PAUL SCHERRER INSTITUT

PSI Proceedings 02-01
September 2002
ISSN 1019-6447

Proceedings

Papers of the Third International Symposium on Ultrasonic Doppler Methods for Fluid Mechanics and Fluid Engineering Co-organized by EPFL and PSI

Lausanne EPFL, Switzerland
Sptember 9-11, 2002

ÉCOLE POLYTECHNIQUE
FÉDÉRALE DE LAUSANNE

Third International Symposium on Ultrasonic Doppler Methods for Fluid Mechanics and Fluid Engineering (3rd ISUD)

Swiss Federal Institute of Technology
EPFL, Lausanne, Switzerland
September 9 - 11, 2002

PROCEEDINGS

Editor
Dr. G. De Cesare (EPFL, Hydraulic Constr.)

co-organised by

PAUL SCHERRER INSTITUT

hosted by

LABORATOIRE DE CONSTRUCTIONS HYDRAULIQUES

Editorial

Dear Symposium participant, dear reader,

After the first two successful editions of the Symposium on Ultrasonic Doppler Methods for Fluid Mechanics and Fluid Engineering (ISUD), held at PSI, Villigen, Switzerland in 1996 and 1999, we are very pleased to organize this third edition for the first time at the Swiss Federal Institute of Technology (EPFL) in Lausanne, Switzerland. In a certain sense, present Ultrasonic Doppler technique users will come to the place where some of the bases of this technique were elaborated.

The ultrasonic Doppler method for velocity profile measurements has recently shown its potential in the fields of general fluid mechanics and fluid engineering. Its application has been broadened from fundamental research to industrial use. It is attracting increasing interest from physicists and fluid engineers for its use as a research tool and the number of users is growing. The purpose of the Symposium is to exchange information on applications of the ultrasonic Doppler method to a variety of flow configurations and liquids including industrial measurements.

The Symposium brings together researchers from all over the world to discuss their applications, results and future work using the ultrasonic Doppler method. The submitted papers present the latest fluid mechanics results that are based on the ultrasonic Doppler technique. In recent years non-Doppler ultrasonic measurement methods have emerged for quantifying various physical parameters. A special section is dedicated to these applications.

On behalf of the organizing committee, I welcome all the participants in Lausanne and wish them an enjoyable and fruitful Symposium. I hope that the participants and the readers alike will find the program of the Symposium of interest.

Dr. G. De Cesare

Contents

A CHARACTERISTIC OF THE FLOW FIELD ON A HEATED ROTATING DISK

Yasuyuki Miwa[1], Noriyuki Furuichi[1] and Masaya Kumada[1]

[1] Gifu Univ. 1-1 Yanagido Gifu, 501-1193, Japan, e-mail:furuichi@cc.gifu-u.ac.jp

Keywords: Mixed convection, Buoyancy, Centrifugal force, Velocity profile, Heated rotating disk, UVP

ABSTRACT

A velocity field on a heated rotating disk was obtained using UVP. The mean velocity on the heated flow field is obtained as a reasonable result and the effect of the heating can be observed near wall region. The unsteady flow field also shows clearly the effect of the heating by using a cross-correlation method. It was found from the variation of the cross-correlation coefficient that the region dominated by natural convection expands toward outside with increasing Grashof number.

1. INTRODUCTION

The purpose of this investigation is to study a flow structure on the heated rotating disk. The flow structure on the rotating disk (un-heated) has been studied by many researchers as it shows a typical flow transition scheme from laminar to turbulence. Moreover, a three-dimensional boundary layer appears as a spiral structure caused by the azimuthal velocity component induced by rotation and radial component by centrifugal force (*ex*. Littel and Eaton, 1994).

In the configuration of this paper, a heating of the disk is added. It is well known that this flow field exhibits a mixed convection, a field consisting of a forced convection induced by rotation and natural convection by buoyancy. It has been clarified well a mechanism of time-averaged heat transfer on the disk (Kreith et al. 1959), the vortex structure on the disk (Ogino et al., 1997) and turbulent heat flux (Elkins and Eaton, 2000). In this flow field, it is expected that the three-dimensional boundary layer is strongly affected by heating. A numerical simulation by Shingai and Kawamura (2002) reports, under the Ekman layer, an influence the heating in the means velocity filed. On the other hand, experimental reports about instability on the heated rotating disk are less, because of difficulty of the measurement. Since this flow field exhibits a three-dimensional boundary layer, as mentioned above, the measurement of the spatial distribution of the velocity is difficult by the visualization method like a PIV. The instabilities including the vortex structure as reported by Ogino et al. might be a function of the radial position. However, the radial variation of the unsteady structure has not been clarified quantitatively although the dependence of the rotating Reynolds and the Grashof number has been clarified.

In this study, we measure the velocity field by Ultrasonic Doppler method and show the vector mapping of the filed on the heated rotating disk for various Grashof number to confirm the correctly measurement under the field with temperature gradient. For unsteady flow structure, we consider it by the cross correlation of the velocity fluctuation.

2. EXPERIMENTAL APPARATUS AND COORDINATE SYSTEM

The schematic of the experimental apparatus and coordinate system are illustrated in Figure 1. A radius of the rotating disk submerged in the water tank (620×720×400mm) is R=85mm and

a height of it is 60mm. A rotating speed of the disk was fixed on π(rad/s) (Rotating Reynolds number is $Re_\omega=R^2\omega/\nu=2.27\times10^4$). A difference of the temperature between the rotating disk and water was varied Δt=0~35°C as a parameter (Grashof number is $Gr=g\beta(T_w - T_\infty)R^3/\nu=1.81\times10^7$ ~4.21×10^7).

Three ultrasonic transducers (8MHz) were set for a vector field measurement with different angle and position as shown in Figure 1 (a) ((i)7, (ii)80, (iii)45 degree, respectively). Three beams were crossed at one point in the flow field to measure the velocity of three components. The arrangement of the transducers shown in Figure 1 (b) is for a measurement of an unsteady flow structure. Both transducers are set with inclination angle 7 degree. The velocity at the nearest point of the rotating wall was selected to compute cross-correlation coefficient. The measuring interval of the each transducer is 26msec. An error rate of the velocity was about 5% and position is 5% since a difference of density of water induced by the heating in this experiment.

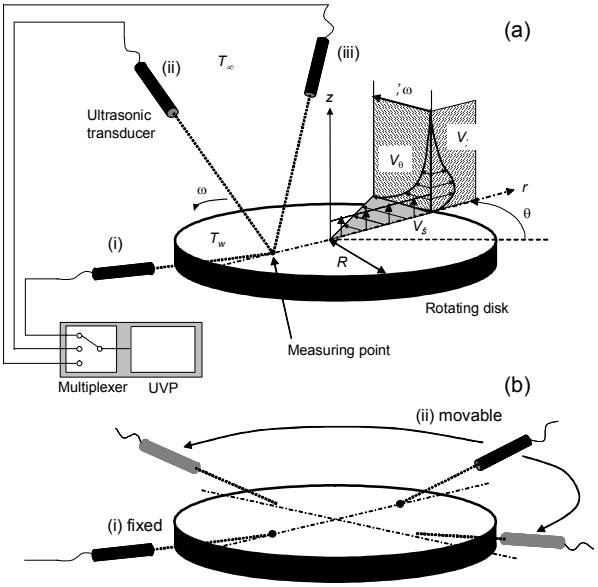

Figure 1. Schematic of the experimental apparatus and coordinate system

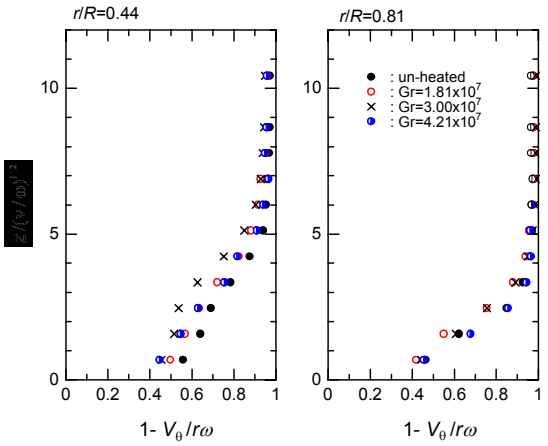

Figure 2. Examples of the velocity profile of azimuthal component

3. RESULTS AND DISCUSSION

3.1 Mean velocity fields

Typical velocity profiles of the azimuthal component are shown in Figure 2. The velocity profile in a boundary layer is obtained clearly. These plots suggest a weak effect of the Grashof number. At r/R=0.44, the velocity profiles of heated case are slightly different with unheated case near disk region, especially $Gr=3.0\times10^7$. At r/R=0.44, although the trend of velocity profiles are almost similar, the velocity near wall region is the largest at $Gr=1.81\times10^7$. On the other hand, it should be noted that the velocity at $Gr=4.21\times10^7$ is almost similar with one of un-heated.

A typical velocity field of the r-z plane obtained in this experiment is shown in the Figure 3. The figure (a) shows an unheated case and the (b) shows the case that a difference of the temperature is 35°C ($Gr=4.21\times10^7$). In both cases, the cross-flow by the centrifugal force directed to outside of the disk can be observed clearly. This velocity component increases with increasing radial position. The flow directed toward the disk (-z) generating to take a balance of a flow rate with the cross-flow can be also observed. The difference of the flow field between figure (a) and (b) can be observed at the vicinity of the rotating disk. The cross-flow near wall of heated case is larger than unheated case since the density of the working fluid is changed by the heating.

To observe detail of the velocity near wall region relating to the heating, the relationship between the cross-flow component V_r and wall normal component V_z is shown in Figure 4. Compared between Gr=1.81×10^7 and unheated case, V_r component increases, however the trend of the relation of two components is almost same. With increasing Grashof number, the gradient of the line is decreases. This results shows that an appearance of an effect of the heating for small V_r component at the centre of the disk. When the cross-flow component is large at large radial position, the effect of the heating is small. Therefore, it is expected that the effectiveness of the heating is a function of the radial position.

To observe the effect of the heating to the three-dimensional boundary layer, the relationship between the azimuthal flow and cross-flow is shown in Figure 5. The plotted data is measured at r/R=0.6-0.9. To clear the trend of the plot, the lines are added. The clearly three-dimensional spiral structure is observed over the every condition and the effect of the heating. Especially, at the Gr=4.21×10^7, the local peak exists near region of 1-$V_\theta/r\omega$=1 comparison with other case. It shows that the wall normal position (z) of the maximum V_r velocity component is higher than other condition since large heating.

Thus, obtained velocity profile clearly shows the effect of the heating. These results might be reasonable one. It is concluded that the velocity under the field with small temperature gradient can be obtained correctly.

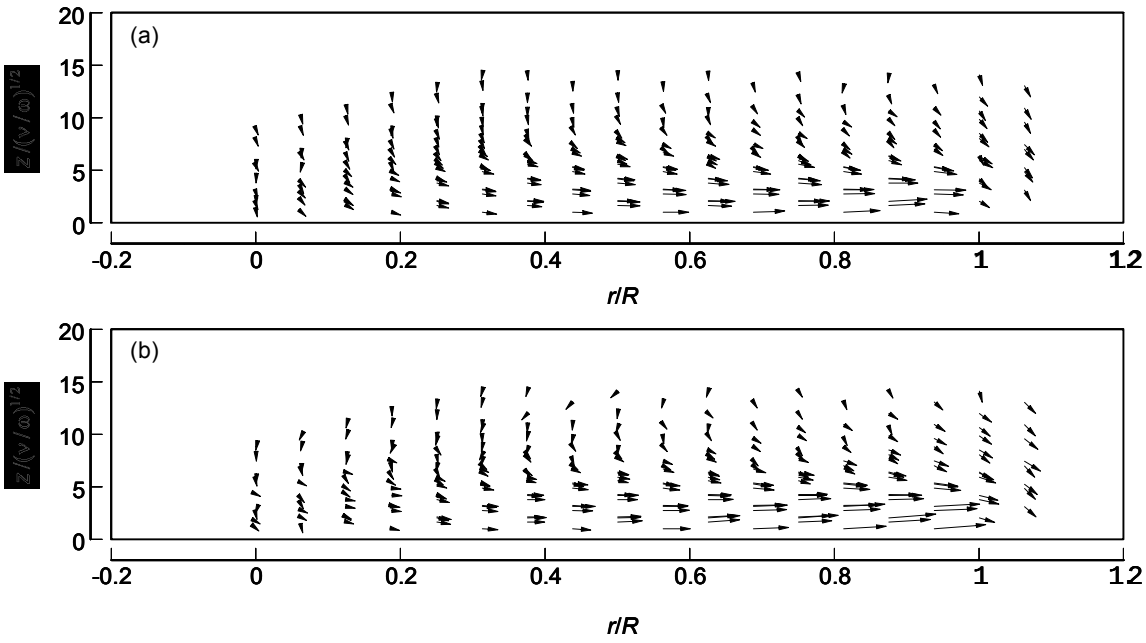

Figure 3. Examples of vector map at r-z plane (a) un-heated (b) Gr=4.21×10^7

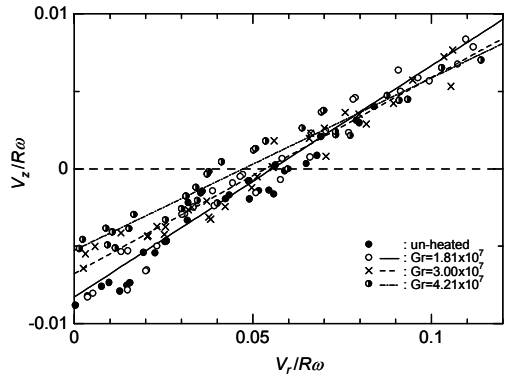

Figure 4. Relationship between V_r and V_z near wall region

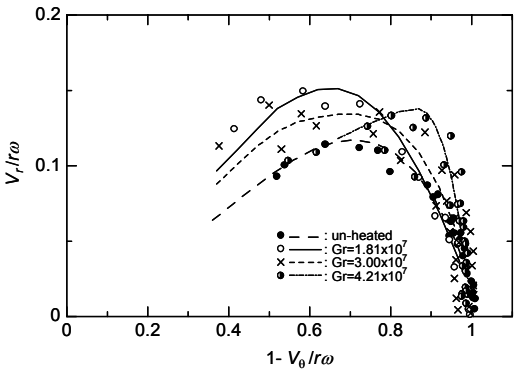

Figure 5. Polar plot of the velocity profile (V_θ-V_r)

3.2 Correlation of the velocity fluctuation

The correlation coefficients of the velocity fluctuation of the radial component are obtained between the fixed and movable transducers. Azimuthal variations of the cross correlation coefficient $R_{vv}(r,r,0,\theta)$ are shown in Figure 6. The local minimums are observed at $\theta=\pi/2$ and maximums are $\theta=\pi$ at $Gr=1.81\times10^7$. This behaviour of the correlation coefficient is similar at each radius positions and similar with unheated case although it is not shown in this paper. On the other hand, this behaviour is different largely with Figure (b); $Gr=4.21\times10^7$. Especially, the $r/R<0.5$, the local minimum is observed at $\theta\approx\pi$.

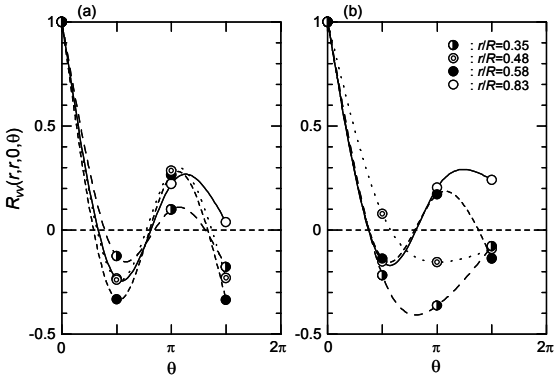

Figure 6. Azimuthal variations of the correlation coefficient (a) $Gr=1.81\times10^7$ (b) $Gr=4.21\times10^7$

Radial variation of $R_{vv}(r,r,0,\pi)$ is shown in Figure 7 to make an attention to the behaviour of it at $\theta=\pi$. The local maximums are observed at each Grashof number. These peaks move toward outside of the disk with increasing a Grashof number. The zero-cross points where the sign of the correlation coefficient changes minus to plus also move toward outside. At $r/R>0.7$, the correlation coefficient is almost same $R_{vv}\approx0.2$ in every conditions. The correlation coefficient is a positive as shown the unheated case at $\theta=\pi$. Therefore, it is suggested that the forced convection is dominant $r/R>0.7$ at every case. It can be concluded that the region dominated by natural convection expands toward outside with increasing with Grashof number.

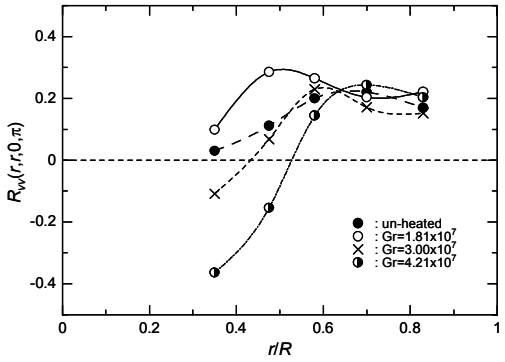

Figure 7. Radial variations of the correlation coefficient

4. CONCLUSION REMARKS

The velocity field on the heated rotating disk was obtained using UVP. The mean velocity of the al component on the heated flow field is obtained as a reasonable result and the effect of the heating can be observed near wall region. The UVP method can be applied to the measurement of flow field with small temperature gradient such as present field. The unsteady flow field also shows clearly the effect of the heating. The cross-correlation coefficient of the cross-flow component between each azimuthal angle varies with azimuthal and radial direction. It was found from the variation of the cross-correlation coefficient that the region dominated natural convection expands toward outside with increasing Gr number.

REFERENCES

Elkins, C.J. and Eaton, J.K, J. Fluid Mech., 402, 2000, 225-253
Kreith, F., Taylor, J.H. and Chong, J.P., ASME J. Heat Transfer, 1959, 95-105
Littell, H.S. and Eaton, J.K., J. Fluid Mech. 266, 1994, 175-207
Ogino, F., Saito, Y., Yoshida, T., Masuda, K. and Mizuta, K., J, Chemical Eng. 23, 5, 1997, 679-686 (in Japanese)
Shingai, K. and Kawamura, H., Thermal Science and Engineering, 20, 1, 2002, 25-33

SIGNAL PROCESSING FOR ADVANCED CORRELATION ULTRASONIC VELOCITY PROFILER

Yousuke Sato[1], Michitsugu Mori[2], Yasushi Takeda[3], Koichi Hishida[1] and Masanobu Maeda[1]

[1] Department of System Design Engineering, Keio University,
Hiyoshi 3-14-1, Kohoku-ku, Yokohama, Kanagawa, Japan, e-mail: yousuke@mh.sd.keio.ac.jp

[2] Tokyo Electric Power Co., Inc., Egasaki-cho Tsurumi-ku, Yokohama 230-8510, Japan, e-mail: mori-mcy@rd.tepco.co.jp

[3] Paul Scherrer Institute, CH-5232 Villigen PSI, Switzerland & Hokkai University, Div. Mechanical Science, Sapporo, Japan e-mail: yft@eng.hokudai.ac.jp

Keywords: high time resolution, signal processing, cross correlation, turbulence measurement

ABSTRACT

The objective of the present study is to develop a high-time resolution ultrasonic velocity profiler system by improving a signal processing algorithm and to apply it to turbulent flow measurement. The time resolution of an existing ultrasonic velocity profiler systems is limited to the order of 10 ms at the best due to its signal processing technique, the fact of which needs more than a few tens echo signals to obtain the velocity distribution. In order to improve the time resolution of a Doppler-shift-typed ultrasonic velocity profiler, we have introduced a cross-correlation technique to estimate a time difference between two echo signals of a pair of emissions of ultrasound pulses. We improved a signal processing procedure for a better durability over noise by using following criteria, 1: a threshold of correlation coefficient at 0.95; 2: a threshold of signal amplitude≒ over 3/128 (in 8bits); 3: exclusive operation to the spurious data that is largely far from average values. A pipe flow was measured by the present high-time resolution ultrasonic velocity profiler system with new signal processing algorithm. Hydrogen bubbles and nylon particles were used as a tracer. A comparison showed that a good agreement was attained, although data rate for hydrogen bubbles was over 90% and nylon particles were less than 10% at the center of pipe region. Moreover, comparing with LDV, a relative error falls within ±1.5%. In conclusion, we could improve the time resolution of the high-time resolution ultrasonic velocity profiler up to 1 ms to obtain a line profile of velocity distribution and demonstrated a possibility to realize a measurement of a smaller time scale velocity fluctuation in flows.

1. INTRODUCTION

The acquisition of instantaneous velocity fields is of utmost importance in understanding flow mechanism. An ultrasonic velocity profiler called as UVP has been developed for this purposes [1][2]. The principle of UVP is to use a pulsed ultrasonic echography together with a derivation of instantaneous Doppler shift frequency of echo. One of its measurement capabilities is capturing an instantaneous velocity distribution on one line. Furthermore, the UVP is applicable to opaque liquid objects and through the wall of closed vessel without making a window. By taking these advantages, UVP measurement clarified a transient process in a rotating Taylor-Couette system successfully [3]. To measure multi-dimensional two-phase flow characteristics, a measurement system combining UVP with a video data processing unit was developed [4], and such characteristics as void fraction profiles of bubbly concurrent flow were investigated [5].

Time resolution of UVP greatly depends on a signal processing algorithm, and in the existing UVP based on pulse Doppler method, it is difficult to detect the Doppler shift from a single

echo and it requires dozens echo receptions. Therefore, time resolution is limited to the order of 10 msec at the best and is insufficient for the measurement of turbulence characteristics.

The objective of the present study is to realize high time resolution measurement which is better than 1 ms by introducing a new signal processing method other than the Doppler shift method. A cross correlation method was adopted to determine a time difference - velocity (tracer movement) - between two successive echoes. Although this method is able to take a large signal shift compared to the Doppler method, the waveform needs to be characterized to differentiate a signal in order to detect the signal shift. Thus, four-cycle sinusoidal tone burst was used. Since data amount obtained is increased from one pair of pulses through the following signal validation processes, it enables to determine velocity by a few times of echo reception, i.e. time resolution is extremely improved.

The present system consists of three enhanced PC boards and a transducer. Both a pulsar-receiver and an analogue to digital converter up to 2GS/s are synchronised by Trigger signal. Trigger timing is configured such that following two processes are repeated. 1: Emitting several successive trigger signals; 2: Leaving constant time interval. Herewith, since data amount was increased, velocity distribution that improved data rate was obtained with durability over noise by the following processes. 1: threshold of correlation coefficient≒ over 0.95; 2: threshold of signal amplitude≒ over 3/128 (in 8bits); 3: exclusive operation to the unusual data which separated most from an average value. It is also advantageous to be able to adjust time resolution sufficiently depending on the time scale of fluctuation.

2. PRINCIPLE

2.1 Determination of Velocity Profiles

A basic concept of the principle of the present signal processing technique is illustrated in Fig. 1. Sinusoidal ultrasonic tone-burst are emitted from the transducer with a short time interval (Δt) along a measuring line, and then the echo signals that is reflected from the same minute tracer bulk are detected by the same transducer. This generates two time series of echo signals with the time coordinate being set at the emission of the ultrasonic pulse.

Position x is determined from time delay τ between emission of pulse and reception of echo by echographic relation as expressed in Eq.1. A displacement of the tracer bulk Δx during the burst interval Δt gives a velocity of the bulk, which is reflected on the echo signal as a time shift $\Delta\tau$. Eq.2 figures out this relationship.

$$x = \frac{c\tau}{2} \quad (1)$$

$$v = \frac{c\Delta\tau}{2\Delta t} \quad (2)$$

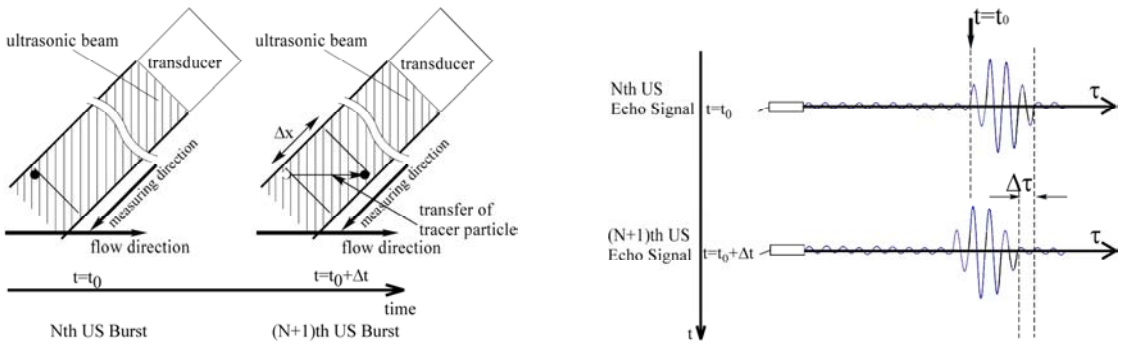

Fig. 1 Determination of time difference between two local echo

2.2 Interpolation of Cross-Correlation for an accurate measurement of time delay

The time shift $\Delta\tau$ at each position would be obtained by cross correlation from two time series of local echo signals, whereby much higher sampling rate, 100 MS/s, is used to build such a time series in the present work. When two signals include the echo from the tracer bulk very clearly and characteristically, a time delay $\Delta\tau$ is easily determined from computation of cross correlation function because of characterized echo signals with 4-cycle successive tone-burst.

However even in this case, the sampling rate is still insufficient to determine the velocity at the position with high accuracy due to its discrete nature of the signal. To improve this, we adopted an interpolation scheme that has been established in the signal processing by LDV [6]. We take a cross-correlation function with the reference window, which is a part of reference echo signals, and the length of the time series is 1 μs, and the search window in search echo signals. The integer index of the peak in the correlation map k is obtained as the discrete value and we obtain a modified time difference by using Gaussian Curve Fitting to find the $\Delta\tau$ corresponding to the real peak value as shown in Eq. 3.

$$\Delta\tau = k + \frac{1}{2}\left(\frac{\log\left(P_{k-1}\right) - \log\left(P_{k+1}\right)}{\log\left(P_{k-1}\right) - 2\log\left(P_{k}\right) + \log\left(P_{k+1}\right)} \right) \quad (3)$$

This adjustment for interpolation of discrete data minimizes a bias error. The present technique enables us to improve the resolution of velocity evaluation. We repeat this procedure over the measurement range

2.3 Trigger Timing

The measurement system was set up such that signal emission, echo reception and its digitisation be synchronized with the trigger signal. The timing is configured such that the following two processes are repeated as shown in Fig. 2. 1: Emitting several, usually 2~4, successive trigger signals**;** 2: Leaving constant time interval. Time during two successive trigger signals is called Duration Time, which is equivalent to Δt in measurement principle. Duration Time and constant time interval are combined and called Interval Time, that corresponds to a time resolution of the system.

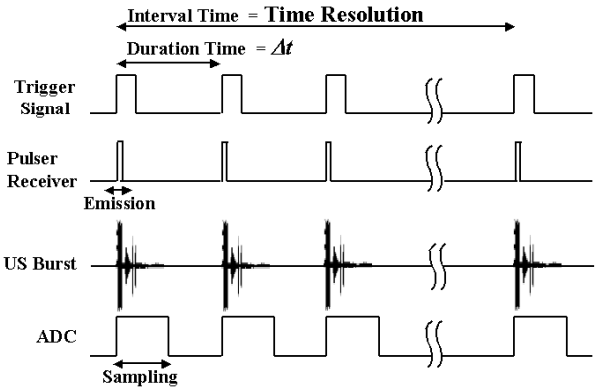

Fig. 2 System controlling

By configuring like this, two advantages are expected: the first is an increase of an amount of total data by increasing the number of time series of echo to be used, and the second is a flexible adjustment of time resolution.

2.4 Validation of Echo Signals

When a concentration of the tracer particles is low, we receive only weak echo and the signal to noise ratio is low. Furthermore, when the peak of the computed cross correlation function between two echo signals is not clear or the peak value is quite low, an accurate measurement of the velocity is difficult. The objective of the present study is to develop a signal processing procedure of velocity measurement with durability over noise for high adaptability in a real flow place. Therefore, we employed three rejection schemes to validate the echo signal. 1: threshold of signal amplitude value; 2: threshold of correlation peak value; 3: exclusive operation to the unusual data which separated largely from average value.

As the amplitude of the echo signal is strongly dependent on various experimental and measurement configurations such as material properties of reflector, its concentration, velocity levels, setting angle of transducer, electronics etc., there is no realistic prescription to determine the threshold values for signal amplitude as well as peak value of cross correlation function. Also, there is no realistic prescription to determine the unusual data to be excluded.

3. EXPERIMENTAL APPARATUS

3.1 Measuring System

Measurement system was built based on PC. Devices installed were pulsar-receiver board, analog to digital converter board, a trigger board and a transducer. To synchronize pulser receiver and analog to digital converter, we built a trigger board to send an external signal. The trigger board has a 1 MB onboard memory (RAM-TABLE). The software here could set a signal pattern in the memory of Trigger Board with 100 ns time resolution. Using this Trigger Board, we could attain any desired Interval Time and Duration time. Fig. 3, 4 and Table.1, 2, 3, 4 show system configuration and parameters, and each system Board specification.

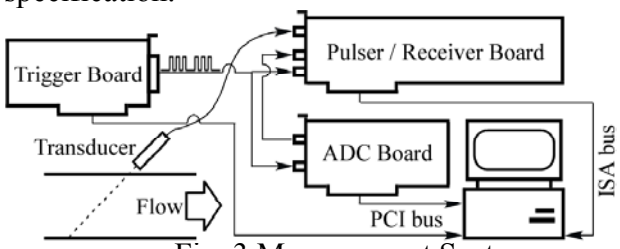

Fig. 3 Measurement System

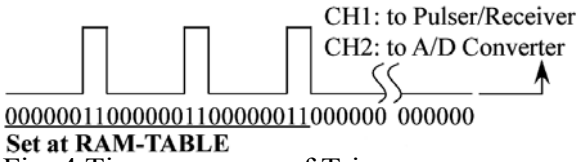

Fig. 4 Time sequence of Trigger

Table. 1 Specifications of Transducer

resonance frequency	4MHz
active diameter	5mm
overall diameter	8mm
overall length	60mm
near field length	16.9mm
divergence half angle	2.2º

Table. 2 Specifications of Analog to Digital Converter

sampling frequency	1kHz to 500MHz
resolution	8bits
on board memory size	512MB
internal sampling clock accuracy	200ppm
DC accuracy	2%

Table. 3 Specifications of Ultrasonic Pulser/Receiver Board

Pulser	
pulse type	gated sinusouid
frequency range	50kHz to 20MHz
pulse width	20ns to 26μs
jitter width	±1/frequency range
Receiver	
bandwidth	50kHz to 20MHz
gain	0dB to 70dB
dynamic range	+70dB

Table. 4 Set of present system parameters

US basic frequency	4 MHz
pulse reptiiton rate	150μs maximum
maximum measurable range	11cm
maximum measurable velocity	60cm/s
velocity resolution	50mm/s
spacial resolution	0.75mm
number of channels	150
bursts per profile	1~3
time resolution	150μs maximum
profile storage	Max: 34133

3.2 Flow Test Section

We examined the measurement system applying to a water pipe flow as shown in Figure 5. An ultrasonic transducer of 4 MHz was installed in the outside of the pipe wall with the 45º inclination. This pipe was made of acrylic polymer and the thickness of the pipe was 2 mm;

thin enough for the ultrasound pulses to pass through this pipe wall. The inner diameter of the pipe was 44mm and the channel around the pipe was filled with water to eliminate a spurious echo returning to the transducer.

The experiments were performed at the Reynolds number of 12000 and 14000. The measurement position was 19D from the entrance of the pipe. For comparison of the effect of echo amplitude, two kinds of tracers were used. They were Hydrogen bubble, 10~20 μm particle diameter and nylon powder, 3~30 μm particle diameter.

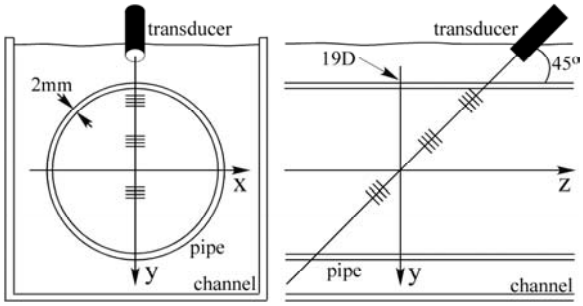

Fig. 5 Test Section

4. RESULTS AND DISCUSSION

4.1 Mean Velocity and Data Rate

In Fig. 6, one result is shown in comparison with LDV measurement. It was measured at the same line and for the same velocity component. In LDV, 3000 data are averaged at each measurement points. In the present new-typed high-time resolution ultrasonic velocity profiler, 3000 profiles were averaged, and time resolution was 10ms with Δt of 200μs. Also, threshold of the present high-time resolution ultrasonic velocity profiler was set to 0.95 (correlation coefficient) and 3/128 (quantized signal amplitude). Only hydrogen bubble was employed as tracer in this measurement. LDV and the present high-time resolution ultrasonic velocity profiler measurements show excellent agreement for averaged velocity distribution and RMS value distribution. In total a difference outside the boundary layer lies in less than 5%. Experimental accuracy (RMS value / average) at the center of the pipe is in the order of 2%. This result indicates that high accuracy measurement on LDV-level was realised in line measurement. Additionally, data rate reached to the order of 90% except near wall region.

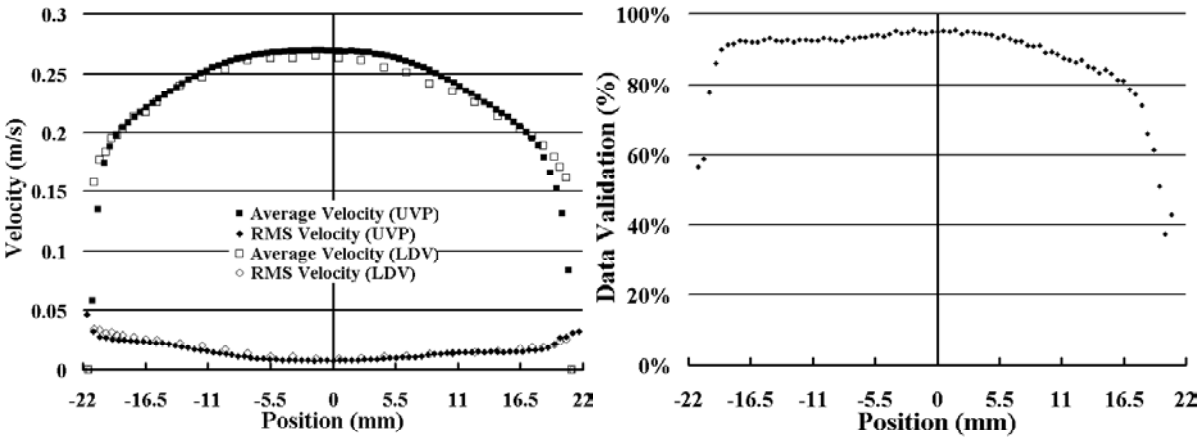

Fig. 6 measurement result of average profiles (left) and data rate through the threshold (right)

4.2 The effect of tracer particles

When applying the present high-time resolution ultrasonic velocity profiler for an actual working flow, hydrogen bubbles cannot not be employed as a tracer. Using a solid particle is also restricted to very small quantity in many cases. The experiments were made in

considering these cases. Amount of data was increased intentionally by emitting successive three times of trigger signal and creating 3 time series of echo in Interval Time, and then, averaging five points on the side of the time series of echo, the unusual data that is separated from average value were excluded. Although data rate was very low, near value resulted by hydrogen bubbles was obtained by this exclusive validation method.

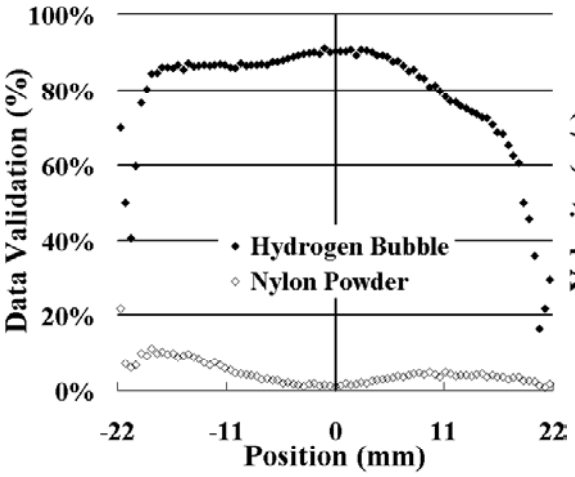

Fig. 7 comparison of data rate

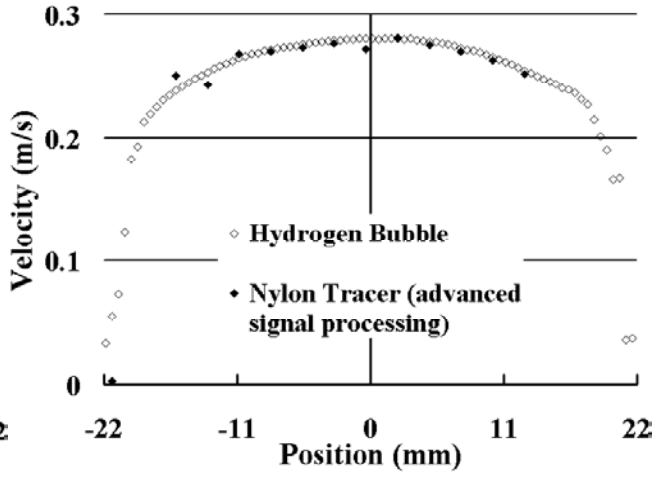

Fig.8 Velocity distribution obtained in low data rate

4.3 Time Series of Measurement

Higher time resolution measurement was made by setting both Interval time and Duration time as 150μs. Fig.9 shows five successive velocity distributions and 400 times successive velocity data at the center of pipe and near wall region. For this time resolution, it was observed that velocity profiling was successful. And, variation is small at the center of pipe. In contrary to this, periodical variation is observed in near wall region.

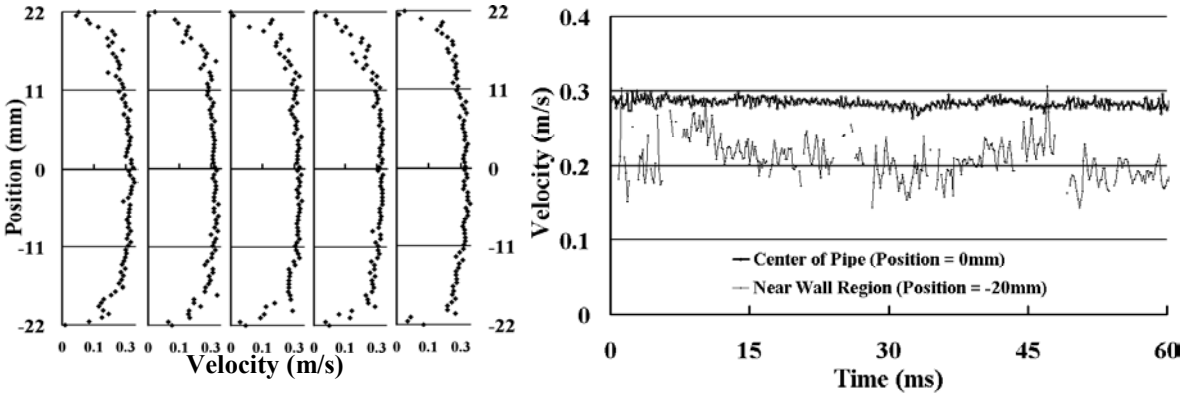

Fig. 9 Instantaneous Velocity Distribution

5. CONCLUSION

The high-time resolution ultrasonic velocity profiler was developed with the signal processing method based on cross correlation; alternative to pulsed Doppler method. The present signal processing method enables us to control the repetition of echo reception with only two times. By this method, we could develop a noble velocity measurement system with high time

resolution. Circular pipe flow was measured with the present high-time resolution ultrasonic velocity profiler system. In comparison to LDV, the relative error of average velocity is less than 2% and RMS value is less than 16% at the center of the pipe. Applicability of the cross correlation method was confirmed. By adjusting acquirement of echo signal, the amount of signal data was increased. Even in the case using nylon particles, which showed only weak reflection echo, we obtained near value of velocity distribution measured using hydrogen bubbles. The high time resolution measurement in 150μs was made. We obtained velocity distribution successively. This measurement is considered to be reliable because the measurement results by the present high-time resolution ultrasonic velocity profiler system showed excellent agreement with those of LDV's.

REFERENCES

[1] William D.BARBER, JEFREY W.EBERHARD and STEVEN G.KARR, A New Time Domain Technique for Velocity Measurements Using Doppler Ultrasound, IEEE Transactions of Biomedical Engineering, Vol.BME-32, No.3, P213-229, 1985

[2] Y.TAKEDA, Development of Ultrasound Velocity Profile Monitor (UVP) and its Experience, 4th International topical meeting on Nuclear Reactor Thermal-Hydraulics, P418-423, 1989

[3] Y.TAKEDA, Quasi-periodic state and transition to turbulence in a rotating Couette system, Journal of Fluid Mechanics, 389, P81-99, 1999

[4] M.ARITOMI and S.ZHOU, Measurement System of Bubbly Flow Using Ultrasonic Velocity Profile Monitor and Video Data Processing Unit, Journal of Nuclear Science and Technology, vol.33, No.12, P915-923, 1996

[5] S.ZHOU, Y.SUZUKI, M.ARITOMI, M.MATSUZAKI, Y.TAKEDA and M.MORI Measurement System of Bubbly Flow Using Ultrasonic Velocity Profile Monitor and Video Data Processing Unit, (3) Comparison of Flow Characteristics between Bubbly Concurrent and Countercurrent Flows, Journal of Nuclear Science and Technology, vol.35, No.5, P335-343, 1998

[6] Y.OZAKI, T.KAWAGUCHI, Y.TAKEDA, K.HISHIDA and M.MAEDA, High Time Resolution Ultrasonic Velocity Profiler, Experimental Thermal and Fluid Science, Volume 26, Issues 2-4, P253-258, June 2002

AN AZIMUTHAL-STREAMWISE STRUCTURE OF AN AXISYMMETRIC SUDDEN EXPANSION FLOW

Noriyuki Furuichi[1], Ikutaro Yamashita[1], Masaya Kumada[1] and Yasushi Takeda[2]

[1] Gifu Univ. 1-1 Yanagido, Gifu, 501-1193, Japan, e-mail:furuichi@cc.gifu-u.ac.jp

[2] Hokkaido Univ., Kita 8, Nishi 5, Kita-ku, Sapporo, 060-0808, Japan, e-mail:yft@eng.hokudai.ac.jp

Keywords: Separation, Reattachment, Azimuthal Structure, Axisymmetric Sudden Expansion, Proper Orthogonal Decomposition

ABSTRACT

An azimuthal-streamwise velocity field was obtained by UVP method using multiple transducers and a streamwise variation of the averaged velocity field, correlation coefficient and eigenvalue spectra decomposed by a proper orthogonal decomposition will be discussed. Several typical inflection points were found in the streamwise variations and a coherent structure was found relating to a large-scale fluctuation around the reattachment region.

1. INTRODUCTION

An objective of this study is to clarify an azimuthal structure of a flow in an axisymmetric sudden expansion. The sudden expansion flow is one of the most popular flow fields involving a separation and reattachment phenomenon. The geometry of the configuration is simple and an analysis has been made, as in the pervious researches, as a two-dimensional field. It is, however, well known that three-dimensional structure exists in this flow field by experiments (ex. Kasagi et al.,1977, Troutt et al.,1984, Hijikata et al., 1991) and by numerics (Neto et al.,1993, Le et. al,1997). We also observed a spanwise structure around a reattachment region of a two-dimensional backward-facing step using UVP (Furuichi and Kumada, 2002) by a spatio-temporal measurement of a spanwise velocity component.

A vortex shedding from the separated shear layer is deformed largely around the reattachment region and causes a reattachment phenomenon. Furthermore, as it is indicated that the flow does not fully recovered at 20 times step-height at downstream (Le et al, 1997), the velocity field is affected by the separation and reattachment with the deformation process even in the wake. The three-dimensional structure as mentioned above might have a strong relationship with the deformation process. Therefore, it is necessary to observe the velocity field on the streamwise-spanwise (azimuthal) direction in order to clarify the three-dimensional structure and analysis by some decomposition methods.

In this paper, the flow field is an axisymmetric sudden expansion; a flow which shows separation and reattachment and eliminates a side wall effect. We obtained the velocity field at various azimuthal angles by using multiple transducers and observed the streamwise velocity component in azimuthal-streamwise plane and temporal field. We will discuss the streamwise variation of the averaged velocity field and of an azimuthal coherent structure by using correlation method and proper orthogonal decomposition.

2. EXPERIMENTAL APPARATUS

A test section of the experimental apparatus with transducers and coordinate system are illustrated in Figure 1. The pipe diameter of upstream is d=25mm and that of downstream is D=45mm (Expansion ratio is 1.8, step height h is 10mm). The bulk velocity in the upstream channel is fixed at V_b=0.152m/s and Reynolds number is Re_d=3820. The sudden expansion is

positioned at 85*d* downstream from the flow conditioner and the inlet flow is fully developed. All transducers were set outside of the step wall at r/h=1.75 (the centre of the step) to obtain the velocity profile $v_z(z,t)$. The velocity profile was obtained at z/h=2~20 with channel distance 1.48mm. In this experiment, we used seven transducers positioned from $\theta=-\pi/2$ to $\pi/2$ with the increment of $\pi/6$ as shown in the figure. We obtained the pseudo velocity field as $v_z(z,\theta,t)$ by switching transducers using a multiplexer. A measuring interval per one transducer is 21ms and one of a series is 147ms.

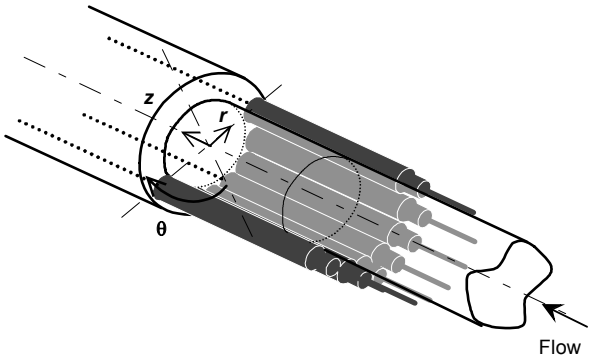

Figure 1. Experimental apparatus and arrangement of transducers

3. RESULTS AND DISCUSSION

3.1 Velocity field

A mean velocity profiles and turbulent intensity profiles at various streamwise positions are shown in Figure 2. As shown in the figure, the both profiles with respect to the azimuthal direction is not uniform except around the redeveloping region (z/h>18), although the difference of the velocity at each azimuthal position is small (i.e. maximum is $0.05V_b$ at z/h=5.5). Armaly et al.(1983) measured the spanwise velocity profile of streamwise component and showed that it is not uniform at Re=3000. Furuichi and Kumada (2001) also showed the same tendency concerning the spanwise velocity component of the two-dimensional backward-facing step. We have no knowledge of the azimuthal velocity profile in the previous paper, however, it is clearly shown that the axisymmetric backward-facing step should not be treated as two-dimensional structure even the mean velocity field, especially around the reattachment region.

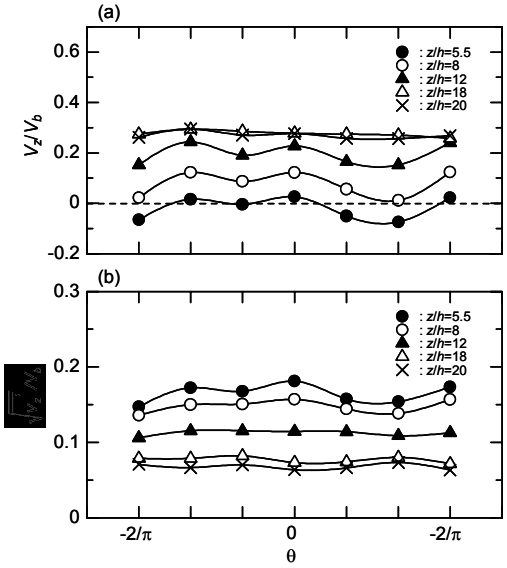

Figure 2. Mean profiles of (a)mean velocity (b)turbulent intensity at variable streamwise positions

An example of an pseudo-instantaneous velocity field of $v_z(z,\theta)$ is shown in Figure 3. The shaded region shows negative velocity, the white is zero and the gradation becomes darker with increasing velocity. The azimuthal variation of the zero region is not uniform with respect to the spanwise direction and the recirculation region shows a complex structure interfered with the separated shear layer. The large-scale structures can be observed z/h>10. The scale of it $z/h\approx$10 is $\Delta\theta<\pi/2$ as shown (a). At further downstream, it grows larger to $\theta\approx\pi/2$ as shown (b).

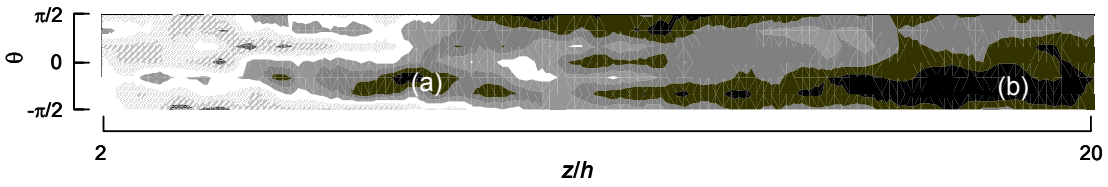

Figure 3. Example of an instantaneous velocity field of $v_z(z,\theta)$

3.2 Cross-correlation

The variation of a cross-correlation coefficient $R_{vv}(z,\theta_1,\theta_2)$ is shown in Figure 4. The subscript 1 and 2 mean the azimuthal measuring points and the $\Delta\theta$ shown right hand in the figure is the angle between θ_1 and θ_2. The positive correlation coefficient is observed up to $\Delta\theta=2\pi/3$ over the measuring region. The length scale of azimuthal direction $L_\theta/\pi=0.41$ at z/h=8 and $L_\theta/\pi=0.48$ at z/h=18. This result is reasonable result as shown in Figure 3. The streamwise variation has some inflection points as shown the dotted line in the figure, if one observes more detail. Although it shows a complex variation around a zero-cross point because of an interaction between the recirculation flow and shear flow, the local minimum can be observed clearly at z/h=8. Troutt et al.(1984) shows also the local minimum around a reattachment region and they supposed that it is caused by the interaction of the wall surface and large-scale vortices. At $\Delta\theta<\pi/3$, the correlation coefficient increases with the streamwise position, while, at $\Delta\theta>\pi/2$, it shows local maxima at $z/h\approx12$ and decreases with the position. At downstream of this region, the turbulent intensity profile as shown in Figure 2 becomes uniform with respect to azimuthal direction. Further downstream, after it shows the local minimum at z/h=16, it increases linearly with the streamwise position. Since the variation with azimuthal direction becomes weaker as shown in the mean velocity field, the scale of the eddy might becomes larger in this region. It should be noted that the tendency of the correlation coefficient does not saturate even at z/h=20. It is indicated that the flow does not fully recovered as indicated by Le et al.(1984).

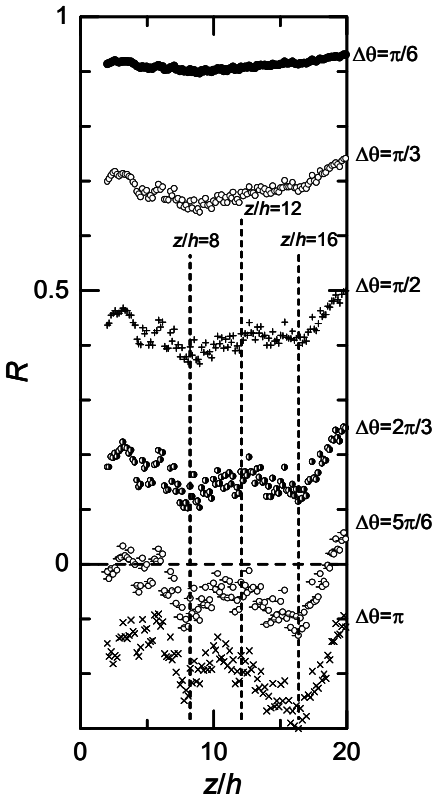

Figure 4. Variation of the correlation coefficient

3.3 POD decomposition

To observe the streamwise variation of spanwise structure as shown in Figure 4 from another viewpoint and identify the coherent structure of this flow field, the velocity field was decomposed by the POD (Proper Orthogonal Decomposition) method. The streamwise variation of eigenvalues of the velocity field $v_z(\theta,t)$ is shown in Figure 5. This result also shows a little change in the variation curve. The first mode shows an almost linear increase with the streamwise position except z/h<6 (in the recirculation region). The mode which shows a typical change is the second and third mode at z/h=8,12,16 as similar with the one of correlation coefficient. It is suggested that the inflection point around the zero-cross point is related to

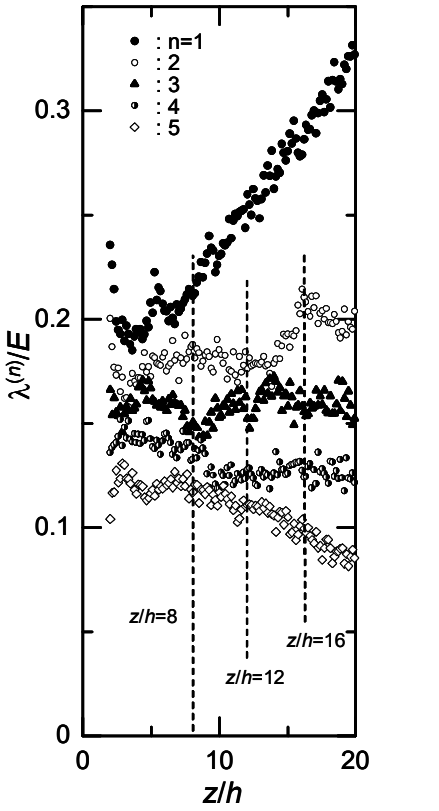

Figure 5. Streamwise variation of eigenvalues

the variation of third mode and the redeveloping region is related to the second mode.

Examples of the decomposed velocity field which were composed of the first and second eigenvectors are shown in Figure 6. The figure (a) is z/h=6, which corresponds to the zero-cross point and (b) is z/h=16. The solid line is the contour line for v_z'/V_b=0.05 and the dotted line is for v_z'/V_b=-0.05. In the figure (a), a certain coherent structure can be observed as a streak structure with a period of $fh/V_b \approx 0.03$, of which the width is $\theta \approx \pi/4$ and flow direction changes alternatingly in azimuthal direction although it is broken around tV_b/h=140. The time length of the streak observed as the contour line v_z/V_b=0.05 is about 35 in dimensionless time. This coherent structure shows non-stationary behaviour with respect to azimuthal direction and it fluctuates within $\theta \approx \pm\pi/6$ as shown by the dotted arrow in the figure. Thus, we found the coherent structure fluctuating with respect to the azimuthal direction around the separated shear layer. It was pointed out that the large-scale fluctuation of $fh/V \approx 0.05$ (Furuichi and Kumada, 2002) is dominant around the reattachment region concerning a flapping motion of the separated shear layer. It is suggested from the figure (a) that the large-scale fluctuation is related to the fluctuation of azimuthal direction as the coherent structure. On the other hand, in the wake around z/h=16 as shown in figure (b), it is found that the coherent structure can not be observed, although the structure becomes lager.

4. CONCLUSION

The azimuthal-streamwise velocity field was obtained by the UVP method using multiple transducers and we discussed about the streamwise variation of the averaged velocity field, correlation coefficient and eigenvalues decomposed by the proper orthogonal decomposition. The typical inflection point was found in the variation of streamwise structure. Furthermore, the coherent structure was found around the zero-cross point relating to the large-scale fluctuation.

REFERENCES

Armaly, B.F., Durst, F., Pereira, J.C.F. and Schonung, B., J. Fluid Mech., 127, 1983, 473-496
Furuichi, N. and Kumada, M., Exp. in Fluids, 32, 2002, 179-187
Hijikata, K., Mimatsu, J. and Inoue, J., ASME-FED Experimental and Numerical Flow Visualization, 128, 1991, 61-68
Kasagi, N., Matsunaga, A. and Yokobori, S., Proc. The International Symposium on Flow Visualization, 1977, 245-250
Le, H., Moin, p. and Kim, J., J. Fluid Mech, 330, 1997, 349-374
Neto, A.S., Grand, D., Metais, O. and Lesieur, M., J. Fluid Mech., 256, 1993, 1-25
Troutt, T.R., Scheelke, B. and Norman, T.R., J. Fluid Mech., 143, 1984, 413-427

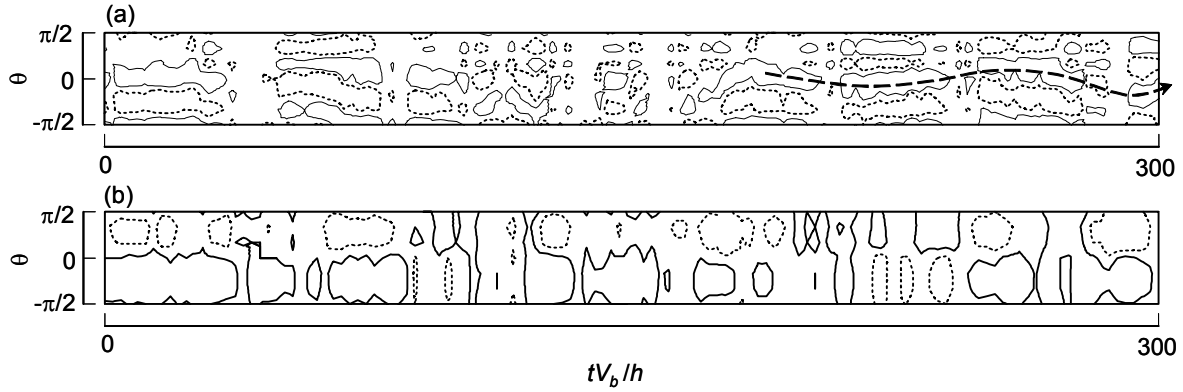

Figure 6. Examples of reconstructed velocity field of $v_z(\theta,t)$ by the first and second eigenvectors at (a)z/h=6 (b)z/h=16.

UNSTEADY FREE-SURFACE FLOW ANALYSIS IN CIRCULAR TUBE USING ULTRASONIC DOPPLER METHOD

Vojtech Bares[1] and Prof. Jaroslav Pollert[2]

[1] Doctorand, Czech Technical University in Prague, Faculty of Civil Engineering, Laboratory of Ecological Risks in Urban Drainage, bares@lermo.cz

[2] Professor, Czech Technical University in Prague, Faculty of Civil Engineering, Laboratory of Ecological Risks in Urban Drainage, pollert@lermo.cz

Keywords: unsteady flow, flood wave, pipe flow, shear stress, ultrasonic Doppler method

ABSTRACT

Turbulence measurements over the smooth wall in both steady and unsteady free-surface pipe flows were done by Ultrasonic Velocity Profile Monitor (UVP) and ultrasonic water-level gauges.

Vertical distribution of longitudinal and vertical velocity (u,v) was measured for 5 different hydrographs. The deviation of the velocity profile from the steady state was confirmed for both rising and falling branches. The friction velocity was determined using the motion equation and the Clauser method for velocity profile in the inner region of turbulent layer. It is shown that the friction velocity (wall shear stress) is higher for rising branch.

1. INTRODUCTION

Waste water in urban drainage systems is governed by many specific factors. That water includes high amount of suspended solid particles and both, cross-section area and pipe material are very often varying. The stationary flow prevails in dry weather periods, while during rain events flow changes to unsteady and can consider effects on hydraulic characteristics and impacts to transport of sewer solids both deposited and suspended.

For the evaluation of sediment transport in drainage systems and for design of longitudinal bottom slope of sewers a criterion of critical bottom shear stress is often used. According to Czech Standard 75 6101 its value should be $\tau_0 = \rho g R i_0 = 4\,Pa$. The value should be reached at least five times per year. However, we can observe the significant deposits in sewer systems. The question is how to set functional criteria.

Many authors (e.g. Cardoso et al, 1989, Kirgoz et al. 1989 and others) evaluated friction velocity or bottom shear stress in steady uniform open-channel flow by different methods and the results showed good applicability above mentioned relation. However, it was shown that there are some differences in free surface pipe flow due to the cross section shape effect (Knight and Sterling, 2000).

Some experimental studies made in last decade were focused on unsteady open-channel flow in rectangular shape flumes (Tu and Graf, 1993, Kabir, 1993, Nezu and Nakagawa, 1995). The authors found out significant differences between bottom shear stress in steady and unsteady state. This study is focused on circular shape channels.

The main goals of the study were experimentally to determinate hydraulic characteristics of steady and unsteady, smooth turbulent free-surface flow in circular tube and to check the suitability of UVP method for determining hydraulic characteristics in above mentioned conditions.

2. METHODS

Experiment was carried out in circular pipe. The pipe was made of plexiglass, with diameter DN 290 mm, length 17 m and bottom longitudinal slope $i_0 = 0.175\ \%$.

The discharge measurements were made on inlet pipe by a flowmeter DN 150 and by a triangular measuring weir. Ultrasonic transducers Pepperl&Fuchs have been used for water level measurements. Maximum water level in both pipes was half of the pipe diameter, i.e. $H/D \leq 0.55$. Measured discharge from 2 to 35 litres per second corresponds with relative water depth H/D from 0,15 to 0,55. At the inlet of the track was automatically added suspension of PVC microparticles and water. Solids had the specific gravity $\rho = 1350\ kg.m^{-3}$ and $d_{50} = 0.15\ mm$.

The steady and unsteady turbulent, smooth free surface flows were observed in the experiment. Different shapes of flood hydrographs were simulated. PC Control Panel (Figure 2) controlled the shape of hydrographs as well as other conditions (discharge, water depth, temperature).

2.1 Velocity measurement

The velocity and turbulence information has been obtained by UVP Monitor (Ultrasonic Velocity Profile Monitor), Met-Flow S.A.. Transducers, with basic frequency $f_{01} = 2\ MHz$ and $f_{02} = 4\ MHz$, were placed outside of the pipe wall in small iron boxes in the axis plane of the circular tube. The space ahead of each transducer was filled in by the ultrasonic gel and was covered with film.

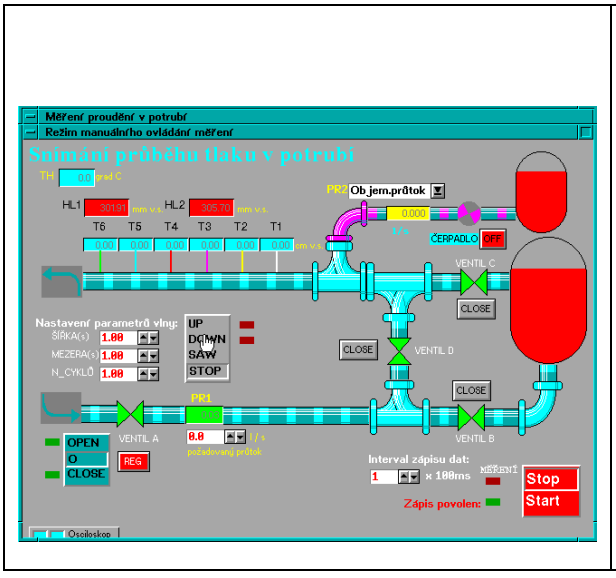

Figure 1 Hydraulic system chart

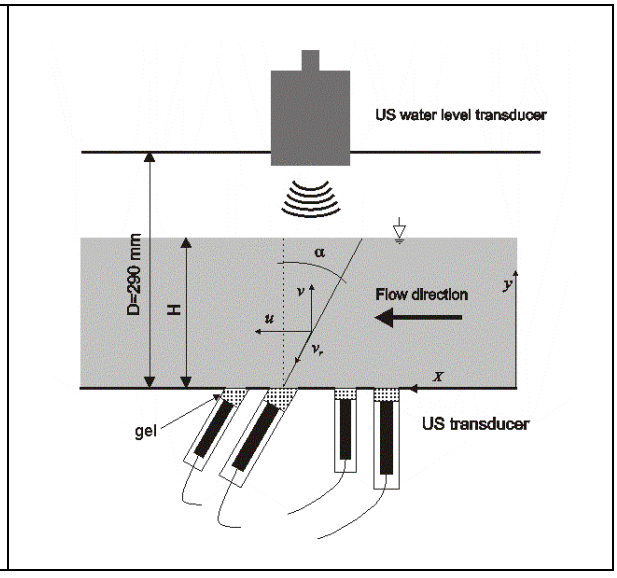

Figure 2 Transducers position

One pair of transducers was perpendicular to pipe bottom and the second one was turned at angle $\alpha = 30°$ against flow direction (Figure 2). Microroparticles of PVC - NERALIT were added to the flowing water due to high quality echo.

3. RESULTS AND ANALYSIS

3.1 Steady flow

3.1.1 Velocity distribution

For description of velocity profiles in fully developed turbulent flow with free surface, generally valid semi-empirical models are used.

Inside inner region of turbulent layer the velocity distribution as a function of height is described by the relation derived by von Kármán (1930) and Prandtl (1932), called logarithmic velocity distribution law. This is expressed as:

$$\frac{u}{u_*} = \frac{1}{\kappa}\ln\frac{u_* y}{\upsilon} + B \qquad (1)$$

Nikuradse (1932) on base of his experiments has found values of $1/\kappa$ and B to be $1/\kappa = 2.5$ and $B = 5.5$ for hydraulically smooth pressure flow in circular pipe. Moreover, also Keulegan (1938) has confirmed the same values for flow with free surface as well. Nevertheless, different values B were found by other authors, in the range between 4,9 (Klebanoff, 1954) and 7 (Townsend, 1956).

The regression analysis has been used to establish B values. The Value B has been found to be in the range from *4* to *6*.

Coles (1956) has introduced the modified logarithmic "law of wake", which describes shape of velocity profile in the outer region of turbulent layer for hydraulically smooth mode of flow, in a form:

$$\frac{u}{u_*} = \frac{1}{\kappa}\ln\frac{u_* y}{\upsilon} + B + \frac{2\Pi}{\kappa}\sin^2\left(\frac{\pi z}{2\delta}\right) \qquad (2)$$

Coles (1956) has also shown that values for $\kappa = 0.4$, $B = 5.1$, and $\Pi = 0.55$ are in agreement with experimental measurements. Different value of Coles parameter $\Pi = 0.2$ were assessed by Nezu and Rodi (1986), and Krikgoz (1989) gives value $\Pi = 0.1$. These are significantly lower values than that of $\Pi = 0.55$ given by Coles.

Values of Coles parameter $\Pi = 0.3$ and constant $B = 4.7$ were found by regression analysis. The velocity distribution is shown in Figure 3.

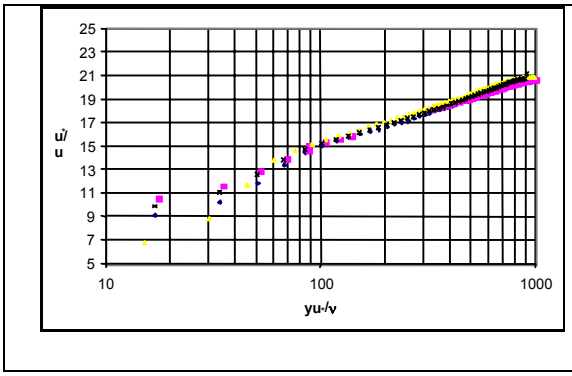

Figure 3 Velocity profiles; steady uniform flow

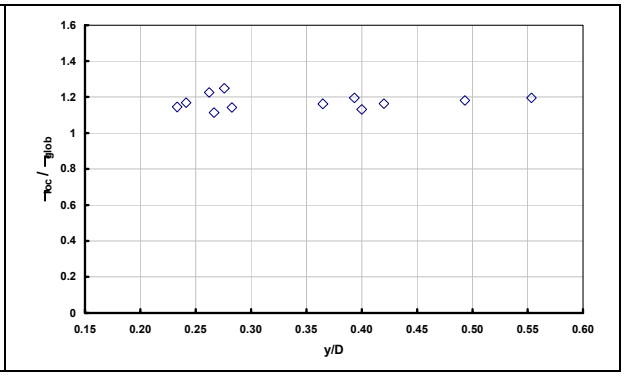

Figure 4 Ratio between $\tau_{0\,loc}$ and $\tau_{0\,glob}$

3.1.2 Friction velocity estimation

The friction velocity is being evaluated by different indirect methods. In our experiment the friction velocity u_* were estimated a) from the channel slope i_0 and hydraulic radius R – u_{*glob} and b) from the inner region data by Clauser method (Nezu and Nakagawa, 1993) – $u_{*loc.}$

The ratio of evaluated bottom shear stress values τ_{0loc}/ τ_{0glob} fluctuated in the range 1.1 – 1.3 (Figure 4), which corresponds well with Knight and Sterling (2000) data.

3.2 Unsteady flow

5 different hydrographs with varied surface slope and length were simulated. The instantaneous velocity profiles were smoothed by moving time average method.

3.2.1 Velocity distribution

The evolution of the mean velocity with the time and water height has shown that the point velocity near the water surface arrives the maximum earlier than those near the bottom.

The velocity profiles in the rising branch were found generally larger than in the falling branch for equal water depth (Figure 5).

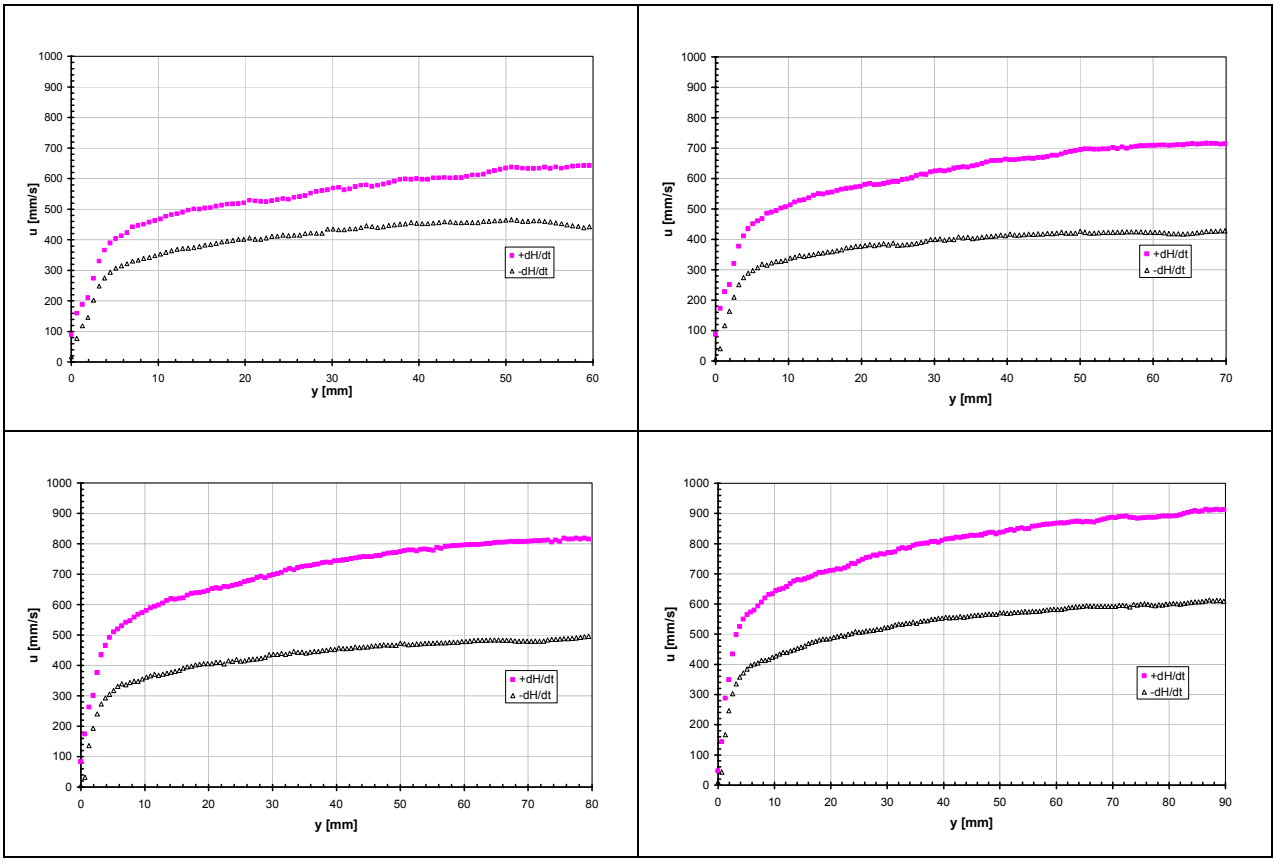

Figure 5 Vertical velocity profiles in the rising and falling branches for given hydrograph and water depths 60, 70, 80 and 90 mm

3.2.2 Friction velocity estimation

The friction velocity was estimated in different ways: a) with steady, uniform formula $u_{,steady} = (gHi_0)^{0.5}$, - b) from the inner region data of velocity profiles, by employing the log – law (1) and c) from the St. Venant equation of motion. By the assumption that the hydrographs are kinematics and/or non-subsiding waves the friction velocity can be obtains (Tu, Graf, 1993):

$$u_{*SV} = \sqrt{gH\left[i_o + \frac{1}{C}\frac{\partial H}{\partial t} - \frac{1}{g}\frac{\partial U}{\partial t}\left(1 - \frac{U}{C}\right)\right]} \qquad (3)$$

where

$$C = U + H\frac{\partial U}{\partial t}\Big/\frac{\partial H}{\partial t} \qquad (4)$$

and

$$U = \frac{1}{H}\int_0^H u \,\mathrm{d}\, y \qquad (5)$$

The results are shown in Figure 6. The similar tendency of u_{*log} and u_{*sv} was observed. The friction velocity is higher in rising branches than in the falling branches. In comparison with steady state values the results are similar and agree well with Tu, Graf (1993).

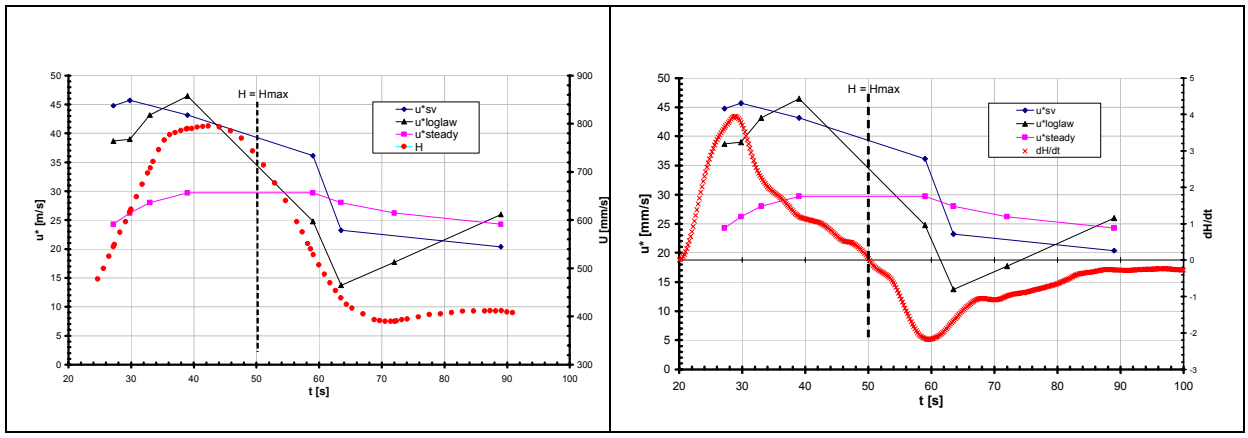

Figure 6 Comparison between the observed values of the friction velocity u_{*log}, u_{*sv} , steady state values $u_{*steady}$ and dU/dt, resp. dH/dt

4. CONCLUSIONS

Using the UVP method the turbulent steady and unsteady flow with free surface over smooth wall in circular tube were observed .

The steady flow measurements showed that a) velocity distribution in the inner region of turbulent flow has been evaluated. The value of parameter B has been found to be in the region from 4 to 6. b) The value of Coles parameter Π for outer region of turbulent layer has been established as $\Pi = 0.3$. c) the ratio $1.1 \div 1,3$ has been found between local bottom shear stress at pipe plane of symmetry, and between average value calculated on base of hydraulic radius R and longitudinal pipe bottom slope i_0.

Unsteady flow measurements showed a) point velocity near the water surface arrive the maximum values earlier than that near the wall. b) for equal water depth the point velocity are generally higher in the rising branch (Figure 5). c) for given hydrograph is the friction velocity larger in the rising branch than in the falling branch (Figure 6). d) calculated and observed friction velocity has the same tendency (Figure 6).

The UVP method provides successfully data of both steady and unsteady turbulent flow with free surface in circular tube. The applicability of this method in non-intrusive measuring mode was confirmed.

ACKNOWLEDGMENTS

This work was supported by the project of Ministry of Education, Youth and Sport of Czech Republic No. MSM 211100002, by the Czech Grant Agency project No. 103/010675 and EU-APUSS-EVK1-2000-22001.

REFERENCES

Cardoso, A. H., Graf, W. H. (1989). *Uniform flow in a smooth open channel*. J. Hydr. Res.. Delft, The Netherlands, 27(5), 603-616.

Graf, W.H., Altinakar, M.S. (1998). *Fluvial Hydraulics*. Laboratorie de recherches hydrauliques, Ecole polytechnyquie federale Lausanne, Suisse.

Kirkgoz, S., Ardichoglu, M. (1997). *Velocity Distribution of Developing and Developed Open Channel Flow*. J. Hydr. Engrg., ASCE, Dec 1997, 1099-1105.

Knight, D., Sterling, M. (2000). *Boundary Shear in Circular Pipes Running Partially Full*, Journal of Hydraulic Engineering, Apr. 2000, 263-275.

Lemmin, U., Rolland T. (1997). *Acoustic Velocity Profiler for Laboratory and Field Studies.* J. Hydr. Engrg., ASCE, Dec 1997, 1089-1098.

Metflow (2000). *UVP Monitor – Model UVP-XW*, Users guide, Met-flow SA, Lausanne, Switzerland

Nezu, I., Nakagawa, H. (1993). *Turbulence in Open-Channel Flows,* IAHR Monograph, A.A.Balkema, Rotterdam

Nezu, I., Nakagawa, H. (1995). *Turbulence Measurements in Unsteady Free-surface Flows,* Flow Measuring Instruments, Vol. 6 No. 1, pp. 49-59.

Nezu, I., Rodi, W. (1986). *Open Channel Flow Measurements with a Laser Doppler Anemometer*. J. Hydr. Engrg., ASCE, 112(5), 335-355.

Takeda, Y. (1995). *Instantaneous Velocity Profile Measurement by Ultrasonic Doppler Method*, JSME International Journal, 8-16

Takeda, Y. (1997). *Ultrasonic Doppler Method for Fluid Flow Measurements – Principle and its Applications*. Bulletin of the Research Laboratory for Nuclear Reactors, special issue no. 2, 1-14

NOTATION

Q	Discharge ($m^3.s^{-1}$)	ν	kinematic viscosity
Π	Coles parameter	i_0	longitudinal pipe bottom slope
B	integration constant	R	hydraulic radius
H	overall depth (m)	α	angle of transducer with vertical
u_*	friction velocity ($m.s^{-1}$)	v	average vertical point velocity
x,y	Cartesian co-ordinates	U	average sectional velocity
u	average longitudinal point velocity ($m.s^{-1}$)	D	pipe diameter
κ	von Karman constant	C	wave velocity

ULTRASONIC MEASUREMENTS OF INSTANTANEOUS VELOCITY AND SUSPENDED CONCENTRATION IN OPEN-CHANNEL FLOW

Massimo Cellino[1]

[1] Hydraulic Engineer, Bonnard & Gardel Consulting, av. de Cour 61, Lausanne, Switzerland, massimo.cellino@bg-21.com

Keywords: open-channel flow, sediment transport, velocity measurement, concentration measurement, burst cycle

ABSTRACT

The Acoustic Particle Flux Profiler (APFP) was developed and assembled at the Laboratoire de Recherches Hydrauliques (LRH) at the Polytechnic School of Lausanne (EPFL), Switzerland.

This non-intrusive instrument permits to measure simultaneously the instantaneous 2-dimensional velocity and the suspended concentration in experimental suspension flows in open channels.

The 2-dimensional velocity was obtained by measuring the Doppler frequency of the backscattered echo. On the same time, by measuring the back-scattered and forward-scattered echo intensity, the instantaneous suspended concentration was also obtained. For the velocity measurement a calibration was not necessary whereas for the concentration a mean suspended concentration measurement by suction had to be performed.

The visual comparison between the instantaneous velocity and suspended concentration shows a strong correlation. The vertical fluctuating velocity seems to be responsible of both erosion and deposition. To try to quantify this phenomenon, the APFP instrument was applied to the analysis of the mutual influence between suspended sediments and coherent flow structures. These structures were studied by using the 4-quadrant analysis. The measurements were carried out in particle laden, open-channel flows. They clearly show the predominance of the ejection and sweep phases that are part of a burst cycle.

The analysis further demonstrates the importance of the ejection and sweep phases in sediment resuspension and transport. Ejections pick up the sediment at the bed and carry it up through the water column close to the surface. It is shown that while ejections and sweeps are in near equilibrium in the near bottom layer, ejections clearly dominate in the remaining water column. The implications of these results for sediment transport dynamics are discussed.

1. THE APFP INSTRUMENT

The APFP (Acoustic Particle Flux Profiler) instrument was developed at the Hydraulic Laboratory of the Ecole Polytechnique Fédérale de Lausanne (Switzerland) by Dr. U. Lemmin (*Lhermitte* and *Lemmin*, 1994, *Lemmin* and *Rolland*, 1997, *Rolland* and *Lemmin*, 1997), Dr. T. Rolland (*Rolland*, 1994) and W.C. Shen (*Shen*, 1997).

This instrument has been set up to measure simultaneously the velocity and the suspended sediment concentration profiles (see *Shen*, 1997). The transducer below the bed and the tilted transducer measure the instantaneous velocity profiles in the same manner than the classical ultrasonic profiler (for example ADVP, *Rolland*, 1994). To measure the instantaneous

suspended sediment concentration profiles the vertical transducers record alternatively the intensity of the ultrasonic echo coming from the targets in the water columns ensonified. *Shen* and *Lemmin*, 1996, showed that the local sediment concentration is proportional to the intensity of the ultrasonic echo.

2. THE EXPERIMENTS

Experiments were carried out in a highly turbulent subcritical flow. Details of the hydraulic conditions and the sediment characteristics for all three runs are given in Table 1. For the investigations into suspension flow, quartz-like sediment particles were gradually added to the flow until a thin (~3 mm of thickness) layer of sediments, remaining stable during the time of the experiments appeared on the bed of the channel. No bed forms were observed. The thickness of the bed sediment layer was sufficient to ensure particle deposition and resuspension at all times without completely eroding the sediment bed layer. No more sediment was added from this moment onward because the capacity charge equilibrium condition was reached and the bottom roughness elements were completely covered with the sediments. The reference concentration c_{sa} was measured by a suction device under isokinetical conditions at the water depth y/h=0.05.

The instantaneous velocity and concentration profiles measured with the APFP instrument which will be discussed here, have been correlated and conditionally averaged to obtain information about ejection and sweep events. Even though ejection and sweep events are defined in the generation region, $5 < yu_*/\nu < 70$, the same conditional averaging technique will be applied over the whole water depth.

run	sand	Q	h	u_c	U	S_b	$Re*10^5$	u_*
		m^3/s	m	m/s	m/s	%	--	m/s
Q50S01	I	0.057	0.12	0.930	0.792	0.100	2.712	0.039
Q50S01	II	0.058	0.12	0.916	0.801	0.100	2.743	0.039

run	sand	ρ_s	d_{50}	v_{ss}	C_s	c_{sa}
		kg/m^3	mm	mm/s	kg/m^3	kg/m^3
Q50S01	I	2650	0.135	12.0	3.61	39.33
Q50S01	II	2650	0.230	21.0	1.57	21.31

Table 1: Summary of experimental conditions

run: name of the run; sand: name of the sand; Q: flow discharge
B: 0.60 m width; h: flow depth; u_c: maximum velocity
U: depth-averaged velocity; S_b: bed slope
Re: Reynolds number; u_*: shear velocity; ρ_s: sediment density (quartz sand)
d_{50}: nominal particle diameter; v_{ss}: settling velocity
C_s: depth-averaged concentration; c_{sa}: reference concentration at $y= a = 0.05h$

From the parameters given in Table 1, the sediment laden flows are in the lower range of transition flows. A value of $y^+ = 100$ corresponds to $y \approx 2.5\,mm$. Only the lowest points of our measured profiles fall into this range. From *Nakagawa* and *Nezu* (Fig. 8.12; 1993) it is obvious that the roughness effect on the coherent structure dynamics is already diminished above that height. Due to the noise constraints mentioned above, these lowest points have to be interpreted with some caution.

3. VISUAL CORRELATION BETWEEN VELOCITY AND SUSPENDED CONCENTRATION

The APFP instrument measures simultaneously, and continuously, the velocity and the suspended concentration of the flow at the centerline of the measuring section. Interesting observations can already be made by visually comparing the instantaneous profiles of velocity and concentration (Fig. 1). In fact, if these profiles are plotted against time, it becomes possible to observe the temporal evolution of the measured velocity and concentration and particularly their correlation.

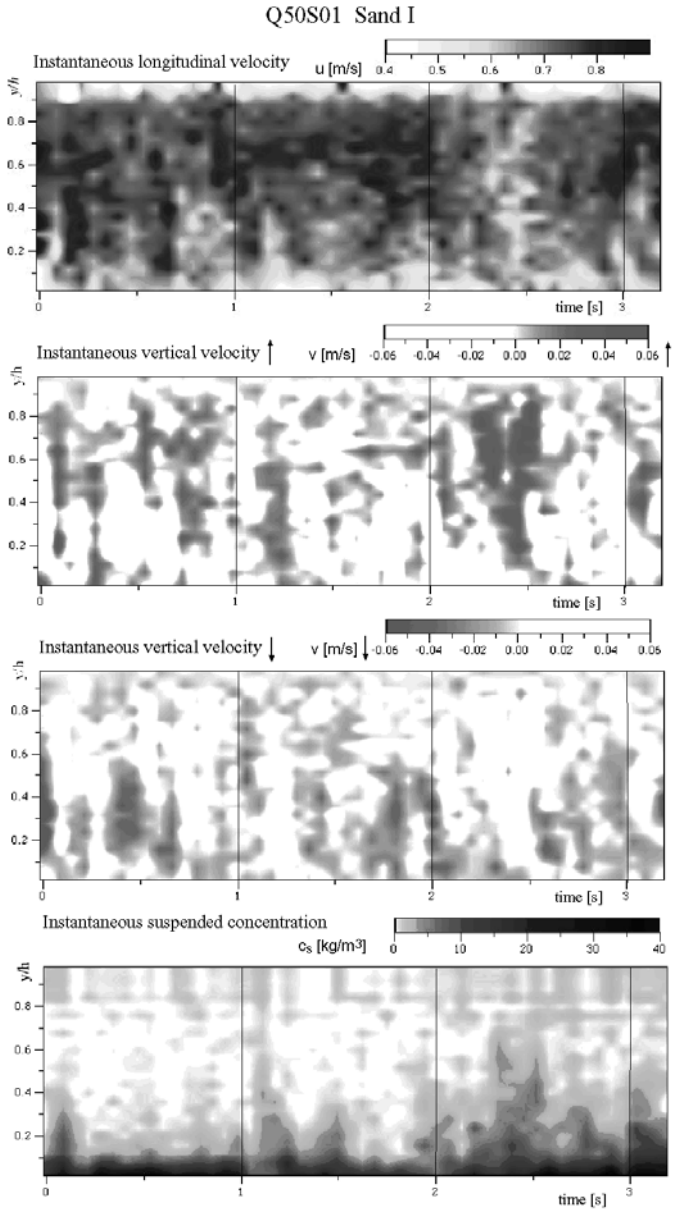

Fig. 1 Instantaneous velocity and concentration profiles

In Fig. 1, an example of the velocity and concentration profiles measured for run Q50S01 (with sand I) is plotted. In order to present sufficient detail, a typical segment measured during three seconds has been presented. Both the longitudinal and vertical velocities are given with the local long-term mean values being subtracted. Note that the flow field is essentially composed of a sequence of correlated high and low longitudinal and vertical velocities showing a certain regularity of the motion of the flow. Superimposed on the

velocity pattern, the simultaneously measured instantaneous suspended concentration is shown.

Close to the bed, y/h<0.2, the high concentration layer is particularly evident. Although this region is thin and always located close to the bed, in certain cases its thickness approaches and temporarily exceeds y/h≈0.3. Several events in Fig. 1 make evident that a sediment "cloud" is generated very close to the bed and is subsequently carried into the outer layer, even up to the surface layer with little change in particle concentration. During these events, the existence of a correlation between the sediment clouds and events of strong instantaneous velocity is already obvious by comparing the two series in this example. Note that the instantaneous velocity vector in these events is always composed of the two components. In the following we will quantify aspects of the statistical correlation between the two signals.

4. RESULTS OF THE 4-QUADRANT ANALYSIS

4.1 FILTRATION OF THE INSTANTANEOUS VELOCITY

The instantaneous (horizontal u, vertical v) as well as the Reynolds stress ($u'v'$) and the sediment flux ($c_s'v'$) have been filtered to compute the contribution coming from each of the four quadrants, (Fig. 2). The filtration has been performed by introducing the discriminating variable, $I_H^i(y,t)$, defined as follows:

$$I_H^i(y,t)=\begin{cases}1, \text{ if } \left[u'(y,t),\ v'(y,t)\right] \text{ is in quadrant i and if } \left|u'(y,t)\cdot v'(y,t)\right| > H\sqrt{\overline{u'^2}}\sqrt{\overline{v'^2}} \\ 0, \text{ otherwise}\end{cases} \quad (1)$$

where H is called the hole size and it is used as a threshold for weakest velocities.

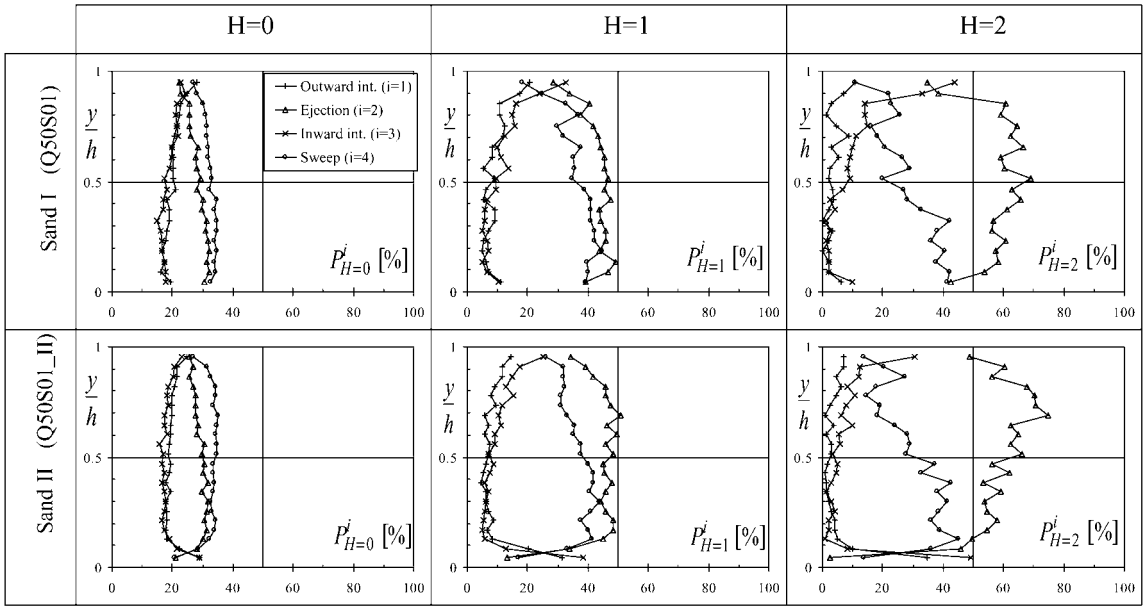

Fig. 2: Event occurrence probability for clear-water and suspension flows (sand I and sand II) for different hole sizes, *H*.

The computation of the occurrence probability of each quadrant has been performed three times by first taking all the events (H=0), and then progressively eliminating the weaker ones (H=1,2) respectively. For H=0, the highest probabilities are found for the sweep events, $P^{i=4}_{H=0}$, followed by the ejection ones, $P^{i=2}_{H=0}$. The other events, namely the outward, $P^{i=1}_{H=0}$, and the

inward, $P_{H=0}^{i=3}$ interactions, have the same but rather small occurrence probability. By increasing the hole size value, H=1, i.e. eliminating the weakest events, the probability of observing an ejection, $P_{H=1}^{i=2}$, increases rapidly, becoming slightly larger than that of the sweep one, $P_{H=1}^{i=4}$.

For H=2, i.e. taking into account only strong events, the ejection occurrence probability dominates the profile and increases towards the surface with a maximum value near the surface. The highest sweep occurrence probability has been detected close to the bed at $y/h \approx 0.1$; at that level, its value is identical to that of the ejection probability but then it decreases rapidly towards the water surface. The probability of observing outward and inward interactions rapidly becomes negligible with increasing the hole-size value.

4.2 FILTRATION OF THE REYNOLDS STRESS

The filtration of the Reynolds-stress profiles, $\overline{u'v'}(y)$, into the four quadrants provides information about the contribution coming from each event. This is particularly interesting because the Reynolds stress is directly related to the beginning of the motion of sediment particles on the bed and their subsequent suspension in the flow. In Fig. 3 the filtered and the unfiltered Reynolds-stress profiles are shown. Again, the contribution to the Reynolds stress coming from the ejection event, $\overline{u'v'}_{H=0}^{i=2}(y)$, is the most important one for both suspension flows. The second most important contribution comes from the sweep event, $\overline{u'v'}_{H=0}^{i=4}(y)$. The outward (i=1) and the inward interaction (i=3) make similar but small negative contributions.

The contribution coming from the ejection event, i=2, is about 80%, while the sweep-event one is about 60% for both suspension flows. *Nakagawa* and *Nezu*, 1977, p. 120, *Nakagawa* and *Nezu*, 1981 and *Lu* and *Willmarth*, 1973, p. 497 obtained similar results investigating the contribution to the Reynolds stress in clear water flows close to the bed. The largest contribution comes from the ejections and sweeps, showing again the importance of these events also in suspension flows. The strong influence of these events on the erosion, deposition and suspension of sediments is confirmed.

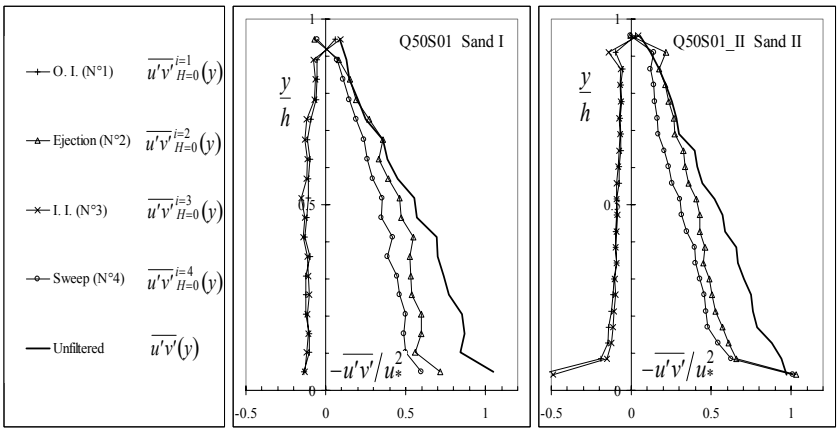

Fig. 3: Filtered Reynolds-stress profiles

4.3 FILTRATION OF THE SEDIMENT FLUX

The sediment flux, $\overline{c_s'v'}$, represents the upward flux of sediment generated by the fluctuating vertical velocity which compensates the downward flux of sediment caused by the gravitational settling, $\overline{c_s} \cdot v_{ss}$, where v_{ss} is the settling velocity. The solution of the equation

obtained by imposing the equilibrium of these two fluxes leads to the Rouse equation expressing the vertical mean concentration distribution.

If the ejection event is the principal contributor to the upward fluctuating velocities and to the Reynolds stress, as was shown by the filtration of velocities, then the sediment flux should also be primarily generated by the ejection event. To verify this hypothesis, the filtration of the sediment flux into the $u'v'$-plane has been performed. In Fig. 4, the filtered and the unfiltered sediment-flux profiles are shown. As expected, the largest contribution to the sediment flux comes from the ejection events, $\overline{c_s'v'}^{i=2}_{H=0}(y)$. The second largest contribution comes from the sweep event, $\overline{c_s'v'}^{i=4}_{H=0}(y)$. In this case the sediment flux is directed towards the bed. The contributions coming from the outward (i=1) and inward (i=3) interactions are once again negligible.

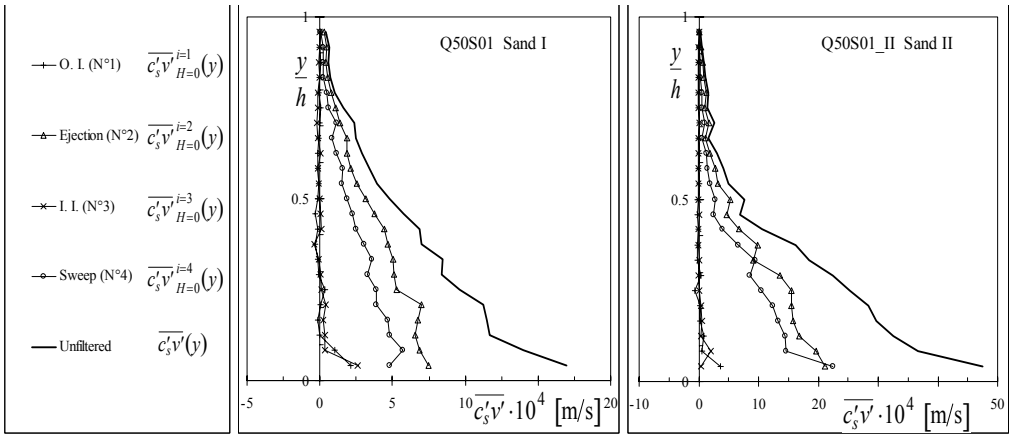

Fig. 4: Filtered sediment-flux profiles

5. CONCLUSIONS

The analysis of this study has been carried out by filtering the instantaneous longitudinal and vertical velocity profiles as well as the suspended concentration profiles according to the well-known four quadrant $u'v'$-plane decomposition.

For all parameters investigated, the ejection events are observed most frequently always followed by the sweep events. The contributions by the remaining two events, namely the outward and the inward interactions are insignificant and can be ignored in the analysis. This discrepancy becomes even more pronounced when the weakest events are filtered out. It is seen that the further one moves up in the water column the more important become strong ejection events. The occurrence probability profiles of each event measured in the two suspension flows are similar. This means that the statistical distribution of the events in the suspension flow is not affected by the size range of the suspended sediments used in the present study. We have also investigated clear water flow under the same hydraulic conditions and found very similar results as for the suspension flows (*Cellino*, 1998). Obviously, the presence of particles in suspension does not alter the dynamics of coherent structures.

For the Reynolds stress, $\overline{u'v'}$, it is evident that the ejection event contributes the most to the unfiltered Reynolds stress. The second most important contribution comes from the sweep event. Thus, the critical Reynolds stress, normally used as a threshold level for the motion of the particles on the bed, could be effectively replaced by an equivalent critical ejection level.

The sediment flux, $\overline{c_s'v'}$, (representing the upward flux of sediment that compensates the downward one, $\overline{c}_s v_{ss}$, due to the gravitational settling), is mainly generated by the ejection

events. The contribution of the sweep events, directed towards the bed and always smaller than the ejection ones, can not be neglected.

Visual inspection of simultaneous time series of the instantaneous velocities and suspended concentration profiles confirms the importance of the ejection and sweep events on the suspended transport mechanics (*Cellino*, 1998). The appearance of sediment clouds in the upper water column, eroded from the bed is always found to be directly correlated to a strong upward vertical fluctuating velocity and a strong ejection event in particular. On the other hand, these sediment clouds disappear in the presence of a vertical downward fluctuating velocity or a sweep event.

In summary, our analysis has clearly shown that the burst cycle plays an important role in sediment suspension mechanics. In particular, the ejection event represents the main cause for the erosion and/or the suspension of particles, whereas the sweep event can be associated with the sediment deposition.

ACKNOWLEDGMENTS

This research was funded by the Swiss National Science Foundation grant 20-39495.93. We are grateful for the support.

REFERENCES

Cellino, M. (1998). *Experimental Study of Suspension Flow in Open Channel*, Doctoral dissertation No. 1824, Ecole Polytechnique Fédérale, Lausanne, Suisse.

Lemmin, U. and **Rolland, T.** (1997). *Acoustic Velocity Profiler for Laboratory and Field Studies*, J. Hydr. Engr., vol. 123, N°. 12.

Lhermitte, R. and **Lemmin, U.** (1994). *Open-Channel Flow and Turbulence Measurements by High-Resolution Doppler Sonar*, J. Atm. Oceanic Tech., vol. 11, N°5, pp. 1295-1308.

Lu, S. S. and **Willmarth, W. W.** (1973). *Measurements of the structure of the Reynolds stress in a turbulent boundary layer*, J. Fluid Mech., vol. 60, part 3, pp. 481-511.

Nakagawa, H. and **Nezu, I.** (1977). *Prediction of the contributions to the Reynolds stress from bursting events in open-channel flows*, J. Fluid Mech., vol. 80, part 1, pp. 99-128.

Nakagawa, H. and **Nezu, I.** (1981). *Structure of space-time correlations of bursting phenomena in an open-channel flow*, J. Fluid Mech., vol. 104, pp. 1-43.

Nakagawa, H. and **Nezu, I.** (1993). *Turbulence in open-channel flows*, IAHR Monograph. A.A. Balkema, Rotterdam, the Netherlands.

Rolland, T. (1994). *Developpement d'une instrumentation Doppler ultrasonore adaptée a l'étude hydraulique de la turbulence dans les canaux*, These de doctorat N° 1281, Ecole Polytechnique Fédérale, Lausanne.

Rolland, T. and **Lemmin, U.** (1997). *A two-component acoustic velocity profiles for use in turbulent open-channel flow*. J. Hydr. Res., vol. 35, N°4.

Shen, C. (1997). *An acoustic instantaneous particle flux profiler for turbulent flow*, These de doctorat N°1630, Ecole Polytechnique Fédérale, Lausanne

Shen, W. and **Lemmin, U.** (1996). "Ultrasonic measurements of suspended sediments. A concentration profiling system with attenuation compensation." Meas. Sci. Tech., vol. 7, pp. 1191-1194.

ULTRASONIC VELOCITY PROFILE MEASUREMENTS IN PIPES AND FLUMES IN A HYDRAULIC LABORATORY

Helmut Knoblauch, Roman Klasinc, Thomas Geisler, Stefanie Breitenstein

Department for Hydraulic Structures and Water Resources Management
Graz University of Technology, Stremayrgasse 10, A-8010 Graz, AUSTRIA, Europe
helmut.knoblauch@TUGraz.at

Keywords: ultrasonic tests, hydraulic model tests, pipes, flume

ABSTRACT

At the Hydraulic Laboratory Graz, Austria, an UVP-Monitor was used to measure flow velocities in pipes and flumes. Moreover the same device was used for measuring the surface level in a flume. Velocity profile measurement was successfully conducted on a physical model of a multi-pipe inverted siphon with three Plexiglas pipes ranging from 62 mm to 246 mm in diameter. Turbulent flow within the pipes was studied under non-intrusive conditions by installing the ultrasonic transducer on the pipe wall. The velocity profiles were obtained by moving the transducer around the pipe to four angles (0°, 45°, 90°, 135°). Measurements in a flume included simultaneous measurement of velocity profiles and fluid surface profiles for wavy flows. These experiments were performed in a horizontal glass channel. The transducer was inserted from above the test section into the medium facing the direction of flow. The transducer axis was placed at various angles to the surface of the water. In the same horizontal channel, water level measurement for wavy flow was performed.

1. TESTS ON PIPE FLOW

1.1 Model stand

The investigation of pipe flow was performed on the test model of an inverted siphon. The model included the inlet and outlet structures, three pressure conduits of various diameters, and adjacent headwater and tailwater areas, as shown in Figure 1.

Figure 1: Test pipes, numbered 1 to 3. Overview (left) and close-up of elbows (right).

The pipes were manufactured from Plexiglas with internal diameters of d_1=62, d_2=172 and d_3=246 mm. The flow conditions were investigated at various discharges to measure velocity profiles at different flows. Table 1 lists the expected flow rates and average velocities for the discharges that were tested. The numbers in the table below are based on the assumed flow distribution among the three pipes.

Pipe 1		Pipe 2		Pipe 3	
Flow [l/s]	Velocity [m/s]	Flow [l/s]	Velocity [m/s]	Flow [l/s]	Velocity [m/s]
1.0 - 1.5	0.35 - 0.51	3.0 - 15.0	0.13 - 0.66	5.0 - 34.0	0.11 - 0.75

Table 1: Expected flow rates and average velocities in the inverted siphon pipes

1.2 Measurement Planes

The flow inside the pipes was investigated by placing the ultrasonic transducer on the pipe wall at an incident angle of 10° from the normal, as shown in Figure 2. Each of the test sections was then divided into four measurement planes, which were evenly distributed over the circumference of the pipe wall.

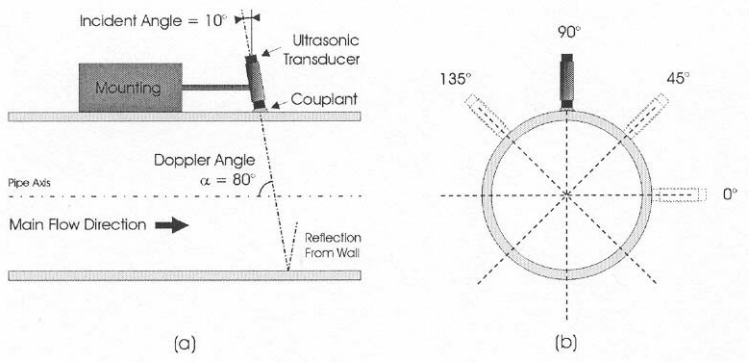

Figure 2: (a) Positioning of the transducer and (b) measurement planes as viewed in the direction of flow

Four measurement planes were used so that the true direction of the velocity vector at one spatial point could be reconstructed. To obtain a suitable amount of profile data, seven test sections on each pipe were investigated. The positions of the test sections along the pipes are shown in Figure 3Figure . The main unit UVP-Monitor (supplied by Met Flow, Lausanne) was operated with a 4-MHz transducer.

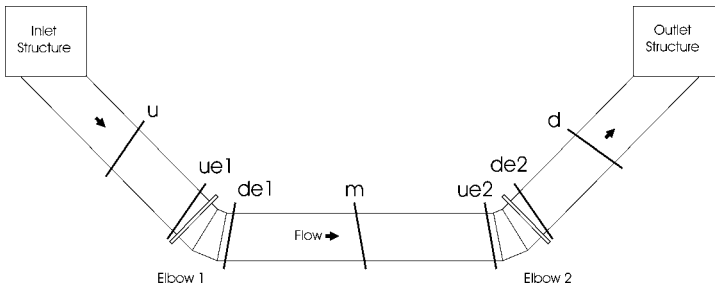

Figure 3: Position of test sections along the pressure pipes of the inverted siphon.

2. RESULTS PIPE FLOW

To give a representation of the obtained results, two measurement sections will be analyzed in more detail. While the first sample deals with measurement at a straight pipe, the second sample covers the measurement that was conducted downstream from a pipe elbow.

2.1 Results straight pipe

The first section to be examined is section **m** on pipe 1 (Figure3), which is right in the **m**iddle of the two elbows. Although the pipe diameter is quite small (d_1=62 mm), decent velocity profiles were obtained because of the excellent spatial resolution of the 4-MHz transducer. Figure 4 displays a typical velocity profile measured at this section. The mean time velocities (dots) and the standard deviation (vertical lines) are shown. This plot displays the velocity component along the line of measurement.

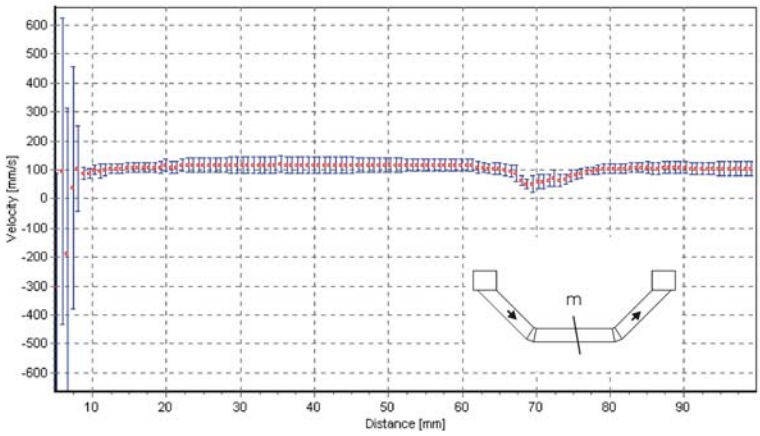

Figure 1: Sample velocity profile obtained at section m on pipe 1 showing undistorted turbulent flow.

The profile in Figure 4 indicates the characteristic velocity distribution for turbulent flow. Outside the near wall boundary layer the fluid moves with the full velocity and may be considered to be practically unaffected by the reduction of velocity close to the pipe walls. The velocity gradient is highest at the pipe wall and becomes progressively smaller with increasing distance from the wall.

The decrease of flow velocity in the range of about 70 mm indicates the position of the back wall of the pipe. Beyond this distance, a mirror image of the velocity profile appears. This imaginary profile is caused by ultrasound reflection at the back wall.

2.2 Results bent pipe

This case is expected to happen **d**ownstream from the **e**lbows, because the flow becomes separated from the inward bend of the pipe. Hence the second test section to be analyzed is section **de2** on pipe 3 (d_3=246 mm). Figure 5 shows a sample profile that was obtained in the vertical measurement plane of this section. Again, the mean time velocities and the standard deviation are shown. In contrast to the previous sample, the flow can neither be considered axially symmetric with respect to the pipe centerline, nor is the highest velocity found in the middle of the stream.

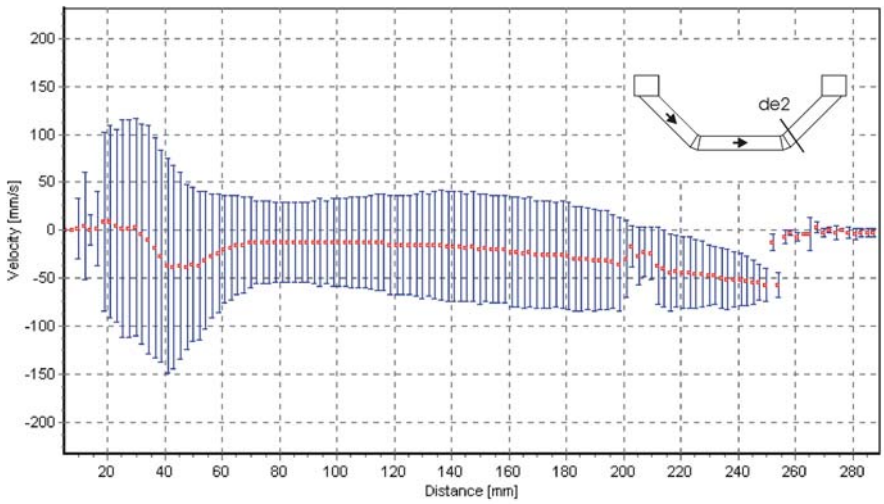

Figure 5: Sample velocity profile obtained at section de 2 on pipe 3

As flow moves through the elbow, it accelerates around the outside of the bend and slows down near the inside of the bend. The profile is distorted with a high velocity zone occurring near the outside of the bend, as shown in Figure 6.

The Doppler angle α varies along the line of measurement due to the converging geometry of the streamlines. In the middle of the stream, flow particles typically travel perpendicular to the measurement line and fail to generate significant frequency shifts. During measurement, however, the flow direction varied so as to generate either a positive or a negative frequency shift, as indicated by the standard deviation in Figure 5.

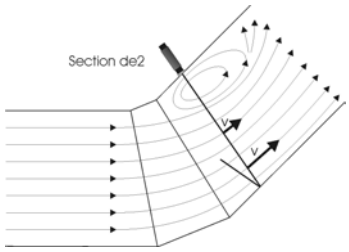

Figure 6: Flow pattern at the elbow showing strong eddies at the inward bend

The velocity is found to be affected by the elbow located upstream from the test section. Flow leaving the elbow is distorted and returns to an undistorted velocity profile after a certain pipe length (6 to 10 times the pipe diameter *d*). If the test section is located within that zone, the computation of the flow rate is likely to be incorrect.

3. STUDY OF OPEN CHANNEL FLOW

3.1 Test stand

The experiments were performed in a horizontal channel about 10 m long, 30 cm wide, and 80 cm high. The bottom of the channel was made from steel, while the sides were manufactured from glass. Water from the overhead reservoir of the laboratory entered the channel through the pipe system. The inflow was adjusted by a control valve, while the depth of the water was varied using a slide gate at the downstream end of the channel.

3.2 Measurement of Velocity Profiles

Our structure produced waves with a small amplitude at the downstream end of the channel where the test section was positioned. The transducer was inserted from above the surface of the water facing the direction of flow, as shown in Figure 7. The axis of the transducer was placed at two different angles to the surface to test the effect of angle variation. In order to validate the obtained velocity profiles, a Höntzsch current meter with a four-vane propeller of 18-mm diameter was used as well. The UVP-Monitor model XW-3-PSi was operated with the same 4-MHz transducer as in the pipe flow experiments.

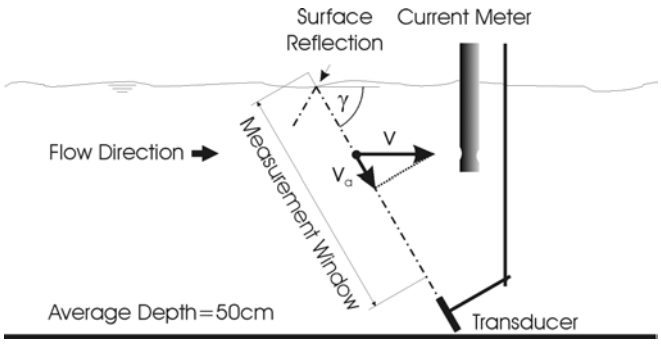

Figure 7: Experimental setup for velocity profile measurements in wavy flow.

The diagram in Figure 8 compares the velocity profiles obtained by the UVP-Monitor with the measurements made by the current meter. The time-averaged velocity profiles were smoothed using a floating average computation. For the most part, the velocity profiles are found to be in good agreement with the samples from the current meter. However, the closer the measurements are to the bottom of the channel, the less the data corresponds, which is caused by disturbances in flow near the ultrasonic transducer.

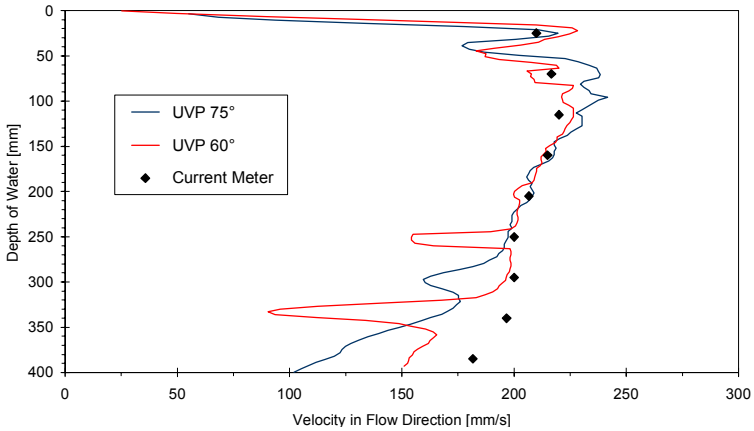

Figure 8: Velocity profiles obtained by UVP-Monitor and current meter.

3.3 Surface Level Measurement

Consideration was given to ways of measuring surface levels with the instrumentation originally designed for velocity profile measurement. For this purpose, separate test runs were conducted to find the most favourable setup for the measurement of surface levels. The largest part of the measurements were made with the 4-MHz transducer, but a 2-MHz transducer was

used as well. The axis of the transducer was placed at three different angles to the surface of the water. The surface level was simultaneously measured by an electrical conductivity method using a pair of parallel wire electrodes (FAFNIR). The results for an angle of 90° to the surface (4 MHz) are displayed in Figure 9.

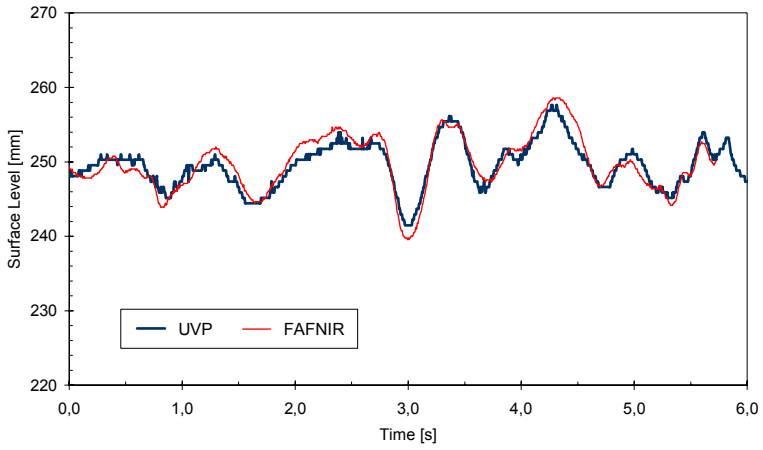

Figure 9: Comparative diagram showing the UVP plot and the output of the FAFNIR probe

4. CONCLUSIONS

Concerning pipe flow the velocity is found to be affected by the elbow located upstream from the test section. Flow leaving the elbow is distorted and returns to an undistorted velocity profile after a certain pipe length (6 to 10 times the pipe diameter *d*). If the test section is located within that zone, the computation of the flow rate is likely to be incorrect.

Additionally free-surface flow in a glass-walled channel was investigated. The instrument performed measurements of both flow velocity and surface level. The data from the identification process was compared to an electrical conductivity method for the measurement of surface level, showing good agreement if the transducer axis is placed perpendicular to the flow direction. Other measurement angles were tested as well, but the identification of the surface level was found to be less precise.

REFERENCES

AMERICAN SOCIETY OF NONDESTRUCTIVE TESTING (1991) *Nondestructive Testing Handbook, Volume 7: Ultrasonic Testing*. Second edition, ASNT, Columbus (USA) www.asnt.org

MASSEY, B. S. (1989) *Mechanics of Fluids*. Sixth edition, Chapman & Hall, London

MET-FLOW (2000) *User's Guide Model UVP-XW*. Second edition, Met-Flow SA, Lausanne. www.met-flow.com

NAKAMURA, H., KONDO, M. and KUKITA, Y. (1996) Simultaneous measurement of liquid velocity and interface profiles of horizontal duct wavy flow by ultrasonic velocity profile meter. *Proceedings of the First International Symposium on Ultrasonic Doppler Methods for Fluid Mechanics and Fluid Engineering (ISUD)*. Paul Scherrer Institute, Villigen (CH)

PANAMETRICS (2001) *Ultrasonic Transducers*. Panametrics Inc., NDT Division, Waltham

VELOCITY AND TURBULENCE MEASUREMENTS IN A SCOUR HOLE USING AN ACOUSTIC DOPPLER VELOCITY PROFILER

Adhy Kurniawan[1] and Mustafa S. Altinakar[2]

[1] Environmental Hyd. Lab., ENAC–EPFL 1015 Lausanne, Switzerland, e-mail: adhy.kurniawan@epfl.ch
[2] Environmental Hyd. Lab., ENAC–EPFL 1015 Lausanne, Switzerland, e-mail: mustafa.altinakar@epfl.ch

Keywords: jet, scour, acoustic measurement, velocity profile, turbulence, signal processing

ABSTRACT

The detailed structure of the 3-D flow (mean velocity, turbulence, and Reynolds stress components) in a scour hole formed by a plane jet is measured using a high resolution Acoustic Doppler Velocity Profiler (ADVP), which can simultaneously measure the profiles of quasi-instantaneous velocity components. The use of pulse-to-pulse coherent technique provides high spatial (O(6mm)), temporal (O(30Hz)) and velocity (O(1mms^{-1})) resolutions. The measurements reveal the importance of the apron on the behaviour of the jet and the structure of the flow. The proper orthogonal decomposition (POD) method is used to extract dynamically significant information on the large-scale coherent structures.

1. INTRODUCTION

The understanding of the scouring process of the sediment bed by a horizontal jet is important in the design of the foundations of hydraulics structures. Until very recently, the researchers were only interested in the parameterization of the equilibrium scour hole geometry (maximum scour depth, deposition height, length of the scour hole, etc.). A review of these studies can be found in Karim and Ali (2000). Recently, researchers have shown interest in the 3D flow pattern within the scour hole. Ali and Lim (1986) and Liriano and Day (2000) have carried out point-velocity measurements using a commercial Acoustic Doppler Velocimeter.

The present study is a part of a PhD thesis project on the experimental investigation of the interaction between flow and mobile sediment bed. The aim of the study being an understanding of the relationship between the flow structure and the scour-hole geometry, the profiles of the three components of the instantaneous velocity vector were measured in an equilibrium scour hole downstream of a plane turbulent horizontal jet. The mean velocity field, and the turbulence characteristics were then evaluated from these measurements. The Proper Orthogonal Decomposition (POD) method was used to investigate the spatiotemporal properties of the velocity field in order to extract information on coherent structures.

2. EXPERIMENTAL SETUP AND ADVP INSTRUMENT

The scouring experiments were carried out in a 17m-long tilting flume with a 0.8m-high and 0.5m-wide rectangular cross section (Fig.1). The raised false floors were built at the upstream and downstream ends of the flume. The 5m-long and 0.30m-deep mobile-bed test reach created in the middle part of the flume was filled with sand having a uniform diameter of 2mm. A submerged plane jet, with or without an apron, was created by passing a constant discharge under a dismountable sluice gate placed on the fixed bed upstream of the test reach.

The equilibrium scour hole was obtained by a continuous operation of the submerged jet under clear-water scour condition during a period of 5 to 6 days approximately. The scour-

hole evolution was recorded using a digital video camera. After reaching the equilibrium scour depth, the flow was stopped and the scoured sand bed was fixed by spraying a glue.

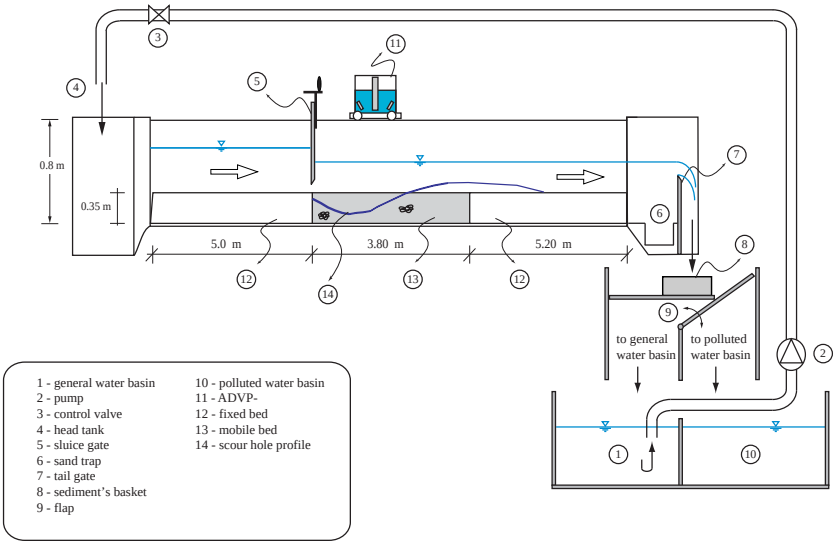

Figure 1. General view of the experimental setup

Flow measurements in the fixed scour hole were then made using both an Acoustic Doppler Velocimeter (ADV) and an Acoustic Doppler Velocity Profiler (ADVP) for the discharge used for creating the scour hole. The hydraulics parameters for the two experiments illustrating the findings of the present study are listed Table 1 (see Kurniawan et al., 2001).

Table 1. Hydraulic parameters of the experiment

Test	Q [m^3/s]	L_a [cm]	h_v [cm]	U_o [m/s]	Fr_o [-]	h_1 [cm]	h_2 [cm]	d_{50} [mm]	Fr_d [-]	d_s [cm]	L_s [cm]
B	0.015	0	5.0	0.846	1.21	25.85	22.2	2.0	4.70	16.8	62.5
C	0.015	10	5.0	0.843	1.20	25.80	22.2	2.0	4.69	13.1	56.6

The ADVP conceived and developed at LRH (Lhermitte and Lemmin, 1994) measures the instantaneous velocity vector at a number of layers within the water column. This instrument has been successfully used to measure the velocity distributions, turbulence characteristics and coherent structures in various free surface flows (Song et al, 1994; Hurther et al., 1996; Yulistiyanto, 1997; Istiarto, 2001; Blanckaert, 2002).

The tristatic configuration of ADVP, used in the present study, consists of one emitter, T_3, and four plane receivers, T_1^-, T_1^+, T_2^-, T_2^+, which are placed symmetrically around the emitter (Fig. 2). This configuration is placed in a water-filled housing covered by a mylar film at the bottom. Mounted on a carriage, the instrument is positioned at the desired location along the flume with the Mylar bottom barely touching the water surface.

The three dimensional instantaneous velocity, is measured by the ADVP as a pair of two-dimensional instantaneous velocities, $\vec{\hat{V}}_1(\hat{u}_1,\hat{w}_1)$ and $\vec{\hat{V}}_2(\hat{u}_2,\hat{w}_2)$. Both velocities are identified by their components along the longitudinal direction, $\hat{u}_1$ or $\hat{u}_2$ and along the vertical direction, $\hat{w}_1$ or $\hat{w}_2$ of the respective plane. Using geometrical relationships, these are combined to give the target velocity, $\vec{\hat{V}}(\hat{u},\hat{v},\hat{w})$. Details can be found in Rolland (1994).

The instantaneous velocity profile was obtained by recording successively the back-scattered signals according to a fixed time interval (time gate), ΔT_{gate} , corresponding to different layers

within the water column. This ΔT_{gate} defines the thickness of the measuring volume, Δd, to be calculated from the relation $\Delta d = \Delta T_{gate} \cdot c_s/2$, where ΔT_{gate}=8 [μs] is the time gate and c_s=1486 [m/s] the sound speed in water. In the present experiment, the pulse-repetition frequency (PRF) was done at 1000 [Hz]. A value of number of pulse-pairs (NPP) of 32 is used, resulting in a measuring frequency, f_v, of 31.25 [Hz]. The measurement duration for individual profiles was 60[sec]-180[sec]. Due to the size of the housing, the measurements were started at x = 20 [cm] from the sluice gate. The profiles were measured at every 2 [cm] up to x = 200 [cm].

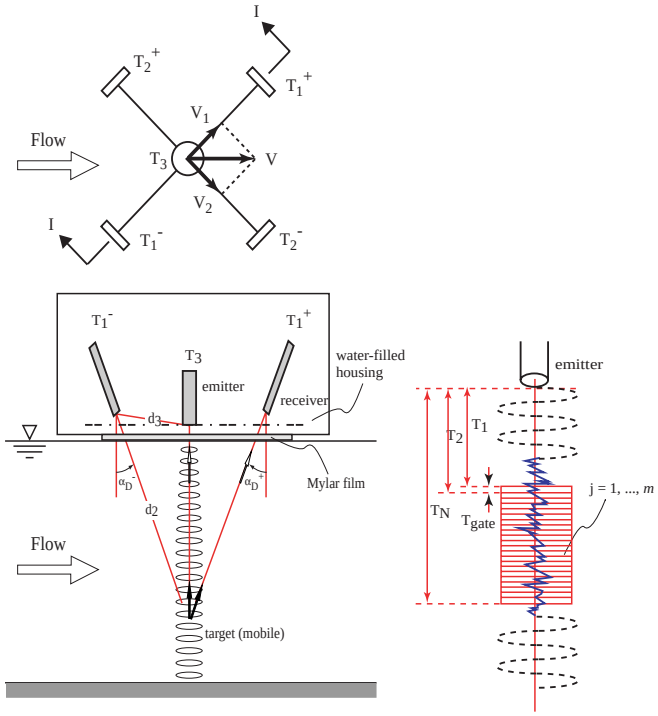

Figure 2. The configuration of *tristatic* mode

3. RESULTS AND DISCUSSIONS

Only the results for the runs listed in Table 1 are presented in this paper. Note that, the velocity data for $x/h_v < 4$ were obtained from ADV-Nortek instrument and they are not included in POD analysis. The ADVP measurements cover the region $x/h_v \geq 4$.

3.1 Velocity Distributions

Fig. 3 shows the distribution of the magnitude of the 2D mean velocity for the tests B and C. For the Test B, without apron, the measurements show that the flow issues from the sluice gate as a plane, turbulent free-jet and impinges on the bed at about x = 40 [cm]. Downstream of the impingement point the main flow continues as a plane, turbulent wall-jet. These results are in good agreement with those of Ali and Neyshaboury (1991) and Liriano and Day (2000). For the Test C, with apron, however, the jet is deflected towards the surface and there is no impingement on the bed. Rajaratnam and Berry (1977) makes a similar observation.

3.2 Reynolds Stresses Distributions

The Reynolds stress, $\tau_{zx} = -\rho\overline{u'\,w'}$, is readily calculated from the measured u(z,t) and w(z,t) data. The Fig. 4 shows the spatial distribution of the Reynolds stress, normalized with ρU_o^2, on the vertical central plane, for the Tests B and C. Qualitatively these distributions compare quite well with the data reported by Rajaratnam (1976). The maximum Reynolds stress is

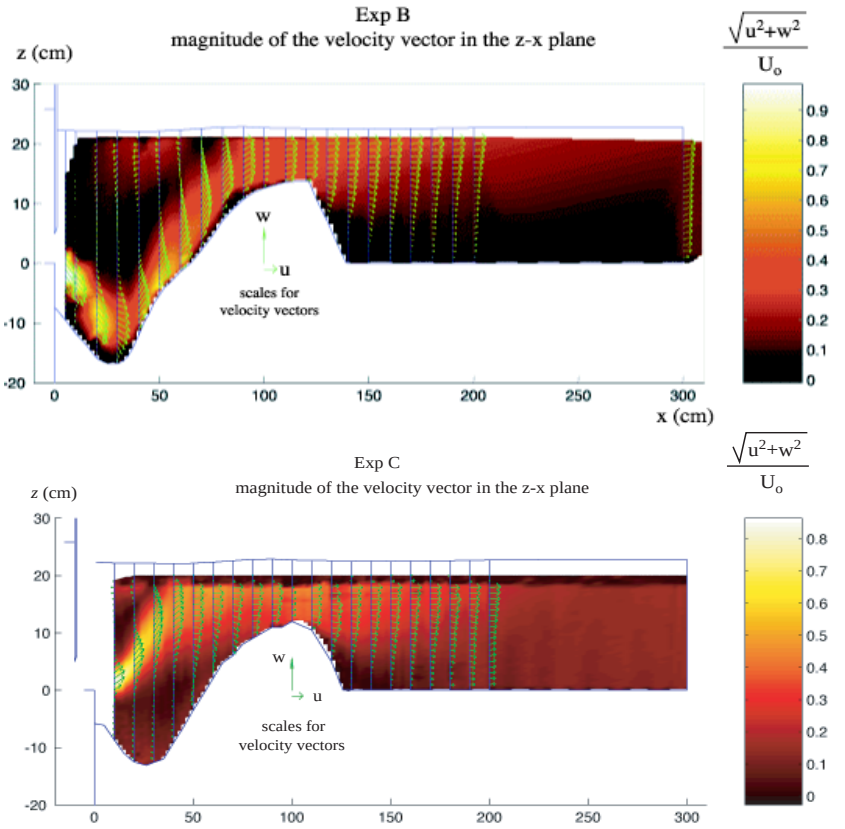

Figure 3. Magnitude of velocity vector in the *z-x* plane

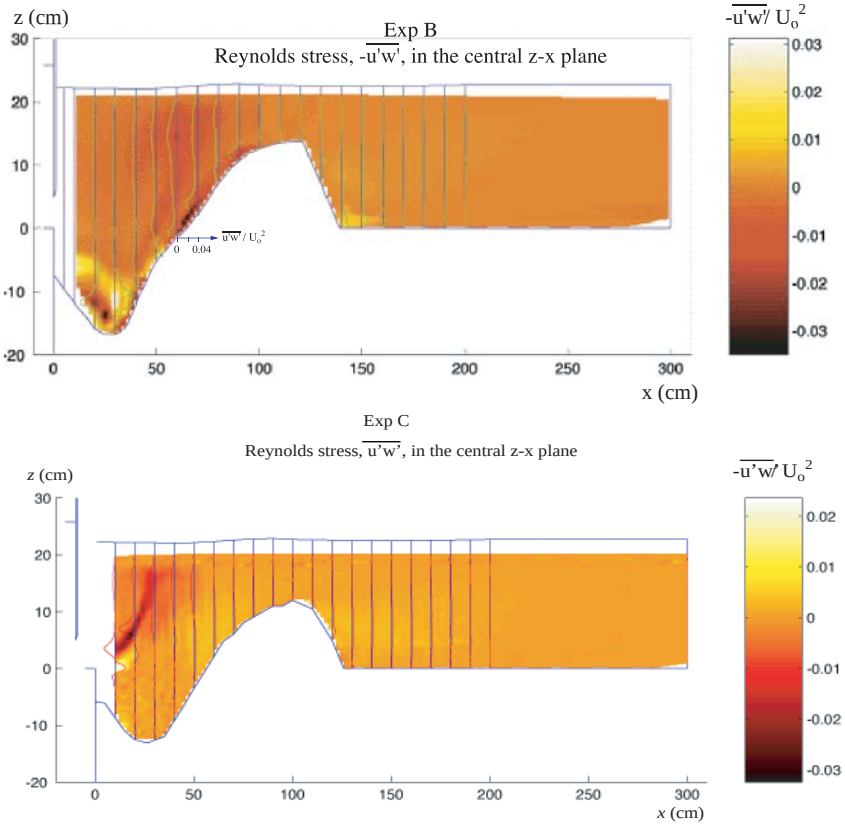

Figure 4. Magnitude of Reynolds stress in the *z-x* plane

usually situated at the line of maximum velocity. In the vicinity of the bed the Reynolds stress is vanishing considerably, implying the incapacity of transporting sediments for the equilibrium scour-hole situation. The negative Reynolds stresses are observed in the upper part of the scour hole where the velocity gradient is negative.

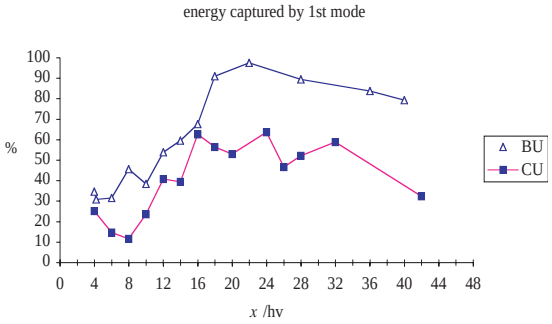

Figure 5. Energy captured by 1st POD mode

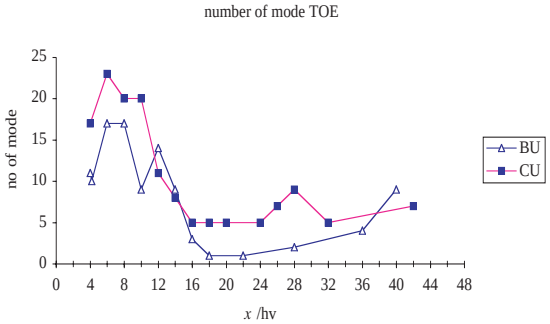

Figure 6. Number of POD modes which catch at least 90% of total energy

3.3 POD analysis and coherent structures

Consider a velocity measurement with ADVP on a vertical. The N instantaneous u-velocity measurements from *m* gates along the vertical are stored in the N×*m* matrix A. The singular value decomposition (SVD) is applied to calculate the eigenvalues (singular values), λ_k , of this matrix A. If $\phi_k(z)$'s are the spatial eigenfunctions or modes corresponding to the eigenvalues λ_k, according to the POD method, the spatiotemporal velocity data can be decomposed as follows (Holmes, et al., 1996)

$$u(z,t) \approx \sum_{k=1}^{m} a_k(t)\, \phi_k(z) \qquad (1)$$

where *a*'s are temporal coefficients and *z* is the spatial coordinate along the vertical. Each mode makes an independent contribution to the total flow energy. The total energy captured in the POD decomposition (sum of all the eigenvalues), *E*, and the relative energy captured by the *k*th mode, E_k, is defined as

$$E = \sum_{k=1}^{m} \lambda_k \quad ; \quad E_k = \lambda_k / \sum_{k=1}^{m} \lambda_k = \lambda_k / E \qquad (2)$$

In Fig. 5, the amount of energy captured by the first mode (the most energetic mode) is plotted against dimensionless distance x/h_v for the tests B and C. In both tests, for the region $x/h_v < 17$ the energy captured by the first mode is relatively low; meaning that a lot of modes are involved in the dynamics of this region. For $x/h_v > 17$ the first mode captures considerably more energy. The number of modes required to capture 90% of the total energy are plotted in Figure 6 as a function of x/h_v. The results presented in Figures 5 and 6 are relatively in good agreement with the values reported by Caraballo, et al. (2001) for a circular jet flow.

It is interesting to note that the reconstruction the flow field using the first POD mode at x/h_v=6, shows the presence of large scale coherent structures indicating a pulsation of the jet. These may correspond to periodic rotational structures (see Faghani, 1997).

4. CONCLUSIONS

A tristatic ADVP was used to measure the 3D velocity field in an equilibrium scour hole created by a horizontal, plane turbulent jet issuing under a sluice gate. The tests were carried out for the cases with and without apron using the same tail-water depth. The measured velocity fields show important differences. In the case with the apron, the jet is deflected towards the free surface whereas the jet without apron flows downwards and impinges on the bed at x/h_v=8 approximately. It then continues as a wall-jet. Although not given here, the resulting equilibrium scour hole geometries for these two cases are also quite different.

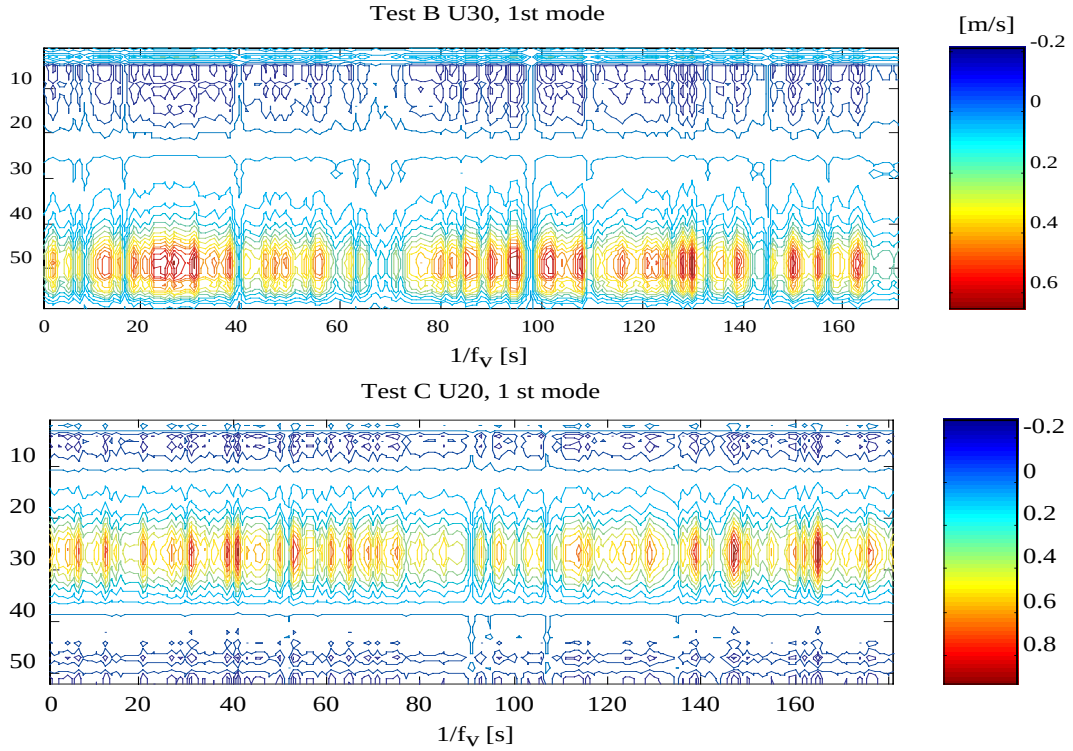

Figure 10. Contour of longitudinal velocity using the first POD mode at *x*/hv=6

The spatiotemporal signals obtained with ADVP were analysed using the POD technique. The results show that a large number of modes are needed to capture the flow dynamics in the near field. The reconstruction of the velocity measurements at x/h_v=6 using only the first mode shows the presence of periodically released rotational structures.

REFERENCES

Ali, K.H.M. and Lim, S.Y. (1986), *Local Scour Caused by Submerged Wall Jets*, Proc., Instn. Civil Engineers, Part 2, 81, pp. 607-645

Ali, K.H.M. and Neyshaboury A.A.S. (1991), *Localized Scour Downstream of a Deeply Submerged Horizontal Jet*, Proc., Instn. Civil Engineers, Part 2, 91, pp. 1-18

Blanckaert, K. (2002), *Flow and turbulence in sharp open-channel bends*, Doctoral Dissertation, No. 2545, EPFL, Lausanne, Switzerland

Caraballo, E. , Samimy, M., Narayanan, S., DeBonis, J. and Scott, J. (2001), *Application of Proper Orthogonal Decomposition to a High Speed Axisymmetric Jet*, 31st Fluid Dynamics Conference, Anaheim CA

Faghani, D., (1997), *Etude des structures tourbillonnaires de la zone proche d'un jet plan : approche non stationnaire multidimensionnelle*, thèse, INP Toulouse

Holmes, Lumley and Berkooz (1996), *Turbulence, Coherent Structures, Dynamical Systems and Symmetry*, Cambridge University Press

Hurther, D., Lemmin, U., and Arditi, M. (1996), *Using an annular curved array tranducer for bistatic ADVP application*, Rapport Annuel, Laboratoire de Recherches hydrauliques, EPFL, B.201.1-B.201.19

Istiarto, I. (2001), *Flow around a cylinder in a scour channel bed*, Doctoral Dissertation, No. 2368, EPFL, Lausanne, Switzerland

Karim, O.A. and Ali, K.H.M. (2000), *Prediction of Flow Patterns in Local Scour Holes caused by Turbulent Water Jets*, J. of Hydr. Research, Vol.38 pp.279-287

Kurniawan, A., Altinakar, M.S. and Graf, W.H. (2001), *Flow Pattern of an Eroding Jet*, Proc. of XXIX IAHR Congress, pp. 537-544, Beijing, China

Lhermitte, R., and Lemmin, U. (1994), *Open-Channel flow and Turbulent measurement by high-resolution Doppler sonar*, J. Atm. Ocean. Tech., 11, 1295-1308

Liriano, S.L. and Day, R.A (2000), *Structure of Turbulent Flow in Scour Holes Downstream of Submerged Jets*, in *Stochastic Hydraulics*, Wang and Hu (eds), Balkema, Rotterdam.

Rajaratnam, N. (1976), *Turbulent Jets*, Elsevier Scientific Publ. Company, Amsterdam, NL

Rajaratnam, N. and Berry, B. (1977), *Erosion by Circular Turbulent Wall Jets*, J. of Hydr. Research, IAHR, Vol.15, pp. 277-289

Rolland, T. (1994), *Developpment d'une instrumentation Doppler ultrasonore adaptée à l'étude hydraulique de la turbulence dans les canaux*, Doctoral Dissertation, No. 1281, EPFL, Lausanne, Switzerland

Song, T., Graf, W.H., and Lemmin, U. (1994), *Uniform flow in open channels with movable gravel bed*, IAHR, J. Hydr. Res., 32(6), pp. 861-876

Yulistiyanto, B. (1997), *Flow around a cylinder installed in a fixed-bed open channel*, Doctoral Dissertation, No. 1631, EPFL, Lausanne, Switzerland

NOTATION

Fr_o = Froude number (-)
Fr_d = densimetric Froude number (-)
L_a = apron length (cm)
L_s = scour length (cm)
PRF = frequency of the pulse emission (Hz)
Q = discharge (m^3/s)
T_1^-, T_1^+, T_2^-, T_2^+, T_3 = ADVP transducer
U_o = initial jet velocity (m/s)
d_{50} = mean diameter of the sediment (mm)
d_s = maximum scour depth (cm)
h_V = sluice gate opening (cm)
u, v, w = time average of longitudinal, transversal and vertical velocity components (m/s)
$\hat{u}$, $\hat{v}$, $\hat{w}$ = instantaneous velocity components (m/s)

ELBE RIVER MODEL: UVP FLOW MAPPING

Vojtech Bares[1] and Prof. Vojtech Broza[2]

[1] Doctorand, Czech Technical University in Prague, Faculty of Civil Engineering, Laboratory of Ecological Risks in Urban Drainage, bares@lermo.cz

[2] Professor, Czech Technical University in Prague, Faculty of Civil Engineering, Department of Hydraulic Engineering and Hydraulic Structures, milecova@fsv.cvut.cz

Keywords: open channel flow, velocity distribution, flow measurements, hydraulic structures, flow simulation

ABSTRACT

The aim of the study was to appreciate the navigation conditions at the planed Elbe river water work Prelouc. For the flow field investigation the physical and mathematical modeling methods were used. The main important role in the physical modeling of navigation conditions in hydraulic models plays the flow field determination, especially in water way branch areas and moreover in significant water intakes. The criteria for navigation safety reviewing are mostly the vertical velocity components to the to the crafts movement direction, determined in the range of 0.15-0.4 $m.s^{-1}$, which in hydraulic model scale correspond to values in order of 10^{-2} $m.s^{-1}$. Moreover, for accurate measurement of the velocity components the ultrasonic Doppler method was used. Furthermore, the physical modeling results were used for the mathematical model calibration and verification.

1. INTRODUCTION

Elbe river navigable length in Czech Republic is 230km. Also it is a natural connection to the European waterways net.

Recently the attention is focused on navigation conditions improvement and moreover on the waterways modernization. The manful reality is, that the Elbe water way consists mostly from low dams cascade, which independently on river flow provide requisite water level, excluded the lower rich of the river (more than 30km) by the Czech – German border. Furthermore, at some water structures, built 60 years ago, the adjustments are needed.

The attention of the office for development water ways (The water ways directorate) mostly focused on above mentioned problems. Besides projecting works in the lower rich of the river (Strekov - Czech – German border), the navigation conditions improvement of the upper rich (Pardubicko) is arranging. Therefore the new navigation step realization is prepared. It consists in use of gated weir (included the head water section), with the new navigation channel (length 3.2km) in right side line.

The total slope 8.5m is at the end part of the channel overcoming by two lock chambers. The water energy should be used in water power plant with total discharge of 75 $m^3.s^{-1}$.

The conception method of solution was influenced by environmental and/or culture – historical points of view. Since the original weir with the water power plant from 1928 is an architectonical memory, and moreover in the neighborhood of the planned water structure are ecologically protected areas, the solution with the right side line is taken as a compromise. In

the frame of the proposed conception the most sensitive localities from the navigation conditions view are:

A the right side channel branch from dam reservoir,

B the channel section upstream the lock chambers with the water power plant inlet

C the section downstream the navigation chambers influenced by outlet from water power plant

D the navigation channel and Elbe river junction.

2. METHODS

For the navigation conditions in above mentioned river parts clarification the investigation by physical and mathematical modeling (1D, 2D) was realized.

2.1 Experimental apparatus

The experiment was done in two independent hydraulic models:

a) the navigation channel branch from the dam reservoir – model H (Figure1).

b) the section including water power plant, lock chambers, channel section under the lock chambers, water power plant outlet and the navigation channel and Elbe river junction – model K+D (Figure 2).

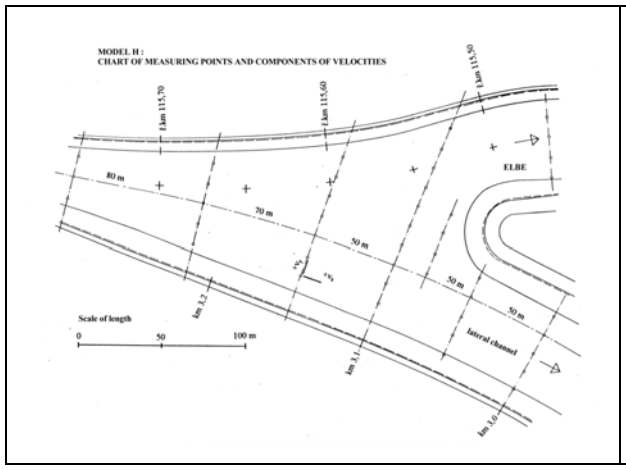

Figure 1 Model H layout

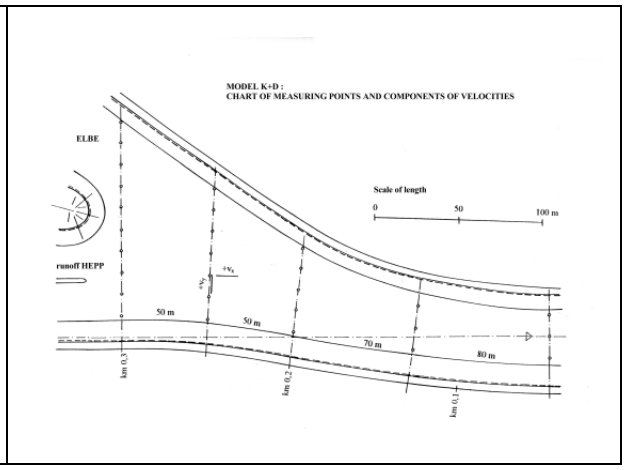

Figure 2 Model K+D layout

Moreover, the main attention was concentrate at velocity field measurement numerical calculation in studied areas.

Hydraulic models were constructed in the model scale of 1:50, velocity scale of 1:7.071, discharge scale of 1:17678 and surface roughness 1:1.93. The model dimension were constructed in range of 12x4m or 26x4m, respectively. The measuring weirs were clapped at the models inlet and outlet. The water level quota was measured with point square.

Several different operations conditions of water power plant and various flow stages, which influence entrance and exit from the navigation channel, until the maximal navigation throw-flow $Q_{max} = 277\ m^3.s^{-1}$ (in model scale $Q_{max\ model} = 15.67\ l.s^{-1}$).

The velocity vectors were investigated in the net of 77 measuring points placed in three levels below the water level, which correspond to 462 values velocity components in the x, y co-

ordinates. The values were measured with micro propeller meters NIXON and UVP monitor (Ultrasonic Velocity Profile Monitor), Met-Flow S.A. Moreover we used six ultrasound probes with basic frequency f_0 = 4MHz. In each point three probes for longitudinal velocity components and three probes for lateral speed components at three independent levels (Figure 3) Each probe was 100mm away the measuring points, which corresponds to the 65thpoint in the ultrasound probe measuring line. The velocity vector average components were obtained from continual measurement for the duration of 45 s.

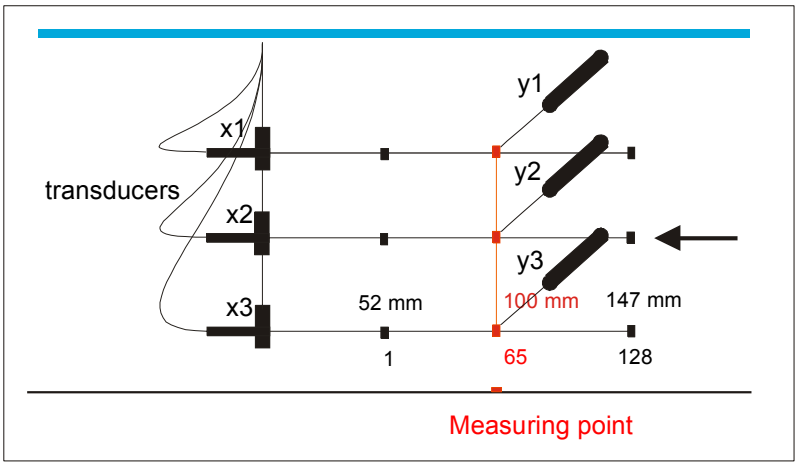

Figure 3 The probes position in the measuring point

For better signal obtain the micro-particles PVC – NERALIT 581 (measuring weight ρ = 1350 kg.m^{-3} and d_{50} = 0.15 mm) were added into the flowing water.

2.2 Mathematical model

For the mathematical simulations the software SHALLOW was used. This software was developed in the Department of Hydraulic Engineering and Hydraulic Structures, CTU for 1D and 2D steady flow simulations with free water surface in open channels. Moreover, this model applies finite elements method (FEM) and stem from the vertical integrated Reynolds equation scheme for turbulent flows, known as “shallow water equations”.

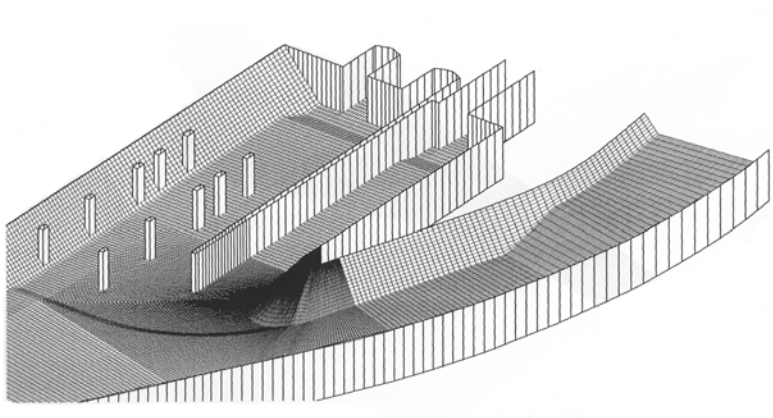

Figure 4 Geometry of mathematical model K+D

For the turbulence modeling, the constant effective viscosity principle was used. This principle is dedicated with use of algebraic relations for the turbulent dispersion coefficient, based on analogy between dynamics and mass transfer in turbulent flows.

3. RESULTS

In both models the water flows conditions modeling approved the suggestion, that the project solving ensure good navigation conditions.

Furthermore, in the fairway of all the modulated conditions, the average longitudinal speed did not exceeded 1.9 $m.s^{-1}$ and the average lateral velocity did not exceed 0.2 $m.s^{-1}$ (0.3 $m.s^{-1}$). Therefore the critical clauses for navigation Czech Standards were not exceeded.

The water power plant plays a positive role in the velocity field shape in the entrance and exit of the navigation channel, where lower lateral velocity components were measured (Figure 6, Figure 8). In contrast, there was shown the negative effect in the water power plant inlet. In consequence of these findings, the geometry changes of the upper docks were brought in.

The UVP method obtained values were also used for the mathematical model calibration and verification. With this model were considered other flow conditions. The measured and calculated data comparison is shown in Figure 5 – Figure 8. The agreement was found in very high level, just in the higher gradients of longitudinal velocity area the deviations in lateral components were observed.

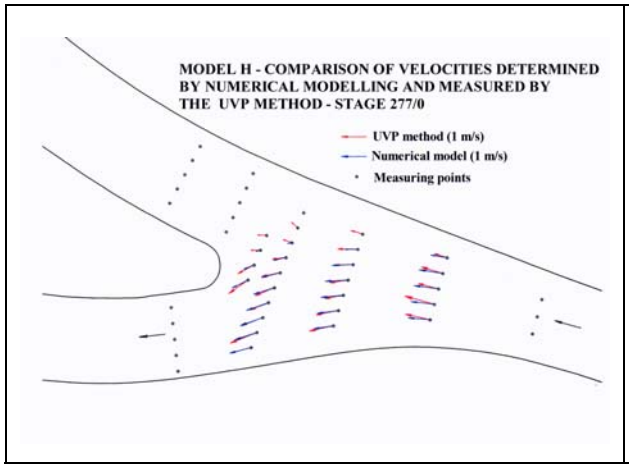

Figure 5 Flow field model H – stage 1

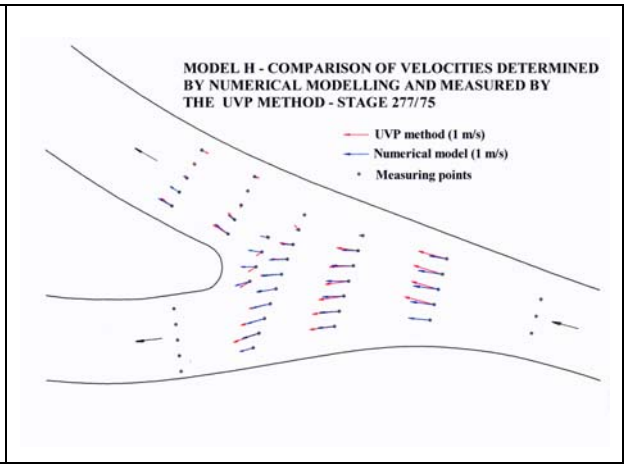

Figure 6 Flow field model H - stage 2

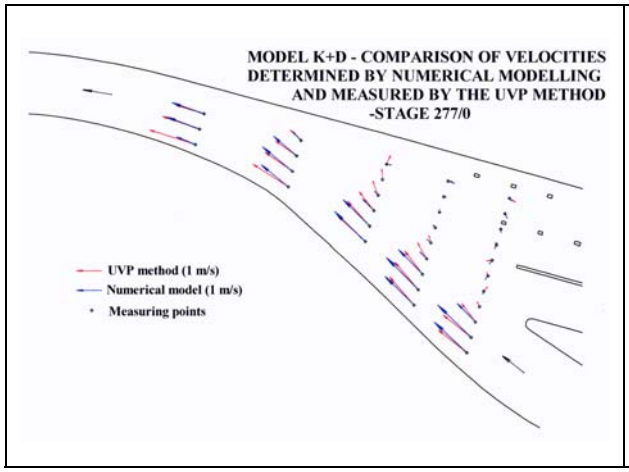

Figure 7 Flow field model K+D – stage 1

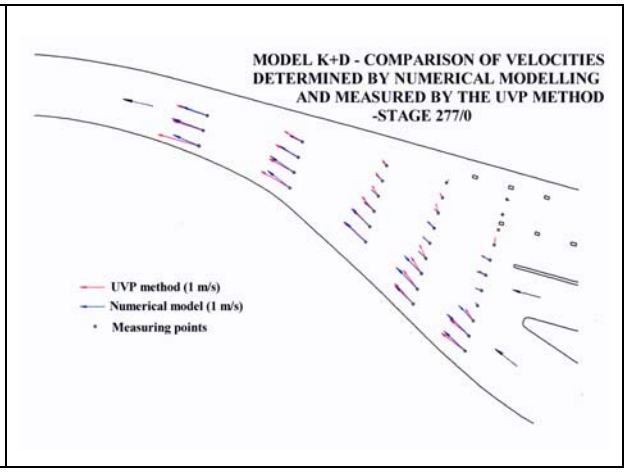

Figure 8 Flow field model K+D – stage 2

4. CONCLUSIONS

The flow field investigation with small values of speed components is common problem, which follows the evaluation of safety conditions of navigation. The Ultrasonic Doppler Method is in this cases very applicable and rationally useful method. Moreover, in the combination with a mathematical modeling, this method allowed to obtain correct image about the water construction system.

REFERENCES

Bares V. (1999), *Gated weir at Elbe River in Prelouc – stage solution,* Diploma thesis, CTU - Prague

Broza, V., Medricky, V., Valenta P. (2000). *Modelovy vyzkum noveho plavebniho sutpne Prelouc,* Stavebni obzor 7/2000, pg. 204-211

Lemmin, U., Rolland T. (1997). *Acoustic Velocity Profiler for Laboratory and Field Studies.* J. Hydr. Engrg., ASCE, Dec 1997, 1089-1098.

Metflow (2000). *UVP Monitor – Model UVP-XW*, Users guide, Met-flow SA, Lausanne, Switzerland

Takeda, Y. (1995). *Instantaneous Velocity Profile Measurement by Ultrasonic Doppler Method*, JSME International Journal, 8-16

Takeda, Y. (1997). *Ultrasonic Doppler Method for Fluid Flow Measurements – Principle and its Applications.* Bulletin of the Research Laboratory for Nuclear Reactors, special issue no. 2, 1-14

ANALYSIS OF COHERENT FLOW STRUCTURES IN A BEND BASED ON INSTANTANEOUS-VELOCITY PROFILING

Koen Blanckaert[1]

[1] Res. Ass., Lab. Hydr. Environ., LHE-ENAC EPF Lausanne, Switzerland, koen.blanckaert@epfl.ch

Keywords: turbulence, coherent structure, open-channel flow, bend, velocity profiling, experiment

ABSTRACT

Coherent flow structures hold the key to a better understanding and modelling of hydrodynamic processes. This paper highlights the unique capabilities of an Acoustic Doppler Velocity Profiler (ADVP) for the experimental investigation of coherent flow structures. Contrary to most commercial velocity meters that measure point-by-point, the ADVP simultaneously measures the quasi-instantaneous velocity vector along an entire profile. This allows to obtain detailed spatial-temporal flow information, and by adopting Taylor's frozen turbulence hypothesis even to visualize flow planes. Whereas most available data on coherent flow structures were obtained in straight uniform flow, this paper illustrates ADVP-measurements of two kinds of coherent flow structures in open-channel bends, where the highly three-dimensional flow is characterized by the existence of cross-stream circulation (helical flow). The first kind concerns the turbulent bulk-oscillation of the pattern of cross-stream circulation cells, whereas the second concerns turbulent coherent structures associated with the bursting process.

1. INTRODUCTION

Turbulence plays a dominant role in the river environment. It dissipates the flow energy, influences the mean-flow pattern, determines the sediment transport as bed-load and suspended load, spreads and mixes transported quantities such as heat, pollutants, oxygen or sediment, triggers the exchange of oxygen at the water surface, etc.

Turbulence modelling in the past aimed at describing the effects of turbulence in a time-averaged way (velocity distribution, conveyance capacity, spreading and mixing characteristics, etc.). It is now generally accepted that the above mentioned processes cannot adequately be described by the averaged effects of turbulence, but are closely related to and conditioned by highly intermittent turbulence events, such as coherent structures.

A prerequisite to enhance our understanding of the relation between these coherent structures at the one side and the mentioned hydrodynamic processes at the other is the availability of detailed experimental data. Such data can give guidance in the model development and form an important tool for the validation of numerical simulations. They are particularly relevant with respect to Large-Eddy-Simulation (LES) techniques. High-quality experimental data on coherent structures are scarce and almost exclusively concern the case of straight uniform flow (Nezu & Nakagawa, 1993; Cellino & Lemmin, 1999; Hurther, 2001), which may not be representative of the highly three-dimensional flow in natural rivers (Blanckaert & Graf, 2001, Blanckaert & de Vriend, 2002).

This paper highlights the capabilities of an Acoustic Doppler Velocity Profiler (ADVP) in the experimental investigation of coherent flow structures. This unique instrument, conceived and built in our laboratory, is briefly presented. The paper subsequently illustrates two different kinds of coherent flow structures measured in open-channel bends, where the highly three-dimensional flow is characterized by the existence of cross-stream circulation (also called

helical motion or secondary flow). The first kind concerns the turbulent bulk-oscillation of the pattern of cross-stream circulation cells, whereas the second kind is associated with turbulent bursting events. While this paper concentrates on the capabilities of the Acoustic measuring technique, the illustrated flow structures will be presented and analysed in detail in forthcoming papers (for example Blanckaert & de Vriend, 2002, for the bulk oscillation).

2. ACOUSTIC DOPPLER VELOCITY PROFILER (ADVP)

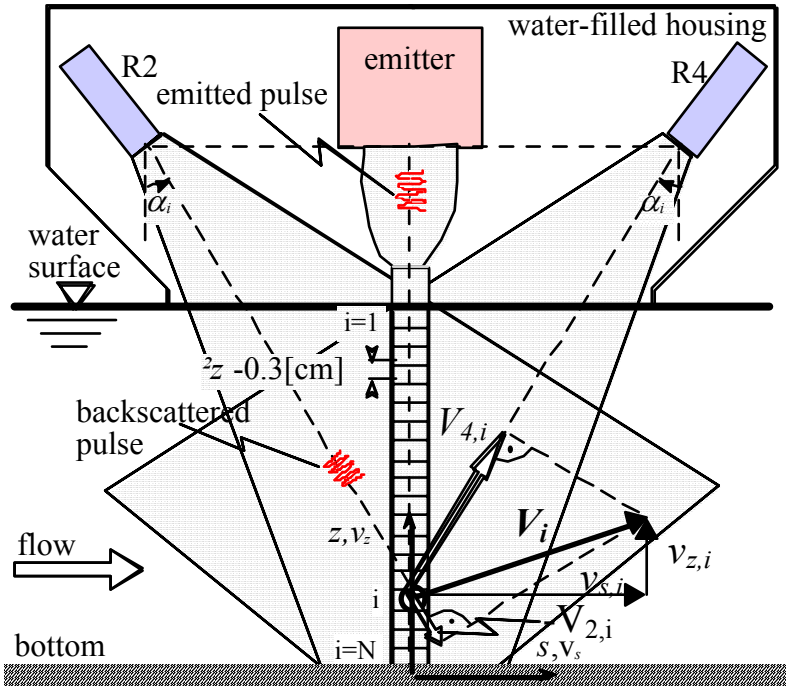

Figure 1. The Acoustic Doppler Velocity Profiler (ADVP)

The non-intrusive Acoustic Doppler Velocity Profiler, conceived and built in our laboratory, measures the quasi-instantaneous velocity vector with a resolution of turbulence scales. It consists of a central emitter, symmetrically surrounded by four wide-angle receivers, R1 to R4 (only two are visible in Figure 1). From these data, the mean velocity vector, $\overline{v}(v_s,v_n,v_z)$, can be derived, as well as the fluctuating velocity vector, $\overrightarrow{v'}(v'_s,v'_n,v'_z)$, the turbulent stress tensor, $\overline{v'_j v'_k}$ ($j,k=s,n,z$), and even higher-order turbulent correlations, $\overline{v'^a_j v'^b_k}$ ($j,k=s,n,z$ and a,b integer).

This ADVP has important advantages over most commercially available acoustic Doppler velocity meters:

(i) Whereas most commercial instruments measure point-by-point, our ADVP simultaneously measures all the velocities along its main axis. The measured profiles are subdivided into a string of equal measuring volumes of size $(\pi 0.7^2/4)\text{x}(0.3)=0.12$ cm^3. This profiling capability allows to do measurements much faster, hence to cover much finer measuring grids than with point-wise instruments. Furthermore, it provides a unique possibility to investigate experimentally spatial-temporal flow characteristics like coherent flow structures, and to visualize flow planes (see below).

(ii) Whereas three receivers are required to measure the three-dimensional velocity vector, our ADVP disposes of four receivers. The fourth receiver yields a redundant velocity information, which is used to improve the turbulence resolution of the measurements (Hurther & Lemmin, 2001; Blanckaert & Lemmin, 2002).

The working principle of the ADVP can be summarized as follows. 1Mhz acoustic pulses sent by the emitter with the pulse-repetition frequency (*prf*), are backscattered along the entire water column by targets (micro air-bubbles) moving with the water, and recorded by the four receivers. The actual measuring volume corresponding to a recorded signal is determined by the time of flight with respect to the emitter. From a number *NPP* (number of pulse-pairs) of recorded Doppler information, one quasi-instantaneous velocity can be estimated. The velocity sampling frequency is thus defined by $f=prf/NPP$, which is typically about 25 Hz, but depends on the flow characteristics. More information on the working principle of the ADVP, its experimental accuracy and its comparison with other velocity meters can be found in Lemmin & Rolland (1997), Hurther & Lemmin (1998, 2001), Blanckaert & Graf (2001) and Blanckaert & Lemmin (2002).

As mentioned before, coherent flow structures are the key to a better understanding and modelling of hydrodynamic processes. Conditional sampling techniques are required to detect and investigate coherent turbulence structures. In their monograph, Nezu & Nakagawa write (1993, p.171): "In order to detect coherent motions from measurements of velocity fluctuations, one must first know the basic features of the coherent structures from flow visualizations; only then can one determine a procedure such that only certain significant information is observed". The profiling capability of our ADVP is a powerful tool for the visualisation of flow planes. The transversal (section 3) or vertical (section 4) dimension of the flow field is covered by measuring simultaneously all the velocities along the acoustic beam. The horizontal dimension is obtained by transforming the measured temporal flow evolution into a longitudinal spatial evolution, according to Taylor's frozen turbulence hypothesis, $x=-Ut$ (the minus sign expresses that events measured at a later time t originate from further upstream).

Previous investigations on coherent turbulence structures in clear water flow as well as flow carrying suspended sediments (Cellino & Lemmin, 1999; Hurther, 2001) testify of the ADVP's reliability in the investigation of coherent flow structures. Hereafter, ADVP-measurements of two types of coherent structures in open-channel bends are presented.

3. BULK-BEHAVIOUR OF CROSS-STREAM CIRCULATION CELLS

Flow in open-channel bends is characterized by the existence of cross-stream circulation (also called helical flow or secondary flow). The bulk-behaviour of the pattern of cross-stream circulation cells was investigated in the laboratory flume shown in Figure 2. It has vertical Plexiglass sidewalls and consists of a 2 m long straight entry reach, followed by a 120° bend with constant centreline radius of curvature, R=2 m. The bar-pool bottom topography is in static equilibrium with the flow, which characteristics are summarized in Table 1. Transversal velocity profiles were measured in the cross-section at 60° in the bend, with the ADVP mounted in a box attached to the outer bank. The measuring grid covered only the outer half of the cross-section (Figure 2). The measuring frequency was 44.6 Hz and the sampling period was 180 s. This experiment has been reported in detail by Blanckaert & Graf (2001) and Blanckaert (2002b).

R [m]	B [m]	Q [l/s]	H [m]	S_s [‰]	U [m/s]	C [m/s]	Re [10^3]	Fr [/]	R/B [/]	R/H [/]	B/H [/]
2	0.40	17	0.11	1.89	0.38	35	42	0.36	5	17.9	3.6

Q: flow discharge
H: reach-averaged flow depth
$\boldsymbol{S_s}$: reach-averaged water-surface gradient
U: reach-averaged velocity
C: Chezy friction factor
$\boldsymbol{Fr}=U/(gH)^{1/2}$: reach-averaged Froude number
$\boldsymbol{Re}=UH/\nu$: reach-averaged flow Reynolds number
$\boldsymbol{\nu}$: molecular viscosity

Table 1. Hydraulic conditions

Two cells of cross-stream circulation are discernable in the pattern of cross-stream motion, (v_n,v_z), shown in Figure 2. Besides the classical helical motion – termed centre-region cell – a smaller and weaker counter-rotating outer-bank cell occurs in the corner formed by the outer-bank and the water surface.

Although the existence of this outer-bank cell has been reported long before (Mockmore 1943, Einstein & Harder 1954, Rozovskii 1957, etc.), it is still poorly understood, which is mainly due to a lack of high-quality experimental data. The visualization of outer-bank cells requires measurements on a fine grid with a high precision (velocities of O(1cm/s)). Our ADVP allowed us to systematically investigate these outer-bank cells. Outer-bank cells measured under different hydraulic conditions have been reported by Blanckaert (2002a).

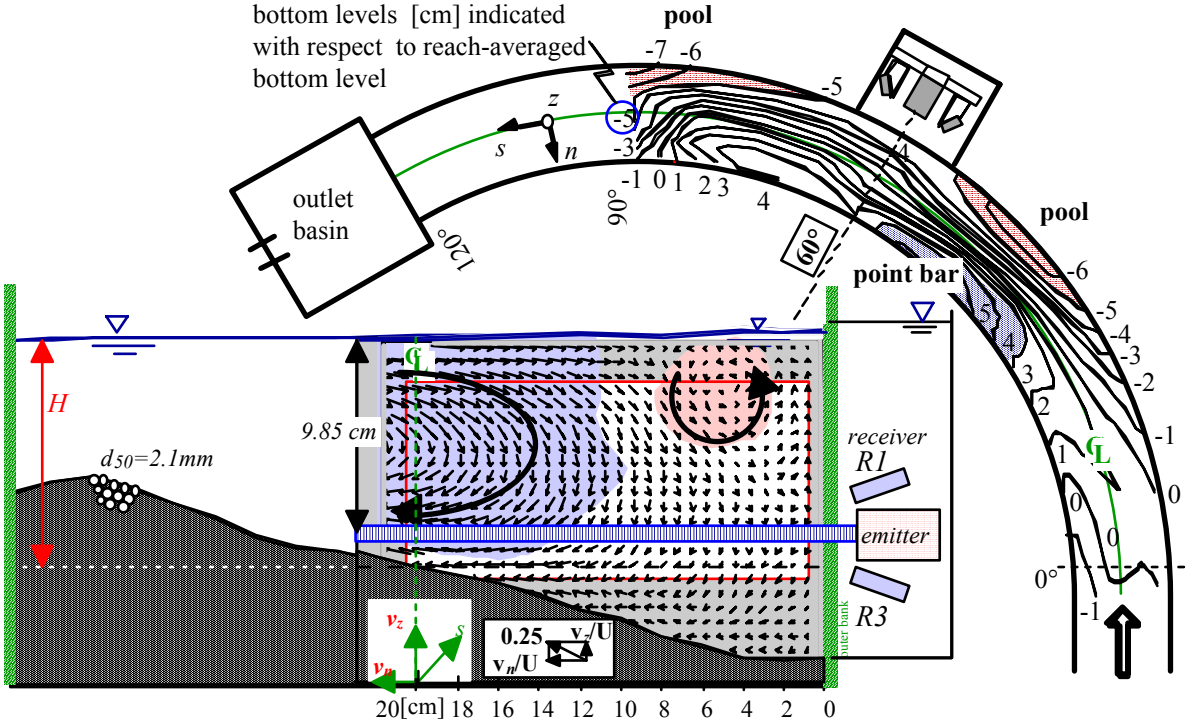

Figure 2. The small-flume experiment

Moreover, the profiling capability of our ADVP allowed us to investigate the bulk-behaviour of this pattern of circulation cells. Figure 3 visualizes the transversal velocity fluctuations in the horizontal plane 9.85 cm below the water surface (cf. Figure 2). The vertical axis covers the measured profile from the outer bank onto near the centreline, whereas the horizontal axis represents the longitudinal spatial evolution, which is obtained from the measured temporal evolution according to Taylor's frozen turbulence hypothesis.

The resulting flow image indicates an a-typical coherence of the transversal velocity fluctuations over the width. Blanckaert and de Vriend (2002) have made an in-depth analysis of this observation and came to the following conclusion:

These width-coherent transversal fluctuations represent a turbulent bulk-oscillation of the pattern of circulation cells in the longitudinal and transversal directions, which has the characteristics of a wave-like motion: it contributes significantly to the turbulent kinetic energy but hardly generates turbulent shear stresses. The reduction of part of the turbulence into a wavelike motion changes the turbulence structure in the investigated bend: for a given amount of turbulent kinetic energy, there is less turbulent shear than in straight flow. This modified turbulence structure leads to a general reduction of turbulence activity in the bend. Differences with straight-flow turbulence can be parameterised by the streamline curvature.

This modified turbulence structure and resulting reduced turbulence activity are potentially important phenomena with respect to environmental processes as sediment transport and spreading and mixing of transported quantities. They had not been observed before, and could only be resolved thanks to the profiling capability of our ADVP.

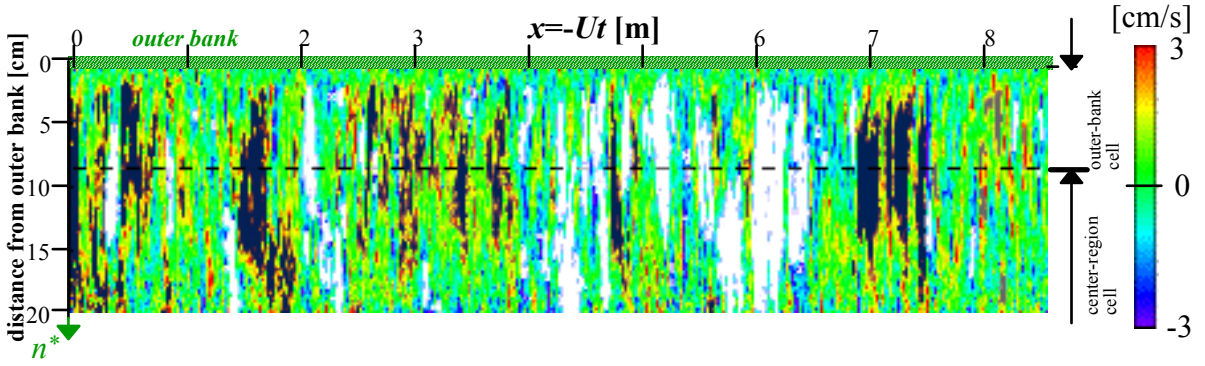

Figure 3. Bulk-oscillation of the pattern of cross-stream circulation cells

4. TURBULENT COHERENT STRUCTURES

As mentioned before, turbulent coherent structures are the key to a better understanding and modelling of hydrodynamic processes. Turbulent coherent structures associated with the bursting process are more efficient in the spreading and mixing of transported quantities (suspended sediment, pollutants, oxygen, heat, etc.) over the entire water column than small-scale turbulence, they dominate the transport of sediment as bed-load and suspended load and they are primary mechanisms in the generation of turbulent kinetic energy and turbulent shear stresses.

By reorienting these turbulent coherent structures, the cross-stream circulation in open-channel bends is expected to alter their characteristics over the entire water column. The available experimental data on turbulent coherent structures associated with the bursting process is mostly limited to the case of straight uniform flow (Nezu & Nakagawa, 1993; Cellino & Lemmin, 1999; Hurther, 2001), and data in three-dimensional flows are particularly scarce.

Turbulent coherent structures were measured in the laboratory open-channel bend shown in Figure 4. It consists of a 9 m long straight entry reach, followed by a 193° bend with constant centreline radius of curvature, R=1.7 m, and a 5 long straight exit reach. The vertical sidewalls are made of Plexiglas and the horizontal bottom is covered with a nearly uniform sand, 1.6 mm < d < 2.2 mm, that was fixed by spraying a paint on it, thus preserving its roughness. The measuring frequency was 31.25 Hz and the sampling period was 90 s. The hydraulic conditions are summarized in Table 2. The parameters R/B = 1.31, R/H = 8 and B/H = 6.1 correspond to a sharp bend that is narrower than usual natural lowland rivers. These ratios do occur, however, in mountain rivers and man-made channels. The experiment has been reported in more detail by Blanckaert (2002b).

R [m]	B [m]	Q [l/s]	H [m]	S_s [‰]	U [m/s]	C [m/s]	Re [10^3]	Fr [/]	R/B [/]	R/H [/]	B/H [/]
1.7	1.3	104	0.21	0.56	0.38	35	81	0.26	1.31	8.0	6.1

Table 2. Hydraulic conditions (see Table 1 for the legend)

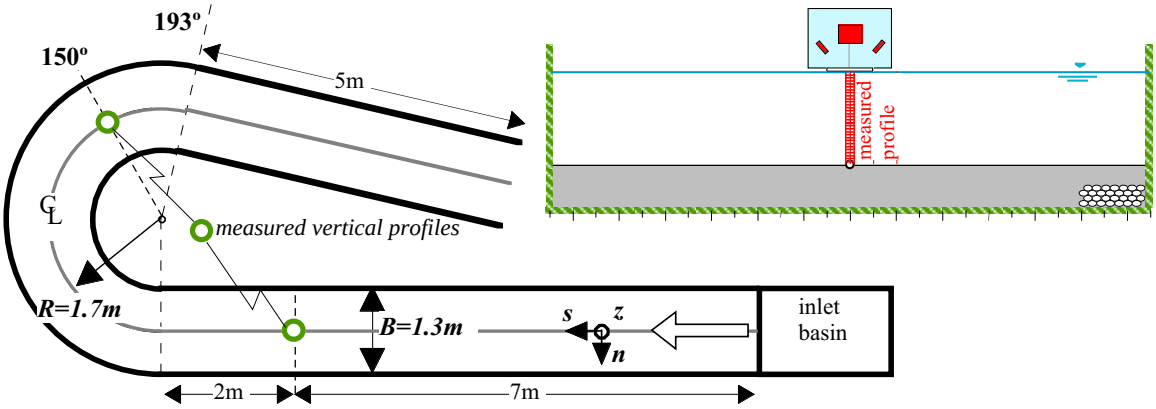

Figure 4. The large-flume experiment

This paper presents visualizations of turbulent coherent structures in vertical planes, obtained by measuring vertical profiles at the centreline of the flow (cf. Figure 4). Figure 5 shows the signature in vertical planes of the instantaneous Reynolds-stress signal, normalized with the overall shear velocity, $v'_s(t)v'_z(t)/u_*^2$ (unfortunately, only a crude representation is possible in black and white printing mode). This quantity is an appropriate detector since it is directly related to the turbulent coherent structures that characterize the bursting process. Figure 5a shows the measurements in the straight flow 2m upstream of the bend, whereas Figure 5b shows the measurements at 150° in the bend (cf. Figure 4).

In the straight flow, the average Reynolds stress $\overline{v'_s v'_z}$ (right side of Figure 5a) has a typical triangular distribution. The instantaneous Reynolds-stress signal clearly reveals the existence of intermittent flow regions with high positive and negative values, which are mainly located in the lower half of the water column. The negative values, corresponding to the so-called sweep and ejection events, dominate over the positive values, corresponding to inward and outward interactions, which is in agreement with the negative sign of $\overline{v'_s v'_z}$ and with data reported by Nezu & Nakagawa (1993) and Hurther (2001).

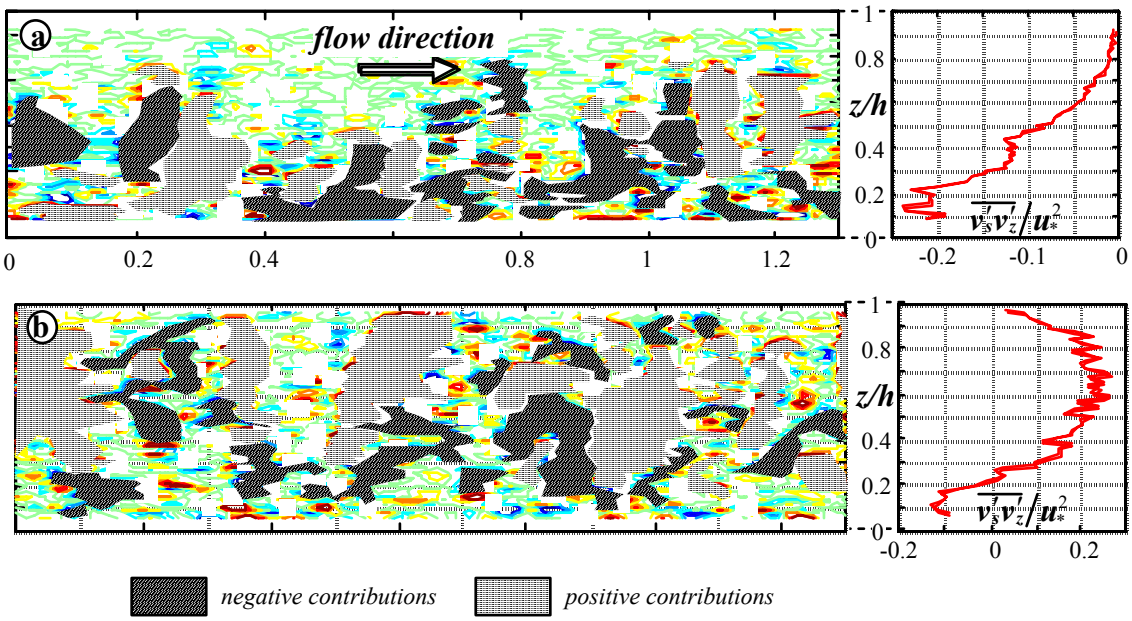

Figure 5: Turbulent coherent structures at the centreline: (a) in the straight flow 2m upstream of the bend; (b) at 150° in the bend, visualized by means of the normalized instantaneous Reynolds stress, $v'_s(t)v'_z(t)/u_*^2$.

At 150° in the bend, the average Reynolds stress $\overline{v_s' v_z'}$ (right side of Figure 5b) is positive over most of the flow depth. Near the bottom, it decreases strongly to attain negative bottom values of comparable magnitude as in the straight flow. In the lower part of the water column, the turbulent coherent structures have a similar signature as in the straight flow. Contrary to the straight flow, important coherent structures exist in the upper part of the water column in the bend. The positive contributions are dominant, which is in agreement with the average Reynolds stress.

These observations confirm that the existence of cross-stream circulation (helical flow) fundamentally modifies the characteristics of the turbulent coherent structures, and thus of the turbulence dynamics in general. The characteristics of turbulent coherent structures in open-channel bends and their relation with the cross-stream circulation will be presented and analysed in more detail in a forthcoming paper.

5. CONCLUSIONS

This paper highlights the unique capabilities of an Acoustic Doppler Velocity Profiler (ADVP) in the investigation of coherent flow structures. Whereas most instruments measure point-wise, the ADVP simultaneously measures the quasi-instantaneous velocity vector along an entire profile. This allows a visualisation of the spatial flow structures. This paper illustrates ADVP measurements of two different kinds of coherent flow structures in open-channel bends, where the highly three-dimensional flow is characterized by the existence of cross-stream circulation (helical motion). Previous measurements were mostly limited to the case of straight uniform flow, and experimental data on coherent flow structures in three-dimensional flows are particularly scarce.

The first kind of coherent flow structure concerns the bulk-behaviour of the pattern of cross-stream circulation cells. The visualization of a horizontal flow plane indicates a turbulent oscillating behaviour of the entire pattern of circulation cells. Blanckaert and de Vriend (2002) have presented an in-depth analysis of these observations.

The second kind of coherent flow structure is associated with the turbulent bursting process. It is investigated by visualizing a vertical flow plane at the centreline of the flow. In the straight flow upstream of the bend, turbulent coherent structures are mainly found in the lower part of the water column. There, ejection and sweep events dominate over inward and outward interactions. At 150° in the bend, the turbulence signature is similar in the lower part of the water column. The upper part of the water column, however, is now characterized by the existence of significant turbulent coherent structures. There, inward and outward interactions are dominant, which is in agreement with the positive sign of the corresponding Reynolds stress. These observations indicate fundamental differences in the turbulence dynamics between curved flow and straight flow.

The presented results testify of the unique capabilities of our ADVP to illustrate and investigate coherent flow structures. Data of the presented kind are needed to improve our understanding and modelling of hydrodynamic processes in the river environment.

ACKNOWLEDGMENTS

This research was sponsored by the Swiss National Science Foundation under grants Nr.2100-052257.97/1 and 2000-059392.99/2. The author gratefully acknowledges Dr. U. Lemmin, for developing and making available the Acoustic Doppler Velocity Profiler.

REFERENCES

Blanckaert K. (2002a). "Secondary currents measured in sharp open-channel bends." *Proc. River Flow 2002,* Louvain, Belgium.

Blanckaert K. (2002b). *Flow and turbulence in sharp open-channel bend*, PhD thesis 2545, Swiss Federal Institute of Technology Lausanne (EPFL).

Blanckaert, K., &de Vriend, H. J. (2002). "Turbulence structure in an open-channel bend." (*submitted for publication*).

Blanckaert, K. & Graf, W. H. (2001). "Mean flow and turbulence in open-channel bend." *J. Hydr. Engng*, ASCE, 127(10), 835-847.

Blanckaert, K., & Lemmin, H. J. (2002). "Improving acoustic turbulence measurements." (*submitted for publication*).

Cellino M. & Lemmin U. (1999). "Coherent flow structure analysis in suspension flows." *Proc. (CD-ROM) 28th IAHR congr.*, Graz, Austria.

Einstein, H.A. & Harder, J.A. (1954). "Velocity distribution and the boundary layer at channel bends". *Trans. AGU*, 35(1): 114-120.

Hurther D. (2001). "Sediment transport assessment in suspension flow based on coherent structure characteristics." *Proc. JFK student paper comp., 29th IAHR congr.*, Beijing, China.

Hurther, D. & Lemmin, U. (1998). "A constant beamwidth transducer for three-dimensional Doppler profile measurements in open channel flow." *Meas. Sciences Techn.*, IOP, 9(10), 1706-1714.

Hurther, D. & Lemmin, U. (2001). "A correction method for turbulence measurements with a 3-D acoustic Doppler velocity profiler." *J. Atm. Oc. Techn.*, AMS, 18, 446-458.

Lemmin, U. & Rolland, T. (1997). "Acoustic velocity profiler for laboratory and field studies." *J. Hydr. Engng*, ASCE, 123(12), 1089-1098.

Mockmore, C.A. (1943). "Flow around bends in stable channels". *Transactions ASCE* 109: 593-628 (incl. discussions).

Nezu, I. & Nakagawa, H. (1993). *Turbulence in open-channel flows*, IAHR-monograph, Balkema.

Rozovskii, I.L. (1957). *Flow of Water in Bends of Open Channels*. Jeruzalem: Isr. Progr. Sc. Transl.

MEASUREMENT OF 3D FLOW FIELD IN A 90° BEND WITH ULTRASONIC DOPPLER VELOCITY PROFILER

Daniel S. Hersberger[1]

[1] Research associate, Laboratory of Hydraulic Constructions (LCH), Swiss Federal Institute of Technology (EPFL) Lausanne, Switzerland, daniel.hersberger@epfl.ch

Keywords: Ultrasonic Doppler Velocity Profiler (UVP), velocity measurement technique, scour in bends, 3D flow field, flow mapping, velocity distribution.

ABSTRACT

In the frameset of a research work on scour in river bends, the influence of vertical ribs placed on the outer sidewalls on the maximum scour depth and the modification of the flow field was studied. The velocities were measured by means of an Ultrasonic Doppler Velocity Profiler, which allows an instantaneous measurement of the 1D velocity profile over the whole flow depth. The measurement probes were mounted on a support in groups of three, allowing the measurement of the 3D flow field. The probes were inclined at 20° to the vertical. The velocity measurements were integrated in an acquisition device also permitting the measurement of the water- and bed-levels with automatic positioning of the probes at about 1500 measurement points.

The secondary flow in river bends induces radial velocities of about 10% of the value of the tangential velocities (which are of positive and negative sign). A method is presented to measure velocities exceeding the measured velocity domain due to a shifting of the raw Doppler signal. Furthermore, the data treatment to obtain the average flow field in the tangential direction and in the cross section is described.

A brief description of the obtained results is given. The flow field in a river bend undergoes some important modifications compared with the one in a straight river reach. These modifications as well as the influence of the vertical ribs on the velocity profiles are presented and briefly discussed. The analysis of the flow field allowed observing a secondary outer bank cell located at the free water surface having a bank protection effect. With increasing wall roughness, this cell gets more important.

1. INTRODUCTION

In the framework of a study on scour (erosion in river bends), the 3D-velocity field was measured. The aim of the study was to investigate the flow distribution and the scour depth in a bend with special emphasis on the influence of vertical ribs applied to the outer wall serving as macro-roughness (Figure 1). These measurements were performed in a 1 m wide 90° bend (Radius of 6 m) at various longitudinal bed slopes and discharges for different rib spacings and depths, as well as without ribs.

2. ACQUISITION SYSTEM

2.1 Components of the acquisition device

2.1.1 Hardware

In order to measure the 3D velocity field, a measurement frame (2 x 2 m, Figure 2) was put on the channel every 15° at eight predefined positions. Within the measurement frame, a regular grid of measurement points (9 x 9 cm) was chosen to perform the measurements.

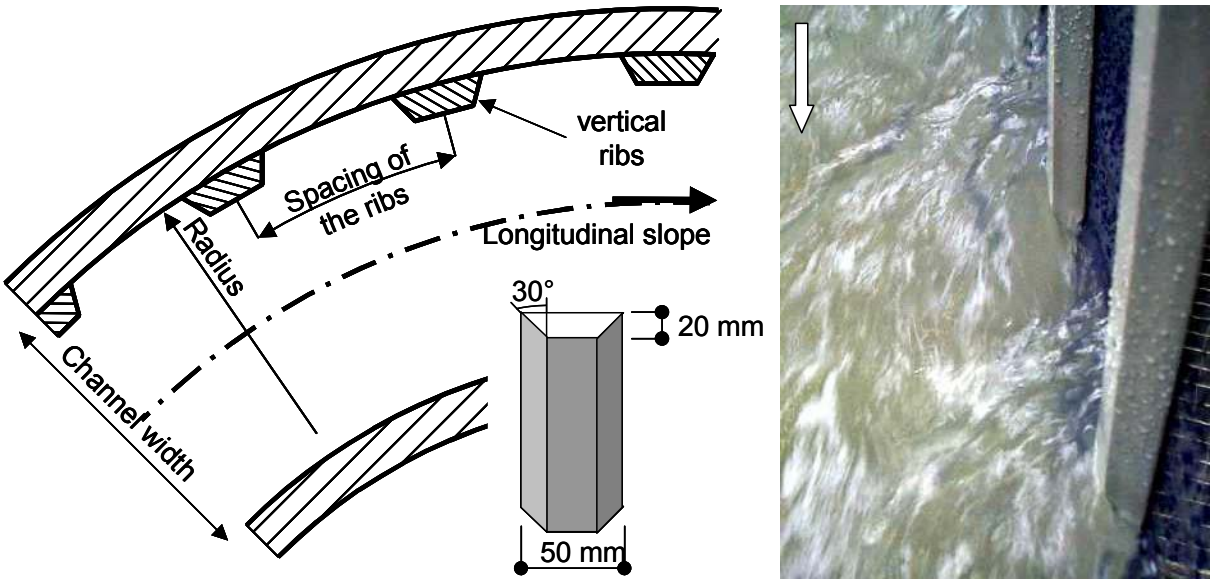

Figure 1 Vertical ribs (macro-roughness) applied on the outer sidewall

The velocities were measured with an Ultrasonic Doppler Velocity Profiler (Metflow, Model UVP-XW) allowing for an immediate obtention of a 1D-velocity profile over the whole channel depth (see METFLOW, 2000). To measure the 3D-flow field, three 2 MHz-probes were mounted on a probe support plate (Figure 2 and Figure 3). Since the number of measurement points was very high (about 1500 points over the whole channel), three plates were mounted on the measurement frame, permitting the simultaneous recording of three groups of three 1D profiles (constituting one 3D profile) which accelerated the data acquisition.

A multiplexer (Figure 2, on the left of Nr. 5) allowed for the switching from one UVP-probe to another.

Due to the complexity of the flow field in bends, several specific problems had to be solved: (1) The measured velocities in the tangential direction are rather high (up to 1.5 m/s), (2) the radial velocities are of an order of magnitude smaller than the velocities in the tangential direction and (3) the radial velocities are both positive and negative due to the secondary flow. Therefore, the scale of the measurements had to be fixed to allow for good quality recording of high as well as small records with positive and negative values.

Two measures were taken to reduce the value of the measured velocity. (1) The UVP-probes were inclined at a 20° angle, thus reducing the highest velocities to 34% (sin 20°). The inclination was not increased to higher values since a very small error in the frame geometry

would lead to an important measurement error. Furthermore, this inclination still gives a satisfying resolution for low velocities. In spite of this, some velocity peaks were somewhat too big to be measured. (2) As a result, an interesting characteristic of the used Doppler measurement was explored. If the measured velocity is higher than the maximum velocity (similar for the minimum velocity), the UVP shifts the measured value by 2 times the velocity range into the negative measurement domain (ROLLAND, 1995). If the sign of the velocity is known, the recorded velocity profile can be corrected by shifting the negative values into the positive domain again. This was done for the high velocities in a tangential direction whose sign was clearly given.

Since the UVP-probes could not be placed vertically, the vertical control volume has a conic shape with a diameter of up to 3 to 6 cm, depending on the distance to the measurement plate.

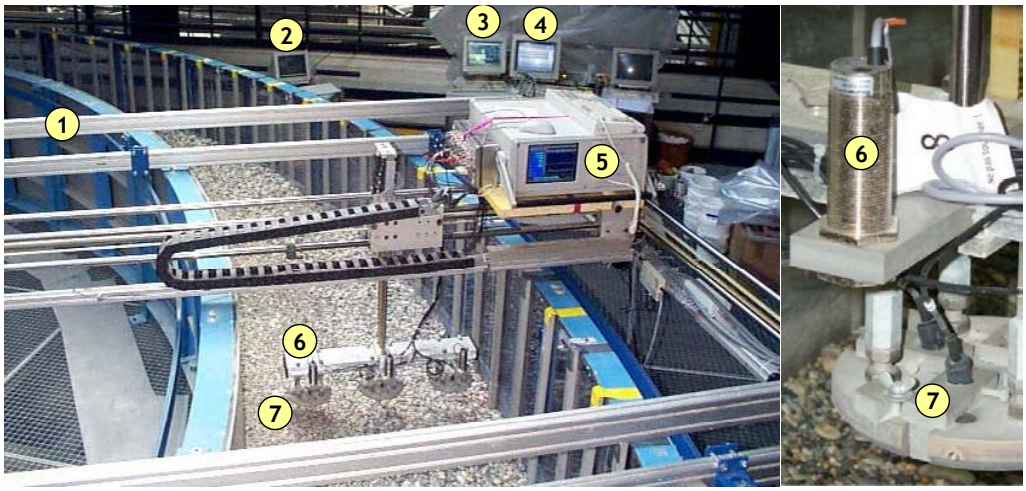

Figure 2: The measurement frame with probe support
1 Measurement frame, 2 Discharge controller, 3 Frame controller, 4 Level acquisition, 5 Velocity acquisition, 6 Levelling probe, 7 Velocity probe and support

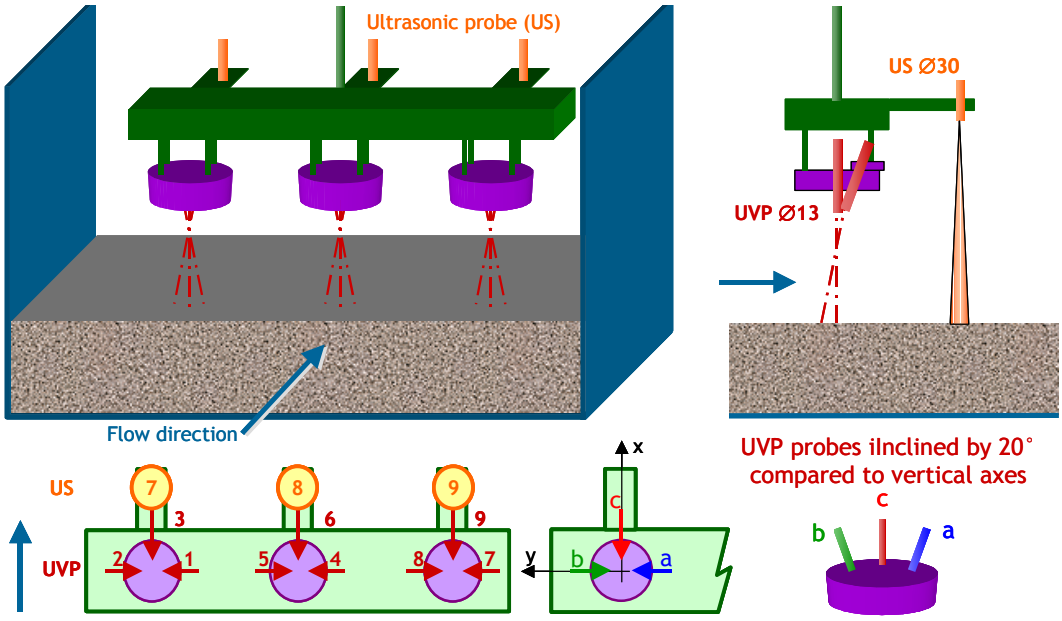

Figure 3: Scheme of the probe support for UVP-Doppler velocity measurement and US bed levelling

2.1.2 Software

A special software was developed to control and automate the whole acquisition process including movement of the measurement frame to the desired position, recording of water and bed levels and recording of the velocity field (Figure 4).

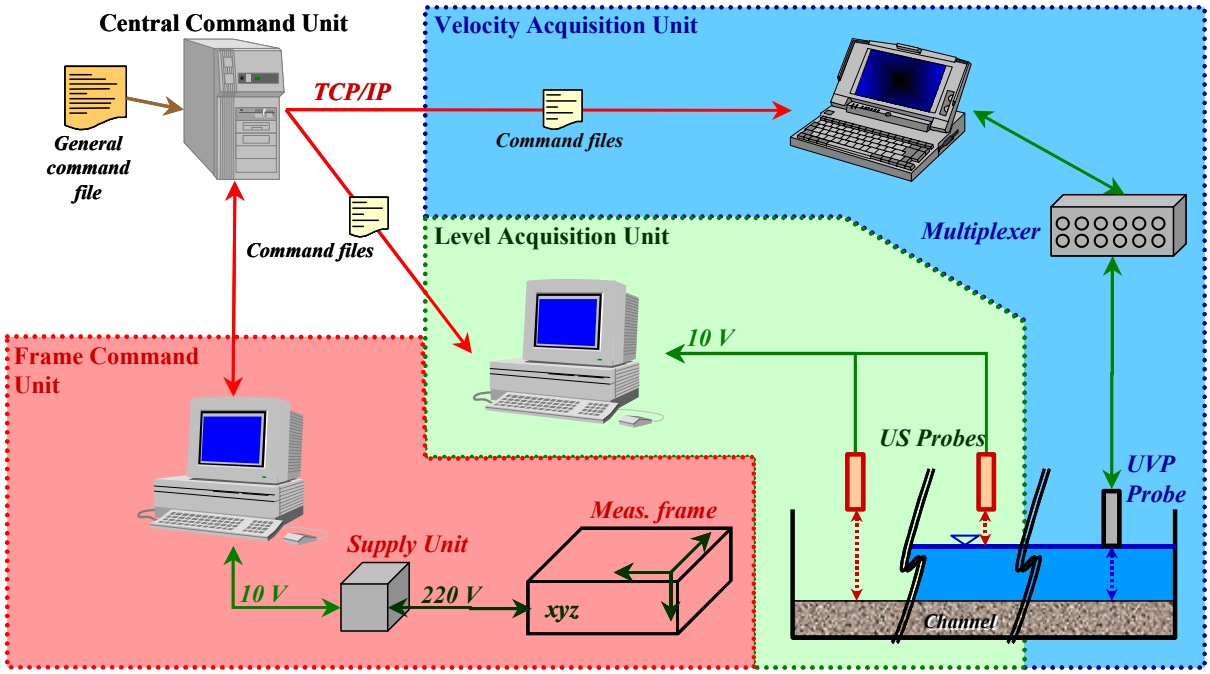

Figure 4: Scheme of the acquisition device

A central command file – fixing frame positions and measurements to be performed – was introduced into the central command unit. This Unit generated small data packages, which were sent to the three different devices[1]. A direct connection to the measurement frame allowed for the control of the measurement location. A special tool introduced the commands into the level acquisition device and into the UVP over the local network. All operations were recorded in a log-file.

2.2 Velocity measurements

In the present study, the main interest is the average flow field. Therefore a rather short measurement was performed. For each 1D-velocity profile, 64 data points (in time) were recorded with a resolution of 128 points (in space). The multiplexer switched to the next probe after 64 measured profiles. Consequently the measured flow field is not an instantaneous 3D-field, but for average values, it can be assumed to be constant considering the short recording time. The acquisition frequency was at about 70 Hz, which would even allow an analysis of turbulence characteristics for one probe for longer samples; therefore longer recordings were performed over 2048 samples (in time) for some selected cases. A set of nine 1D-profiles performed at a given frame location was stored in a specific binary file for later treatment and analysis (§ 3).

[1] The three devices were located on different machines due to incompatibilities between data acquisition cards.

3. DATA TREATMENT

The three 1D records at the three positions were extracted from the raw data file (Figure 5). The high velocities in tangential direction with a negative sign[2] were then corrected so as to be located in the positive range.

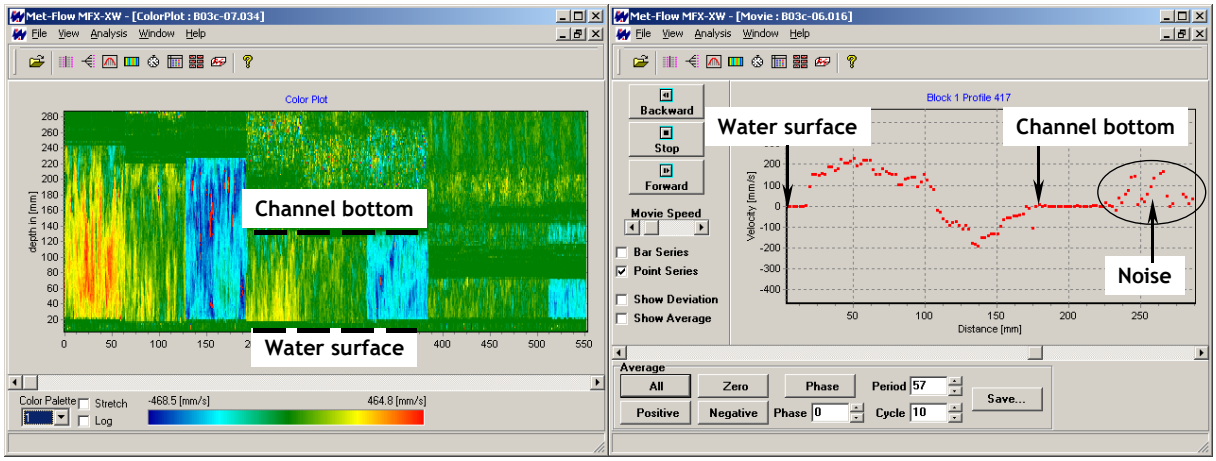

Figure 5: Used UVP Software showing a sample file

Next, the measured components at a given location had to be projected into a cylindrical coordinate system fitting the bend (tangential, radial and vertical velocities). Assuming that the measured velocity components are a, b and c (see Figure 3), the velocity components in one point are given with

$$u = \frac{a + b - 2 \cdot c}{2 \cdot \sin\alpha}, \quad v = \frac{-a + b}{2 \cdot \sin\alpha}, \quad w = \frac{a + b}{2 \cdot \cos\alpha}$$

The thus obtained velocity components cover the whole measurement depth. As can be seen on Figure 5, the bottom of the flume is clearly detectable. Due to the high amount of velocity profiles, it is useful to be able to detect the bottom automatically. In the present study the ground was fixed at the level for which the two following conditions applied: the velocity as well as the variance are close to zero (absolute value below a given threshold). Another way in which to detect the bottom consists of looking for the peak of the bed shear stress, which is proportional to the derivation of the velocity over the depth du/dz. Both approaches give excellent results.

4. DATA ANALYSIS

A detailed analysis of the 3D velocity field in a bend can be found in HERSBERGER (2002). A brief summary of the flow field analysis is presented hereafter.

4.1 Modification of flow field in bends

4.1.1 Tangential velocities

The velocities in a tangential direction (along the channel axis) are somewhat modified in the bend. Instead of a classical "log"-velocity profile as can be seen on top in Figure 6, it undergoes the following modifications in a curved channel. The maximum velocity is no longer found close to the free water surface but close to the bed surface, particularly in the

[2] Values close to zero were not corrected since some near bed fluctuations are possible.

scour holes; this can be very well seen in the cross-section 40°, in the second profile from the left. The highest velocities are now found in the outer half of the cross-section.

With macro-roughness, the near bed velocity is reduced and the maximum velocity shifts towards the free water surface (Figure 6 right, first two profiles at the outer bank).

The measurements showed that the highest main velocities are located in a straight reach next to the free water surface. In the bend, this zone of maximum velocity first shifts towards the outer sidewall where it plunges down along the wall towards the channel ground. At the maximum scour location, high velocities can be observed close to the ground (Figure 7, left).

XS	Without macro-roughness	Ribs spaced at 2 x the mean water depth
10°	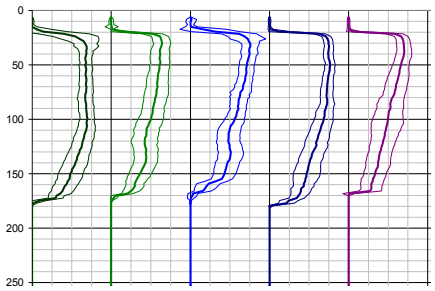	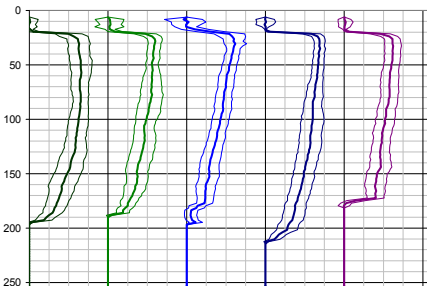
40°	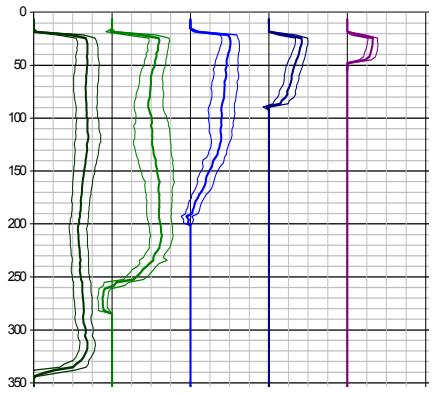	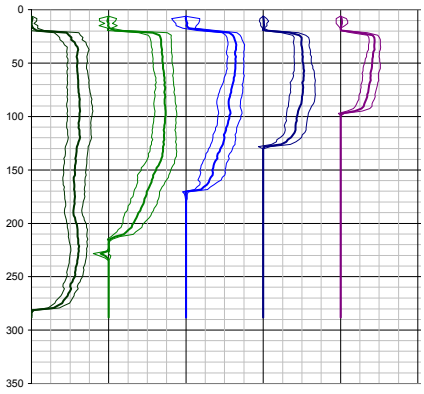
	outer bank inner bank	outer bank inner bank

Figure 6: Mean velocities and standard deviations in tangential direction. View in the downstream direction. Left profile at 90 cm from the outer bank, radial distance between profiles 180 cm. Vertical axis: free water surface in mm.

With macro-roughness, the zone of maximum velocity remains close to the surface over the whole bend with a rib spacing of about two times the mean water depth. By introducing additional ribs, (spaced at about the mean water depth) the maximum velocity moves towards the channel ground, but at fair distance from the outer wall (at about the average flow depth). For the smallest rib-spacing, the high-velocity zone gets even closer to the ground, but once again at fair distance from the outer side wall. Since the highest velocities are kept away from the outer bank, wall foundations are less endangered by scouring.

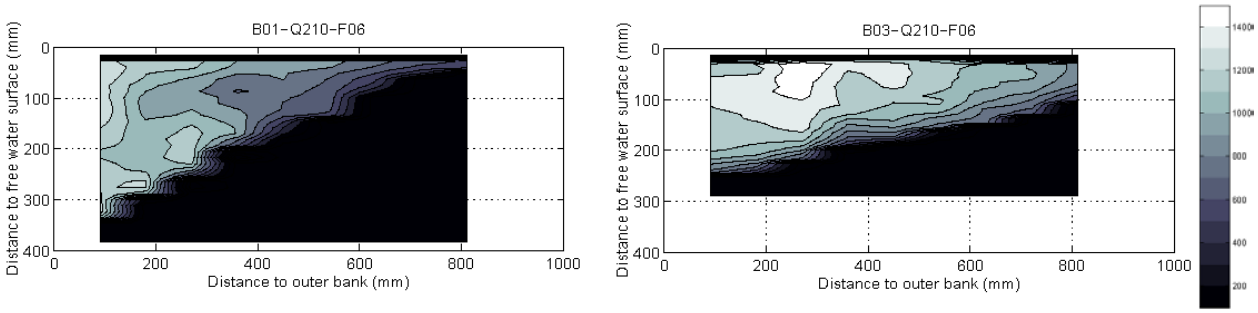

Figure 7: Tangential velocities at 40° without macro-roughness (left) and with ribs spaced every 2° (right); velocities in mm/s.

4.1.2 Velocities in the cross-section - secondary current

The flow field in the cross-section (radial and vertical components combined) shows the growth of the secondary current starting just after the beginning of the bend, increasing in the downstream direction and reaching its maximum intensity in the first scour hole (Figure 8, top). Towards the second scour hole, the main cell again becomes greater, but not as great as for the first scour. The near bed radial velocities are of the same order of magnitude over the whole channel (about 10% of the tangential velocity components).

By placing ribs at the outer side wall (every 4°), a secondary current of almost constant intensity over the whole bend is well visible.

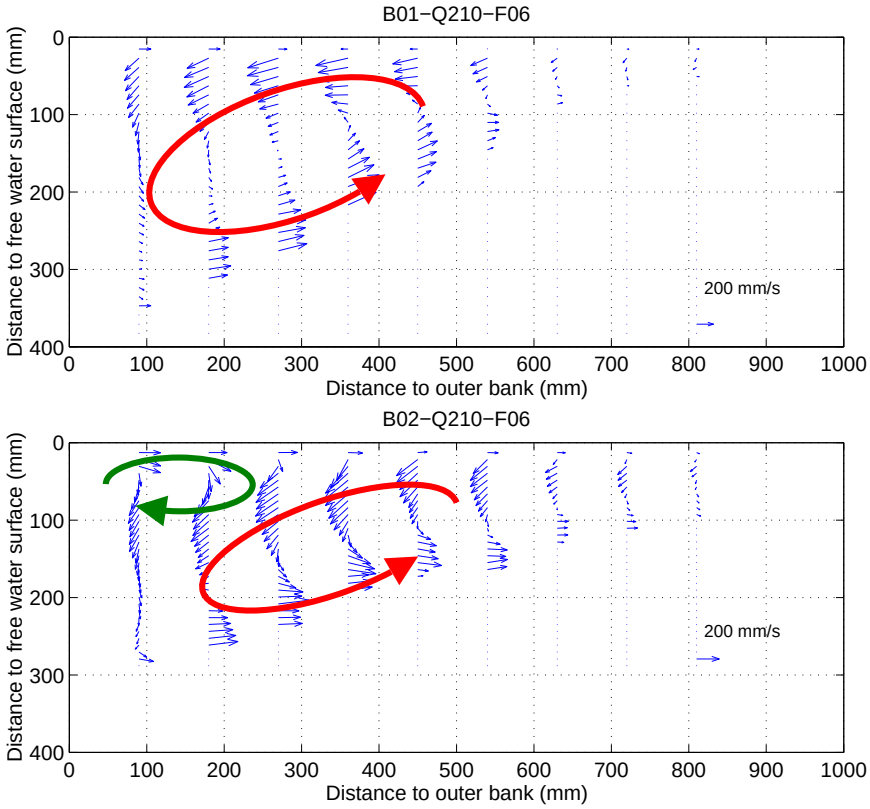

Figure 8: Main and inner bank secondary cells in the first scour hole (no macro-roughness, on top) and main secondary cell and outer bank secondary cell protecting the wall of the channel (rib spacing 2°) at 70° (bottom)

At the outer bank at the free water surface, a very small secondary cell (outer bank cell) becomes visible (Figure 8). This cell was described by BLANCKAERT & GRAF (2001). For the tests, this cell keeps the same intensity over the whole bend. If more ribs are added (2°), the cell increases. But if the rib spacing is too dense (1°), it decreases again, but does not disappear (see 55°). Knowing that the scour reduction is most important for rib spacings of 4 and 2°, it can be concluded that the cell reaches the greatest size for the tests with the most important scour reduction.

Blanckaert observed the highest tangential velocities at the interface between the two cells. If we compare Appendix 11.4 with 11.5 we find high velocities at the interface, but the highest velocities occur inside the main secondary cell either towards the free water surface or near the outer bank.

The intensity of the radial velocity components on the ground with all rib spacings is of the same order of magnitude as without macro-roughness. This leads to the conclusion that the radial velocity components cannot explain the difference in the scour depth. If the radial components cannot explain this difference, then the secondary current cannot explain it either, even if it contributes to the erosion process. But looking at the tangential velocities, we see a significant reduction of the near bed velocities if we apply vertical ribs on the outer bank. Furthermore the tangential velocities are about 10 times bigger than the radial ones. Therefore we must to conclude that the modification of the tangential flow field seems to be a determining factor for the reduction of the scour due to macro-roughness.

ACKNOWLEDGMENTS

This research is being sponsored by Met-flow SA, Lausanne, Switzerland, the Swiss National Science Foundation under Grant No. 2100-052257.97/1 and the Swiss Federal Office for Water and Geology (FOWG).

REFERENCES

Blanckaert, K. & Graf , W.H. (2001). *Mean flow and turbulence in open-channel bend*. Journal of Hydraulic Engineering, ASCE 127(10), 835-847

Hersberger, D.S. (2002). *Roughness effect of outside protection walls on flow and scouring in bends of sediment transporting mountain rivers*, Ph.D. thesis Nr. 2632,Laboratory of Hydraulic Constructions (LCH), Swiss Federal Institute of Technology (EPFL), Lausanne, Switzerland

Metflow (2000). *UVP Monitor – Model UVP-XW*, Users guide, Metflow SA, Lausanne, Switzerland

Rolland T. (1995). *Développement d'une instrumentation Doppler ultrasonore: Application aux écoulements turbulents*, Ph.D. thesis 1281, Laboratory of Hydraulic Research (LRH); Swiss Federal Institute of Technology (EPFL), Lausanne, Switzerland, 159 pp.

NOTATION

a, b, c	velocity components in probe direction
u, v, w	velocity component in tangential, radial and vertical direction
α	inclination angle of the probes compared to a vertical line (20° in the present study)

AN OVERVIEW OF EXPERIMENTAL ACTIVITIES AT THE THERMAL FLUID SCIENCES LABORATORY, UNIVERSITY OF MISSOURI-ROLLA (USA)

Akira Tokuhiro

Assist. Prof., Department of Nuclear Engineering, University of Missouri-Rolla, 1870 Miner Circle, Rolla, Missouri 65409-0170, USA, e-mail:tokuhiro@umr.edu

Keywords: artificial heart valve, heat transfer measurements, near-wake dynamics, ultrasound Doppler velocimetry, particle image velocimetry

ABSTRACT

The Thermal Fluid Sciences Laboratory (TFSL) at the University of Missouri-Rolla, Nuclear Engineering Department was inaugurated in summer 2000. TFSL is presently centered on two velocimetry systems for detailed flow measurement studies; that is, ultrasound Doppler (UDV) and particle image velocimetries (PIV). The lab is currently has four ongoing investigations as follows:

1) flow characterization of artificial heart valve designs using the Met-Flow UVP,
2) flow (UVP) and heat transfer measurements of natural convection flow in a thin rectangular cell with hydrophilic particles,
3) measurement of near-wake dynamics of a single bubble in downward flow of water using PIV, and
4) measurement of near-wake dynamics of a single oil droplet in downward from of water using PIV.

The presentation will describe some initial results from the experiments, comments on student involvement using the UV/PIV and future plans to expand the use of both UVP/PIV.

IN-LINE ULTRASOUND BASED RHEOMETRY OF INDUSTRIAL AND MODEL SUSPENSIONS FLOWING THROUGH PIPES

Johan Wiklund[1,2], Mattias Johansson[1], Jeelani Shaik[1], Peter Fischer[1], Erich Windhab[1], Mats Stading[2] and Anne-Marie Hermansson[2]

[1] Food Process Engineering Laboratory, Institute of Food Science, Swiss Federal Institute of Technology (ETH), Schmelzbergstrasse 9, 8092 Zürich, Switzerland, jeelani.shaik@ilw.agrl.ethz.ch or windhab@ilw.agrl.ethz.ch

[2] SIK, Swedish Institute for Food and Biotechnology, 402 29 Gothenburg, Sweden, johan.wiklund@sik.se

Keywords: In-line rheometry, non-Newtonian rheology, surfactant solution, suspension, ultrasound, velocity profile.

ABSTRACT

A pulsed ultrasound (U) Doppler based technique is experimentally evaluated for in-line rheometry of viscoelastic surfactant solutions (shampoo) and non-Newtonian aqueous cellulose fibre suspensions flowing in a pipe over a wide range of volume throughputs and concentrations. The method involves the simultaneous measurement of radial velocity profile (VP) determined by the time delay and frequency of ultrasound reflected by particles, and pressure drop (PD) in a pipe section. The experiments are carried out in a flow loop fitted with a flow adapter having optimum acoustic properties, a transducer, which emits ultrasound at a frequency of 4 MHz and receives the echo signal, and a Met-Flow UVP-Monitor. For each volume throughput, a non-linear regression analysis of the velocity profile measured by the in-line UVP-PD rheometer is carried out using the integrated form of power-law rheological model to obtain the exponent and consistency index for both surfactant solutions and cellulose suspensions. In addition, Herschel-Bulkley model is used to obtain the yield stress for cellulose suspensions. The model parameters and the shear rate dependent viscosities for the shear thinning surfactant solutions determined using the in-line UVP-PD technique agree well with those obtained using the conventional commercial rotational off-line rheometers (Bohlin CS-50, Rheometric Scientific ARES, and Paar Physica MCR-300). Off-line rheometric measurements could not be made using cellulose fibre suspensions due to compression and drainage of the sample. For the surfactant solutions tested, the viscosity at the pipe wall decreased by an order of magnitude corresponding to an order of magnitude increase in the wall shear rate. In contrast, the viscosity at the pipe wall for the cellulose fibre suspensions decreased only slightly corresponding to the same increase in the wall shear rate. However, increasing the concentration of cellulose fibres from 1 to 3 % by weight increased the suspension viscosity at the pipe wall by a factor of about 2 to 3 depending on the shear rate. In general for a given throughput, as the concentration of the cellulose fibres increases, the suspension becomes stress, shear rate and shear viscosity distributions in the pipe, which are directly related to the more shear thinning as indicted by the decreasing values of the power-law exponent. The non-invasive in-line UVP-PD rheometric method also enabled the determination of the radial shear local microstructure (ie. the orientation) of particles in the suspension. In the absence of the present in-line method, it would not have been possible to study the rheological behaviour of non-Newtonian systems such as aqueous cellulose fibre suspensions even in conventional off-line rheometers.

1. INTRODUCTION

The rheology of industrial suspensions depends on the processing conditions, which affect the microstructure, and the shear and elongational flow fields. The product quality is usually controlled based on shear rate dependent viscosity information obtained using off-line rheometers as there exist no in-line rheometers for suspensions, which are usually opaque. This method is not reliable as its flow field could be significantly different to that in the actual flow process. In addition off-line rheometers cannot be used for in-line purpose because of the lack of suitability of their geometry and invasive nature. They are also difficult to use for suspensions with extreme rheological properties. Takeda (1-7) developed a pulsed ultrasound echographic method for the measurement of velocity profiles in flowing suspensions, which was expanded and manufactured as an Ultrasound Velocity Profile (UVP) Monitor by Met-Flow SA (8). Using this Monitor, Windhab and Ouriev (9-15) developed a system and a methodology for in-line rheometry of concentrated opaque suspensions by measuring simultaneously the velocity profile (UVP) and the pressure difference (PD) in a pipe section of a process. This was successfully tested on industrial and model suspension systems such as chocolate transport in pipes during chocolate and fat crystallisation processes (9-15), and starch in glucose syrup. The present paper investigates experimentally the above UVP-PD methodology for industrial surfactant solutions (shampoo) and model cellulose fibres in water suspensions using the UVP-PD in-line rheometer system. It also compares the shear rate dependent viscosities measured by UVP-PD in-line rheometric method with those measured by conventional off-line rheometers.

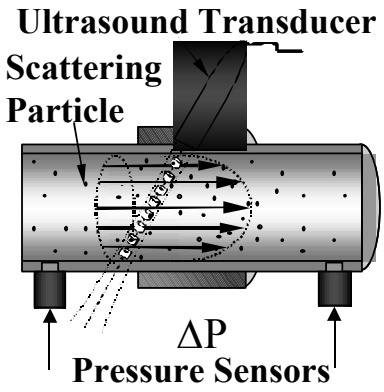

Figure 1. Flow adapter, ultrasound transducer and pressure sensors for the UVP-PD method.

2. THEORY

The principle of measurement of velocity profile by the Ultrasound Velocity Profile (UVP) Monitor is explained in detail by Takeda (1-7) and is summarised in the Met-Flow users guide (8). The in-line methodology developed by Windhab and Ouriev (9-15) involving the measurement of UVP and pressure difference (PD) to obtain the shear rate dependent viscosity using rheological models is explained by these authors and is discussed briefly here (see Fig.1 for working principle). The instrument measures instantaneous spatial velocity distribution in a flowing suspension along the axis of an emitted Pulsed Ultrasound beam by measuring the Doppler shift in the frequency of the reflected ultrasound and time delay. Equations for the radial velocity profiles during the flow of shear thinning (or thicknening) and yield-stress suspensions in a pipe are presented below using respectively power-law and Herschel-Bulkley rheological models.

For laminar flow of a liquid of viscosity η in a pipe of radius R and length L, the variation with radius r in the shear stress is $\tau = r\Delta P / 2L$ (1)
in which ΔP is the pressure drop, the wall shear stress being $\tau_w = R\Delta P / 2L$. If v is the velocity at any radius r, then the shear rate $\dot{\gamma} = -dv/dr$ and shear viscosity $\eta = \tau / \dot{\gamma}$. Power-law and Herschel-Bulkley rheological models are considered below to obtain the radial velocity, shear rate and shear viscosity for shear thinning (or thickening) fluids with and without an yield stress respectively.

2.1 Power-law model

The variation in shear stress τ with the shear rate $\dot{\gamma}$ for a power-law liquid is $\tau = K\dot{\gamma}^n$ (2) where K is the consistency index and n is the power-law exponent. Eqs.(1) and (2) can be combined and integrated (assuming zero velocity at pipe wall) to give the radial velocity, shear rate and viscosity profiles :

$v = \left(nR/(1+n)\right)\left(R\Delta P/2LK\right)^{1/n}\left(1-(r/R)^{1+1/n}\right)$ (3); $\dot{\gamma} = \left(r\Delta P/2LK\right)^{1/n}$ (4)

$\eta = \tau/\dot{\gamma} = K\left(r\Delta P/2LK\right)^{1-1/n}$ (5). At the pipe wall, the shear rate and viscosity are given by $\dot{\gamma}_w = \left(R\Delta P/2LK\right)^{1/n}$ (6) and $\eta_w = \tau_w/\dot{\gamma}_w = K\left(R\Delta P/2LK\right)^{1-1/n}$ (7).

Although Power-law model predicts (Eq.(5)) an unrealistic infinite shear viscosity at the centre of the pipe for shear thinning liquids (n < 1), it predicts a realistic finite viscosity at the pipe wall. Eq.(3) can be used to obtain the volume flow rate :

$$Q = 2\pi\int_0^R vrdr = \frac{\pi nR^3}{(3n+1)}\left(\frac{R\Delta P}{2LK}\right)^{\frac{1}{n}} \qquad (8)$$

2.2 Herschel-Bulkley model

Some fluids behav like solids and do not flow until a critical yield stress τ_0 is exceeded. Application of stress is greater than the yield stress results in the formation of a moving plug in the centre of the pipe. For fluids with an yield stress and power-law behaviour above yield stress, Herschel Bulkley model can be used :

$\tau = \tau_0 + K\dot{\gamma}^n$ (9). This and Eq.(1) can be combined and integrated (assuming zero velocity at pipe wall) to give the radial velocity, shear rate and viscosity profiles :

$v = \left(n/(1+n)\right)\left(\Delta P/2LK\right)^{1/n}\left((R-R_*)^{1+1/n} - (r-R_*)^{1+1/n}\right)$ (10)

$\dot{\gamma} = \left(\Delta P/2LK\right)^{1/n}(r-R_*)^{1/n}$ (11); $\eta = \tau/\dot{\gamma} = K\left(\Delta P/2LK\right)^{1-1/n} r/(r-R_*)^{1/n}$ (12)

where $R_* = 2L\tau_0/\Delta P$ is the plug radius. At the pipe wall, the shear rate and viscosity are given by $\dot{\gamma}_w = \left(\Delta P/2LK\right)^{1/n}(R-R_*)^{1/n}$ (13)

and $\eta_w = \tau_w/\dot{\gamma}_w = K\left(\Delta P/2LK\right)^{1-1/n} R/(R-R_*)^{1/n}$ (14)

Herschel-Bulkley model also predicts (Eq.(12)) an unrealistic infinite shear viscosity at the centre of the pipe for both shear thinning and thickening liquids, it also predicts a realistic finite viscosity at the pipe wall.

$$Q = \pi v_* R_*^2 + \frac{\pi nR^2(R-R_*)^{1+1/n}}{(n+1)}\left(\frac{\Delta P}{2LK}\right)^{\frac{1}{n}}\left[1 - \frac{2n}{(3n+1)}\left(1-\frac{R_*}{R}\right)^2 - \frac{2nR_*}{(2n+1)R}\left(1-\frac{R_*}{R}\right) - \left(\frac{R_*}{R}\right)^2\right]$$

in which the plug velocity v_* can be obtained by setting $r = R_*$ in Eq.(10).

3. EXPERIMENTAL

3.1 Set-up

The present experimental set-up and procedure is described in detail by Wiklund and Johansson (2001) and is similar to that used by Ouriev (2000). However, a few relevant details are given here. The flow loop consists of a stainless steel tank with a propeller agitator, a positive displacement pump, a 23 mm diameter stainless steel pipe, a flow adapter made of a plastic composite PEEK30 fitted with a 1mm diameter 4 MHz frequency Ultrasound (U) Transducer in a 8 mm housing, a UVP Monitor (Met-Flow SA, Model UVP-X3-Psi, Switzerland), a Digital Oscilloscope (Yokogawa, Japan), two silicon diaphragm pressure sensors (PS), a PC for pressure and suspension weight data acquisition and a valve at the exit of the pipe to re-circulate the suspension.

3.2 Procedure

Prior to the flow experiments, a pulse of an ultrasound is generated in a measured sample of the suspension using a 4 MHz U transducer and UVP Monitor, the time difference for the reflected pulses being detected by the oscilloscope at two different vertical positions. The velocity of sound is then calculated using the distance between the two points measured by a digital height gauge (Tesa Brown and Sharpe SA, Switzerland). The tank is filled with the suspension, agitated mildly, the pump is set to the desired flow rate and the flow is allowed to attain the steady-state. The pressure difference in a pipe section of 1.16 m is measured by the PS connected to a PC (inverted manometer used for low pressure differences) which also simultaneously measures the weight of the suspension collected in a bucket put on a digital weighing balance in a given time. The Met-Flow UVP Monitor is triggered for measurement after setting the ultrasound parameters corresponding to the appropriate frequency and velocity of sound. Each raw velocity profile consists of Doppler frequency shift units at 128 points along the ultrasound beam, only less than about 30 points lying within the pipe diameter. 1024 such radial raw velocity profiles are recorded and stored on the hard disc of the in-built PC. These are then converted into velocity units along the pipe diameter allowing for the $20^{\mathbf{0}}$ angle of the ultrasound transducer with the normal to the pipe axis. Best velocity profiles are selected by comparing the measured volume flow rate with that obtained by integrating the velocity profiles. For comparison purposes, the shear rate dependent viscosties are measured using conventional off-line rotational rheometers such as Physica, ARES, Bohlin. Two industrial viscoelastic surfactant solutions and three cellulose fibres in water suspensions at three different weight percentages of fibres are investigated. However, off-line rheometers could not be used for fibre suspensions as fibres came out leaving mostly water in the cup.

4. RESULTS AND DISCUSSION

4.1 Surfactant solutions

The experimental (symbols) velocity profiles along the pipe diameter during the flow of viscoelastic surfactant (Shampoo AFi) solution (density ρ = 1022 kg/m^3, velocity of sound c = 1503 m/s) at different flow rates measured by the in-line UVP-PD method is shown in Fig.2. These are well represented by the theoretical profiles (curves) obtained by fitting the experimental data and pressure drop using the power-law model (Eq.(3)) with the values of constants n and K listed in the Table 1a. The flow is laminar since the maximum value of the

Reynolds number (Re_{max}) is less than 725 validating the use of the model equations. This is also true for shampoo XI (ρ = 1012 kg/m^3 , **c** = 1518 m/s) for which $Re_{max} < 253$.

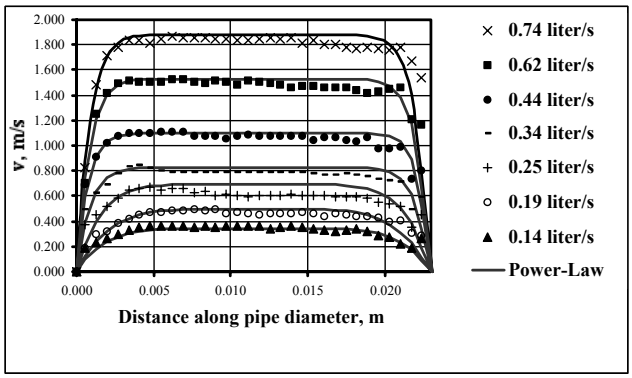

Fig.2. Experimental and Power-Law fitted velocity profiles for Shampoo AFi.

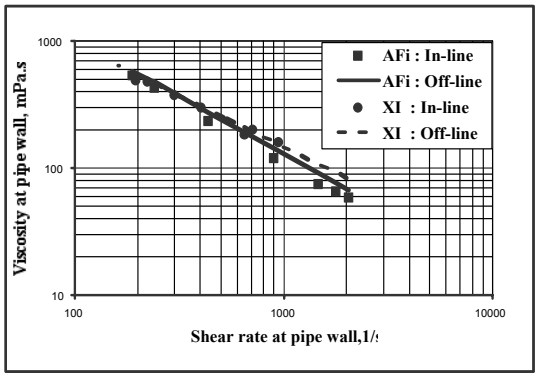

Fig.3. Shear rate dependent viscosities measured by in-line UVP-PD and off-line Physica rheometers.

Table 1. Power-Law model parameters obtained from experimental velocity profiles.

(a). Shampoo AFi

Flow rate, liter/s	Pressure drop, Pa	n	K
0.14	20680	0.19	37.7
0.19	20619	0.22	30.6
0.25	20500	0.16	38.3
0.34	21812	0.09	59.4
0.44	22330	0.07	66.0
0.62	23433	0.08	62.9
0.74	24012	0.09	60.9

(b). Shampoo XI

Flow rate, liter/s	Pressure drop, Pa	n	K
0.14	19499	0.28	22.4
0.19	21528	0.30	21.2
0.25	22495	0.28	22.6
0.33	24306	0.26	25.3
0.43	24033	0.19	33.9
0.61	29013	0.24	29.8
0.72	30870	0.19	41.1

The variation in the viscosity η_w with shear rate γ_w at the pipe wall obtained using the in-line UVP-PD method (symbols) and Eqs.(7) and (6) with the values of the power-law constants n and K for the data shown in Figure 2 and for shampoo XI, is shown in Figure 3. This agrees well with the variation in viscosity with shear rate measured by off-line Paar Physica MCR-300 rheometer are also shown by the full lines for AFi (n = 0.09, K = 69.4) and broken lines for XI (n = 0.19, K = 39.2) shampoos respectively, the off-line power-law constants corresponding to the whole range of shear rates encountered in the in-line experi-ments. Other off-line rheometers such as Rheometric Scientific ARES and Bohlin CS-50 are also used to measure the shear rate dependent viscosity. However, these could not be used at higher shear rates as the highly shear thinning shampoos started leaving the Couette geometry.

4.2 Aqueous cellulose fibre suspensions

Figure 4 shows the experimental (symbols) velocity profiles along the pipe diameter during the flow of 2% by weight of cellulose fibres in water suspension at different flow rates measured by the in-line UVP-PD method. Once again these are well represented by the theoretical curves obtained by fitting the experimental data and pressure drop using the power-law model (Eq.(3)) with the values of constants n and K listed in the figure. Similar agreement is obtained using Herschel-Bulkley model (eq.(10)). This is also true for cellulose

concentrations of 1% and 3%. The flow is once again laminar since the maximum value of the Reynolds number (Re_{max}) is less than 504 validating the use of the model equations.

Figure 5 shows the variation in the viscosity with the shear rate at the pipe wall obtained using the measured velocity profiles using Power-law (Filled symbols) and Herschel-Bulkley (open symbols) for 1%, 2% and 3 % cellulose in water. Both the models seem to predict about the same viscosity for a given shear rate at the pipe wall, the agreement between them depending on the accuracy of the plug radius R_* assumed. In general the cellulose fibre suspensions are shear thinning as indicated by the decrease in the viscosity at the pipe wall with the shear rate. The viscosity of 3% cellulose fibre suspension is about thrice that of the 1% suspension at low shear rates, the factor being about 2 at high shear rates. However, off-line rheometers could not be used to measure the shear rate dependent viscosity as the fibres got separated from the water in the suspension during measurement.

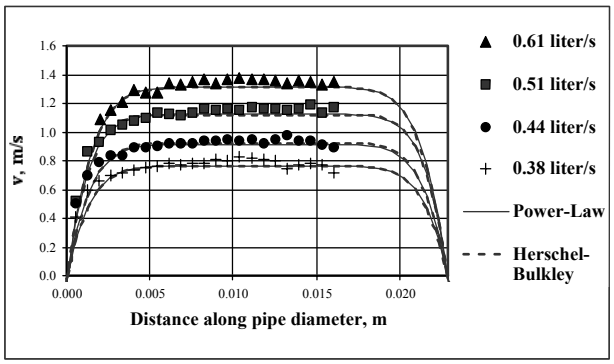

Fig.4. Experimental and fitted velocity profiles obtained by in-line UVP-PD method for 2% cellulose fibre in water suspension .

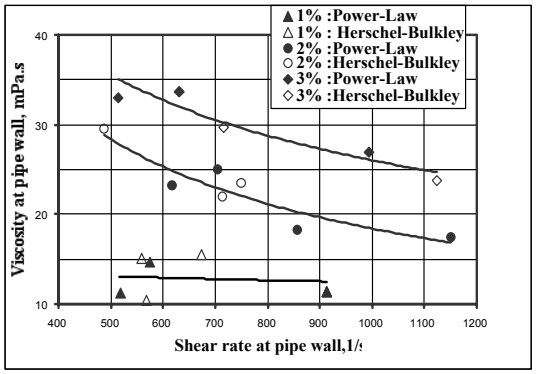

Fig.5. Variation in viscosity with shear rate at pipe wall determined by in-line UVP-PD method for different % cellulose fibre in water suspensions.

Table 2. Power-Law and Herschel-Bulkley model parameters obtained from experimental velocity profiles for 2% cellulose in water suspensions (ρ = 1000 kg/m^3 , **c** = 1502 m/s).

Flow rate, liter/s	Pressure drop, Pa	Power-Law n	K	Herschel-Bulkley n	K	R_* mm
0.38	2916	0.13	6.24	0.24	2.12	4
0.44	3164	0.13	6.49	0.24	2.10	4
0.51	3564	0.13	7.50	0.19	3.69	3
0.61	4076	0.14	7.50	0.27	2.19	4

For each of the measured velocity profiles in Figures 2 and 4, the shear rate decreases along the pipe diameter from a maximum value at the pipe wall to zero at the centre of the pipe. This corresponds to an increase in viscosity along the pipe diameter from a minimum value (corresponding to wall shear rate) to a constant maximum value at the centre of the pipe for the shear thinning Shampoo solution and cellulose in water suspensions. However, both Power-law and Herschel-Bulkley models predict an unrealistic infinite viscosity at the centre of the pipe where the shear rate is zero. The volume flow rates obtained by integrated velocity profiles represented by Power-law or Herschel-Bulkley model and pressure measurement by UVP-PD method has an error of 10 to 30% compared with those measured by the gravimetric method ; the error decreased with the flow rate as the accuracy of pressure drop measurement

increased. The accuracy also increased with the extent of shear thinning as reflected by the Shampoo solutions. The deviation could also be due to the fact that the consistency index K and exponent n may not be constant over the entire range of shear rates encountered along the radius of the pipe.

5. CONCLUSIONS

The in-line UVP-PD methodology developed by Windhab and Ouriev (9-15) using the Met-Flow UVP Monitor is successfully tested to obtain shear rate dependent viscosities of shear thinning viscoelastic surfactant shampoo solutions and aqueous cellulose fibre suspensions. These agreed well with those obtained using conventional off-line Paar Physica rheometer for shampoo solutions. The rheological behaviour of cellulose fibre suspensions could not be measured using the off-line rheometers due to compression and drainage of the sample, thereby making the in-line UVP-PD method as the only alternative method.

REFERENCES

1. **Takeda, Y.** (1985). *Fluid Control and Measurements*, 2-6 September, Proceedings, Tokyo.
2. **Takeda, Y.** (1986). *Int. J. Heat Fluid Flow*,7 (4), 313.
3. **Takeda, Y.** (1989). *Nuclear Eng.Design J.*, **126**, 277.
4. **Takeda, Y., Samec, K. & Kobayashi, K.** (1991). *Experimental & Numerical Flow Visualisation*, FED-Volume **128**, Book No. H00706.
5. **Takeda, Y.** (1995). *Experimental Thermal & Fluid Science*, **10**, 444.
6. **Takeda, Y.** (1997). *Proceedings USD1997: A seminar on flow measurements using ultrasound Doppler methods*.
7. **Takeda, Y.** (1999), *Experiments in Fluids,* **26**, 177.
8. **Met-Flow** (1996, 1999, 2000), *UVP Monitor : Models UVP-X3-PSi, UVP-XW*, Users Guide, Met-Flow SA, Lausanne, Switzerland.
9. **Windhab, E., Ouriev, B., Wagner, T. & Drost, M.** (1996). *Proceedings 1st International Symposium on Ultrasonic Doppler Methods for Fluid Mechanics and Fluid Engineering*, PSI, Villigen, Switzerland, 9-11 September.
10. **Ouriev, B.; Windhab, E.** (1996). *Tagungungsband-Fachtagung, VDI/GMA*, Düsseldorf, 1-2 February.
11. **Ouriev, B.; Windhab, E.** (1996). *Proc. 5th Int. Tagung zur Lebensmittelrheologie*, Granum Press, BFA Detmold.
12. **Ouriev, B.; Windhab, E.** (1997). Proc. 1st Int. Symposium on Food Rheology and Structure, ETH Zürich, 16-21 March ; Ed.: Windhab, E.; Wolf, B., Vincentz Verlag, Hannover, 378-384.
13. **Ouriev, B.; Windhab, E.** (1999). *Proc. 2nd Int. Symposium on Ultrasonic Doppler Methods for Fluid Mechanics and Fluid Engineering*, PSI, Villigen, Switzerland,

20-22 September.

14. **Ouriev, B.; Breitschuh, B.; Windhab, E.** (2000). *Colloid Journal*, **62** 234-240.
15. **Ouriev, B.** (2000). *Ph.D. Dissertation ETH No. 13523*, Swiss Federal Institute of Technology, Zürich.
16. **Wiklund, J. and Johansson, M.** (2001). *Master's Dissertataion*, Swiss Federal Institute of Technology (Zürich), Swedish Institute for Food and Biotechnology (Gothenburg), Chalmers University of Technology, May.
17. **Wiklund, J., Johansson, M., Shaik, J., Fischer, P., Windhab, E., Stading, M., Hermansson, A.M**. (2001). *Annual Transactions - The Nordic Rheology Society ,* **8/*9,*** 128-130, 2000/2001 *at The Nordic Rheology Conference,* Trondheim, 14-16 June.

APPLICATION OF ULTRASOUND DOPPLER VELOCIMETRY TO FLOWS OF HOT METALLIC MELTS

S. Eckert[1], G. Gerbeth[1], V.I.Melnikov[2], C.-H. Lefhalm[3], J. Knebel[3]

[1]Forschungszentrum Rossendorf, P.O.Box 510119, D-01314 Dresden, Germany, s.eckert@fz-rossendorf.de
[2]University Nishni-Novgorod, Minin street 24, 603 600 Nishni-Novgorod, Russia, melnikov@nntu.sci-nnov.ru
[3]Forschungszentrum Karlsruhe, P.O.Box 3640 , D-76021 Karlsruhe, Germany, lefhalm@iket.fzk.de

Keywords: ultrasonic Doppler velocimetry, acoustic wave guide, liquid metals, flow velocity measurement, two-phase flow, bubbles

ABSTRACT

During the last decades the Ultrasound Doppler Velocimetry (UDV) became a very powerful tool to measure the velocity structure of liquid flows. Because of the ability to work in opaque fluids and to deliver complete velocity profiles in real time it becomes very attractive for liquid metal applications. But, in case of hot metallic melts the user is confronted with a number of specific problems: First of all, the application of the ultrasonic transducers is usually restricted to maximum temperatures of 150°C. The transmission of a sufficient amount of ultrasonic energy from the transducer to the fluid has to be guaranteed. Here, the acoustic coupling and the wetting conditions have to be considered as important issues. Moreover, the flow has to be seeded with reflecting particles to obtain Doppler signals from the fluid.

The feasibility of velocity profile measurements by UDV has already been demonstrated for low temperature liquid metals as mercury (Takeda, 1987) and gallium (Brito et al., 2001). Now, first successful measurements in liquid sodium at 150°C are published by Eckert & Gerbeth (2002). We will present mean profiles of a sodium flow in a rectangular duct exposed to an external, transverse magnetic field. To demonstrate the capability of UDV the transformation of a well-known turbulent, piston-like profile to a M-shaped velocity profile with growing magnetic field strength was observed.

An integrated ultrasonic sensor with acoustic wave guide has been developed to overcome the limitation of ultrasonic transducers to temperatures lower than 200°C. This sensor can presently be applied at maximum temperatures up to 600°C, but an extension up to 800°C can reasonably be expected. In this presentation we show some experimental results obtained in flows with eutectic PbBi at temperatures up to 350°C and in a CuSn alloy up to 620°C.

US frequency	4 MHz
Doppler angle	70°
Pulse repetition rate	6700 Hz
Measurable depth	175 mm
Bursts per profile	128
Velocity resolution	9 mm/s
Number of gates	140
Number of profiles	256
Spatial resolution in sodium	1.25 mm

Table 1. Set of system parameters adjusted in the sodium experiment

1. VELOCITY MEASUREMENTS IN LIQUID SODIUM

1.1 Experimental set-up

To demonstrate the capabilities of the UDV technique with respect to the applicability for sodium flows, we determined velocity profiles of a MHD channel flow exposed to a homogeneous, transverse magnetic field. We will give here a brief summary of our measurements and refer the reader to Eckert & Gerbeth (2002) for further details.

The experiments were performed at the sodium loop, NATAN, of Forschungszentrum Rossendorf (FZR). The facility operates with a sodium flow in the temperature range between 120°C and 350°C. An electromagnetic pump is used to generate the mean flow with maximum velocities of about 1.7 m/s in a square test section of 44 × 44 mm^2. The horizontal test section is equipped with a homogeneous transverse magnetic field over a length of 1100 mm. For all variations of the magnetic field strength the liquid flow rate was kept constant.

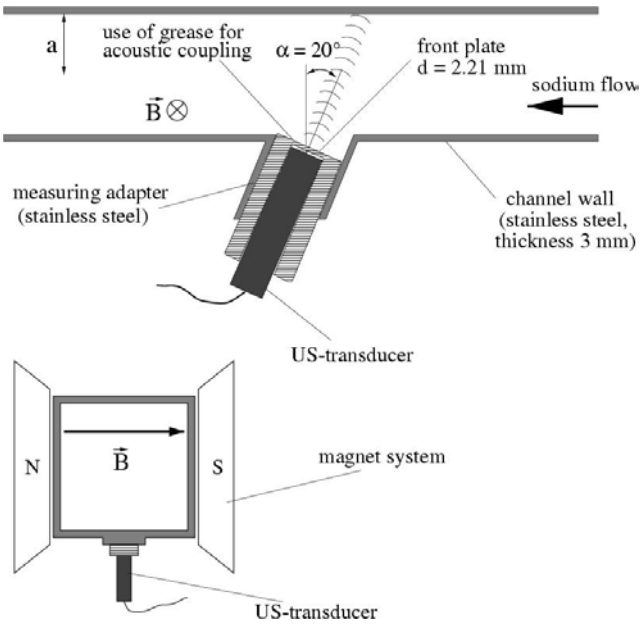

Figure 1. Schematic view of the arrangement of the sodium experiment at FZR

The velocity profiles were measured in the direction perpendicular to the magnetic field lines. As shown in Figure 1 the US transducer was installed inside a cylindrical measuring adapter with an angle of 70 ° with respect to the mean flow parallel to the channel axis. Silicon grease was used to achieve the acoustic coupling between US transducer and the adapter wall. The front plate of the adapter is machined stainless steel with a thickness of 2.21 mm. To guarantee a sufficient transmission of US energy into the flow, the adapter surface must be well wetted by the liquid sodium. For this reason both sides of the adapter front plate were polished. The outer surface that would be in direct contact with the liquid metal was cleaned using phosphoric acid.

The DOP2000 (Signal Processing Lausanne) was used to carry out the velocity measurements. The US transducers are 4 MHz probes of a high temperature series (TR40405). The application range for this transducer is limited to maximum temperatures of 150°C (long term load) and 200°C (short term load), respectively. The measurements were performed at sodium temperatures of 145°C which was carefully controlled by a thermocouple in the vicinity of the measuring domain. The parameter sound velocity was

corrected according to the actual value of the temperature. Taking into account temperature fluctuations of about ± 1 K the resulting uncertainties in the determination of the measuring depth due to the corresponding sound velocity modifications were about 0.1 mm.

The device parameter configuration used in the experiments is shown in Table 1. The mean velocity profiles were calculated averaging 256 single profiles corresponding to a measuring time of about 5.6 s.

1.2 Results of the velocity measurements

Two examples of velocity profiles measured with and without magnetic field, respectively, are displayed in Figure 2. The effect of the magnetic field on the flow structure can be clearly detected. However, the occurrence of some artefacts becomes obvious:

An inherent shortcoming of the UDV is the ringing effect of the US transducer that follows immediately after the emission of the pulse. It results in a saturation of the transducer preventing reliable measurements at depths just a few mm behind the surface of the transducer. In the present case additional perturbations arise by the influence of the adapter front wall because the US waves travelling also inside this wall contribute to the saturation of the piezoelectric element.

At a depth of 44 mm corresponding to the location of the opposite channel wall we do not find the velocity going to zero. Multiple reflections in the vicinity of the channel wall are considered to be the reason for this artefact. Because of this bias the velocity profiles have been truncated. The maximum negative velocity gradient measured in the boundary layer was chosen as criterion for truncation.

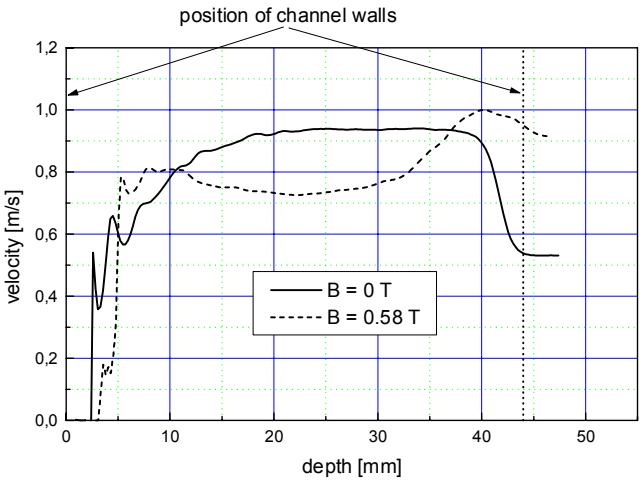

Figure 2. Measured raw profiles of the velocity of the sodium duct flow with and without applied transverse magnetic field

Figure 3 shows mean velocity profiles of the sodium duct flow obtained at a Reynolds number of about 56700 for variations of the Hartmann number, i.e. the magnetic field strength. In the case without magnetic field a velocity profile as known for turbulent channel flows was detected. A significant modification of the velocity structure can be observed if the flow is exposed to the transverse magnetic field. In the end regions of the pole faces the resulting electromagnetic force is not homogeneous in the cross-sectional area leading to a M-shaped profile of the velocity [4]. The development of such a M-shaped profile with increasing magnetic field can be clearly observed in Figure 3.

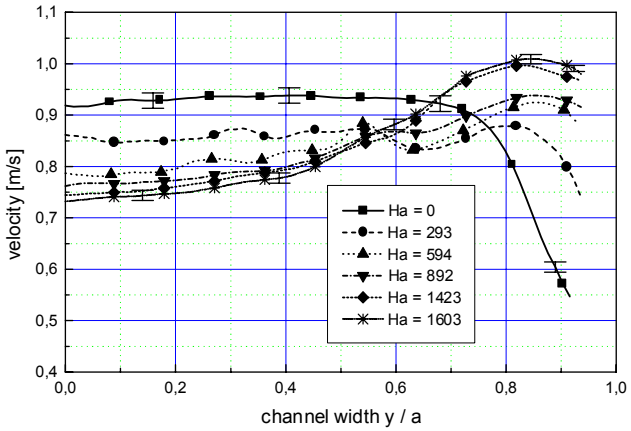

Figure 3. Effect of a transverse magnetic field on the mean velocity profiles in a turbulent sodium duct flow

2. VELOCITY MEASUREMENTS BY MEANS OF AN ULTRASONIC SENSOR WITH INTEGRATED ACOUSTIC WAVE GUIDE

2.1 Sensor concept

To overcome the thermal restrictions of the existing US transducer an integrated ultrasonic probe consisting on a wave guide and a piezoelectric transducer equipped with electronic components and a stainless steel housing was developed by the University of Nishni-Novgorod in collaboration with FZR (see Fig. 4). The acoustic wave guide is fabricated from a stainless steel foil with a thickness of 0.1 mm and a length of 200 mm which is wrapped axially around a capillary tube. The wave guide has an outer diameter of 7.5 mm. The wave guide was closed at the front end by means of laser beam welding. The piezoelectric element is welded directly on the rear end of the wave guide. The working frequency of the ultrasonic transducer is 4 MHz.

2.2 PbBi-channel flow

The THESYS loop of the KALLA laboratory of the Forschungszentrum Karlsruhe (FZK) focuses on the development and application of fundamental lead-bismuth technologies. At the THESYS loop velocity profiles of a eutectic PbBi flow (Pb44Bi56, T_{melt} = 125°C) in a round tube (∅ 60 mm) were successfully obtained by means of the integrated sensor. As shown in Fig. 5 the sensor is installed in a measuring port with an inclination of 45° with respect to the tube axis. The front end of the acoustic wave guide was in direct contact with the flow.

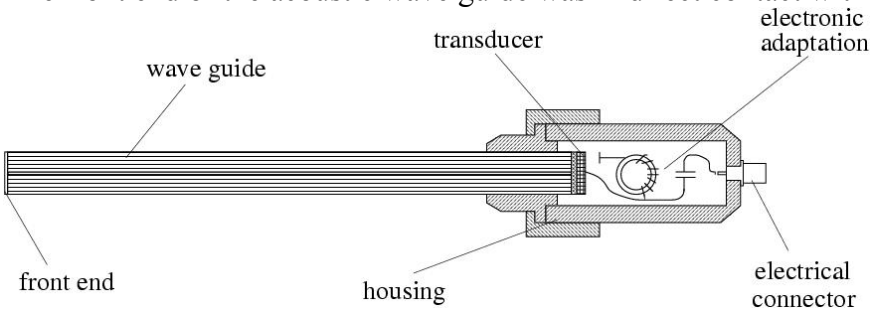

Figure 4. Schematic view of the integrated ultrasonic transducer

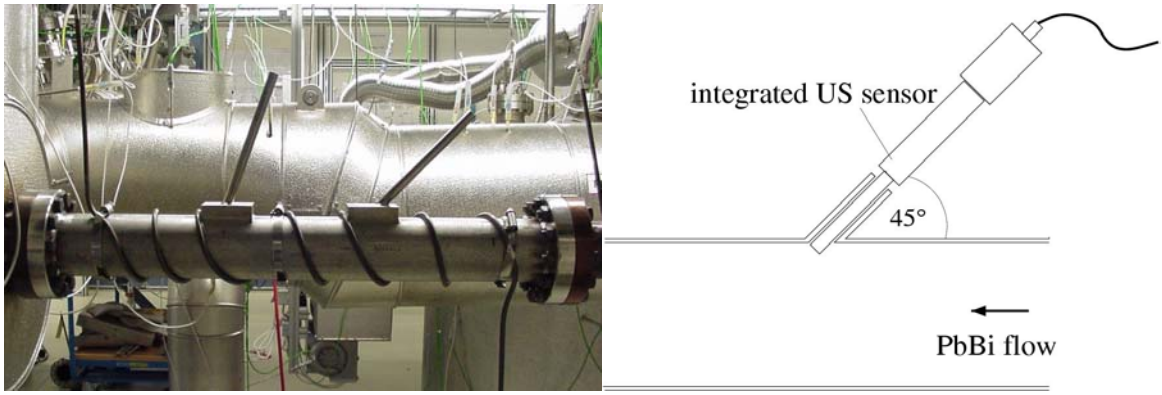

Figure 5. Schematic view of the arrangement of the PbBi experiment at FZK

Stable velocity signals could be received during a period of about 72 hours at temperatures between 180°C and 350°C. Velocity profiles have been obtained at different temperatures for variations of the liquid flow rate (see Fig. 6).

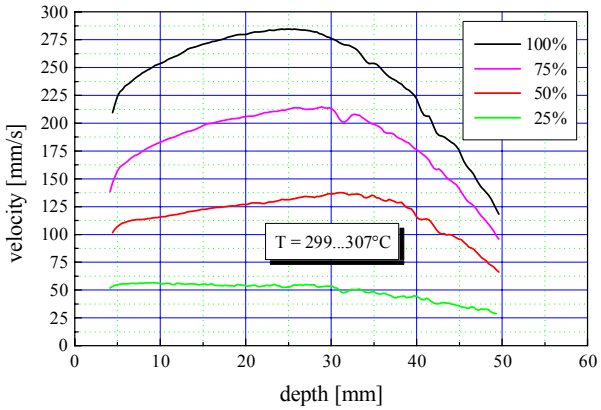

Figure 6. Measuring results obtained at temperatures of about 300°C for variations of the liquid flow rate (parameter: power of the electromagnetic pump)

2.3 Measurements in CuSn

Another demonstration was done in a flow of a CuSn alloy (Cu35Sn65, T_{melt} = 550°C) at a temperature of about 620°C. The liquid metal was molten inside a rectangular alumina crucible (130 × 80 mm^2) by means of an inductive heating system. The depth of the melt was about 40 mm. The melt temperature was controlled using a bolometer. As shown in Fig. 7 the integrated sensor was dipped into the metallic alloy through the free surface with an angle of 35° with respect to the horizontal line. A mechanical stirrer was used to generate a flow.

Results obtained from this experiment are shown in Fig. 8. The velocity profiles determined at both measuring positions are similar with respect to the shape and the amplitude and show different signs in accordance with the chosen rotation direction of the mechanical stirrer. Several repetitions of the measurements showed the reproducibility of the results.

3. CONCLUSIONS

It has been demonstrated that UDV can be used successfully to determine velocity profiles in metallic melts at high temperatures up to 600°C. The application of acoustic wave guides is shown as a promising way to overcome the thermal restriction of US transducers.

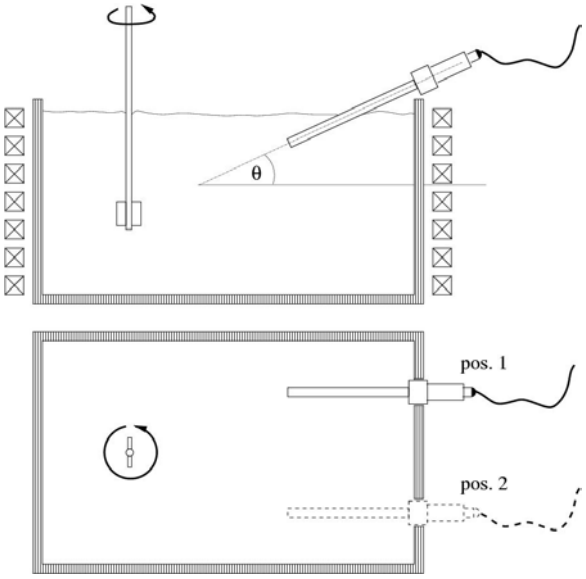

Figure 7. Schematic view of the arrangement of the CuSn experiment at FZR

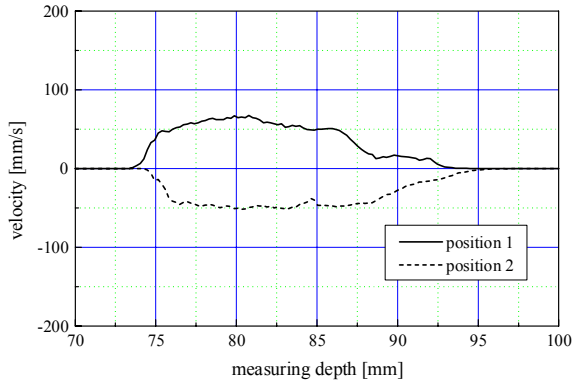

Figure 8. Velocity profile measured in the CuSn melt at both sensor positions

The developed integrated sensor delivered clear signals leading to reproducible results. This approach may open a new field for applications of UDV. On the other hand, with UDV a powerful measuring technique could be available for investigations of the velocity structure in liquid metals improving the poor situation for such kind of opaque fluids. However, besides the high temperatures some other problems have to be taken into consideration for liquid metal applications such as the wetting problem, the handling of the oxide layers or chemical reactions between the wave guide material and the metallic melt.

REFERENCES

Brito D., Nataf H.-C., Cardin, Aubert J., Masson J.P. (2001). *Ultrasonic Doppler Velocimetry in liquid gallium*, Exp. Fluids 31: 653-663

Eckert S., Gerbeth G. (2002). *Velocity measurements in liquid sodium by means of ultrasound Doppler velocimetry*, Exp. Fluids 32: 542-546

Moreau R. (1990). *Magnetohydrodynamics,* Kluwer Academic Publisher, Dordrecht

Takeda Y. (1987). *Measurement of velocity profile of mercury flow by ultrasound Doppler shift method,* Nucl. Techn. 79: 120-124

2D TIME AVERAGED FLOW MAPPING OF DIE ENTRY IN FLOW OF HIGHLY CONCENTRATED SHEAR-THINNING AND SHEAR-THICKENING SUSPENSIONS

Boris Ouriev (Ur'ev)

Bühler AG, Uzwil, CH-9244, Switzerland, e-mail: boris.ouriev@buhlergroup.com

Keywords: Channel flow; Fluid flow; Two-dimensional flow map; Non-Newtonian fluid; Concentrated suspension; Elongation flow; Die entry; Shear-thickening; Shear-thinning; Ultrasound Doppler

ABSTRACT

In this work a methodology for high-resolution time averaged 2D flow mapping (e.g. Takeda, 1999) of converging flows was explored. Flow of non-transparent, highly concentrated shear-thinning and shear-thickening suspensions was circulating through the entrance flow adapter with the adjustable position of the die entry. The entrance region was scanned with the distance resolution of 2.7 x 1 mm, radial to axial displacement respectively. Time averaged flow map was composed from 1D flow profiles measured along the ultrasonic sensor beam using Ultrasonic Pulsed Echo Doppler technique (UVP product of Met-Flow SA, e.g. Takeda 1986, 1991, 1995). Priory to die entry visualization an investigation of flow properties was performed using a novel in-line non-invasive measuring technique. The method is based on combination of the UVP velocity monitoring and pressure difference (PD) method (e.g. Windhab et. al., 1996 and Ouriev, 2000, Ouriev et. al. 1995, 1998, 1999, 2002). The rheological flow properties were derived from simultaneous recording and on-line analysis of the velocity profiles across the tube channel and related radial shear stress profiles calculated from the pressure loss along the flow channel. Comparison between flow of mentioned above model suspensions was qualitatively analyzed. For the first time the flow divergence of shear-thickening suspension could be visualized. From comparison between entrance flow of viscous shear-thinning and shear-thickening suspensions a strong viscoelastisity of shear-thickening suspensions in elongation flow has been proposed. This method opens an opportunity of precise flow mapping of viscoelastic and viscous, non-transparent and highly concentrated fluids. This is important for industrial type of fluid processing machinery, where characteristics of elongation flow (flow geometry) has global impact on quality of fluid processing.

1. INTRODUCTION

Highly concentrated suspensions play important technological role in various branches of industry as food, chemistry, pharmaceutics, cosmetics, ceramics, paper and etc. Traditionally, knowledge gained in rheological studies using off-line rheometers is transferred to "real" flow situations in different types of flow processes. According to study of Uriev (1980, 1988, 1992) a close relationship between rheology, microstructure and fluid macro properties can be drawn (e.g. Windhab, 1986). In that contact in-line rheological measurement of suspensions flow become one of first priority solutions on the way to improved process control especially if elongation type of flow is concern.

In present work the advantages of relatively small ultrasound and pressure sensor dimensions and the ability of ultrasound to propagate through the solid walls and opaque fluids was used.

A detailed study of model suspensions in pressure driven and drag shear flows was performed priory 2D flow mapping. The flow behaviour of shear-thinning and shear-thickening model suspensions was analyzed in drag shear experiments using rotational rheometer and pressure driven shear flows using UVP-PD technique (e.g. Ouriev, 2000). From such experiments a variety of rheological and flow information was derived and used for further comparison between pressure driven and drag shear flows of highly concentrated suspensions.

2. EXPERIMENTAL SET-UP AND INSTRUMENTATION

Using a time averaged flow mapping the flow of shear-thinning and shear-thickening suspensions through a cylindrical contraction was investigated. In Fig. 1 a schematic of the setup to investigate the entrance region is illustrated. It consists of two basic components for pressure measurement and velocity visualization. The geometry is equipped with micro-pressure transducers for direct pressure measurement of the steady state flow in the upstream section. At the walls of the upstream tube the two UVP transducers were installed opposite to each other. Note that y-axis denotes here the radial direction across the measuring cell and x-axis denotes the flow direction, along the measuring cell axis. Thus, V_y denotes the velocity in radial direction and V_x is the velocity in flow direction. The velocity profiles were obtained along the measuring line Pm of the ultrasonic sensor (see Fig. 1 and Table 1).

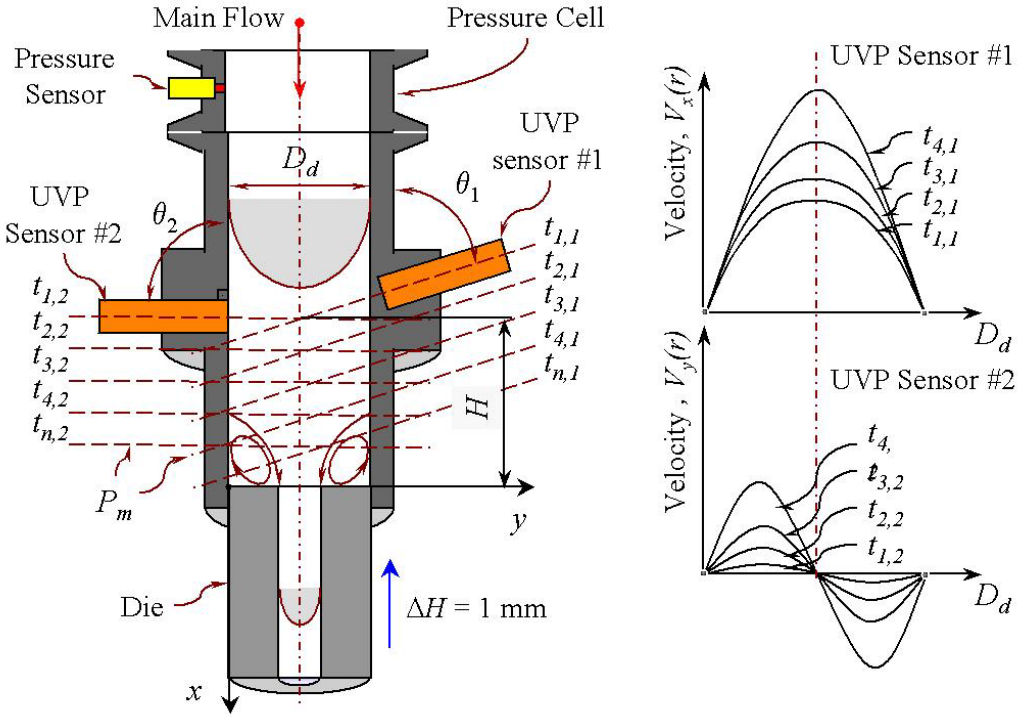

Fig. 1: Schematics of measuring cell and illustration of measuring procedure for 2D velocity mapping of converging flow.

The radial velocity $V_y\,(P_m)$ was measured using UVP sensor #2 and velocity profiles $V_x\,(P_m)$ in flow direction were obtained with UVP sensor #1 (see Fig. 1), where D_d is diameter of upstream section. For conversion of the velocity in flow direction, the results obtained from sensor #1 was multiplied by a factor of $1/\cos\theta$, where θ is the Doppler angle. The absolute velocity was not corrected if measured with the UVP sensor #2. In this case the Doppler angle is $\theta_2 = 90°$ ($1/\cos\theta_2 = 1$). The dimensions of the flow adapter $D_d = 23$ mm and $D_{DIE} = 4$, 6 and 8 mm, where D_{DIE} is die diameter. Consequently, the ratio between die diameter and inner diameter of the upstream tube varied between 2.87 and 5.27.

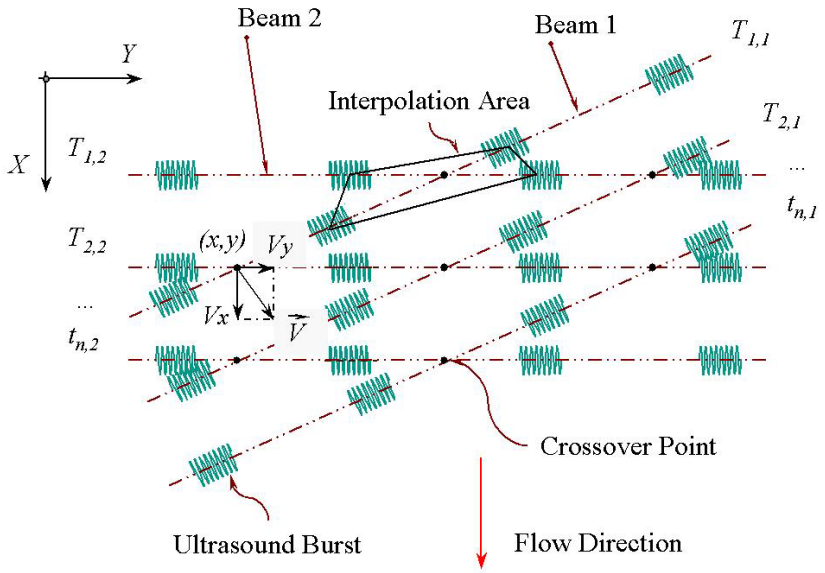

Fig. 2: Principle of 2D time averaged flow mapping.

Since the ultrasonic transducers have a direct contact to the fluid sample. The location of the sensor front was optimized in order to avoid a disturbance of the flow field around the sensor front. As shown in Fig. 1, the die entry was moved from the lowest position upper position H in steps of $\Delta H = 1$ [mm]. As shown in Fig. 2, time averaged flow map was obtained from the crossings of the ultrasonic beams of both UVP sensors. As already mentioned, the starting point of the scanning procedure was at the lowest die entry position (see Table 1). This sensor was installed with the Doppler angle $\theta_2 = 90°$ and was used for recording velocities in the radial direction $V_y(P_m) \equiv V_y(D_d)$. The dimensions of the sensor housing limited the minimum distance between the die entry and the UVP sensor #2. Having a sensor diameter of 8 mm, the shortest distance between the center of the acoustic beam and the die entry was 4 mm. The velocity in flow direction was visualized using UVP sensor #1 which was installed with an incline of $\theta_1 = 70°$ (Doppler angle) to the flow direction of the mainstream.

Table 1: Dimensions of the measuring cell

Parameter	[mm]	*Comments*
L_{DIE}	30	Length of the die
D_{DIE}	4, 6 and 8	Inner diameter of the die
D	23	Inner diameter of the upstream flow channel
θ_1	70	Doppler angle of UVP sensor #1
θ_2	90	Doppler angle of UVP sensor #2
H_{max}	70	Maximum distance between die entry and center of the UVP sensor #2
H_{min}	4 to 5	Minimal distance between die entry and center of the UVP sensor #2

As already mentioned above, priory to entrance flow velocity mapping a reference measurement of the steady pressure driven shear flow velocity profile was obtained. The aim

of this measurement is to obtain an averaged velocity profile for further evaluation of the profile shape symmetry around the tube axis and calculation of the volumetric flow rate Q_{UVP}. This was performed simultaneously with the pressure sensor calibration. As mentioned above, priory 2D flow visualization, the concept of the UVP-PD measuring technique was used beside volumetric flow rate measurement. The shear viscosity function, wall slip velocity and yield value. Detailed description of UVP-PD technique is given in work of Ouriev (2000).

The following methodology was applied for measurement and computation of the entrance flow for highly concentrated suspensions.

- Measurement of time averaged velocity profiles $V_x\,(P_m)$ and $V_y\,(P_m)$.
- Control of boundary flow conditions using instantaneous pressure and velocity information
- Volumetric flow rate computation from the velocity profile $V_x\,(P_m)$ of laminar pressure driven shear flow at maximum distance H. The result of this measurement was compared with the reference volume flow rate calculated from measured online mass flow rate and the sample's density.
- Calculation of time averaged flow map of entrance flow.

In present work only 8 mm diameter die is considered. Detailed discussion of experiments with 4 and 6 mm dies is given in work of Ouriev (2000).

3. MATERIALS

General information about shear-thinning and shear-thickening suspensions chosen for flow mapping is summarized in Table 2. The following parameters were chosen for characterization of the suspension sample: concentration of solids φ_{Sl} (by weight), shear viscosity at upper Newtonian plateau η_∞, maximum flow velocity Vy_{MAX} and volumetric flow rate Q_{UVP}.

Table 2: Highly concentrated suspensions of native cornstarch in Newtonian fluid matrix used in flow mapping experiment (T = 25°C ± 0.1°C).

Suspension	D_{DIE} [mm]	φ_{Sl} [%w]	η_∞ [mPas]	Re [-]	Vy_{MAX} [mm/sec]	Q_{UVP} [1] [l/h]
* Shear-thinning	8	40	51.4	192.76	543	590.8
* Shear-thickening			159.4	60.61	690.74	558.5

* Both suspensions consist of Newtonian fluid matrix of equal shear viscosity level, $\eta = 10$ *[mPas]*.

[1] For shear-thickening suspensions the volumetric flow rate is corrected with the wall slip velocity using UVP-PD method.

Flow of suspension sample was stationary and developed throughout the scanning procedure. Such flow conditions were controlled by means of Standard Mean Deviation (*SMD*) of absolute flow velocity and absolute pressure signals (e.g. Ouriev 2000).

According to observations described in work of Ouriev (2000), fully developed pressure driven shear flow of shear-thickening suspensions shows a strong effect of dilatancy at solids concentration above 30 %w. In this case the flow is accompanied by slip of the suspension

sample at the tube wall. Therefore a correction of volumetric flow rate was performed beside wall shear rate and finally viscosity slip correction (see Table 2).

4. RESULTS

4.1 2D Flow Mapping of highly concentrated suspensions

The flow map was obtained from the velocity vectors located in crossing points of two grid systems (see Fig. 2). One grid is based upon time-space positions of UVP sensor #2 beam.

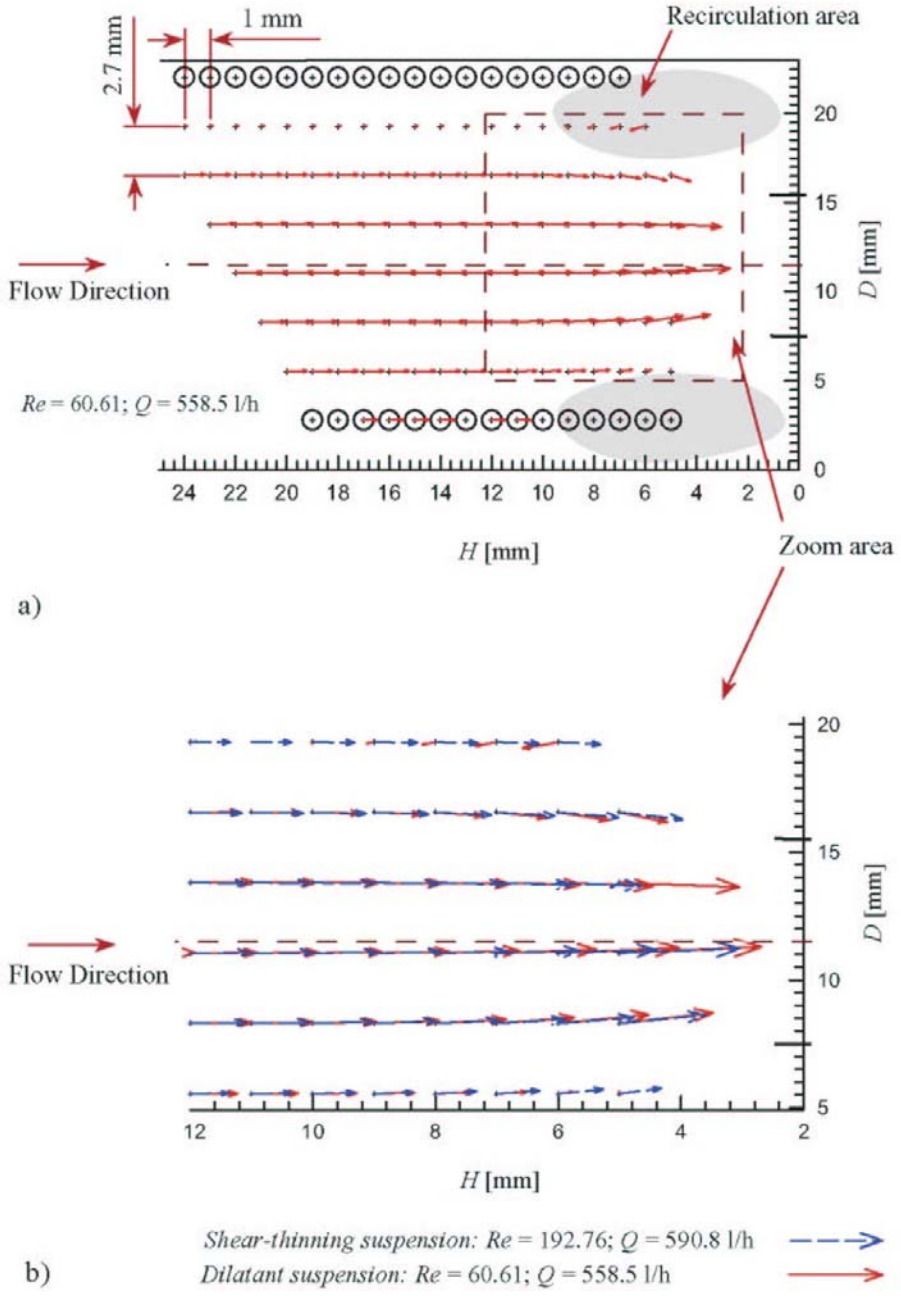

Fig. 3: Velocity map of the converging flow approaching a 8 mm die: a) flow map of shear-thickening suspension of starch φ_S = 40 % in GlS50; b) comparison between flow maps of shear-thinning (starch φ_S = 40 %w suspended in AK10) and shear-thickening (starch φ_S = 40 %w in GlS 50) suspensions.

1D velocity profiles were recorded along the ultrasound beam, P_m, at different axial positions H with displacement ΔH kept within 1 ± 0.015 mm (see Fig. 1 and Fig. 2). The second grid is obtained from displacement of the UVP sensor #1 beam inclined to the mainstream direction. The detailed information about the scanning procedure and grid design is given in work of Ouriev (2000).

The results of time averaged flow mapping are shown in Fig. 3a, a 2D-flow map of the shear-thickening suspension of 40 %w starch in GlS50 is shown. The comparison between the flow maps is illustrated in the enlarged Fig. 3b.

According to observations of Boger (1987), the vortex growth for shear-thinning fluids increases with increase of sample elasticity at given volumetric flow rate. For shear-thinning suspension, which is treated as viscous fluid, no secondary flow area (vortex) was observed. Contrarily to shear-thinning suspensions, shear-thickening suspensions showed large secondary flow area (see Fig. 3). Such increase of vortex at low *Re* and higher viscosity level (see Table 2) in comparison with shear-thinning suspension points appearance of viscoelastic properties of shear-thickening suspension in elongation flow.

According to comparison between shear-thinning and shear-thickening suspensions shown in Fig. 3b, it is noticed that the centerline velocity is higher for the shear-thickening suspension compared to the shear-thinning suspension, though the volumetric flow rate of shear-thinning suspension slightly larger compare to the shear-thickening suspension (see Table 2). The flow patterns shows a broader vortex boundary in case of shear-thinning suspension compare to the flow pattern of shear-thickening suspension. Likewise, the first sign of the vortex boundary is located at a distance of 9 mm above the die entry for shear-thickening suspension. No secondary flow regime was found down to the scanning area limit at 5 mm above the die entry in flow of shear-thinning suspensions.

5. CONCLUSIONS

From the results of introduced UVP 2D flow mapping the following advantages and disadvantages are concluded.

- Method works in Non-transparent and highly concentrated fluids of non-Newtonian type.
- High-resolution flow map was generated. In present work the dimensions of the mash elements reduced to 2.7 x 1 mm area (see Fig. 3) at given UVP sensor housing of 8 mm in diameter.
- Applicable to small channel dimensions of any geometry has been successfully tested.
- SMD (Standard Mean Deviation) of time averaged flow velocity profiles was used for control of flow conditions.
- Introduced scanning procedure assume stationary and developed flow. Pulsating flow can not be measured.
- Lost of velocity information close to the pipe walls due to the UVP starting depth restrictions (e.g. Ouriev 2000).
- Acoustic dissipation by means of strong scattering of ultrasound energy reduces velocity information which can be used for flow mapping. Lost of velocity data close to the opposite to UVP sensor location wall.
- Area of the secondary flow (Vortexes) could not be measured due to limitation of the lowest position above the die entry.
- Limitation of the maximum measurable velocity Vx_{MAX}. An overflow of velocity data at UVP Monitor could be observed due to exponential increase of Vx_{MAX} while approaching die entry.

Introduced technique could find a wide application field in industrial processes as: mixing, pipe transport, extrusion and etc., where extensional flows are dominating and desired to be characterized and controlled. It would be also of advantage to improve this technique and to step in real time flow mapping besides solving mentioned above disadvantages. In contrast to time averaged flow mapping where only stationary and developed flows can be considered; the real time flow mapping will be of advantage if non-stationary, pulsating flows must be investigated.

The results of fundamental research on model highly concentrated suspensions gave a sufficient background for further development of the UVP based in-line rheometry for industrial applications at Bühler AG.

6. ACKNOWLEDGMENTS

The author wishes to thank Prof. Windhab and Prof. Takeda, ETH LMVT workshop and Mr. Gogniat for their help.

7. REFERENCES

Ouriev, B., (2000) Ultrasound Doppler Based In-line Rheometry of Highly Concentrated Suspensions. PhD Thesis, ISBN: 3-905609-11-8, Zurich.

Ouriev, B., Koller, S., Korvink. J., Baltes, H., Windhab, E., (1995) On-Line Rheometry with Microsensors. ETH ILW-VT and ETH PEL Report, Zurich

Ouriev, B., Windhab, E., (1998) In-line rheological measurements and flow visualization using Doppler ultrasound method. 5th Europ. Rheo. Conf., Ljublijana, Slovenia

Ouriev, B., Windhab, E., (1998) On-line rheological measurements and process monitoring with flow visualization of non-transparent highly concentrated multiphase systems using Doppler ultrasound method. Intern. Conf. on Colloid Chem. and Phys.-Chem. Mechanics, Moscow, Russia

Ouriev, B., Windhab, E., (1999) Rheological Investigation of Concentrated Suspensions using a Novel In-line Doppler Ultrasound Method. Colloid Journal, Vol. 62 (2)

Ouriev, B., Windhab, E., (2002) Experiments in Fluids, Vol. 32, p. 204

Takeda, Y., (1986) Int. J. Heat Fluid Flow, Vol. 7, p. 313.

Takeda, Y., (1986) Velocity Profile Measurement by Ultrasound Doppler Shift Method. Int. J. Heat Fluid Flow 7 (4): 313.

Takeda, Y., (1991) Development of an Ultrasound Velocity Profile Monitor. Nuclear Engineering and Design 126 (2): 277-284.

Takeda, Y., (1995) Experimental Thermal and Fluid Science J., Vol. 10, no. 4, 444-453.

Takeda, Y., (1995) International Journal Series B-Fluids and Thermal Engineering, Vol. 38, no. 1, p. 8.

Takeda, Y., J., (1999) Experiments in Fluids, Vol. 26, no. 3, p. 177.

Uriev, N.B., (1980) Highly concentrated disperse systems, Khimiya, Moscow, p. 320

Uriev, N.B., (1980) Dynamics of structure of concentrated disperse systems. Physico-chemical mechanics and leofilic properties of dispers systems, Naukova Dumka, Kiev, pp. 3-12

Uriev, N.B., (1988) Physico-chemical Fundamentals of the Technology of Disperse Systems and Materials, Khimiya, Moscow, p. 256

Uriev, N.B., (1992). Structure, rheology and stability of concentrated disperse systems under dynamic conditions. J. of Colloids and Surfaces, 87, pages 1-4.

Windhab, E., (1986) Untersuchungen zum rheologischen Verhalten konzentrierter Suspensionen. Thesis VDI,

Windhab, E., Ouriev B; Wagner T; Drost M (1996) Rheological study of non-Newtonian fluids. 1st Inter. Symp. on Ultrasonic Doppler Methods for Fluid Mechanics and Fluid Engineering, PSI Villigen, Switzerland

ULTRASONIC VELOCITY PROFILER UVP-XW FOR ICE-SLURRY FLOW CHARACTERISATION

D. Vuarnoz, O. Sari , P.W. Egolf, H. Liardon

University of Applied Sciences of Western Switzerland
CH-1401 Yverdon-les-Bains, Switzerland

ABSTRACT

To analyse flows and to determine the flow patterns the investigation of velocity profiles can lead to valuable informations. For example, they can be on the rheological nature of the fluid or on the type of flow (laminar, transitional or turbulent flow). Ice slurries consist of suspensions containing a large number of small ice particles. They yield a pumpable ice for environmentally friendly cooling purposes in research and industrial applications. From their velocity profiles, which show a plug, the rheogram can be constructed. The results compare well with the measured data, obtained by applying an Ostwald rheometer. Two UVP sensors were placed on a rectangular horizontal channel to measure the downstream velocity component in the horizontal and the vertical direction and to investigate deviations, caused by a variation of the mass flow and the buoyancy force acting on the ice crystals. Furthermore, the influence of an additional heat transfer (with a constant heat flux) in a horizontal heat exchanger on the horizontal temperature and velocity profiles was investigated. When the heat transfer rates are increased, higher degrees of asymmetry of the velocity and temperature profiles are observed.

1. INTRODUCTION

At present multifunctional fluids are developed, which show very high energy densities. They are applied for storage and transportation of thermal energy. At high solid particle fractions of 25 to 40 mass % their energy density and viscosity is high. The first is advantageous and the second a drawback. If both effects are taken into consideration - compared to conventional brines - approximately five to thirty times improved transport fluids are obtained. Usually they are mixtures of a heat transfer fluid (e.g. glycol, water, etc.) with a storage material (e.g. paraffin wax, salt hydrates, or ice (in the case of ice-slurries), etc., which is finely dispersed in the carrier fluid. These new fluids define multi-component and multi-phase suspensions, which are named *Phase Change Slurries (PCS)* [1]. An important subgroup of this class of fluids are the *Ice Slurries.* Usually they are generated by a mechanical-scraper type ice generator. A commercially available type (also used in our laboratory) creates particles of ellipsoidal shape, the largest diameter is approximately 300 μm and the width to length ratio 0.7 [2].

In the flow at least two forces act on the ice particles. Viscous forces are transferring kinetic energy from the ice particles motion to the carrier fluid by friction and the density difference between the ice and the fluid leads to buoyancy forces, described by Archimede's law. The buoyancy force may separate the components of the fluid and, therefore, lead to additional complexities of the flow and thermodynamic behaviour. This implies the occurrence of different flow patterns. Flow pattern diagrams are constructed, which show in which domain of a parameter space, what kind of flow pattern occurs. These are mainly homogeneous, heterogenous, moving-bed, and stationary-bed flow (see e.g. [3]).

Numerous of these multiphase fluids are opaque in respect to an optical observation. Measurements of velocity profiles with Pitot tube sondes are extremely difficult to apply and even completely fail in the case of moving and stationary bed flows (see Kitanovski et al. [3]), and Kawaji et al [4]). Numerous other techniques also have their disadvantages or even failings, but such cannot be discussed here. The ultrasonic Doppler Echography method permits to measure velocity profiles without any perturbation of the flow. The velocity profiles are influenced by numerous physical quantities, e.g. the composition of the fluid, the ice fraction, the ice particle size distributions, cluster creation and Ostwald ripening, etc. The non-intrusive UVP method must be applied carefully, and an open question is how the measured particle velocity is related to the bulk velocity. It is assumed that in most cases the difference is small.

2. METHODS

2.1 Experiments

The goal of all our experiments was to characterize ice-slurry (two-phase) flow by an ultra sound visualization and a following analysis of the averaged ice particle velocity profiles.

Measurement	Objective	Main parameter
A	Determination of rheogram	-
B	Influence of mean velocity	Mass flow
C	Disturbance by heat transfer	Heat flux

Table. 1 : Experiments performed with UVP, which are presented in this article.

2.2 Device

As in the experiment by Mori [5] (FIG. 1), the material of the pipe is plexiglass. The positions of the sensors for each class of experiments is shown in Table 2. All the measurements, presented in this article, were performed in a horizontal pipe or channel (see Sari et al. [2]).

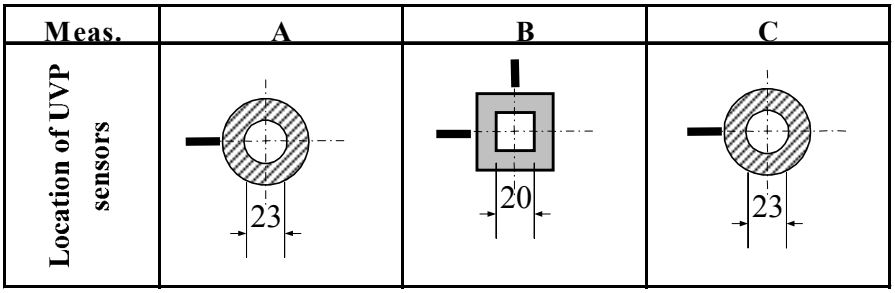

Figure 1 : Positioning of measuring probes shown in cross sections.

2.3 Parameters of the measurements

In case A and C each measurement of a velocity profile is determined by averaging over 1028 profiles and in case B over 500 profiles. Only the projections of the velocity vectors to the main direction of the flow is taken into account. Unfortunately, up to present, no data on ultra sound speed in ice slurries are available. During the measurements the applied instrument UVP XW-3-Psi records data with a sound speed assumed to be 1480 m/s. The frequency of the ultra sound beam is 2 MHz. Comparison between (relative) profiles are meaningful even

by directly evaluating the output data of the instrument (see measurements B and C). Absolute velocity profiles - as shown in case A - need an additional scaling, which only leads to correct results, if the flow is homogeneous. The scaling factor is determined by the mass conservation law. An integration of the product "density times velocity" over the tube cross flow area must be in agreement with the mass flow measured by a coriolis mass flow meter.

3. RESULTS

3.1 A – Construction of ice slurry rheograms

In a horizontal pipe with laminar ice slurry flow the downstream velocity component is measured at different locations in the radial direction. The obtained profiles show a cylindrical plug, which is in correspondance with the theory of laminar Bingham flow. The obtained profiles are symmetric to the axis of the pipe. The mass flow was 0.5 kg/s.

From an average velocity profile - if additionally the pressure drop is measured (see Ref [2] - it is possible to construct a complete rheogram [6]. Taking the laminar flow theory of a Bingham fluid into consideration (see Ref. [7]), one finds for the critical shear stress (eq. 7) and for the viscosity (eq. 8):

$$\tau_0 = -\frac{1}{2} r_1 \frac{dp}{dz} \qquad (7)$$

$$\mu = -\frac{1}{4} \frac{1}{u(r_1)} \frac{dp}{dz} (r_2 - r_1)^2 \qquad (8)$$

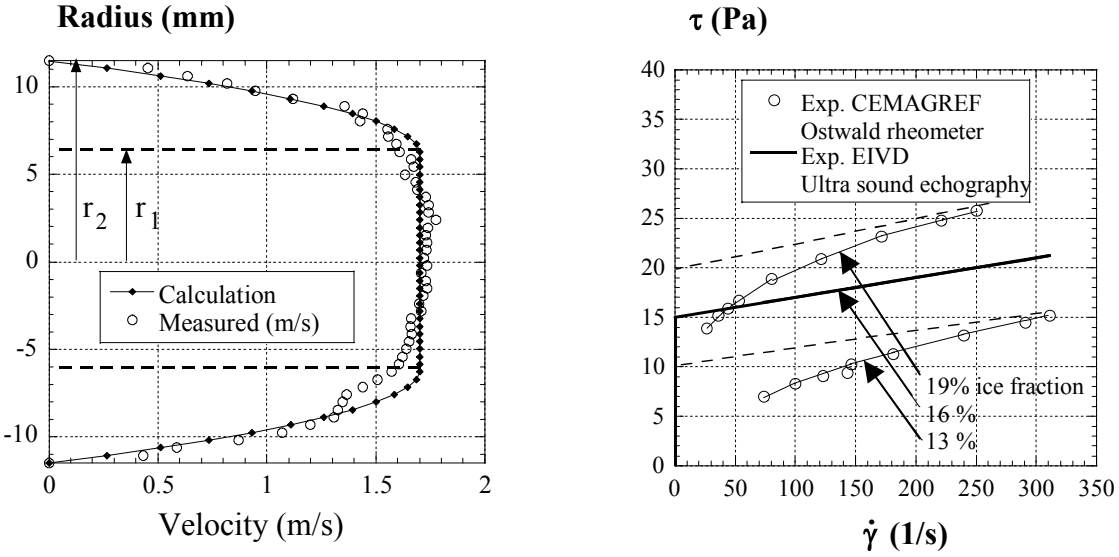

Figure 2 : On the left hand side the measured and calculated velocity profiles are compared. On the right rheograms measured with 13% and 19 % ice fractions at CEMAGREF, in Paris, France [8] and the idealized rheogram, constructed with the viscosity and critical shear stress determined with the UVP method (data obtained from the figure on the left) are shown.

Velocity profiles were thoroughly investigated with the UVP method, but without taking data on the pressure drops. Ben Lakhdar shows experimentally determined rheograms with the same concentration of talin in water [8]. That gives us the possibility to calculate the pressure drop of a pipe of 1 m length, 23 mm diameter, with a mass flow of 0.5 kg/s as adjusted in our

experiments. The density was determined to be 967.7 kg/m^3. The result is dp/dz =-4850 Pa/m. With these data the velocity profiles were calculated (see FIG. 2).

Because of small disturbances in the measurement of the velocity profile, the radius of the rectangular plug r_1 may be difficult to determine. The result can be improved by fitting parabolic curves into the two flanks of the measured profile and afterwards estimating the positions of the maxima of these two parabolas, which define direct measures of r_1.

3.2 B – Dependence of the ice particle velocity profile on mass flow

Optimal conditions for optical observation are given with a diascopic neon light, a translucent glass, which leads to a homogeneous light difussion, and a colour filter. After the experimental imaging, some treatments of the pictures are performed, whereby a specially adapted software was applied. Particle velocity profiles, measured with UVP, are obtained with two transducers located as shown in FIG. 1. The first sensor produces a picture of the profile from the top to the bottom. The second UVP measurement is performed in a horizontal plane from the right to the left. We plot the two resulting velocity profiles in the same diagram, with the aim to visualize some differences between them. It is expected that the horizontal profile is perturbed by buoyancy, especially at low velocities. To control the stability of the flow, during experimentation the time evolutions of the velocity profiles were observed. The alterations were negligible.

Meas.	C_I (%)	ρ (kg/m^3)	T (°C)	ṁ (kg/s)	u (m/s)	Δp (Pa)	Re	He
1	7.6	979	-4.32	0.21	0.54	189	500	9334
2	7.5	976	-4.31	0.09	0.23	72	122	9305
3	7.5	980	-4.31	0.06	0.15	38	0.7	9344

Table 2 : Experimental parameters and measured values of three experiments.

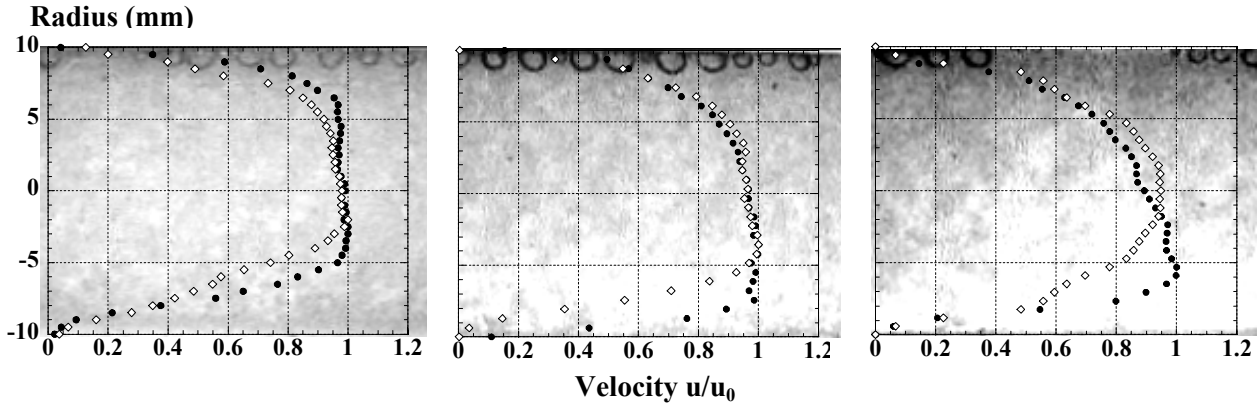

Fig. 3 : Variation of the particle velocity profiles depending on the mass flow. From the left to the right: 0,21 kg/s, 0,09 kg/s, 0,06 kg/s. Black pointers show vertical profiles and white ones belong to horizontal profiles. In the background ice slurry particles flowing through the tube can be recognized.

The results show that the vertical profiles are more sensitive to a reduction of the mass-flow than the horizontal profiles. The horizontal profiles show a reduction of the plug diameter with decreasing mass flow, but the symmetry is conserved. In the vertical profiles it is seen that the dynamic axis of the flow (see in Ref. [3]) is decreasing toward smaller mass flows. Some problems of US beam reflexion at the wall opposite to the transducer must be solved.

3.2 C – Influence of heat transfer

The experimental device is described in Ref. [2]. Because horizontal profiles are less dependent on buoyancy, they were chosen for a study of the influence of heat transfer on the flow patterns. Table 4 presents the conditions of the experiments with heat transfer. The velocity profiles with three different heat transfer rates are shown in FIG. 4.

Mesures	Q (W)	ρ_{in} (kg/m^3)	ρ_{out} (kg/m^3)	$\dot{m}$ (kg/s)	u (m/s)	Δp (bar)	Re out	He out
1	0	967.49	967.74	0.50091	1.246	0.0131	847.48	1228
2	621	967.43	967.94	0.50061	1.246	0.0134	878.62	1306
3	2409	967.56	968.81	0.51681	1.246	0.0118	1058	1393

Tab 4 : Experimental parameters and measured values of three experiments.

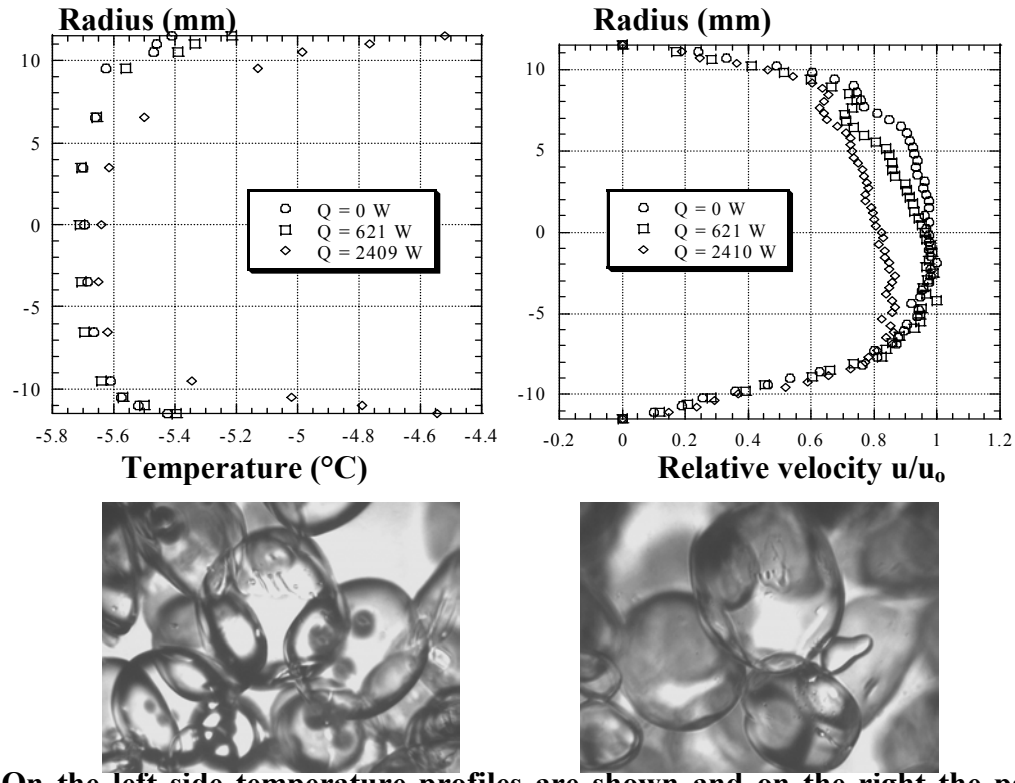

Fig. 4 : On the left side temperature profiles are shown and on the right the particle velocity profiles corresponding to the parameters presented in Table 4. Photographs (1061*762 μm) show ice slurry particles at the inlet of the heat exchanger.

According to the measurements, the plug region (seen in the velocity profiles) is largest when the highest heat transfer rate is applied. It is difficult to exactly determine the central plug region of the flow. But it can be seen that with an increasing heat transfer rate an asymmetry develops. This is also observable in the temperature profile.

4. CONCLUSIONS

In a horizontal channel averaged horizontal and vertical velocity profiles have been determined. The influence of the mean velocity or mass flow and a perturbation by a heat transfer rate has been experimentally studied. Data on ultra sound velocity measurements in ice slurries are still missing and would lead to a further substantial improvement to interpret and evaluate such measurements.

ACKNOWLEDGMENTS

We are grateful to the HES-SO for funding our work. Furthermore, we thank Met-Flow SA for supporting us with high-tech material. M. Takeda we are thankful for very useful remarks.

REFERENCES

[1] **Inaba, H.,** "New challenge in advanced thermal energy transportation using functionally thermal fluids." Int. J. Therm. Sci, **39**, 991-1003, 2000.

[2] **Sari, O., Vuarnoz, D., Meili, F., Egolf, P. W., 2000.** "Visualization of Ice Slurries and Ice Slurry Flows." Proceedings of the Second Workshop on Ice Slurries of the International Institute of Refrigeration, Paris, France, 25-26 May.

[3] **A. Kitanovski, A. Poredoš, P. Reghem, B. Stutz, J.P. Dumas, D. Vuarnoz, O. Sari, P.W. Egolf, T.M. Hansen, 2002.** "Flow patterns of ice-slurries flows." Proceedings of the Fifth Workshop on Ice Slurries of the International Institute of Refrigeration, KTH, Stockholm, Sweden, 30-31 May.

[4] **Kawaji. M., Stamatiou, E., Hong, R., Goldstein, V., 2001.** "Ice-slurry flow and heat transfer characteristics in vertical rectangular channels and simulation of mixing in a storage tank." Proceeding of the Fourth Workshop on Ice Slurries of the International Institute of Refrigeration, Osaka, Japan, 12-13 November.

[5] **M. Mori, Y. Takeda, N. Furuichi, M. Aritomi, H. Kikura, 1999.** "Development of a new type flow metering system using UVP." Proceeding of the Second International Symposium on Ultrasonic Doppler Methods for Fluid Mechanics and Fluid Engineering, Paul Scherrer Institute, Villigen, Switzerland, 20-22 September.

[6] **Windhab, E., Ouriev, B., Wagner, T., Drost, M., 1996.** "Rheological Study of Non-Newtonian Fluids." Proceeding of the First International Symposium on Ultrasonic Doppler Methods for Fluid Mechanics and Fluid Engineering, Paul Scherrer Institute, Villigen, Switzerland, 9-11 September.

[7] **P. W. Egolf, J. Brühlmeier, F. Özvegyi, F. Abächerli, P. Renold, 1996.** "Kältespeicherungseigenschaften und Strömungsverhalten von binärem Eis." Forschungsbericht zuhanden der Stiftung zur Förderung des Zentralschweizerischen Technikums, June.

[8] **M. A. B. Lakhdar, 1998.** "Comportement thermohydraulique d'un fluide frigoporteur diphasique : le coulis de glace ." Ph D thesis, Institut National des Sciences Appliquées de Lyon, Paris, April.

NOTATION

p	Pressure	Pa	r	Radius	mm
z	Axial distance	mm	u	Velocity	m/s
C_I	Concentration	%	f	Frequency	Hz
T	Temperature	°C	w	Water	-
$\dot{m}$	Mass flow	kg/s	a	Additive	-
Δp	Pressure drop	Pa	$\dot{\gamma}$	Shear velocity	s^{-1}
Re	Reynolds number	-	μ	Dynamic viscosity	Pa·s
He	Hedström number	-	ρ	Density	kg/m^3
$\dot{Q}$	Thermal heat flow	W	τ	Shear stress	Pa

MEASUREMENT OF REYNOLDS STRESS IN BUBBLY FLOW USING ULTRASONIC DOPPLER METHOD

Hideki Murakawa[1] and Hiroshige Kikura[1] and Masanori Aritomi[1]

[1]Research Laboratory for Nuclear Reactors, Tokyo Institute of Technology, 2-12-1 Ohokayama, Meguro-ku, Tokyo, 152-8550 Japan, e-mail:murakawa@2phase.nr.titech.ac.jp

Keywords: Bubbly flow, Ultrasonic Doppler Method, Reynolds stress

ABSTRACT

Microscopic structure in bubbly flows is a topic of interest in the study of fluid flows. In the present paper, the Ultrasonic Doppler Method was applied to the measurement of bubbly flows from which Reynolds stress profiles were obtained. Experiments were carried out for an air-water dispersed bubbly flow in a 20mm x 100 mm vertical rectangular channel having a void fraction smaller than 3%. Two ultrasonic transducers were set on the outer surface of the test section with a contact angle of 45° off the vertical, one facing upward and the other facing downward. By applying statistical methods to the two directional velocity profiles, Reynolds stress profiles were calculated. By comparing the Reynolds stress in bubbly flow with that in single-phase flow, it was found that Reynolds stress profiles varied with the amount of bubbles present in the flow. Peak values of the Reynolds stress near the wall increased. This tendency was more pronounced as void fraction increased.

1. INTRODUCTION

Two-phase bubbly flow is one of the most fundamental flow fields appearing in many industrial applications. However, two-phase flow structure has not completely been understood and still needs further investigation in detail. The main reason is the difficulty of measuring without disturbing the given bubbly flow. At the early stage of two-phase measurements, most techniques required intrusion into the flow fields. Examples are the electrical resistivity method, hot-film anemometry, and so on. To avoid disturbing the original flow, non-intrusive measurements have been developed. One of them is the Ultrasonic Doppler Method. The authors have tried to adapt the Ultrasonic Doppler Method to bubbly flow measurements. Advantages of this method include spatial-temporal measurement of the flow, applicability to opaque liquids such as liquid metal and magnetic fluid, line measurement for flow mapping, and adaptability to an existing pipe flow.

Two-phase measurements have been carried out for the last thirty years using several methods. Serizawa et al. (1975) pioneered performance of detailed experiments in bubbly flows using hot-film anemometers. They investigated not only the velocity and void fraction profiles, but also the turbulent intensity profiles and turbulent energy production. Michiyoshi & Serizawa (1986) reported the effects on flow structure of injecting bubbles into liquid flows. Wang et al. (1987) investigated flow quantities in bubbly flow in a vertical pipe and showed that the local void fraction reached a peak value near the pipe wall and the Reynolds stress was increased as a result of bubble injection.

The objective of this study is to clarify the effects of bubble injection on the liquid flow structure using the Ultrasonic Doppler Method. The experiments were performed at Reynolds numbers less than 3200, the transition region in single-phase flow.

2. EXPERIMENTAL APPARATUS

The flow set-up consisted of a vertical rectangular channel made of acrylic, a water circulation system, an air supply system, and the Ultrasonic Doppler Method measurement. The working fluids were air and tap water. The water was seeded with nylon micro tracer particles (Daicel Hüls, WS-200P) at the ratio of 0.1g/l. The specific density of theses particles is 1.02. Their average diameter is 80 μm. The pump circulated water through the lower tank, test channel and upper tank. The water flow rate was controlled and adjusted by operating a valve together with an orifice flow meter. Air was injected through seven needles (i.d. 0.19mm) at the bottom of the test section. The air flow rate was regulated by an air control valve and measured by a float flow meter. Experiments were carried out at atmospheric pressure, water temperature was kept between 19.5 and 20.5ºC using a subcooler. The Ultrasound Doppler Method system included an X-3 PS-I model UVP monitor (Met Flow AG), and a personal computer, which record the water and gas flow rates. For each measuring condition, 30,000 instantaneous velocity profiles were recorded along each measuring lines.

The test section located between the upper tank and air-water mixer. The size of the vertical rectangular channel is 100mm x 20mm x 1700mm. Two ultrasonic transducers were set on the outer surface of the test section with a contact angle of 45º off the vertical one facing upward and the other facing downward. The outer surface of the test channel and the ultrasonic transducers were submerged in the water in order to equalize acoustic impedance.

3. DATA PROCESSING METHOD

3.1 The separation of liquid phase velocity

Since ultrasonic pulses reflected on the bubble's surface and micro particles suspended in liquid phase, the data measured in the bubbly flow using the Ultrasonic Doppler Method included both the liquid phase velocity and bubble's rising velocity. The authors have established a technique for separating the velocity distribution of the gas phase and the liquid phase by using statistical methods (Suzuki et. al. 1999,2002). In this paper, the outline of this technique is described.

A bubble's rising velocity is faster than the liquid velocity; so, an instantaneous velocity profile has a typical peak if a bubble crosses the measuring line in the measurement of a bubbly flow. The maximum value of velocity profiles that measured the bubble rising velocity is bigger than those that did not measure it. Figure 9 illustrates the typical data patterns of instantaneous velocity profiles. By adopting an appropriate threshold velocity, the recorded instantaneous velocity profiles were divided into two groups, that is, profiles either including bubbles (GroupA) or not (GroupB). In this study, to clarify the time averaged liquid structure in bubbly flow, GroupA data was calculated.

3.2 The calculation of the Reynolds stress

The Reynolds stress profiles can be calculated from the two directional velocity components (u and v). Ultrasonic transducers were set at different angles (α and β) from the flow direction. The mean Reynolds stress profiles were calculated as follows (Durst et al. 1976 and Tropea 1983):

$$\tilde{Q} = \tilde{U}\cos\theta + \tilde{V}\sin\theta \qquad (6)$$

$$U = \bar{U} + u, \qquad V = \bar{V} + v \qquad (7)$$

$$q_1 = v\cos\alpha + u\sin\alpha, \qquad q_2 = v\cos\beta + u\sin\beta \qquad (8)$$

where $\widetilde{U}$ and $\widetilde{V}$ are instantaneous vertical and horizontal velocities and $\widetilde{Q}$ is the instantaneous velocity along the measuring line. $\overline{U}$ and u are the time averaged velocity, and the velocity fluctuation, respectively. The fluctuating velocity components (q_1, q_2) on the two measuring lines can be expressed in Eq.(8). If α equals to β, the Reynolds stress can be expressed as follows from Eq.(6) -(8):

$$-\rho\overline{uv} = \rho\frac{\overline{q_1^2} - \overline{q_1^2}}{2\sin 2\theta} = \rho\frac{q_1'^2 - q_2'^2}{2\sin 2\theta} \qquad (9)$$

where q' is standard deviation of the velocity fluctuation on the measurement line directions.

4. RESULTS AND DISCUSSION

4.1 Velocity profiles in bubbly flow

The graph in Figure 10 illustrates the universal velocity distribution in single-phase flow. In this graph, u^+ and y^+ are defined as follows:

$$u^+ = \frac{\overline{u}}{u_\tau}, \quad y^+ = \frac{yu_\tau}{\nu} \qquad (10)$$

where u is the axial velocity, y is the distance from the wall, and v is the kinematic viscosity of the water. The value of y is corrected for the error considered to arise from the part of the measurement line overlapping with the wall surface and reported by Taishi et al. (2002). The value for u_τ is the friction velocity in single-phase flow, which is given by the follow equations (Durst et al. 1996):

$$C_f = 2\left(\frac{u_\tau}{u_m}\right)^2 = 0.073\,\mathrm{Re}_m^{-1/4}, \quad \mathrm{Re}_m = \frac{u_m \cdot 2D}{\nu} \qquad (11)$$

where $2D$(=20mm) is the width of the channel and u_m is the mean velocity.

Generally, it is well known that the velocity distribution in a turbulent flow region near the wall can be written as

$$u^+ = 5.75\log y^+ + 5.5 \qquad (12)$$

In single-phase flow, the velocity profiles approach the form defined by Eq.(12) with increasing Reynolds number. This tendency agrees well with the findings reported by Durst et al. (1996). From these results, it is proven that single-phase flow was in the turbulent transition region under this condition.

Figure 11(a),(b) show the mean velocity profiles in bubbly flow for different gas flow rates. These figures are calculated only used for liquid velocity (Group A). These results indicate that bubbles influence liquid structure at the vicinity of the wall. This tendency is more pronounced at low Reynolds number. Under conditions that place the flow in the transition region, were the flow single-phase (i.e. Figure 11(b)), the mean velocity increased with in the vicinity of the wall increasing gas flow rate. On the contrary, the mean liquid velocity in the logarithmic region decreases with increasing gas flow rate. Thus it can be seen that in the channel flow, bubbles accelerate the liquid and promote the liquid structure to the turbulent flow regime because of the bubbles' buoyancy. However, Figure 11(a) shows a slightly different phenomenon from other conditions. As gas flow rate increase, the velocity distributions increase at most of channel positions. This tendency is seems to be related to the liquid phase being laminar flow.

4.2 Reynolds stress profiles in bubbly flow

Reynolds stress profiles measured in single-phase flow appear in Figure 12(a). Reynolds stress increases as Re_m increases. The Reynolds stress profiles normalized by u_τ^2 used in Eq.(11), are shown in Figure 12(b) also. The maximum values of the normalized Reynolds stress are different in each profile. These maximum values are inversely proportional to Re_m. These results are good agreement with Wei et al. (1989).

From Figure 13, it is found that Reynolds stress profiles are affected by bubble injection such that the values of the Reynolds stress increased with increasing bubble injector. The differences between the value of the Reynolds stress in single-phase flow and the one in bubbly flow decrease as liquid flow rate increases. Further more, Reynolds stress is strongly affected near the wall (y/D<0.4). These results show that bubble injection takes a strongly role in promoting turbulence transition, particularly in the near-wall region, and this effect decreases with decreasing liquid flow rate. Michiyoshi et al. (1985) and Wang et al. (1986) measured Reynolds stress profiles in bubbly flow in a vertical pipe. They reported that the Reynolds stress normally increased with increasing gas flow rate. But for some flow rates, the Reynolds stress is less than it is at higher gas flow rates. In the present study's results, similar tendency appeared. The results showed that some gas injection tended to reduce the turbulence in the liquid. However those conditions depend on gas, and liquid flow rates, bubble size, and channel geometry.

5. CONCLUSIONS

Measurements of liquid structure in bubbly flow were performed using the Ultrasonic Doppler Method. As a result, the following phenomena occurring in a vertical rectangular channel are clarified:

- Bubbles accelerate the liquid velocity in the vicinity of the wall, and this tendency is enhanced as liquid flow rate is reduced.
- Reynolds stress profiles are affected by bubble injection, and these effects become stronger at low liquid flow rates.
- The Reynolds number as increases, the value of the Reynolds stress is increased in the near-wall region (y/D<0.4).

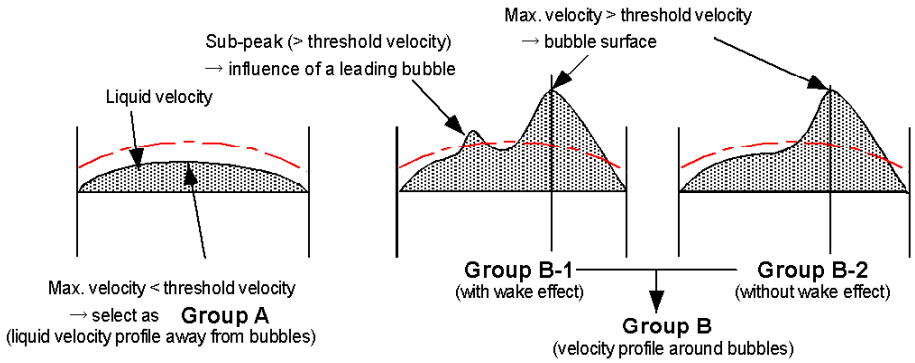

Figure 9 Typical data pattern and their classification

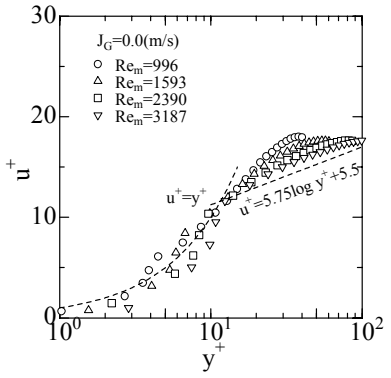

Figure 10 Mean velocity profiles in single phase flow

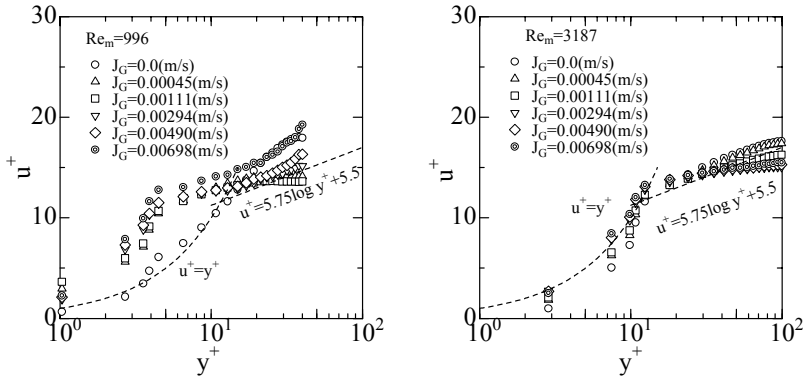

(a) Re_m=996 (d) Re_m=3187

Figure 11 Mean velocity profiles for different gas flow rate

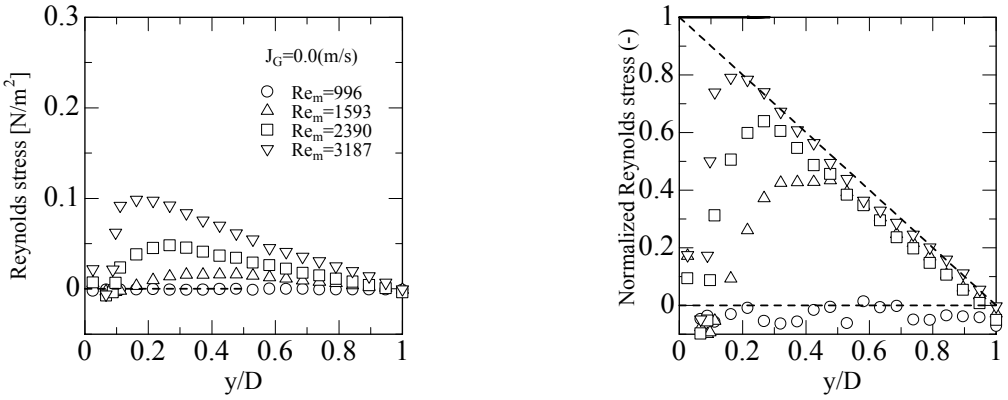

(a) Reynolds stress profiles (b) Normalized Reynolds stress profiles

Figure 12 Reynolds stress profiles for different Reynolds numbers in single phase flow

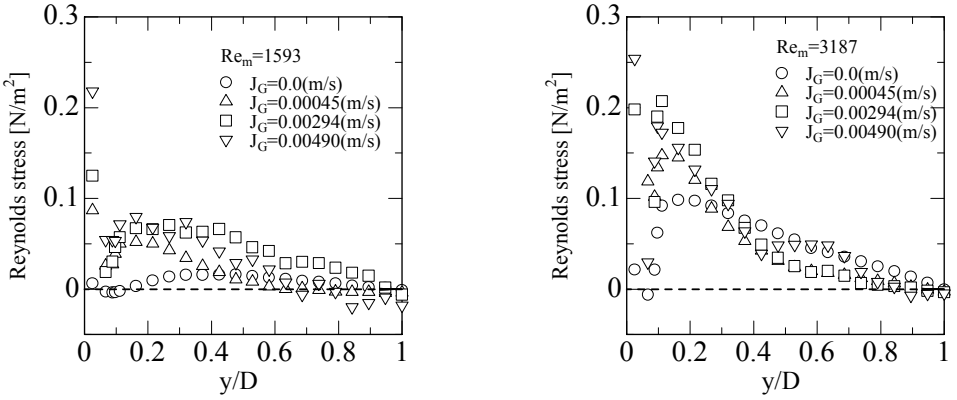

(b) Re_m=1593 (d) Re_m=3187

Figure 13 Reynolds stress profiles for different gas flow rate in bubbly flow

REFERENCES

Serizawa, A., Kataoka, I., Michiyoshi, I. (1975). *Turbulence structure of air-water bubbly flow-II. Local properties*, Int. J. Multiphase Flow 2: 235-246

Michiyoshi, I., Serizawa, A. (1986). *Turbulence in two-phase bubbly flow.* Nuclear Engineering and Design 95: 253-267

Wang, S.K., Lee, S.J., Jones Jr, O.C., Lahey Jr, R.T. (1987). *3-D turbulence structure and phase distribution measurements in bubbly two-phase flows*. Int. J. Multiphase Flow 13: 327-343

Suzuki, Y., Aritomi, M., Takeda, Y., Mori, M. (1999). *Effect of bubble motion on liquid flow structure surrounding bubbles in bubbly flows.* In Proc. 7th Int. Conf. Nucl. Eng.(ICONE7), ICONE-7163

Suzuki, Y., Nakagawa, M., Aritomi, M., Murakawa, H., Kikura, H., Mori, M. (2002). *Microstructure of the flow field around a bubble in counter-current bubbly flow,* Experimental Thermal and Fluid Science, in print

Durst, F., Melling, A., Whitelaw, JH. (1981). *Principle and practice of laser Doppler anemometry.* London: Academic Press 407-425

Tropea, C. (1983). *A note concerning the use of a one-component LDA to Measure shear stress terms.* Experiments in Fluids Vol. 1 Technical notes: 209-210

Durst, F., Kikura, H., Lekakis, I., Jovanovic, J., Ye, Q. (1996). *Wall sheare stress determination from near-wall mean velocity data in turbulent pipe and channel flows.* Experiments in Fluids 20: 417□428

Taishi, T., Kikura, H., Aritomi, M. (2002). *Effect of the measurement volume in turbulent pipe flow measurement by the ultrasonic velocity profile method.* Experiments in Fluids 32: 188□196

Wei, T., Willmarth, W.W., (1987). *Reynolds-number effects on the structure of a turbulent channel flow.* J. Fluid Mech 204: 57-95

APPLICABILITY OF ULTRASONIC CAVITATION BUBBLES FOR THE MEASUREMENT USING ULTRASONIC DOPPLER METHOD

Tsuyoshi Taishi[1], Hiroshige Kikura[1], Masanori Aritomi[1], Yoshikazu Koike[2] and Michitsugu Mori[3]

[1]Research Laboratory for Nuclear Reactors, Tokyo Institute of Technology, 2-12-1 Ohokayama, Meguro-ku, Tokyo, 152-8550 Japan, e-mail: ttaishi@2phase.nr.titech.ac.jp
[2]Shibaura Institute of Technology, 3-9-14 Shibaura, Minato-ku, Tokyo 108-8548, Japan
[3]Tokyo Electric Power Company, 4-1 Egasaki-cho, Tsurumi-ku, Yokohama, 230-8510 Japan

Keywords: ultrasonic Doppler method, cavitation bubbles, flow rate measurement, ultrasonic piezoelectric oscillator, ultrasonic cavitation bubbles generating system

ABSTRACT

In the present study, the applicability of ultrasonic cavitation bubbles is investigated for flow rate measurement using the ultrasonic Doppler method. The velocity of the ultrasonic cavitation bubbles is evaluated from instantaneous and mean velocity profiles inherently applied in the ultrasonic Doppler method. The experimental results show that the present ultrasonic cavitation bubbles approach is in good agreement with the experiments using the conventional seeding of micro particles. The flow rate measurement employing the ultrasonic cavitation bubbles results in 1% error compared with the measurement from the orifice flow meter.

1. INTRODUCTION

Flow rate measurement has been acknowledged as one of the most important aspects in various industrial and engineering fields. Until now, numerous flow rate measurement techniques have been established. In general, even though the method employing pressure difference in the piping has mainly been utilized, it is still necessary to carry out the correction concerning the variation of time. In addition, the processing is also required for the piping.

The ultrasonic Doppler method has been developed by Takeda [1][2] and utilizes a pulsed echo-graphic technique of ultrasound. This method has many advantages compared with conventional method. The advantages are as follows: The information on the velocity profile in the measurement line's direction can be made available instantaneously. It can also be applied for various liquid flow velocity measurements such as opaque liquids flows or flow inside non-transparent channels [3]. The flow rate measurement applied the ultrasonic Doppler method has been developed the by authors [4]. In addition, this method can be applied for transient flow measurement [5], the flow rate measurements in the industrial metal pipes [6][7].

The current principle of the method is based on the detection of the echoes of ultrasonic pulses reflected by seeding materials suspended in the fluids. So the ultrasonic Doppler method requires putting the seeding materials into the flow as the ultrasonic reflector. However, in the case of the nuclear power plant, it is difficult to apply the seeding materials in the fluid loop. There are two options to be applied into the power plant as a reflector for ultrasonic method, namely cavitation bubbles and hydrogen gas bubble injection [6]. In the present study, the ultrasonic cavitation bubbles by the ultrasonic oscillator is proposed as

ultrasonic reflectors. The ultrasonic cavitation bubbles are generated by inducing stationary wave using the ultrasonic oscillator in the rectangle box [8]. Applicability of the ultrasonic cavitation bubbles for the measurement using ultrasonic Doppler method is therefore investigated.

2. EXPERIMENTAL SET-UP

2.1 Ultrasonic cavitation bubbles generating system

Ultrasonic cavitation bubbles generating system consists of a rectangular box with ultrasonic oscillator for generating the bubbles in a water-loop and the ultrasonic oscillator driver unit. The ultrasonic cavitation bubbles are generated by ultrasonic piezoelectric oscillator (D48820: NTK) on rectangular box with two resonance boards. The ultrasonic piezoelectric oscillator is attached to the ultrasonic horn, and mounted altogether to the resonance board with bolt joint. The oscillator is driven by function-generator (Yokogawa: FC110) and wide range amplifier (Tokin: WB-500). The function generator emits the sinusoidal-wave signal at the frequency of 16 KHz. The signal is then amplified by the wide range power amplifier. Schematic diagram of the system is shown in Fig.1.

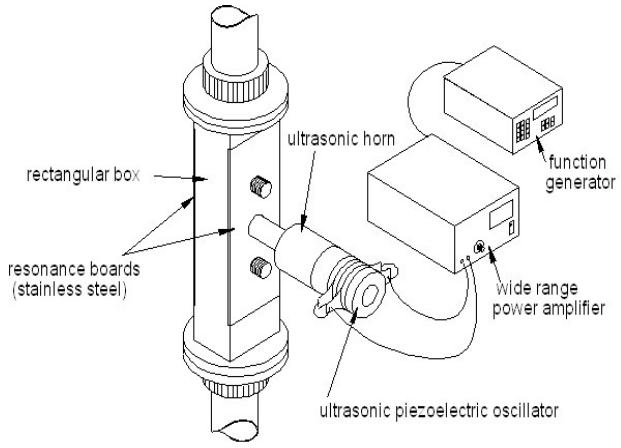

Fig.1. Ultrasonic cavitation generating system

2.2 Experimental apparatus

A schematic diagram of the experimental apparatus is shown in Fig.2. The experimental apparatus can be used to investigate both upward and downward liquid flows. It consists of water circulation system, ultrasonic cavitation bubbles generating system and measurement system. Therefore, in the present study, both upward and downward flows of a single-phase turbulent pipe flow are studied. In the case of upward flow, the water contained in the storage tank is circulated by a centrifugal pump to an overflow tank through the test section and measurement section. In downward flow, the water in a storage tank is pumped up direct to an overflow tank by a centrifugal pump and enters the test section. The flow rate is controlled by a needle valve and monitored by two orifice flow meters. One orifice flow meter is used for Re < 8000 and the other for Re □ 8000. They are located in the bottom part of the water loop. During the experiments, water temperature is maintained at 10C using a sub-cooler. The flow measurement

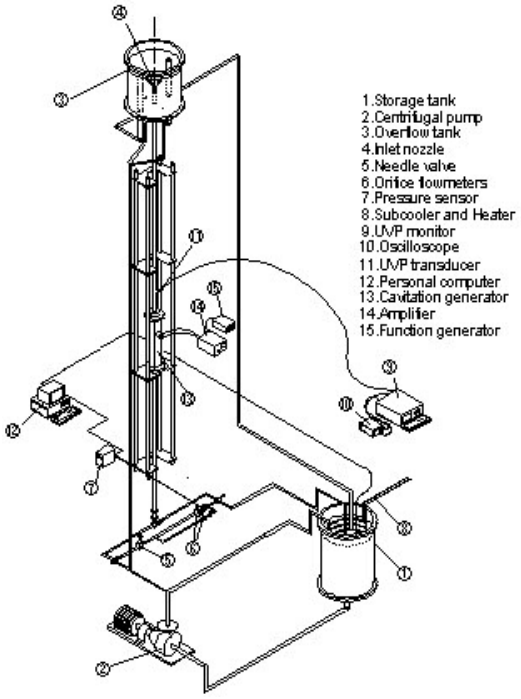

Fig.2. Experimental apparatus

system consists of the UVP monitor (X-3 PS-i model: Met Flow AG) and a personal computer, which records flow rate and temperature data. The test pipe is made of the Plexiglas of total 7 m in length and installed vertically. Its inner diameter is 50mm. The ultrasonic cavitation generating section is located at 50D (D = pipe inner diameters) from bottom and 90D from the top of the loop. The measurement section is shown in Fig.3. The UVP transducer is set on the surface of outer wall with a contact angle of θ degrees perpendicular to the flow direction. Wall thickness of the pipe in this section is 1mm, because the ultrasonic beams have good permeability. The test section is set in a container filled with water to facilitate firm coupling between the wall and transducer. The measurements are carried out at several different positions along the vertical pipe. For upward flow, the measurement positions are set respectively at 8D, 28D, 48D and 68D from ultrasonic cavitation generating section. For downward flow the measurement position is set at 16D from ultrasonic cavitation generating section. The configuration is illustrated in Figure 4.

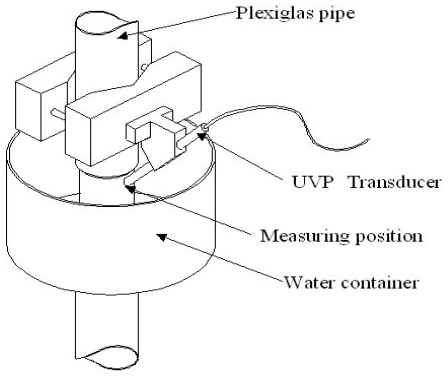

Fig. 3. Measurement section

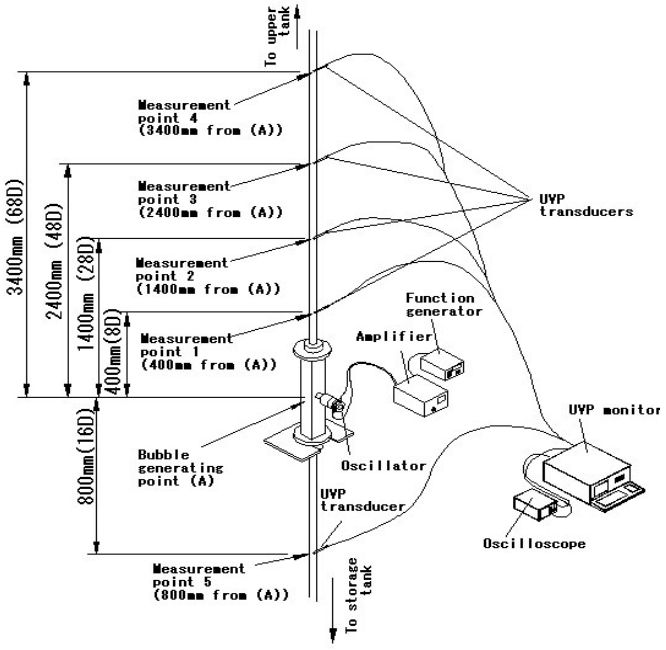

Fig.4. Configuration of measurement position

3. EXPERIMENTAL CASES AND RESULTS

3.1 Experimental cases

In the present study, the following experimental cases were carried out in order to confirm whether the ultrasonic cavitation bubbles could be utilized as an ultrasonic reflector.

- In order to obtain the relations between ultrasonic cavitation bubbles and the detected ultrasonic echo in this method, the experimental case with the ultrasonic cavitation bubbles was compared with the case in which the reflector was not used. Subsequently, the comparison of the instantaneous velocity profiles measurement concerning to the on/off operating condition is carried out.
- Since the ultrasonic cavitation bubbles disappear with time, the average velocity profile shall be measured at several different positions in downstream direction.
- The case in which nylon particle as ultrasonic reflector was applied was compared with the case in which the ultrasonic cavitation bubbles was used for the average velocity profile and flow rate measurements.

- In order to confirm the tractability characteristic of the ultrasonic cavitation bubbles, experiments with several different flow rates and directions were carried out. The results were then compared with the measurement using orifice flow meter. In addition, in order to investigate the effect of flow direction, the flow rates calculated from the average velocity profiles between upward flow with downward flow were also compared.

3.2 Experimental results

Figure 5 shows the colour density of the velocity data from the UVP in time domain at the ultrasonic cavitation bubbles generating system on/off position. In this figure, position A is the starting point of Ultrasonic cavitation bubbles generating system and electrical noises are detected. At position B, the ultrasonic echo from the Ultrasonic cavitation bubbles is

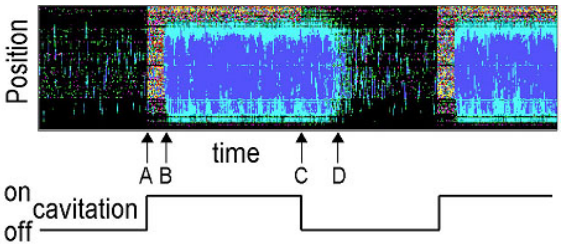

Fig.5. Colour density of the velocity data

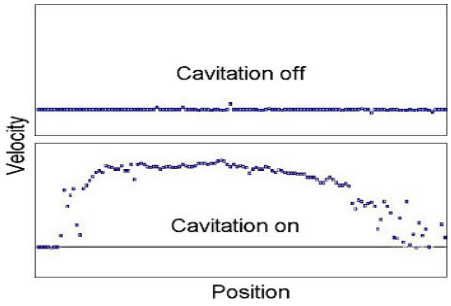

Fig.6. Instantaneous velocity profiles

clearly detected. The delay between positions A and B is the time required by the bubbles to travel from the Ultrasonic cavitation bubbles generating system to reach the measurement position. The ultrasonic cavitation generating system is stopped at position-C and the electrical noise disappears. Ultrasonic echo is detected until position-D, and then the ultrasonic echo fades out. In the region between positions C and D, the ultrasonic echo is still detected. This implies that the ultrasonic reflection from the ultrasonic cavitation bubbles is measured by UVP. The comparison between the instantaneous velocity profiles employing the ultrasonic cavitation bubbles with the case without ultrasonic cavitation bubbles is shown in Figures 6. When the ultrasonic cavitation bubbles generating system stopped, instantaneous velocity profile is not detected. In the opposite, when the system is turned on, the velocity profile is clearly detected. From this result, it is revealed that the velocity profile can be measured by generating the ultrasonic cavitation bubbles. The measuring position was shifted along the downstream direction of the flow as shown in Figure 4 in order to investigate the effect of the measuring position from the position of ultrasonic cavitation bubbles generating system. Figure 7 shows that the data of instantaneous velocity profile began to scatter at the position of 48D. The disturbance increases as the measuring position was shifted farther (i.e. at 68D). In figure 8, it is shown that the average velocity profile is reliably measured at positions 8D and 28D. Therefore, it was confirmed that the measurement using this method was possible if it 30D from the ultrasonic cavitation bubbles generating system. The measurement result of average velocity

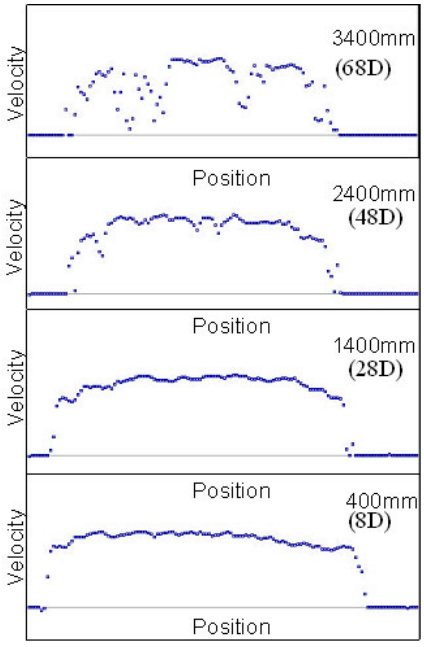

Fig.7. Instantaneous velocity profiles in the different positions

profile by this technique was compared with that of applying nylon particle in order to confirm the accuracy of the flow velocity measurement by this technique. The result shown in

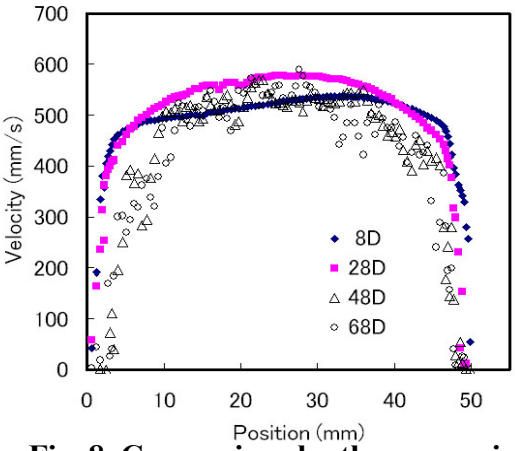

Fig. 8. Comparison by the measuring positions in average veracity profiles

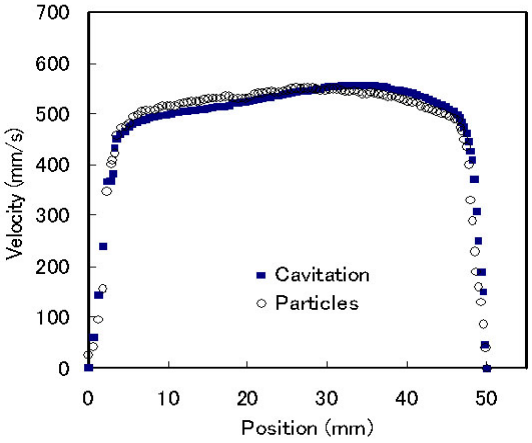

Fig. 9. Comparison between ultrasonic cavitation and particles in average velocity profiles

Figure 9 is in a good agreement. In addition, the flow rates calculated from each average velocity profiles agree well in the error of about 0.82% as shown in Figure 10. The flow rate was calculated from average velocity profile as follows [9]:

$$Q(t) = \pi/3 \left\{ \frac{R_0^3 - R_1^3}{R_0 - R_0} v_0 + \sum_{i=0}^{n-2} \frac{R_{i+1}^3 - R_{i+2}^3}{R_{i+1} - R_{i+2}} \left(v_{i+1} - v_i \right) + R_n^2 v_n \right\}$$

where R is the distance from centre of the pipe, i is the position of velocity data, and v is the velocity value.

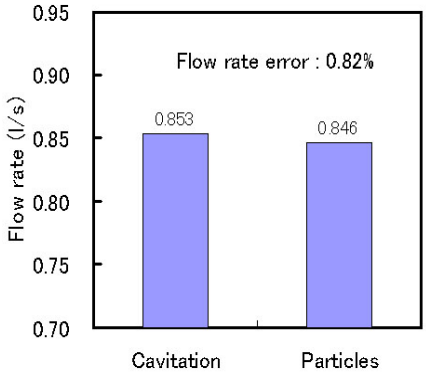

Fig.10. Comparison between ultrasonic cavitation and particles in flow rate measurement

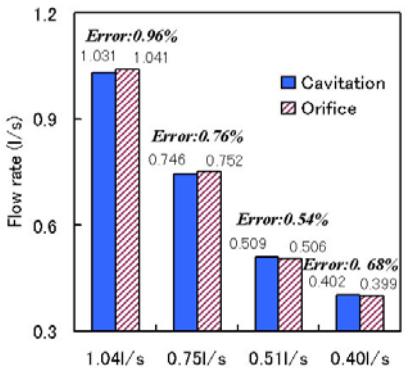

Fig.11. Flow rate measurement using the ultrasonic cavitation compare with Orifice flow meter

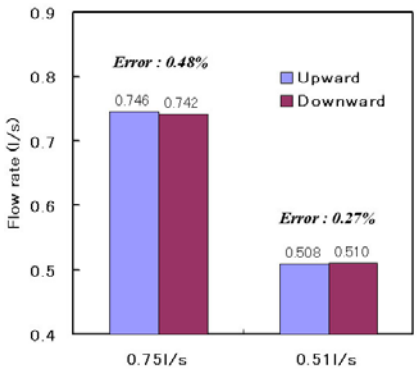

Fig.12. Flow rate measurement error between upward and downward flow

The flow rate measurement errors calculated from the respective average velocity profiles in flow rate difference are less than 1% when compared with the measurement using orifice flow meter. This is shown in Figure 11 that the flow rate measurement of 1.04 l/s has the measurement error of 0.96%. Therefore, it can be understood that there is no effect caused by the change of the flow rate. In addition, Figure 12 shows the comparison between the flow rate measurement calculated from each average velocity profiles for upwards flow with the downward flow in two different flow rates. The flow rate measurement errors for 0.75 l/s is 0.48%, and for 0.51 l/s is 0.27%. Therefore, it can be confirmed that the ultrasonic cavitation bubbles have good tractability in the liquid flow for the downward flow measurement.

4. CONCLUSIONS

In the present study, the experimental results concerning the applicability of ultrasonic cavitation bubbles for the measurement using the ultrasonic Doppler method can be clarified as follows:

- Ultrasonic cavitation bubbles generated by ultrasonic wave oscillator is sufficient to be employed as a reflector for the ultrasonic Doppler method.
- Ultrasonic cavitation bubbles can be used for velocity profile measurement along the vertical channel at any positions before 30D from the ultrasonic cavitation bubbles generating system with the flow rate of 1.0 l/s.
- The flow rate measurement error using the ultrasonic cavitation bubbles method is less than 1% when compared with the measurement using flow orifice meter.
- Ultrasonic cavitation bubbles can be applied for flow rate measurement in the ultrasonic Doppler method

The future direction of this experimental work will be to improve the efficiency of the ultrasonic cavitation bubbles generating system by conducting the simulation of ultrasonic field analysis. In addition, the experimental study will also be carried out to analyse the intensity in the ultrasonic field.

REFERENCES

[1] Takeda Y. (1987). *Measurement of velocity profile of mercury flow by ultrasound Doppler shift method.* Nucl Technol Vol,79 120pp-124pp

[2] Takeda Y. (1995). *Velocity profile measurement by ultrasonic Doppler Method.* Exp Thermal Fluid Sci. Vol.10, 444pp-453pp.

[3] Takeda Y; Kikura H. (1998). *Measurement of mercury flow by ultrasonic Doppler Method.* ASME 1998 Fluids Engineering Division Summer Meeting. FEDSM98-5974.

[4] Takeda Y., et al. (2000). *Development of new flow metering system using UVP. (Preliminary performance assessment using flow standards)*. ASME 2000 Fluids Engineering Division summer meeting. FRDSM2000-11102.

[5] Takeda Y., et al. (1999). *Application of Ultrasonic Doppler Method to Flow Rate Measurements, (1) Principle and Realization - Laboratory Experiment,* Proc. of FEDSM'99, 3rd ASME/JSME joint Fluid Engineering Conference, San Francisco, USA, (1999-7), FEDSM99-7140.

[6] Kikura H., et al. (1999). *Application of ultrasonic Doppler method to flow rate measurement, (2) Measurement using industrial stainless-steel.* Proc. of FEDSM'99, 3rd ASME/JSME Joint Fluid Engineering Conference. San Francisco, USA, FEDSM99-7141.

[7] Mori M., et al. (2002). *Development of a novel flow metering system using ultrasonic velocity profile measurement*, Experiments in Fluids. 32, 153pp-160pp

[8] Henglein, A. (1987). *Sonochemistry: Historical developments and modern,* Ultrasonics, 25, 6pp-16pp

[9] Wada S., et al. (2002). *Multiline Flow Rate Measurement using Ultrasonic Doppler Method.* 3rd ISUD EPFL, Lausanne, Switzerland, September 9 - 11, 2002

STUDY ON THE DEVELOPMENT OF NOVEL VELOCITY PROFILE MEASURING METHOD USING ULTRASOUND TIME-DOMAIN CROSS-CORRELATION

Gentaro Yamanaka, Hiroshige Kikura, Masanori Aritomi[1]

[1] Research Laboratory for Nuclear Reactors, Tokyo Institute of Technology, 2-12-1 Ohokayama, Meguro-ku, Tokyo, 152-8550 Japan, e-mail: gen@2phase.nr.titech.ac.jp

Keywords: high resolutions, Nyquist's sampling theorem, cross-correlation

ABSTRACT

This paper presents a velocity profile measurement by a novel method using pulsed ultrasound. The method is called ultrasound time-domain correlation method (UTDC) and is based on the cross-correlation between two consecutive echoes of ultrasonic pulses to detect the velocity. The UTDC has two advantages over a conventional ultrasound pulsed Doppler method. First, the method has higher time and spatial resolutions than the pulse Doppler method. Second, the system does not have a limitation in maximum measurable velocity and range, which are limited by Nyquist's sampling theorem. In the paper, the velocity profile measurement in turbulent pipe flow using the UTDC is performed.

1. INTRODUCTION

This paper presents that the application of the ultra- sound time-domain correlation method (UTDC) [1, 2] to the velocity profile measurement in a turbulent pipe flow. We applied this method to the steady turbulent flow in a pipe, and have obtained the ensemble averaged velocity profile and have not obtained the higher statistical momentum.

The ultrasound flow measurement system has been used in many industrial and scientific fields, because they are non-intrusive and usable in opaque materials, including solids in flow condition. The time-of-flight ultrasound flow-meter using a pair of ultrasound transducers [3, 4] is especially widely used in industry for flows in large pipes. This method can be used for longer without maintenance than orifice flow-meter and venturi nozzle. In addition, this method offers the advantage that it can be applied to pipes with no modification. However, they require a profile factor to assume the velocity profile of a flow or the calibration one between the real flow-rate from the measured one.

The ultrasound Doppler method is a technique, which utilizes the Doppler shift frequency f_D from the scatterers suspended in a working fluid to obtain the velocity of the scatterer v

$$v = c\frac{f_D}{2f_0} \tag{1}$$

where c is the sound velocity in the working fluid and f_0 is the central frequency of the transmitted ultrasound. Since Satomura[5] discovered the ultrasound Doppler shift from blood, this method has been applied in many types of blood flow-meters in biomedical engineering.

The system can be classified into two categories by its measurement principle. One is the continuous wave Doppler method. Its advantage is the limitless measurable velocity. However, it is impossible to detect the position of scatterers by this method. The other is the pulse Doppler method, by which it is possible to obtain both the position and the velocity

information of scatterers. The defect of this system is in the limitation of the measurable velocity due to Nyquist's sampling theorem, which is expressed by

$$v_{max} = c\frac{f_{prf}}{4f_0} \tag{2}$$

where v_{max} is the maximum measurable velocity, and f_{prf} is the pulse repetition frequency. One of the measuring instruments based on the pulse Doppler method, the ultrasound velocity profile monitor (UVP)[6] has been developed at Paul Scherrer Institut (PSI) for both the engineering and academic demand. Although the spatial and time resolution are poor compared with the laser Doppler velocimetry (LDV), the ultrasound pulse Doppler technique has an advantage of the measurement of instantaneous velocity profiles. As a consequence, in the measurement of flow-rate by the UVP, it is that the calibration is not necessary, since the flow-rate can be directly obtained by the integration of measured velocity profile. However, the UVP system cannot be applied to the high speed flow in large pipes because of the measuring limitation due to Nyquist's sampling theorem. The UTDC uses the repetition of ultrasound pulses, but uses different procedure to detect velocity data from the pulse ultrasound Doppler method. In order to detect the velocity profile, the UTDC utilize the cross-correlation function between two echoes from two pulses is calculated. Therefore there is no limitation in the maximum measurable velocity due to Nyquist's sampling theorem and the method has advantages, which the pulse Doppler method has. Additionally it has a better time resolution than the pulse Doppler.

2. ULTRASOUND TIME-DOMAIN CORRELATION METHOD

2.1 Principles

Figure 1 shows the concept of UTDC. An ultrasound transducer is set at the angle of with respect to the flow direction. An echo signal is reflected from position 1, when an ultrasound pulse is transmitted at the time of $t = t_0$. The elapsed time between the pulse emission and its reception is $t = t_1$. If another ultrasonic pulse is emitted at the time of $t = t_0 + T$, the echo signal from the same scatterer is from position 2. If the elapsed time of second ultrasonic pulse is $t = t_2$, the distance that the scatterer moved towards the axial direction of the ultrasound beam path, is obtained and the velocity of the scatterer can be obtained from the following equation

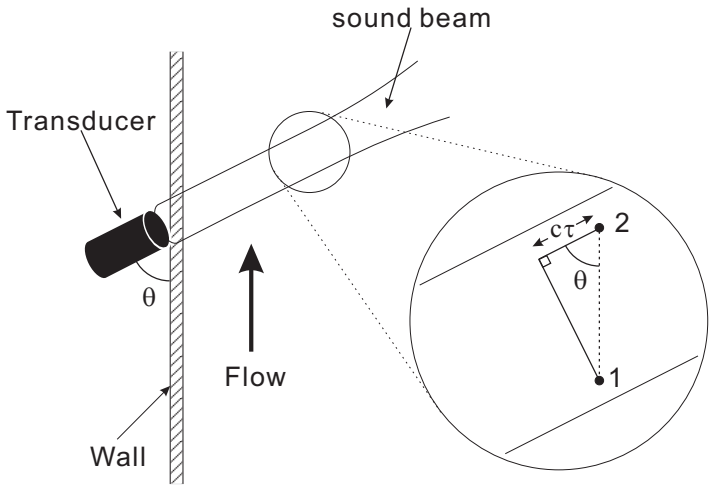

Fig.1 Relationship between a transducer, a flow field and scatterers

$$v = \frac{(t_1 - t_2)c}{2T\cos\theta} \tag{3}$$

where T is equal to $1/f_{prf}$ and $(t_1 - t_2)$ is denoted by τ, the Eq.(3) can be described as

$$v = c\tau\frac{f_{prf}}{2\cos\theta} \tag{4}$$

In the real measurement, the ultrasonic echo is reflected by the scatterers within the ultrasonic pulse as illustrated in Fig. 2. An echo signal E1 is due to the scatterers in volume 1 (V1). At time T (= 1 / fprf) seconds later, scatterers in V1 moves to V2. Then the echo signal E2 can be obtained. V1 and V2 include the same region in the ultrasound path which is illustrated as shaded area in Fig.2. Therefore a set of echo signals which have similar shapes can exist in somewhere between E1 and E2. If the time shift is known, the velocity of the scatterers included in volume 1 can be obtained using Eq.(4).

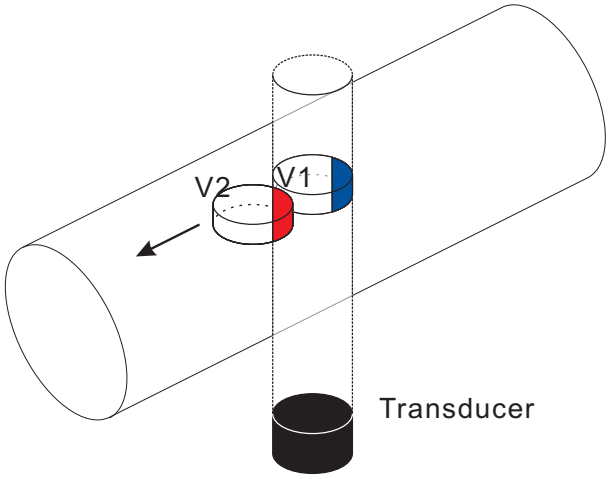

Fig.2 Real image of UTDC

The time shift is obtained by calculating a cross-correlation function R(s) between E1 and E2 (see Fig. 2), which is expressed as

$$R(s) = \frac{\int E_1(t)E_2(t+s)dt}{\sqrt{\int E_1(t)^2 dt \int E_2(t+s)^2 dt}} \tag{5}$$

The digitized cross-correlation factor $R(s)$ is represented by

$$R(s) = \frac{\sum_{i=1}^{N} E_1(i)E_2(i+s)}{\sqrt{\sum_{i=1}^{N} E_1(i)^2 \sum_{i=1}^{N} E_1(i+s)^2}} \tag{6}$$

The valuable s is selected so that $R(s)$ reaches the maxi- mum, and is set to s. Using the determined value of τ, the scatterer velocity can be obtained from Eq.(4).

3. CORRELATION INTERPOLATION

Because the echo signal is sampled at discrete times, the correlation function can be also calculated at discrete time delays and the maximum value of the correlation factor exists at between two points. To predict the maximum value, the maximum discrete correlation and its two neighboring points should be found and fitted by any interpolating functions.

Concerning the particle image velocimetry (PIV), in which the cross-correlation function is used for detecting the movement of scatterers crowd, the solution of light scattering by a small particle is known as Airy function which can be assumed as Gaussian function. From these reasons, Gaussian function is well used as the interpolating function to

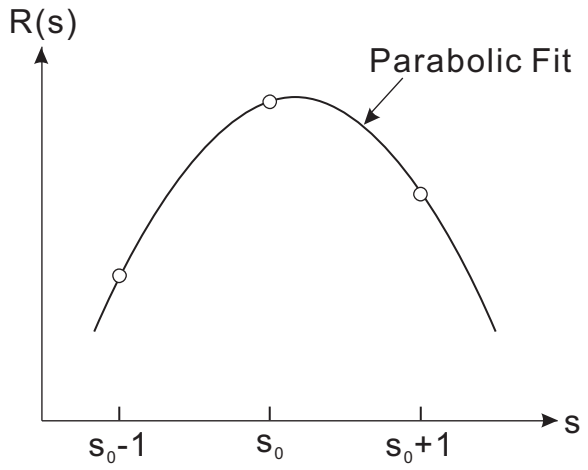

Fig.3 Interpolation of the correlation function

obtain the movement in PIV.

Because the solution of the time evaluation of acoustic scattering is unknown, we used the parabolic function to interpolate the correlation function. This is illustrated in Fig. 3.

4. EXPERIMENTAL APPARATUS

The schematic diagram of the experimental apparatus is shown in Fig. 4, which consisted of a test section and a measurement system.

A working fluid was tap water. Micro particles of nylon powder were suspended in the water to be used as scatterers of ultrasonic pulses. The average diameter of the particle was about 80μm, and the specific density was 1.02. The test pipe is made of Plexiglas, and has an inner diameter of D=50mm, an outer diameter of 60mm and a length of 4800mm.

Water flowed downward into the vertical circular test section from the upper entrance through bell-mouth nozzle and tripping ring to reduce entrance length. The water flow rate was controlled by a needle valve and measured by an orifice flow meter, both of which were located at the bottom part of the apparatus.

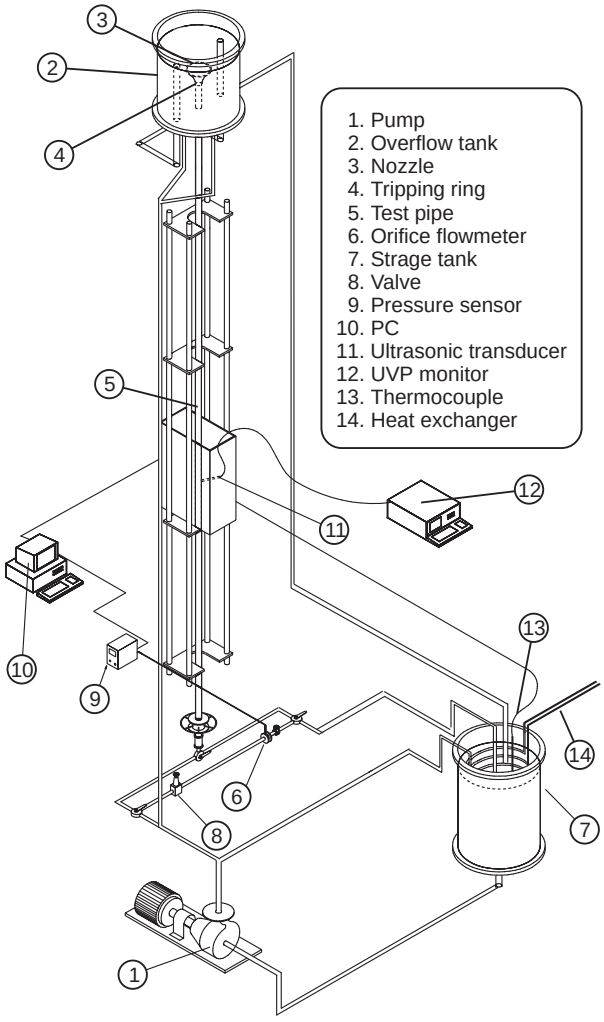

Fig.4 Experimental apparatus

Figure5 shows the measurement section. The wall thickness at the measuring position was 1 mm. An ultrasonic transducer was set on the outer surface at the contact angle of 45° toward the liquid main flow direction, and was fixed at 80D far from the inlet of the test pipe. The gap between the transducer and the wall surface was filled with water to prevent the reflection of ultrasonic pulses on the wall. Experiments were performed at Re=12000, which was based on the bulk velocity and the pipe diameter.

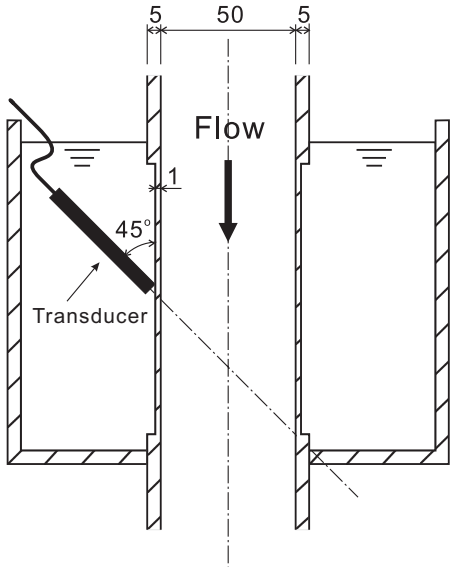

Fig.5 Test section

Figure 6 shows the setup of the measuring system, which consisted of a ultrasound pulser/receiver DPR-35+ (JSR Co. Ltd.), an ultrasound transducer (Imasonic S.A.), and a digital oscilloscope LC-574A (Lecroy Corp.).

The center frequency of the ultrasound pulse emitted from the transducer was 4MHz, because the ultrasonic transducer was designed for center frequency of 4MHz. After the pulse emission, the transducer was changed to receiver mode. The LC-574A has the 8-bit A/D converter, whose maximum sampling rate is 4GS/s. The RF and the position signals were tapped from the pulser/receiver. The RF signal were digitized at 100MS/s in the experiment and placed into the memory of the LC-574A. The RF echo was triggered by the pulse repetition frequency at the pulse emission. The pulse repetition frequency f_{prf} is 2000Hz.

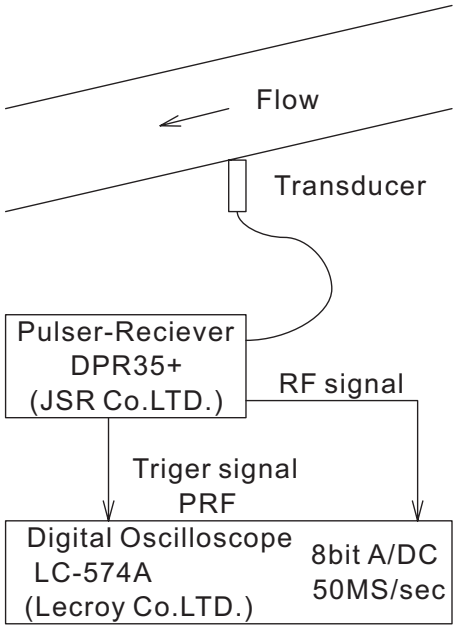

Fig.6 Block diagram of hard ware system

5. RESULTS AND DISCUSSION

Figure 7 shows an example of consecutive ultrasound echoes with respect to the elapsed time from the emission of the ultrasound pulse. Because of the deference of acoustic impedance between the working fluids and the scatterers, the echo from scatterers can be divided from electrical noise by setting the threshold, which is shown in Fig.7. When the three sets of signals are compared, it is observed that every signal has similar wave form in a region.

By separating signals into windows and comparing the windows with those for the following signal, the correlation factor can be calculated. The window length was set to 100 samples, and the sampling rate was 100 MSamples/s.

Figure 8 shows the ensemble averaged velocity profile and the data valid rate with respect to the distance from the pipe wall. The circle plots are the average of 26000 instantaneous velocity profiles. The data valid rate is shown as the blue bar. From the figure, the data valid rate is very low, and the mean velocity at each point is the average of approximately 2000 data.

Figure 9 shows the non-dimensional velocity profiles. In Fig.9 the circle is the present result, the blue curve is the DNS data by Eggels et al. and the red curve is the LDV measurement by Durst et al.. The figure shows that the present data is in agreement with the LDV data and the logarithmic low. But the present data is little bit scatter, because the data valid rate is very low.

REFERENCES

[1] Hein, I.A., et al., A real-time ultrasound time-domain correlation blood flowmeter: part 1, IEEE Trans. Ultrason. Ferro. Freq. Contr., 40, pp. 768-775, (1993).

[2] Hein, I.A., et al., A real-time ultrasound time-domain correlation blood flowmeter: part 2, IEEE Trans. Ultrason. Ferro. Freq. Contr., 40, pp. 776-785, (1993).

[3] Yamamoto, M. and Ito, Ultrasound flow meter in a large pipe, IEICE Trans. Jpn., 48-11, pp. 1956-1963, (1965), in Japanese.

[4] Augenstein, D. and Regan, J., The basis for a 1% power increase: LEFM3 technology, In Proc. 8th Int. Conf. Nucl. Eng., ICONE-8575, Baltimore, (2000).

[5] Satomura, S., Study of the flow patterns in peripheral arteries by ultrasonics, J. Acoust. Soc. Jpn., 15, pp. 151-158, (1959).

[6] Takeda, Y., Velocity profile measurement by ultrasound Doppler shift method, Int. J. Heat Fluid Flow, 7, pp. 313-318, (1986).

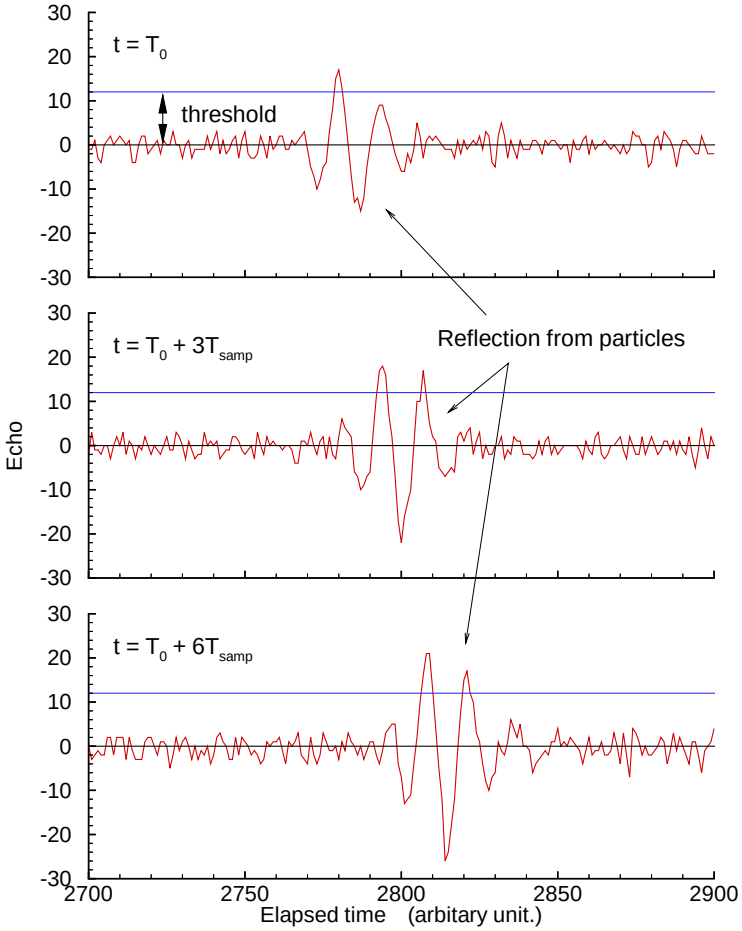

Fig.7 Typical consecutive echoes

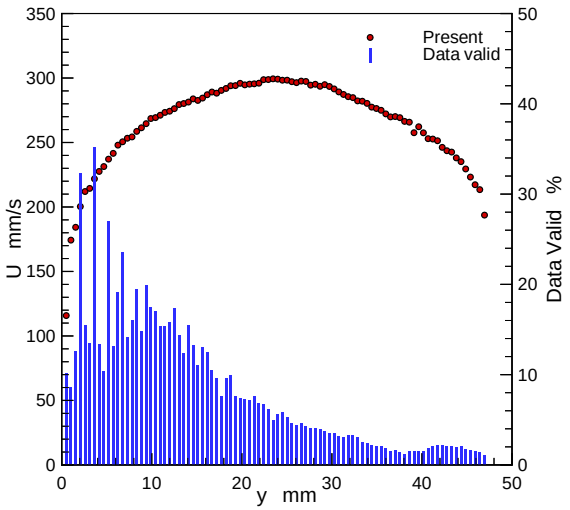

Fig. 8 Ensemble averaged velocity profile and the data valid rate

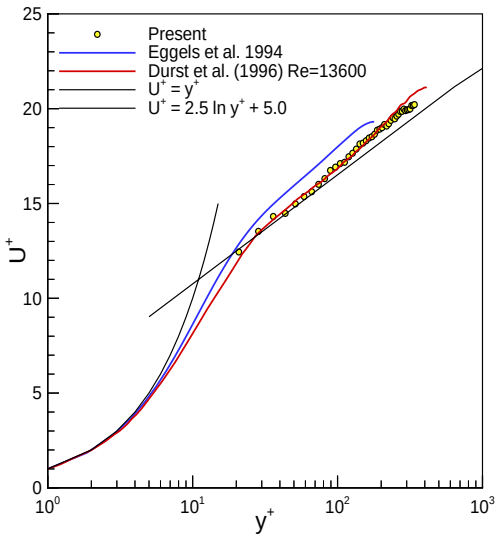

Fig. 9 Ensemble averaged velocity profile and the data valid rate

INDUSTRIAL APPLICATION EXPERIENCES OF NEW TYPE FLOW-METERING SYSTEM BASED ON ULTRASONIC-DOPPLER FLOW VELOCITY-PROFILE MEASUREMENT

Michitsugu Mori[1], Kenichi Tezuka[1], Hideaki Tezuka[1],
Noriyuki Furuichi[2], Hiroshige Kikura[3], and Yasushi Takeda[4]

[1] Tokyo Electric Power Co., Inc., Yokohama 230-8510, Japan, mori-mcy@rd.tepco.co.jp
[2] Gifu University, Gifu 501-1193, Japan [3]Tokyo Institute of Technology, Tokyo 152-8500, Japan
[4] Hokkaido University, Sapporo 060-8628, Japan

Keywords: ultrasonic-Doppler, velocity profile, flowmeter, industrial application, calibration

ABSTRACT

Velocity-profile measurement by ultrasonic-Doppler method has recently much advanced for fluid flow measurement; however, the actual application is in uncharted territory for high temperature/pressure and high velocity fluid in thick and large industrial piping. The measurement tests of the flow rate using ultrasonic-Doppler flow velocity-profile measurement were carried out at the test loops in NIST (National Institute of Standard and Technology of the United States), NMIJ (National Metrology Institute of Japan), and industrial piping of ~400 mm in diameter. The tests showed errors of ~0.2% for NIST and ~0.4% for NMIJ.

1. INTRODUCTION

A technology to instantaneously determine flow rates by spatially performing continuous line-measurement of flow velocity-profile in piping is considered to provide an advanced ultrasonic flowmeter, superior to the conventional flowmeter using a transit time or time of flight (TOF) method. The conventional one based on the TOF method depends largely on the accuracy of a profile factor as it finally determines the flow rate of a fluid by multiplying it. This is also true of a one-point ultrasonic-Doppler flowmeter. Accordingly these conventional methods are limited in the scope of application as they are effective only in measuring flows with steady-state developed flow. In other words, the methods have to use an approximation that is applicable only in a narrow flow range.

Meanwhile, the feedwater and circulating water systems of a power plant are generally exposed to high temperature/pressure conditions or consist of large pipes. Therefore, determining a profile factor under the same flow and shape conditions is impracticable and results in certain errors in measurement. In fact, it is impossible at the present stage to determine a profile factor by a high-precision calibration loop using a weighing method under such high temperature/pressure conditions as in the feedwater or large-bore piping as in the circulating seawater system for a nuclear power plant. Consequently the profile factor has to be determined with a Reynolds number approximately one digit smaller than that of the actual plant. In the case of a circulating water system with a piping bore of ~3 meters for instance, a profile factor determined with the piping bore set at a fraction of the actual size is applied to the system because of constraints from the calibration facilities. The conventional ultrasonic flowmeters as described above round off all indeterminate errors by a profile factor as shown in Figure 1.

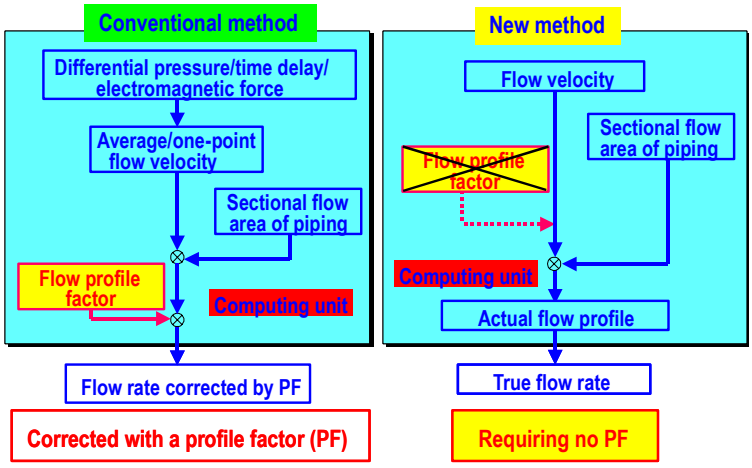

Figure 1. Conceptual Comparison between Conventional Flowmeter and Ultrasonic-Doppler Flow Velocity-Profile Flowmeter.

To get rid of these errors, efforts are needed to eliminate the profile factor by determining flow rates based on the calculation of true flow profile in the piping. This concept is described in Figure 1. The ultrasonic-Doppler flow velocity-profile flowmeter proposed in this paper can accurately determine the true value of flow at the work site of a plant, not depending on such conditions as the piping bore, temperature and pressure, as far as the basic frequency of ultrasonic waves, Doppler-shift signals, sound velocity and measuring configuration are known. Apparently this capability gives the proposed flowmeter a wide range of industrial applications and advantages in measuring principle and applicability to operational plants over the conventional TOF or one-point ultrasonic-Doppler flowmeter, which involves wider errors whenever the flow velocity-profile or configuration in piping varies.

2. MEASURING PRINCIPLE

The proposed ultrasonic-Doppler flow velocity-profile flowmeter is a method of simultaneously measuring multiple points on the line of flow velocity-profile using a Doppler-shift in ultrasonic pulse echo, and it features capability of instantaneously obtaining spatial information(**Takeda**, 1987, 1995). Figure 2 shows a concept of its measuring principle. The new flowmeter calculates flow velocity-profile by processing signals on the line of measurement based on Doppler signals of an ultrasonic wave that is transmitted from ultrasonic transducers installed on the piping and reflected from bubbles, etc. in the fluid to be measured. This method, with the same meaning as the process of solving Navier-Stokes equation, is capable of determining flow rates more accurately than previous methods and expected to have a wide area of applications. The flow of a fluid even in round piping with a circular cross section would have unsteady-state three-dimensional distribution wherever it is not provided with a sufficient entrance-run length or it is affected by such temporal fluctuations as valve opening and closing or pump startups and stops. In a strict sense, therefore, a three-dimensional map should be prepared by a time-dependent process to determine the flow in the piping under these conditions. In this process, the flow can be determined by the following equation (**Takeda**, et.al. 1998):

$$Q(t) = \int V(t)ds = \iint V_x(r,\theta,t)rdrd\theta$$

Where Vx denotes an axial component of the flow on the cross section of the piping. Assuming that the flow is of approximately one dimension, given

$$V_x >> V_r \approx V_\theta$$

the flowmeter can be simplified as follows:

$$Q(t) = \sum_i^N \{\Delta\theta \int_{-R}^{R} v(r,\theta_i,t) / \sin(\alpha) rdr\} \qquad ;\Delta\theta = 2\pi / N$$

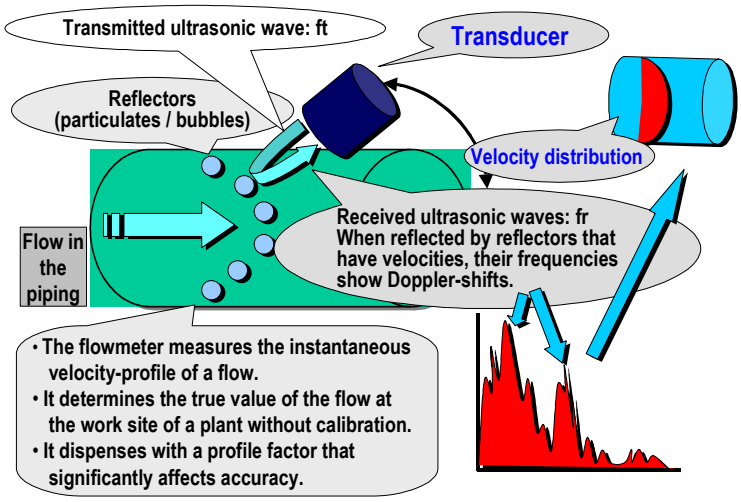

Figure 2. Measuring Principle of Ultrasonic-Doppler Flow Velocity-Profile Flowmeter

In this instance, N units of transducers are installed at the same place on the pipe wall with their circumferential angle varied, but only one line of measurement is sufficient to determine the flow in a passage of piping with stable flow profile. The lines of measurement should be inclined at a certain angle with a perpendicular to the pipe wall and arranged in such a way that all of them will cross the pipe axis.

3. ADVANTAGES OVER CONVENTIONAL FLOW MEASUREMENTS

The conventional measuring methods which also use ultrasonic waves could not accurately measure flow rates if postulated conditions of calibration, such as fully-developed flow profile and conditions, are disturbed because these methods determine flows using flow velocity at one point on the pipe axis or average flow velocity on the pipe diameter. Meanwhile, the proposed ultrasonic-Doppler flow velocity-profile flowmeter measures the flow velocity of the fluid instead and consequently it has many advantages for industrial applications, including those mentioned below:

(a) Profile factors for the calibration can be eliminated in the measurement of flow rates in the work site of a plant.

(b) The accurate measurement of flows is enabled for those like a flow not to be fully developed shortly after a bent pipe.

(c) The whole piping filled up with a fluid is not indispensable essentially for the measurement.

(d) It is applicable to opaque fluids and viscous fluids, in which the calibration can be hardly performed to measure a flow rate, to mention a few of its other advantages.

(e) In addition, as common in ultrasonic flowmeters, the measurement does not disturb the flow in the piping, as it is generally capable of noncontact measurement.

4. CURRENT STATE OF DEVELOPMENT

The development of a flow velocity-profile measuring method using ultrasonic-Doppler effect progressed in recent years for the purpose of measuring the flow velocity-profile of fluids in general and it has come to be used in many areas of fluid experiments and measurement. However, its application to the measurement of high-velocity flows in large-bore, thick-wall industrial pipes as those installed at power plants still remains an unknown field.

4.1 Transient Flow Measuring Tests

Up to now, a series of tests has been carried out on the proposed new method in measuring the flow velocity-profile and flow rate of a fluid in steel piping of ~400A class at normal temperature and normal pressure, and the results have been compared with the values

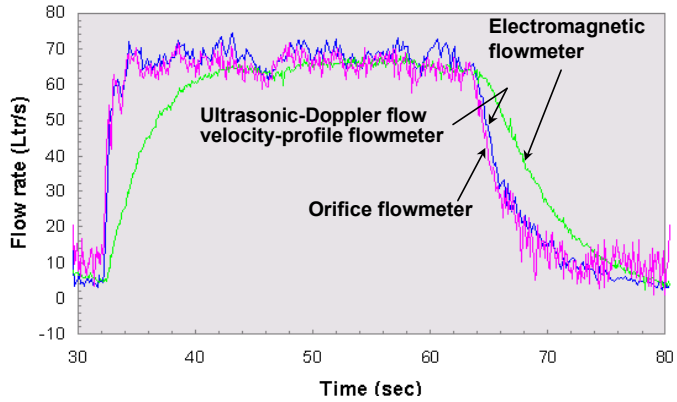

Figure 3. Comparison in Transient Flow Test on Ultrasonic-Doppler Flow Velocity-Profile Flowmeter

measured by a differential-pressure flowmeter and an electromagnetic flowmeter(**Mori**, 1999). An example of the measured results is given in Figure 3. The ultrasonic-Doppler flow velocity-profile flowmeter in these tests achieved desirable results of measurement. As is apparent from the diagram, the conventional differential-pressure method and the ultrasonic-Doppler flow velocity-profile flowmeter showed the same tendency with respect to fluctuations in transient flow, indicating that both of them well responded to fluctuations at a velocity of around 100 msec. The test findings led to the prediction that the proposed method will attain sufficient capability to measure water flows in the piping systems of operational plants, taking into account the arrangement of pipes and measuring conditions in these facilities.

4.2 Verification Test at NIST

Based on the foregoing knowledge and information, a measuring test was conducted at the National Institute of Standard Technology (NIST), a unit under the U.S. Department of Commerce. Figure 4 gives an outline of the loop test section of the reservoir system for standard calibration flow-metering at NIST. A branch line to a tank for volumetric flow measurement is provided on the downstream side of the loop. The flow rate of water per unit length of time can be determined by accumulating in the tank the fluid flowing down the test section in a given period of time and dividing the volume of the fluid thus accumulated by the time elapsed. The nominal measurement error is 0.12%. In this test, the flow of water was measured at the part where it reached the stage of full development.

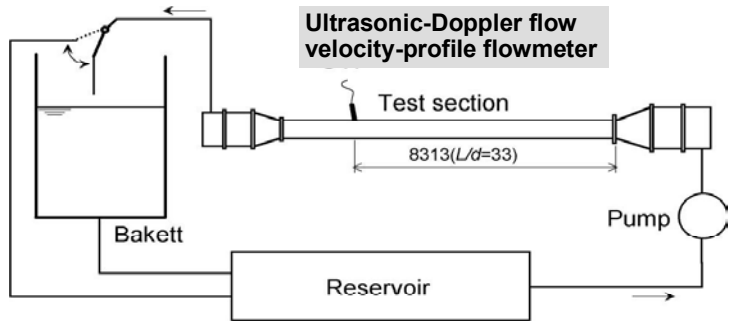

Figure 4. Standard Calibration Volumetric Flowmeter at NIST

The proposed ultrasonic-Doppler flow velocity-profile flowmeter was found to meet the approved values of the standard loop with an error well within 1%, proving to have sufficient accuracy. Table 1 compares the approved values of the NIST standard

Table 1. Comparison of Ultrasonic-Doppler Flow Velocity-Profile Flowmeter and Standard Calibration Volumetric Flowmeter at NIST

	UdFlow	(L/s)	NIST Weight		Re=400k	
File	Average	Deviation	GPM	L/s	Difference	% error
N0355.dat	69.760	2.958	1103.30	69.600	-0.161	-0.23%
N0356.dat	69.670	3.191	1103.51	69.613	-0.057	-0.08%
N0357.dat	69.725	3.233	1103.49	69.612	-0.113	-0.16%
N0358.dat	69.444	3.152	1103.65	69.622	0.178	0.26%
N0359.dat	69.569	3.218	1103.44	69.609	0.040	0.06%
Average	69.634	0.128	1103.48	69.611	-0.022	-0.03%

loop and corresponding data on the ultrasonic-Doppler flow velocity-profile flowmeter at Re = 400,000. The values of the NIST loop are based on the average of weighing time while those of the ultrasonic-Doppler flow velocity-profile flowmeter are based on the time average of instantaneous values. As indicated in the table, the measuring test found a deviation of only 0.03% between the two devices in terms of the average of the values recorded by five rounds of measurement. From the results of measurement conducted with Re number varied, it was found that the overall average deviation between the two devices was no more than 0.2%. (**Takeda**, 2000; **Mori**, 2002)

4.3 Calibration Test at National Metrology Institute of Japan (NMIJ)

A calibration test was conducted on the ultrasonic-Doppler flow velocity-profile flowmeter by a liquid flowmeter calibration facility, a verification loop, at the National Metrology Institute of Japan (NMIJ), suborgan of the National Institute of Advanced Industrial Science and Technology (AIST), an independent governmental corporation. As shown in Figure 5, the test apparatus flows water from the overflow tank into the measuring pipe for calibration tests and then measures the flow rate of water while sending it by a diverter into the weighing tank installed in the downstream section for a certain length of time. The calibration facility (made to the national standard) has the standard uncertainty set at 0.02% of the reference flow rate.

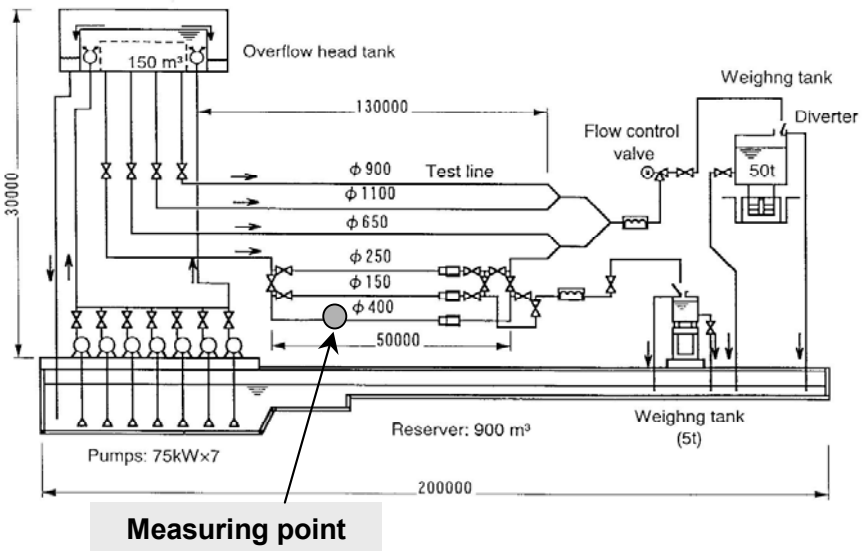

Figure 5. Liquid Flowmeter Calibration Facility at the National Metrology Institute of Japan of AIST

The calibration test on the ultrasonic-Doppler flow velocity-profile flowmeter was carried out with a measuring instrument attached to the 400A piping section of the facility. The results of the test are summarized in Table 2. The test findings indicate the uncertainty of the flowmeter examined in terms of the average of the results recorded in 10 rounds of measurement, compared with the reference flow rate set as a target. Based on the measuring test, the ultrasonic-Doppler flow velocity-profile flowmeter was given a calibration certificate showing an uncertainty range of 0.1% to 0.4%.

5. RANGE OF APPLICATION

The ultrasonic-Doppler flow velocity-profile flowmeter is based on a continuous pulse Doppler linear measuring method, in which uniform distribution of ultrasonic wave reflectors is desirable, specifically micro-bubbles, in the fluid to be measured. This means that the proposed new flowmeter has to effectively utilize cavitation bubbles in the flow after the pump outlet as well as micro-impurities contained in the fluid. Accordingly the flowmeter is considered applicable to the measurement of production lines at pulp and food-processing factories but its application to power plants involves arrangements for mixing bubbles or

some other reflectors into the fluid prior to the measurement of flow rates because, in general, feedwater and other systems in these facilities are exposed to high pressure and the fluid in their piping is not expected to contain impurities. However, some power plants have hydrogen, oxygen or other chemical substances injected into the fluid for water chemistry purposes and, in some instances, these substances could be used as reflectors for the ultrasonic-Doppler flowmeter. Besides, there are greater prospects for its application to the measurement of flow rates in the cooling seawater circulation and some other plant systems that are expected to contain reflectors.

Table 2. Results of Calibration Test on Ultrasonic-Doppler Flow Velocity-Profile Flowmeter at the National Metrology Institute of Japan (NMIJ) of AIST

Round of test	Measuring equipment	Avg. value in 5 rounds □m^3/h□	Avg. uncertainty in 10 rounds
#1	UdFlow No.1	2008.9	0.4%
	Ref. value for weighing tank	2000.1	
#2	UdFlow No.1	2008.9	
	Ref. value for weighing tank	2000.9	
#3	UdFlow No.1	1508.2	0.□%
	Ref. value for weighing tank	1511.8	
#4	UdFlow No.1	1508.2	
	Ref. value for weighing tank	1513.5	
#5	UdFlow No.1	985.5	0.3%
	Ref. value for weighing tank	986.1	
#6	UdFlow No.1	983.7	
	Ref. value for weighing tank	986.0	

The ultrasonic-Doppler flow velocity-profile flowmeter can determine true values at the work site of a plant because it finds the flow rate of a fluid from flow velocity-profile and, consequently, it dispenses with a profile factor that depends on such flow conditions. Accordingly the proposed new type flowmeter is capable of on-site calibration with true values, which it has been impossible to carry out in the past. This implies that the new flowmeter is very effective in reducing the cost of flow measurement as its introduction will eliminate the need to detach flowmeters or large pumps from plant lines and send them to a measuring facility for calibration.

The following are examples of conceivable applications of the ultrasonic-Doppler flow velocity-profile flowmeter:

(a) Measurement, Calibration, and Monitoring of Flow Rates in Pipes Containing Ultrasonic Wave Reflectors.

Those parts that contain bubbles and cannot be accurately measured by any other flowmeter.

Turbid fluids flow rate in pipes carrying high-viscosity fluids.

Surveillance of leaks in pipelines, etc.

(b) Measurement of Flow Rates in Large-Bore Pipes and On-Site Calibration with True Values.

Measurement of flow rates in cooling seawater circulation systems, etc. (with a piping bore of several meters)

On-site calibration of feedwater flow rates, etc. (with the flow rates measured by supplying reflectors mostly from nozzles for cleaning)

(c) Measurement of Flow Profile

Measurement of flow velocity-profile in containers and pits for the improvement of facilities, design changes, troubleshooting service, etc.

6. CONFIGURATION AND EXTERNAL VIEW OF ULTRASONIC-DOPPLER FLOW VELOCITY-PROFILE FLOWMETER

Figure 6 shows the basic configuration of the ultrasonic-Doppler flow velocity-profile flowmeter. The proposed ultrasonic-Doppler flow velocity-profile flowmeter processes signals from ultrasonic transducers with transmitter-receiver functions attached to the piping. The optimization of ultrasonic transmission frequency and repeating frequency is fully attained by a personal computer that also provides remote-control functions for the main unit of the flowmeter. All results of measurement can be seen on the PC display unit. Figure 7 shows an external view of an experimentally made prototype ultrasonic-Doppler flow velocity-profile flowmeter.

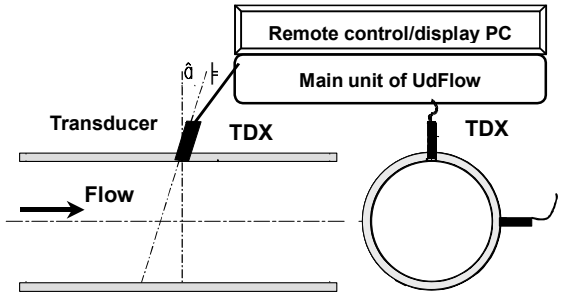

Figure 6. Basic Configuration of Ultrasonic-Doppler Flow Velocity-Profile Flowmeter

Figure 7. Experimentally Made Prototype

One ultrasonic transducer is sufficient to accurately measure flow rates in those parts of piping which carry well-developed flows, as proved by measuring tests at NIST and NMIJ. However, flow rates in the parts which are not far from a bend in the piping or which carry inadequately-developed flows and are subject to disturbance in flow profile have to be measured with two or more ultrasonic transducers properly arranged on one and the same plane. For this purpose, each of the personal computers used for the new flowmeter is provided with capability to respond to signals from three transducers.

Figure 8 gives an example of the ultrasonic-Doppler flow velocity-profile flowmeter measured flow profile shown on a PC display unit. As is apparent from the photograph, the plotted data clearly show the parabolic flow velocity-profile on the diametrical line of the piping.

7. CONCLUDING REMARKS

The ultrasonic-Doppler flow velocity-profile flowmeter proposed in this paper is a new device which, unlike the conventional flowmeters, theoretically dispenses with a profile factor (i.e., adjusting factor) and is capable of accurately measuring true values at the work site of a plant without using some arbitrary adjusting factors. It is expected that the ultrasonic-Doppler flow

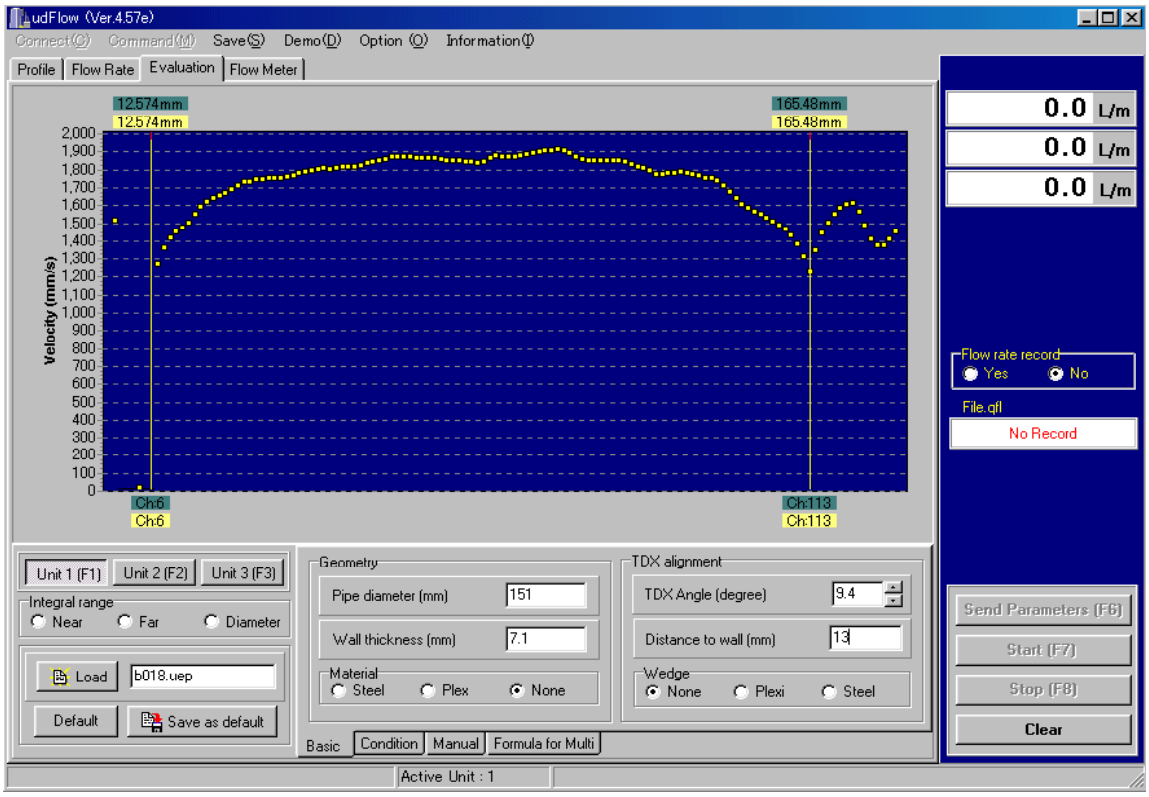

Figure 8. Configuration of Display Unit for Flow Profile Measured in Ultrasonic-Doppler Flow Velocity-Profile Flowmeter, showing the Time-Averaged Flow Velocity-Profile during On-Line Measurement to Compute the Flow Rate by Integrating the Profile.

velocity-profile flowmeter, with these advantages, will be applied to on-site measurement of true flow rates in large-bore pipes or the calibration of existing flowmeters and pumps installed in pipelines, thereby contributing to the improvement of plants and equipment in efficiency and to the reduction of their maintenance costs.

REFERENCES

Takeda Y.(1987). *Measurement of velocity profile of mercury flow by ultrasound Doppler shift method*, Nuclear Technology, 79, pp 120-124.

Takeda Y. (1995). *Velocity profile measurement by ultrasonic Doppler method,* Experimental Thermal and Fluid Sci., 10, pp 444-453

Takeda Y. et. al. (1998). *Development of flow rate measurement using ultrasonic Doppler method (1) Theoretical background,* 1998 Fall Meeting of AESJ, F16, p.343

Mori M. et. al. (1999). *Development of ultrasonic-Doppler velocity profile method for flow rate measurements of power plant,* ICONE-7, FP7429

Takeda Y. et. al. (2000). *Development of a new flow metering system using UVP, Preliminary performance assessments using NIST flow standards,* Proceedings of ASME FEDSM'00, ASME 2000 Fluids Engineering Division Summer Meeting, June 11-15, Boston, Massachusetts.

Mori M. et. al. (2002). *Development of a novel flow metering system using ultrasonic velocity profile measurements, Experiments* in Fluids, 32, pp.153-160

MULTILINE FLOW RATE MEASUREMENT USING ULTRASONIC DOPPLER METHOD

Sanehiro Wada[1], Hiroshige Kikura[1], Masanori Aritomi[1], Yasushi Takeda[2] and Michitsugu Mori[3]

[1]Research Laboratory for Nuclear Reactors, Tokyo Institute of Technology, 2-12-1 Ohokayama, Meguro-ku, Tokyo, 152-8550 Japan, e-mail: sane@2phase.nr.titech.ac.jp

[2]Hokkaido University, Kita 8 Nishi 5, Kita-ku, Sapporo 060-0808, Japan

[3]Tokyo Electric Power Company, 4-1 Egasaki-cho, Tsurumi-ku, Yokohama, 230-8510 Japan

keywords: Ultrasonic Doppler method, ultrasound, flow rate measurement, velocity profile, non developed flow

ABSTRACT

Ultrasonic Doppler method for flow metering system has been developed. The principle is based on the integration of instantaneous velocity profile over a pipe diameter so that it is expected to be able to eliminate installation problems such as entry length as well as to follow transient flow rate precisely. Therefore, in the present study, we reported the results of multiline flow rate measurement employing this method Flow metering principle by ultrasonic Doppler method in a circular pipe depends on the alignment of measuring lines. And in most cases, metallic pipes are used both in industrial factories and power plants.

In this paper, the influence of the number of measuring lines and the comparison among several kinds of metallic pipes on the flow rate measurements have been investigated for non-developed flows in a vertical pipe.

1. INTRODUCTION

A flow metering system has been developed using ultrasonic Doppler method [1][2]. This method has many advantages over other flow measurement techniques. One of the advantages is that it has a capability of measuring the velocity profile in a pipe over a diameter, so it is expected to improve the flow metering principle. All conventional flow metering techniques have to assume the velocity profile in a pipe. This assumption limits the improvement of the measurement accuracy just down to only about 2%. In addition, it induces various constraints such as the necessity of installing a long entry length upstream the measurement position. Ultrasonic Doppler method might be able to eliminate these assumption and constraints.

The system has been developed to be applied for conventional piping system of metallic wall [3][4]. Laboratory experiments has shown a very good agreement with the flow rate measurement using conventional orifice flow meter. Additionally, it shows a good tractability for transient behavior. In order to establish the technique and investigate its absolute accuracy, the comparison among experimental results has been performed at the NIST calibration stand [5].

Ultrasonic Doppler method employs a pulsed ultrasonic echography together and detects instantaneous Doppler shift frequency to form a velocity profile. It can obtain spatio-temporal information of the flow field. A pulsed ultrasound is applied also for flow metering based on the traveling time of ultrasonic pulse. It has, however, unfavorable restrictions on its installation and its application is quite limited. Since the ultrasonic Doppler method can obtain an instantaneous velocity profile, it is expected to be applicable for flow metering with much higher accuracy and to be applied with less restrictions.

Flow metering principle by ultrasonic Doppler method in a circular pipe depends on the alignment of measuring lines. The most accurate way is to make a two or three-dimensional flow mapping at the cross section of the pipe. At one axial location of a cylindrical pipe, the flow rate is estimated by the following equation:

$$Q(t) = \iint V_z(r,\theta,t) r dr d\theta \tag{1}$$

This requires the measurement of two-dimensional time-dependent velocity distribution. However, it does not require the assumption about any flow conditions such as the degree of flow development, Reynolds number and steadiness. Therefore, it can accomplish a flow metering with minimum restriction and the highest possible accuracy. For the purpose of measuring the flow rate, it also does not require any calibration procedures of the device. However, it is considered that this requires a large number of measuring lines, namely transducers and it takes a long time for data collection. In order to overcome this drawback, we made an assumption that the angular dependence of *Vz* is weak. Adopting this assumption and locating all measuring lines on a diameter (going through the center of the pipe) with inclination angle, reduces the equation to

$$Q(t) = \sum \left\{ \Delta\theta \int V_z(r,\theta,t) / \sin(\alpha) r dr \right\} \tag{2}$$

where $\Delta\theta = 2p/N$.

It is expected that this enables one to realize the flow metering with much less number of transducers with reasonably short measuring time. We performed a laboratory experiment in which this simplification is confirmed to be effective using one measuring line. However, it is necessary with regard to the measurement of non-ideal turbulent flows to consider non-axisymmetric or swirl flows.

In the present study, the influence of the number of measuring lines and the difference of some metallic pipes on the flow rate measurements using ultrasonic Doppler method have been investigated for non-developed flow occurring in a bend pipe.

2. TRANSMISSION OF ULTRASONIC WAVE

The propagation and transmission of ultrasound wave follows the common optical law. Reflection, diffraction, and so on occurs at the boundary of two materials which have different acoustic impedance; *Z*. However, when the wall thickness is very small, in the same order of wave length, a sort of resonance transmission of the wave occurs instead at the boundary. We investigated this resonance transmission in this position. When the wall thickness is comparatively small and in the order of the ultrasonic wave length, immersed in a fluid, then the transmission coefficient of the wave, D, is described as follows:

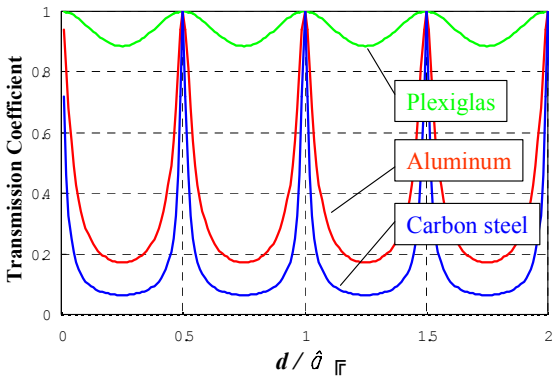

Figure 1. Transmission of ultrasound

$$D = \left[1 + \frac{1}{4}\left(m - \frac{1}{m} \right)^2 \sin^2 \frac{2\pi d}{\lambda} \right]^{-\frac{1}{2}} \tag{3}$$

Where $m=Z_1/Z_2$,. Z is acoustic impedance, d is wall thickness, and λ is wave length.

Due to its trigonometric characteristics, it changes periodically as d/λ . Fig.1 shows the comparison of the ultrasound transmission in the water for three kind of metallic pipe materials, namely Plexiglas, aluminum and carbon steel. For Plexiglas, the amplitude of oscillation is rather smaller between 80 to 100% and its width is quite broad. Whereas, for aluminum and carbon steel, the resonance peaks are very strong and very narrow. However, it does promising that for the resonant wall thickness, the transmission is 100%. From the above equation, the maximum transmission occurs at:

$$d / l = n / 2 , \qquad (n = 1,2,3\ldots) \qquad (4)$$

and the minimum (maximum reflection) at:

$$d / l = (2n + 1) / 4, (n = 1,2,3\ldots) \qquad (5)$$

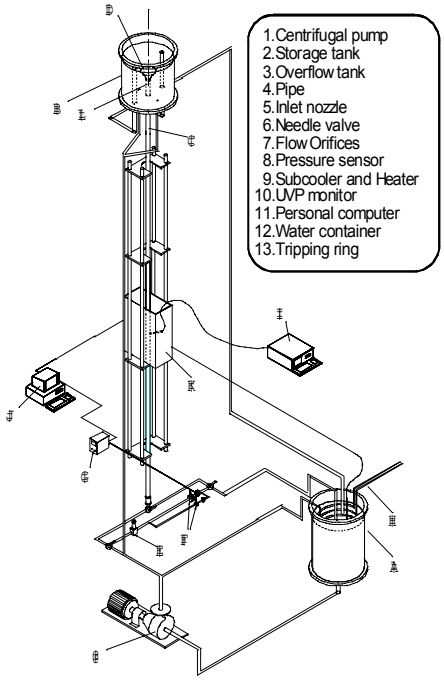

Figure 2. Schematic diagram of the experimental apparatus

3. EXPERIMENTAL APPARATUS

A schematic diagram of the experimental apparatus used in this study is shown in Fig.2. The experimental apparatus consists of a water circulation system, a test section and a measurement system. In this study, single-phase turbulent pipe flow in upward direction was investigated.

The experimental apparatus was designed and built in order to put emphasis on the formation of fully developed turbulent pipe flow in both downward and upward directions. The water was circulated by a centrifugal pump from the storage tank into the pipe. The vertical pipe was made of Plexiglas, with the total length, inner diameter and wall thickness were 6 m, 50 mm and 5 mm, respectively. The flow rate was regulated by the needle valve and monitored by flow orifices and pressure sensor located upstream of the test section.

The test section and the arrangement of ultrasonic (US) transducers are shown in Fig. 3. The water flows into the pipe through the bend pipe and the sudden expansion pipe. The US transducer was mounted on the surface of the outer wall at a contact angle of θ to the normal plane of the wall. The wall thickness of the pipe in this test section was 5 mm (Plexiglas), 1.49mm (Carbon steel), 1.61mm (Aluminum), because the ultrasonic beam demands low resistance against ultrasonic wave propagation.

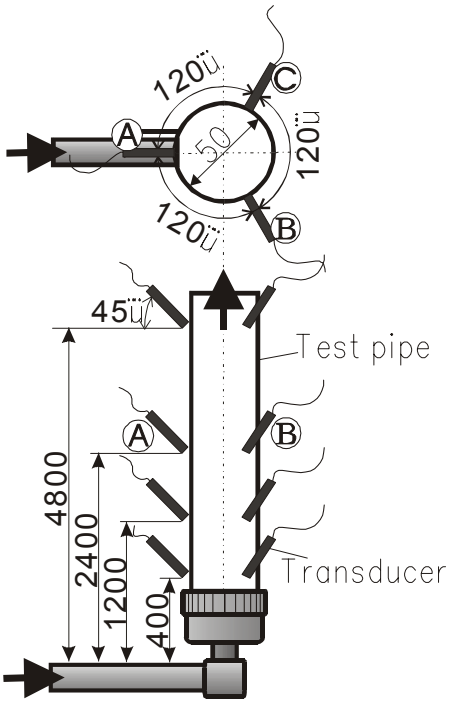

Figure 3. Test section and transducer arrangement in upward direction

Measuring points were located at 0.4 m (8D), 1.2m (24D), 2.4m (48D) and 4.8m (96D) downstream from the bend pipe. Three transducers were set on the outer surface of the each measuring point with an interval angle of 120° and with a constant inclination angle, θ = 45°

(Plexiglas) and 28.5° (Carbon steel and Aluminum). These transducers were switched using a multiplexing function of ultrasonic velocity profile monitor. The test section was surrounded by water to form an acoustic coupling between the wall and transducers.

During the experiment, water temperature was kept constant at about 20°C using a sub cooler and heater installed inside the storage tank. The flow measurement system consisted of the X-3 PS-i model ultrasonic velocity profile monitor (Met Flow AG) and a personal computer, which recorded the flow rate by the flow orifices and temperature data by the thermocouple.

As a reflector material, nylon powder (Daisel Hüls Ltd, WS200P) was suspended in water. The average particle diameter is approximately 80 μm and the specific gravity of particle is 1.02.

4. MULTI-LINE US TRANSDUCER ARRANGEMENTS

Fig.4 shows the arrangement of the transducers and measuring lines. At its most simple configuration, ultrasonic Doppler method for flow rate measurement requires only a single transducer whereby the measurement line goes through the center of the pipe. If the flow is axial symmetric, the flow rate can be obtained accurately by integrating the half of the velocity profile using Eq. 4, which is obtained with the measuring line on the diameter as shown in Fig.5.

$$Q(t) = \frac{\pi}{3}\left\{\frac{R_0^3 - R_1^3}{R_0 - R_0}v_0 + \sum_{i=0}^{n-2}\frac{R_{i+1}^3 - R_{i+2}^3}{R_{i+1} - R_{i+2}}(v_{i+1} - v_i) + R_n^2 v_n\right\} \tag{4}$$

For the flow rate calculation, there are two approaches to integrate the velocity profile. For example, using US transducer-A shown in Fig. 4, one method is that the flow rate is calculated by using a measuring line, 1 or 4, and the others that the flow rate is calculated by using two measuring lines, 1 and 4. In the same manner, many US transducers can be used to integrate each measuring lines, so that the flow rate can be measured more accurately, even if the flow is non-axisymmetric.

In the present study, we used up to three US transducers for the flow rate calculation.

In the case of using multiline for flow rate calculation, some velocity interpolation of circumferential direction is required as shown in Fig.6, which shows a circumferential

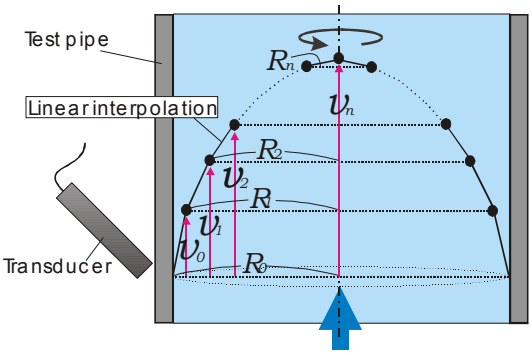

Figure 5. Integration of the velocity profile

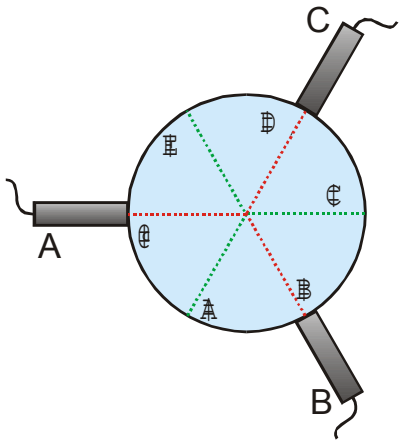

Figure 4. Arrangement of US transducers

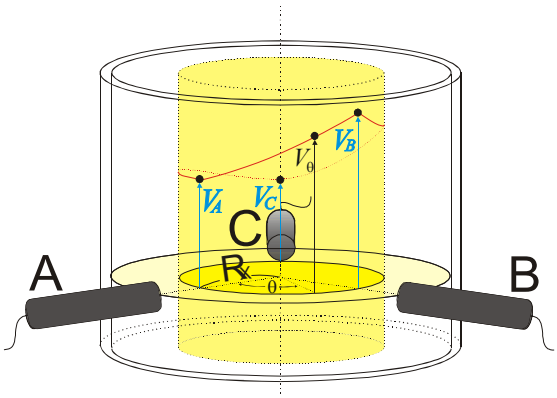

Figure 6. Circumferential velocity interpolation

velocity interpolation using three measuring lines, 1, 3 and 5 as illustrated in Fig.4. The difference of flow rate error between using Liner and Spline interpolation method was 0.018 % in this flow, so that we used Liner interpolation for flow rate calculation in this study.

5. RESULTS AND DISCUSSION

5.1 Mean velocity profile

The mean velocity profiles at the inlet position of 8D and 96D from the measurement line using Plexiglas and each US transducer are shown in Fig.7 (a) and (b). The basic frequency of ultrasonic is 4 MHz and Reynolds number is 24 000. From this figure, it is found that the velocity profiles after the bend pipe depends on the inlet length. As shown in Fig.7 (a), for 8D case, the flow is non-axisymmetric so that it is difficult to estimate the flow rate directly using a single US transducer measurement. However, if the flow condition is axial symmetry as shown in Fig.7 (b), for 96D case, the flow might be fully developed, and the flow rate can be calculated by using a half side of the velocity profile.

Fig.7 (c) and (d) show the mean velocity profiles using aluminum and carbon steel at the inlet position of 8D. The half velocity profile that is near side from the transducer is disturbed by a reflection from the front pipe wall, so that it is difficult to directly estimate the flow rate. However, as shown in this figure, the flow rate can be calculated by using the far side profile.

5.2 Flow rate measurement

As mentioned above, the velocity profile can be obtained so that a flow rate is estimated by using half region of the velocity profile. Mean flow rate calculated by using multiline US

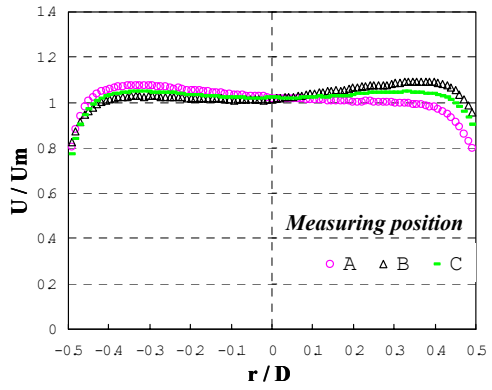

(a) Plexiglas (8D)

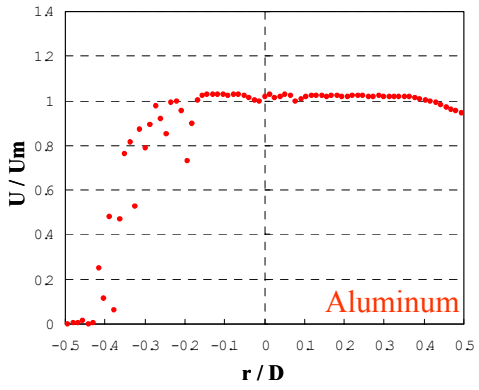

(c) Aluminum (8D)

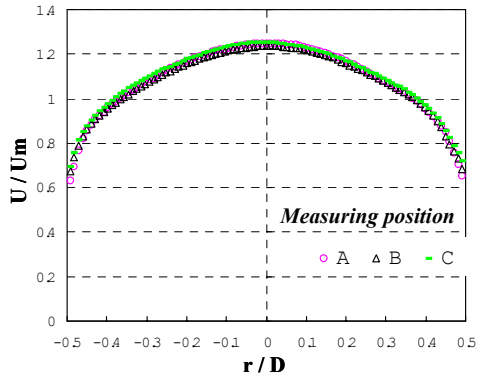

(b) Plexiglas (96D)

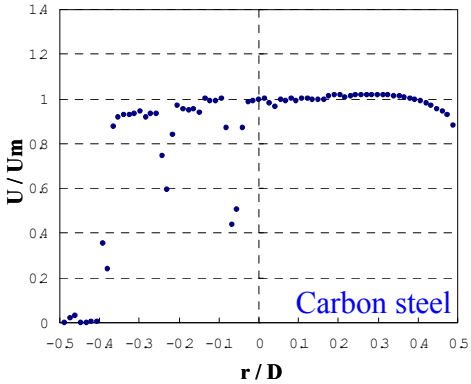

(d) Carbon steel (8D)

Figure 7. Mean velocity profiles

transducer arrangement is compared with the flow rate measured by the volumetric flow rate. Here the tank capacity is about $1m^3$ and the volume of water collected in the tank can be measured with very high accuracy. The volumetric flow rate is estimated from the volume of water collected in the tank and the collection time, so that the expanded uncertainly for this facility is quoted to be 0.08%. Table-1 shows the comparison of errors between the measured flow rate at 8D using ultrasonic Doppler method and the volumetric flow rate with respect to the using line number (ref. Fig.4) for calculating a flow rate. As described above, for the metallic wall, it is difficult to estimate a flow rate directly by using the near side velocity profile from the transducer, so that the errors in the case of aluminum and carbon steel are shown only for those cases using the far side profile. And to estimate the accuracy of each measurement, the standard deviation for Plexiglas is plotted in Fig.8. From Table-1 and Fig.8, it is found that for 8D case, the inlet flow is unstable, so that the standard deviation of the mean flow rate measured by single US transducer is large. However, by using multiple measuring lines, it is achievable to measure the flow rate with high accuracy.

6. CONCLUSION

Flow metering system using ultrasonic Doppler method has been developed. In the present study, we reported the results of multiline flow rate measurement employing this method. In this experiment, even for the non-axisymmetric flow occurred at the inlet position through the pipe bend and sudden expansion pipe, it is possible to measure the flow rate using multiline system with high accuracy.

As mentioned above, it is indicated that the present multiline flow metering system by using ultrasonic Doppler method has very high accuracy. And this method can be considered as a multipurpose system, because the flow rate can be measured under non-ideal flow conditions such as non-developed flow or non-axisymmetric flow.

Table 1. Comparison of errors for each material

Using line number	Error %		
	Plexiglas	Aluminum	Carbon steel
1	1.99	-	-
2	0.55	-3.7	0.03
3	-2.33	-	-
4	-5.63	1.51	-3.14
5	-0.95	-	-
6	4.09	-1.41	-3.18
1, 4	-1.68	-	-
3, 6	0.98	-	-
2, 5	-0.20	-	-
1, 3, 5	-0.40	-	-
2, 4, 6	-0.17	-1.15	-2.07
1 – 6	-0.28	-	-

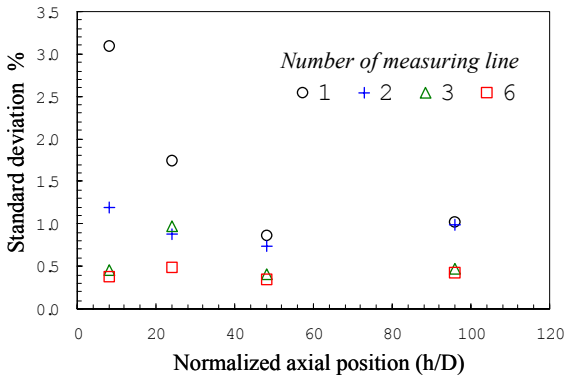

Figure 8. Standard deviation (Plexiglas)

7. REFERENCES

[1] Takeda, Y., Measurement of velocity profile of mercury flow by ultrasound Doppler shift method, Nuclear Technology, 79 (1987), pp 120-124.

[2] Takeda, Y., Velocity profile measurement by ultrasonic Doppler method, Experimental Thermal and Fluid Sci., 10 (1995), pp 444-453.

[3] Kikura, H., et al., Proc. of 3rd ASME/JSME Joint Fluid Engin. Conf. (1999), FEDSM99-7141.

[4] Mori, Metallic., 7th Int. Conf. on Ncl. Engin. (ICONE7), Tokyo (1999), ICONE-7429.

[5] Takeda, Y., et al., ASME 2000 Fluids Engn. Divi. Summer Meet.,(2000), FEDSM2000-11102

ULTRASOUND MEASUREMENT OF TEMPERATURE PROFILES IN CONVECTING OPAQUE FLUIDS

C. David Andereck[1], Hongzhou Xu[2], and Sean Fife[3]

Department of Physics, Ohio State University, 174 West 18th Avenue, Columbus, Ohio 43210, USA
[1] andereck@mps.ohio-state.edu, [2] hongzhou@mps.ohio-state.edu, [3] fife.10@osu.edu

Keywords: Ultrasound, Non-Destructive Testing, Liquid Metals, Rayleigh-Bénard Convection

ABSTRACT

An ultrasonic technique has been developed to non-intrusively measure temperature fields in convecting opaque fluids. As many industrial processes involve opaque fluids with imposed thermal gradients it is important to be able to accurately and simply determine their temperature distributions. However, most current diagnostic techniques involve optical methods, or require mounting probes inside the fluid; these methods either fail altogether in opaque fluids, or require significant invasion of the flow and/or modification of the walls of the container to allow access to the fluid. We have used the temperature dependence of sound velocity to probe the thermal fields of convecting opaque fluids non-intrusively and without the use of seed particles. The technique has been validated by comparing simultaneous ultrasound measurements and visualization using a suspension of thermochromic liquid crystals in a transparent convection cell filled with glycerol. Subsequently we constructed and calibrated an array of ultrasound transducers, relying upon the experimentally determined variation of sound speed in mercury with temperature, and used the array to measure temperature distributions in a mercury-filled Rayleigh-Bénard convection cell. The measurements of cell wavelength and onset Rayleigh number are close to the theoretically predicted values. Limitations and potential improvements will be described.

1. INTRODUCTION AND METHOD

1.1 Background

The buoyancy driven flows of transparent fluids in systems with rigid boundaries at the top and bottom (Rayleigh-Bénard convection) have been extensively studied, both for their potential applications and as beautiful examples of pattern formation in non-equilibrium systems (see Cross and Hohenberg (1993) for a review of convection in single layers and related pattern forming systems). However, most such work has concerned the convection of transparent fluids, owing partially to the available diagnostic tools. Relatively non-intrusive velocity and temperature measurements typically rely on optical techniques, and hence are useful only with transparent fluids. Laser Doppler velocimetry (LDV) and particle imaging velocimetry (PIV) rely on the addition to the flow of small seed particles. A recent development is the ultrasound Doppler velocimeter (Takeda (1986)). As with LDV, it relies on seed particles to scatter Doppler shifted sound back to the detector. In contrast with LDV, Doppler ultrasound works in both transparent and opaque fluids. A very different type of approach, limited to transparent fluids, is to use the variation of the index of refraction of the fluid with temperature to visualize the thermal field through interferometric, Schlieren or shadowgraph techniques (Goldstein (1983), Prakash and Koster (1996)). In each case the result is a 2D map related to the average of the temperature field along the line of observation. An alternative approach, which is not limited to transparent fluids and does not require

seeding, is to use hot-wire or hot-film probes (Blackwelder (1981)). Unfortunately, these probes can be quite invasive. Thus the options for studying opaque fluids such as liquid metals are limited, while the importance of studying their flows is clear; since their thermal properties are quite different from transparent fluids typically used, any attempt to use a transparent fluid to model the detailed flow properties of a liquid metal under thermal stress is doomed to failure. As many industrial processes involve opaque fluids, often in situations in which thermal gradients are important, the need for new diagnostic tools is apparent.

1.2 Experimental Technique

We have used ultrasound to detect the thermal fields of opaque fluids non-intrusively and without the use of seed particles. The technique relies upon the variation of sound speed with the temperature of the fluid. The use of sound speed to measure the temperature of a gas was apparently first proposed by Mayer (1873). The concept has been realized in a particular manner in large-scale gas systems (such as in the interiors of furnaces and boilers) by Morgan (1972), Dadd (1983), Green (1985), Bramanti et al. (1996), and Sielschott (1997). For work with a small laboratory scale apparatus we have adopted the pulse-echo ultrasound technique commonly employed for nondestructive testing of solids. Specifically, a very short ultrasound pulse traverses the fluid-filled chamber in a time determined by the chamber geometry and the average temperature of the fluid through which the pulse passes. We measure the time between the arrival of an echo pulse from the first wall/liquid interface and the arrival of a pulse from the second such interface, the one on the far side of the chamber. The measurement demands are stringent. Nevertheless, with high speed instrumentation we can detect the influence of the fluid temperature on the pulse travel time and thus obtain temperature measurements of the fluid interior. With the present system, spatial resolution of a few millimeters is achievable. Temperature resolution of a fraction of a degree C has been achieved. With an array of transducers a map of the thermal field over the chamber can be produced on a time scale short compared with many convective processes. While we cannot yet achieve the speed or resolution of optical systems, our approach is nonetheless quite adequate for many flow problems.

Figure 1 shows a typical experimental configuration. The contact transducer array, consisting of from 1 to 11 contact transducers (Panametrics M110, for example) arranged linearly, was connected to a Keithley model 7002 switcher, which, under computer control, can shift the electrical connection to the Panametrics pulser/receiver from one transducer to the next with approximately 0.15 s dead time. The output of the pulser/receiver is sent to a preamplifier, which allows us to adjust the voltage offset and gain so that the signal excursions are maximized within the input range of the Perkin-Elmer *Eclipse*, a very high speed signal averager. In the *Eclipse*, signals from a particular transducer accumulate until an averaged output can be transferred to the computer, and the switcher brings the next transducer online. The LabView program responsible for control of the data acquisition then finds the appropriate peaks in the averaged signal and stores their locations for additional processing after the data run is completed. It is possible to obtain a complete scan of the array, with 1024 pulses per transducer, in a few seconds. In addition to control of the data acquisition process, the computer is also responsible for setting the top and bottom plate temperatures, reading thermistor resistances in those plates, and controlling a traversing system that allows us to move the transducer array to provide a 2D thermal map of the chamber. Details of the basic concepts and early work on this technique are found in Fife et al. (2002).

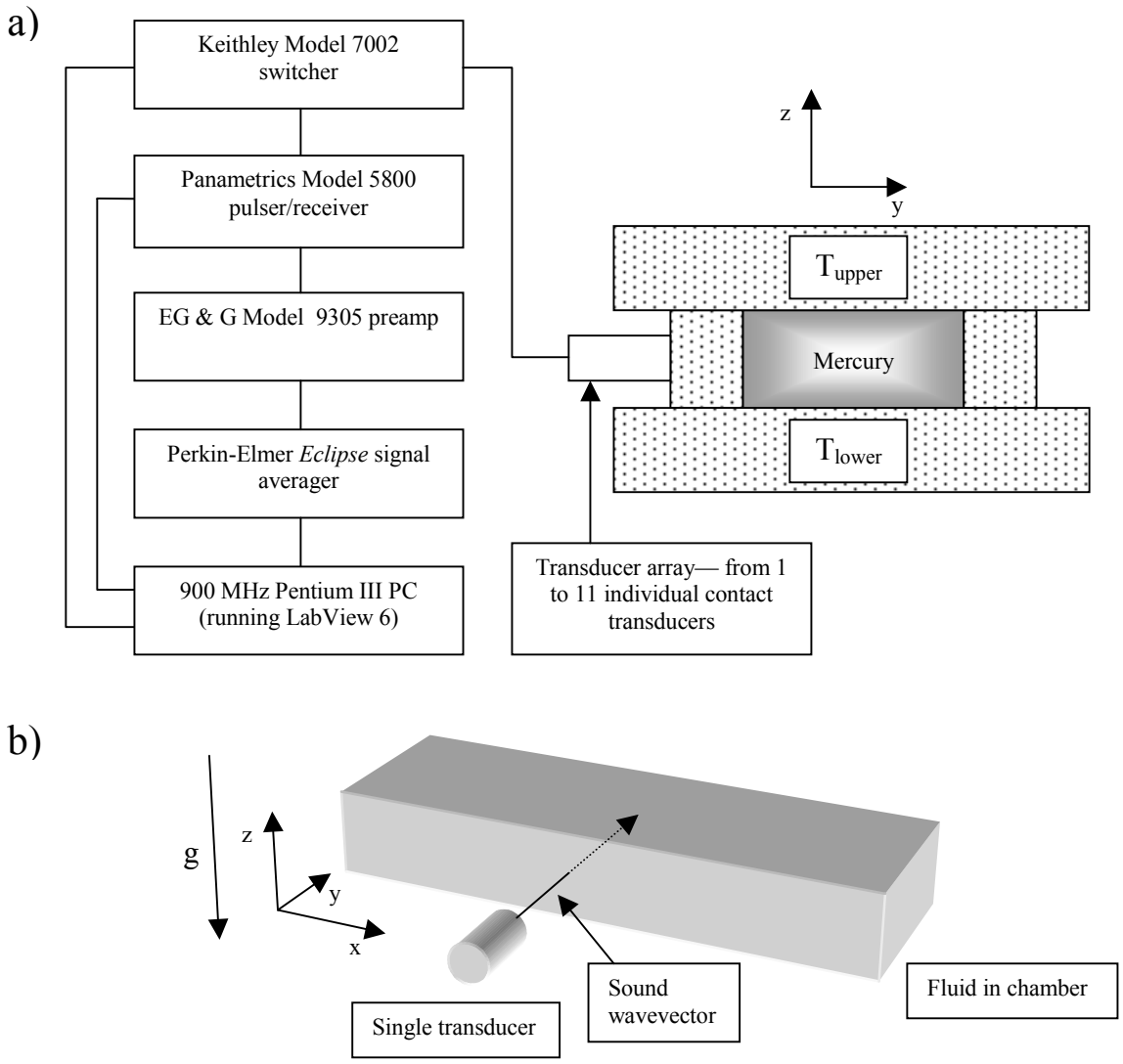

Figure 1. a) Schematic diagram of apparatus. b) Sketch of fluid chamber and its relation to gravity, a representative transducer, and the direction of sound propagation.

2. RESULTS

2.1 Emergence of Patterns

Using a mercury filled stainless steel chamber with depth (z direction) 13 mm, length (x direction) 77 mm, and width (along the direction of sound propagation as in Figure 1b)) 20 mm, we have measured the temperature profile along a line at mid-depth as a function of imposed vertical temperature gradient, heating from below. Figure 2 shows an example data run. At low temperature gradients the profile is essentially flat, uniform across the chamber and indicative of a purely conductive state. As the temperature gradient increases a pattern of rolls emerges, as indicated by the higher and lower temperature regions in the chamber. In this case, the final state consists of four convection rolls, with rising fluid in the chamber center and at either end.

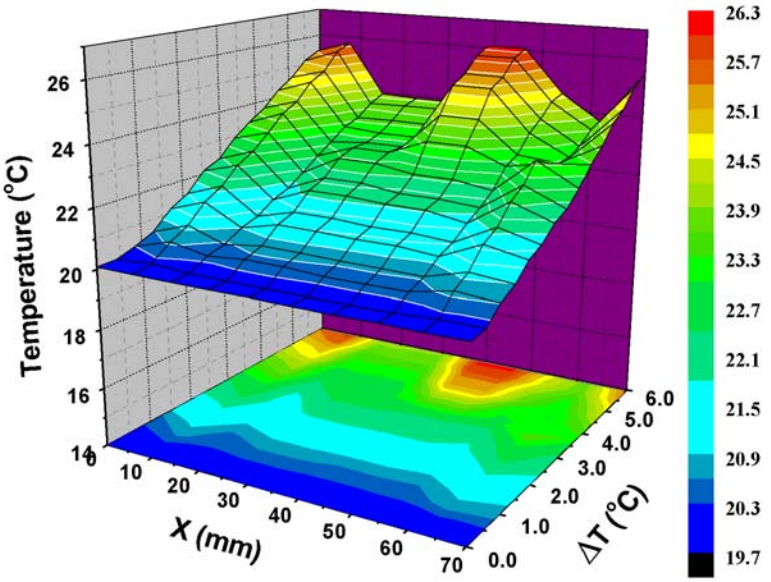

Figure 2. Temperature profile in mercury with increasing temperature gradient, measured at mid-depth along the chamber length.

For a fixed temperature gradient, it is possible to produce a 2D map of the temperature profile by moving either a single transducer or an array of transducers to a set of locations across the external vertical surface of the chamber. A typical result is shown in Figure 3 using a single XMS310 transducer, for an imposed temperature difference of 11.8 C.

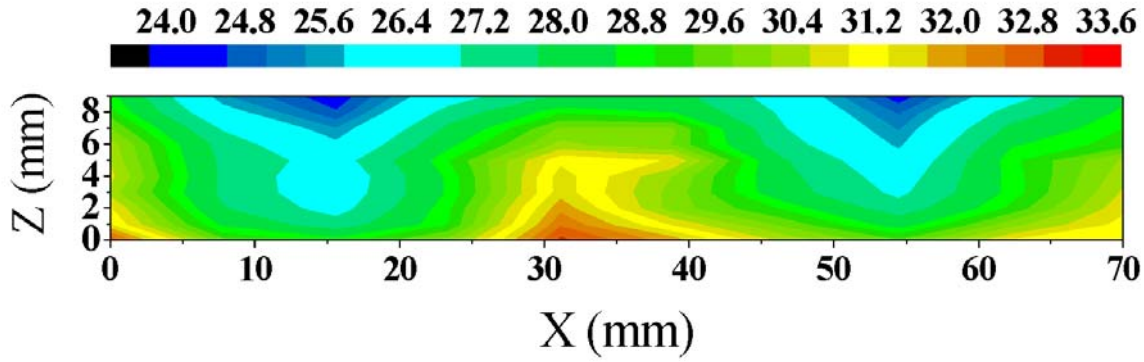

Figure 3. 2D temperature profile for ΔT = 11.8 C

2.2 Pattern Onset

In order to verify the onset of convection, which is predicted to be at a Rayleigh number of 1708 for an infinite system with conducting rigid top and bottom boundaries, we have measured the magnitude of the temperature perturbation as we slowly ramped up or down the imposed ΔT under computer control. The standard deviation of the temperature perturbation obtained from 11 transducers located along a line at mid-depth was plotted against Rayleigh number. It is clear from Figure 4 that an imperfect supercritical bifurcation is occurring at a Raleigh number comparable to the theoretical prediction, and that the result is reproducible over many different experimental runs.

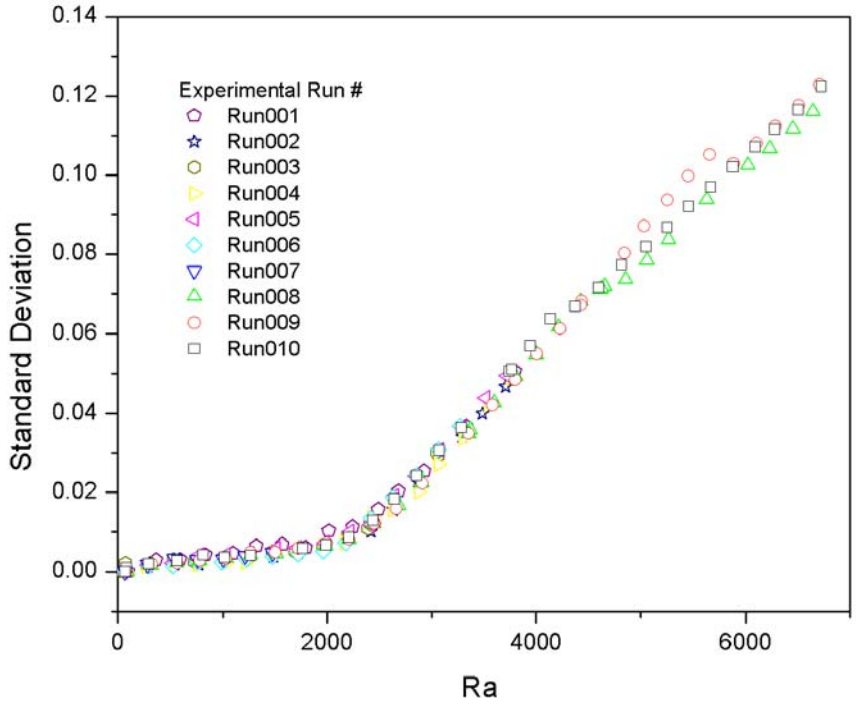

Figure 4. Standard deviation of the temperature profile as a function of Rayleigh number near convection onset

A further test of the technique's capability is provided by measurement of the pattern wavenumber near onset. Again, we have analyzed the data from a mid-depth temperature profile, specifically from run # 9 in the study above, and compared our wavenumber data with the neutral stability curve from Chandrasekhar, S. (1981). Our critical wavenumber, as shown in Figure 5, is quite close to the predicted value.

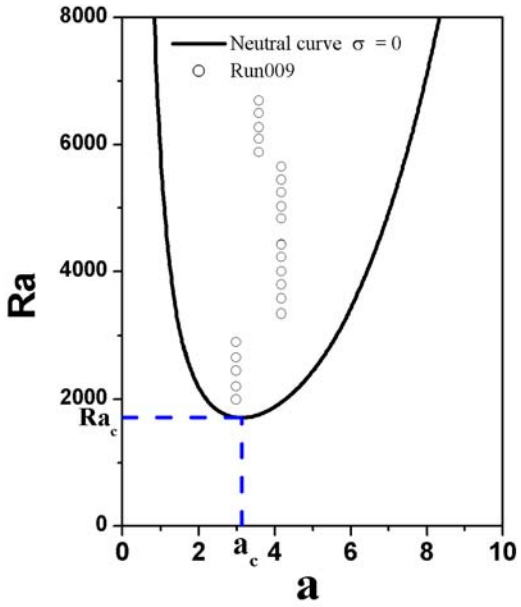

Figure 5. Stability diagram showing the critical Rayleigh number Ra_c, the critical wavenumber a_c, the theoretical neutral curve and measured wavenumbers from run 9

3. CONCLUSIONS

We have demonstrated the usefulness of ultrasound as a probe of the temperature field in liquid metals undergoing convection. The technique has sufficient sensitivity to detect the approximate onset of convection, and sufficient accuracy to yield predicted wavenumbers. We hope to extend this method to other situations in which the unique properties of liquid metals play a role in determining the flow behaviour.

ACKNOWLEDGMENTS

We gratefully acknowledge the support of NASA through grant NAG3-2138. We also wish to thank S. I. Rokhlin, M. Rutgers, and especially Y. Takeda for helpful discussions and useful insights.

REFERENCES

Blackwelder R F (1981) *Hot-wire and hot-film anemometers*. In: Fluid Dynamics, Part A (ed Emrich, R. J.). Methods of Experimental Physics Vol. 18, pp 259-314, New York: Academic

Bramanti M; Salerno E A; Tonazzini A ; Pasini S; Gray A (1996) *An acoustic pyrometer system for tomographic thermal imaging in power plant boilers*. IEEE Transactions on Instrumentation and Measurement 45: 159-167

Chandrasekhar, S. (1981) *Hydrodynamic and Hydromagnetic Stability*. New York: Dover: 58

Cross M C; Hohenberg P E (1993) *Pattern formation outside of equilibrium*. Rev. Mod. Phys. 65: 851-1112

Dadd M W (1983) *Acoustic thermometry in gases using pulse techniques*. TEMCON Conference, London

Fife S; Andereck C D; Rahal S (2002) *Detection of thermal fields in opaque fluids using ultrasound*. Preprint

Goldstein R J (1983) *Fluid mechanics measurements*. Washington: Hemisphere, Springer

Green S F (1985) *An acoustic technique for rapid temperature distribution measurement*. J. Acoust. Soc. Am. 77: 759-763

Mayer A M (1873) *On an acoustic pyrometer*. Philos. Mag. 45: 18-22

Morgan E S (1972) *The acoustic gas pyrometer*. CEGB Rep. RD/L/R 1779

Prakash A; Koster J N (1996) *Steady Rayleigh-Bénard convectionin a two-layer system of immiscible liquids*. Trans. ASME 118: 366-373

Sielschott H (1997) *Measurement of horizontal flow in a large scale furnace using acoustic vector tomography*. Flow Measurement and Instrumentation 8: 191-197

Takeda Y (1986) Velocity profile measurement by ultrasound Doppler shift method. Int. J. Heat Fluid Flow 7: 313-318

ULTRASONIC PROPAGATION IN A MAGNETIC FLUID

Masaaki Motozawa[1] and Tatsuo Sawada[2]

Department of Mechanical Engineering, Keio University, Hiyoshi, Kohoku-ku, Yokohama 223-8522, Japan
[1]motozawa@sawada.mech.keio.ac.jp, [2]sawada@mech.keio.ac.jp

Keywords: Anisotropy, Clusters, Magnetic fluid, Sound velocity, Ultrasonic propagation

ABSTRACT

When an external magnetic field is applied to a magnetic fluid, some of the colloidal particles coagulate and form chain-like clusters. These clusters result in interesting ultrasonic propagation properties, such as anisotropy and hysteresis. We measure the ultrasonic propagation velocity (1 MHz, 2 MHz and 4 MHz) in a magnetic fluid subject to a magnetic field. Measurements were made using the pulse method, first, while the magnetic field intensity was varied from 0 mT to 570 mT, and, second, while the angle between the magnetic field direction and the direction of ultrasonic wave propagation was varied between 0° and 180°. Some interesting results were obtained that seem to be caused by cluster formation in the magnetic fluid.

1. INTRODUCTION

A magnetic fluid is a stable colloidal dispersion of rather small surfactant-coated magnetic particles in a liquid carrier such as water or kerosene. When a magnetic field is applied to a magnetic fluid, interesting flow behaviors have been observed. In order to better understand the characteristics of these interesting flow behaviors, it is useful to make detailed measurements of internal velocity fields. However, because magnetic fluids are opaque, optical methods such as laser Doppler anemometry or flow visualization techniques such as particle image velocimetry can not be applied. Thus, there have been few experimental studies with respect to velocity field in magnetic fluid flows.

A technique called the Ultrasound Velocity Profile (UVP) measuring technique is a method of measuring a velocity profile along a beam line, that is, measuring with respect to the velocity component along the ultrasound beam. This method is useful in that it can be applied to opaque fluids and it has recently been applied to magnetic fluids (Sawada, Kikura and Tanahashi, 1999).

In order to use this method for velocity profile measurement of a magnetic fluid flow, it is first important to have an accurate measurement of sound velocity in a magnetic fluid when the fluid is in a magnetic field. However, the accurate measurement of sound velocity is somewhat more difficult in a magnetic field because, when an external magnetic field is applied to a magnetic fluid, some of the colloidal particles coagulate and form chain-like clusters (Goldberg, Handford and Heerden, 1971). These clusters cause anisotropy of sound propagation in the magnetic fluid. Several studies have been performed to investigate this anisotropy (Skumiel, Labowski and Hornowski, 1995), however its mechanism is still not clear.

In the present paper, we precisely measure sound velocity in a magnetic fluid under a uniform magnetic field and discuss the resulting anisotropy of the propagation.

2. EXPERIMENT

Figure 1 is a block diagram of the experimental apparatus. Figure 2 shows a detailed view of the area the test cell. The ultrasonic measurement scheme is based on the pulse method. The rectangular test cell is filled with a magnetic fluid, has a 32 mm length and is equipped with two ceramic oscillators, an emitter and a receiver. The test cell is placed in a cylindrical container filled with water. In a first experiment, the temperature of the magnetic fluid is varied, while in subsequent experiments, the temperature of the magnetic fluid is kept at 25 °C by circulating water, which is supplied by a temperature control unit. We use three different ceramic oscillators to provide three frequencies of ultrasonic wave: 1 MHz, 2 MHz and 4 MHz. The magnetic field is applied by an electromagnet and the angle between the field's direction and the direction of ultrasonic wave propagation is freely adjustable. The magnetic fluid in the test cell is W-40 with 40 % weight concentration of fine magnetite particles (Fe_3O_4) in a water carrier. The viscosity and density are 1.41 mPa·s and 1.38×10^3 kg/m^3 at 25 °C, respectively.

When a signal from the personal computer (PC) is transmitted to the ultrasonic wave generator, a burst wave is generated and is transmitted to the ceramic oscillator attached to the test cell. An ultrasonic pulse is generated and propagates through the magnetic fluid over a distance of 32mm. The signal is received at the other ceramic oscillator and is amplified. The resulting pulse-echo train is observed on a CRT display. Ultrasonic propagation velocity in a magnetic fluid is calculated by measuring the travel time of the ultrasonic pulses.

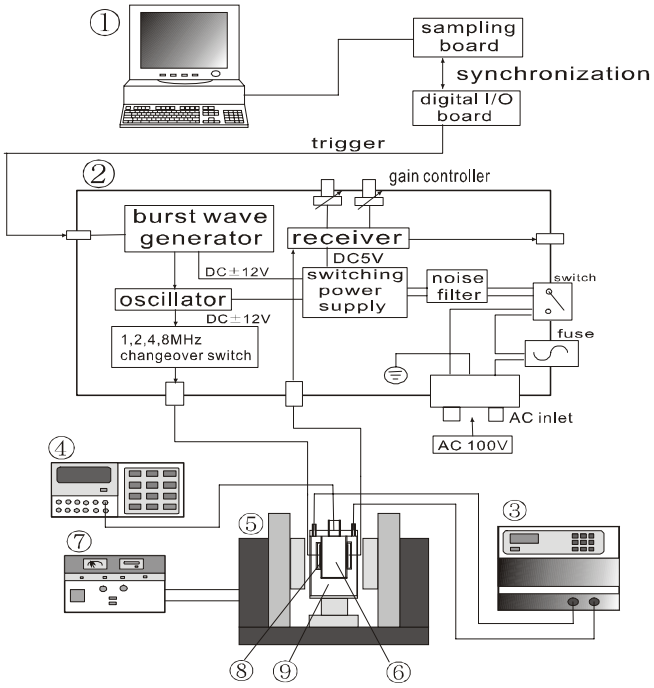

①computer
②Ultrasonic wave generator
③coolnics circulator
④thermister
⑤electromagnet
⑥magnetic fluid
⑦power amplifier
⑧ceramic oscillator
⑨test cell

Figure 1. Experimental apparatus

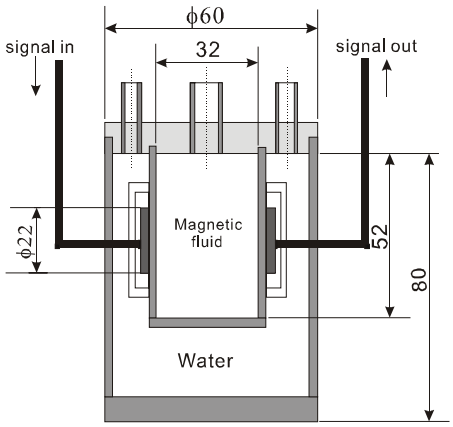

Figure 2. Test cell

3. RESULTS AND DISCUSSION

3.1 Temperature dependence

The temperature dependence of the ultrasonic velocity is shown in Figure 3 for signals of 1 MHz, 2 MHz, and 4 MHz, respectively. The solid line indicates sound velocity in pure water as obtained by Crosso and Mader (1972). In spite of the magnetic fluid being water-based the ultrasonic propagation velocity in a magnetic fluid is smaller than that in pure water. This result is caused by the magnetic particles in the magnetic fluid and surfactant layers. As the temperature increases, the ultrasonic propagation velocity in the magnetic fluid decreases for each signal. This seems to be due to an increase in thermal Brownian motion of the magnetic particles.

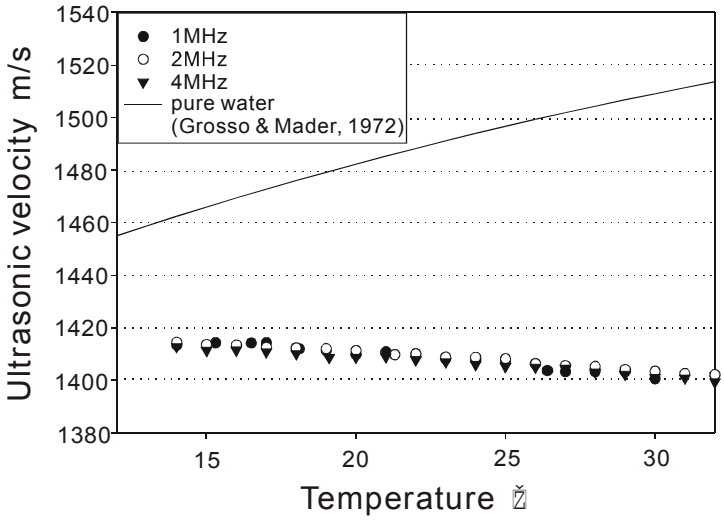

Figure 3. Temperature dependence of the ultrasonic propagation velocity

3.2 Hysteresis

Figure 4 shows 2 MHz ultrasonic propagation velocity V versus the magnetic flux density. Here, ϕ=0 is the angle between the direction of ultrasonic wave propagation and the direction of the external magnetic field, V_0 is the ultrasonic propagation velocity without an external magnetic field, and $\Delta V=V-V_0$. Clearly, there is hysteresis in relation to the applied external magnetic field (Sawada, Nishiyama and Tabata 2002). In this experiment, the magnetic field is applied using the following processes: from 0, increase the magnetic field intensity 15 mT every 2 minutes until reaching 570 mT. Thereafter, decrease the magnetic field intensity by 30 mT every 2 minutes. In the decreasing process $\Delta V/V_0$ increases and shows large variations with changes in the magnetic field intensity.

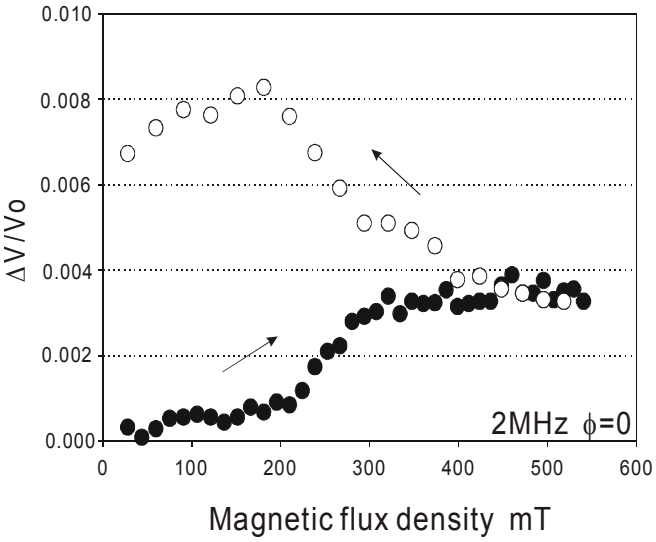

Figure 4. Hysteresis of the ultrasonic propagation velocity

These interesting results are caused by magnetic particle cluster formation in the magnetic fluid. The chain-like clusters are formed in the direction of the magnetic field in proportion to its intensity. The growth of the chains occurs by end-to-end paring or side-by-side

aggregation. When the magnetic field decreases, it is supposed that the chain-like clusters do not break instantly.

3.3 Anisotropy

The anisotropy exhibited for the 2 MHz and 4 MHz ultrasonic propagation velocities are shown in Figures 5 and 6, respectively. In these two experiments, before the measurement begins, the magnetic field is applied for 10 minuets at ϕ=0°. The ultrasonic propagation velocity is then measured every 3°. It can be seen that the minimum ultrasonic propagation velocity is obtained near ϕ=90°. Figure 7 shows 4 MHz ultrasonic propagation velocities obtained using similar measurement techniques to those of Figure 6, however, the measurements are carried out after a one hour application of the magnetic field at ϕ=0°. By comparing Figures 6 and 7, it can be seen that cluster formation develops over time and is not as significant in the initial stages.

4. CONCLUDING REMARKS

The ultrasonic propagation velocity in a magnetic fluid subject to a uniform magnetic field are investigated experimentally. Measurements are made using the pulse method and while changing the angle between the magnetic field direction and the direction of ultrasonic wave propagation. Hysteresis is exhibited as the magnetic field increases and decreases. Anistropy of the ultrasonic propagation velocity is also observed. These interesting results are believed to be dependent on the concentration of magnetic particles, external magnetic field intensity, the frequency of the ultrasonic wave and “excitation” and “relaxation” time connected with magnetization. In order to understand these interacting factors, it is necessary to investigate Brownian motion of the magnetic particles and the process of chain-like cluster formation.

ACKNOWLEDGMENTS

This work was partially supported by a Grant-in-Aid for Scientific Research (B) of the Japan Society for Promotion of Science.

REFERENCES

V. A. Del Grosso and C. W. Mader (1972). *Speed of sound in pure water*, J. Acoust. Soc. Amer., 52, pp. 1442-1446.

T. Sawada, H. Kikura and T. Tanahashi (1999). *Kinematic characteristics of magnetic fluid Sloshing in a rectangular container subject to non-uniform magnetic fields*, Expt. Fluids, 26, pp. 215-221.

T. Sawada, H. Nishiyama and T.Tabata (2002). *Influence of a magnetic field on ultrasound propagation in a magnetic fluid*, J. Mag. Magn. Mater., 250, in press.

A. Skumiel, M. Labowski and T. Hornowski (1995). *Investigation of the ultrasonic propagation velocity anisotropy in magnetic liquids in a constant magnetic field*, Acoust. Lett., 19, pp. 87-92**.**

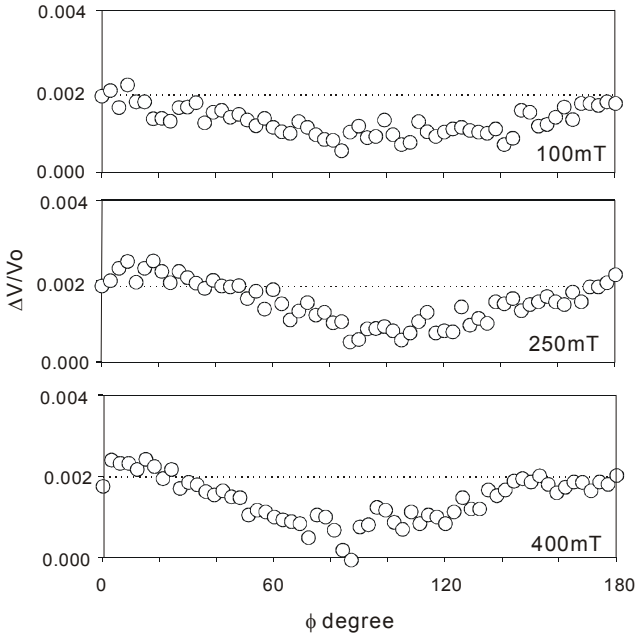

Figure 5. Anisotropy of the ultrasonic propagation velocity (2MHz)

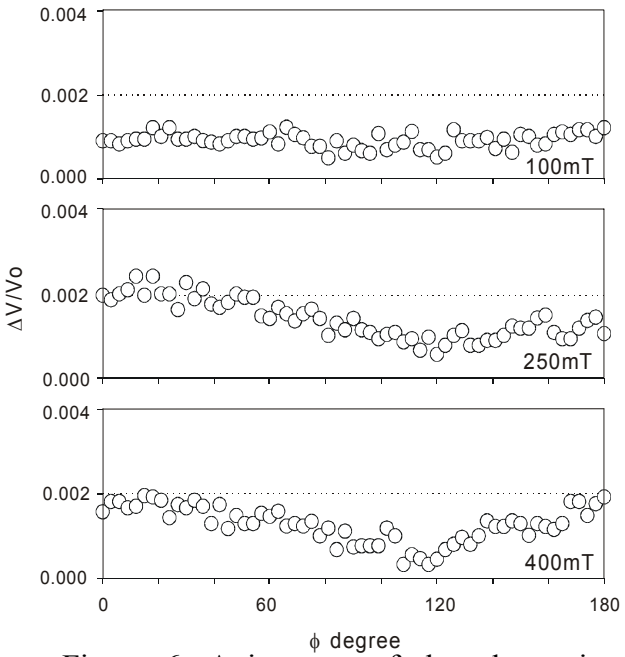

Figure 6. Anisotropy of the ultrasonic propagation velocity (4MHz)

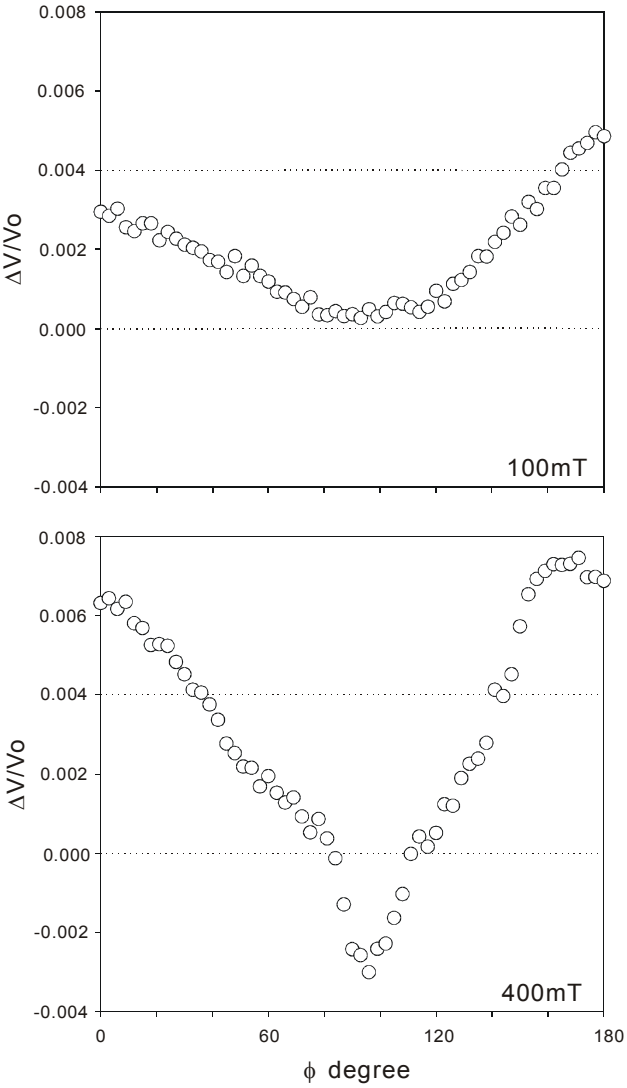

Figure 7. Anisotropy of the ultrasonic propagation velocity (4MHz)

OPENING KEYNOTE LECTURE
DOLPHIN HYDRODYNAMICS: GRAY'S PARADOX REVISITED

Peter W. Carpenter

Fluid Dynamics Research Centre, School of Engineering, University of Warwick, Coventry CV4 7AL, England

ABSTRACT

Belief that some dolphin species possess an extraordinary laminar-flow capability dates back at least as far as Gray (1936). In his analysis of dolphin energetics and hydrodynamics, Gray followed the usual practice of marine engineers to estimate the hydrodynamic drag experienced by the dolphin at the commonly observed swimming speed of 10 /s. According to this approach, if conventional hydrodynamics were involved, the flow over the dolphin would be mostly turbulent and a large drag would be experienced. So large, in fact, that at 10 /s its muscles would have to deliver about seven times more power per unit mass than any other mammalian muscle. This mismatch between the required and expected muscle output has become known as *Gray's Paradox.* It led Gray and others since to argue that the dolphin must be capable of maintaining laminar flow by some extraordinary means.

Resolving Gray's paradox may, at first, seem straightforward. Nevertheless, more than 65 ears later, complete resolution still eludes us. A full appraisal requires a multifaceted and multidisciplinary approach. In this lecture the main aspects will be reviewed. The focus will be on the structure of dolphin skin (see Figure) and the features with a potential laminar-flow function. The artificial analogue dolphin skins (compliant walls), designed by Kramer (1957,1960) and others, will also be described. There is ample evidence that such compliant walls can maintain laminar flow. This will be reviewed and used to provide evidence of the laminar-flow capability of the real dolphin skin.

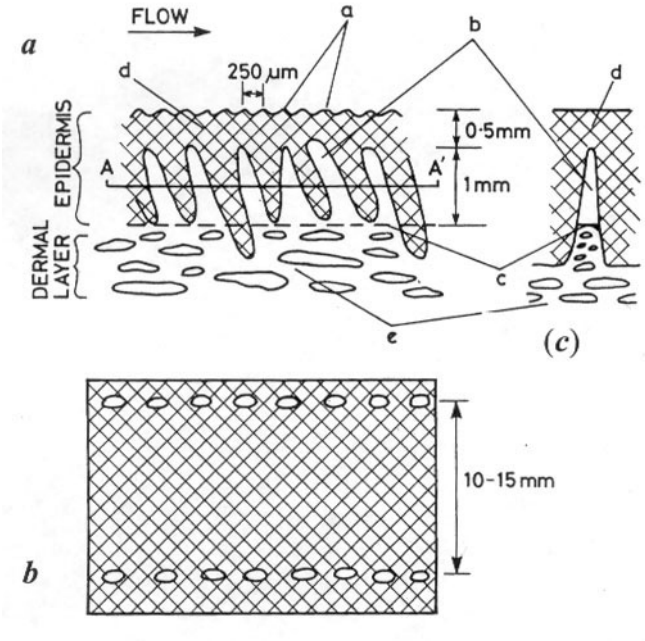

Figure: Structure of dolphin skin. (a) Cross-section; (b) Cut through dermal papillae at AA'; (c) Front view. Key: *a,* cutaneous ridges or microscales; *b,* dermal papillae; *c,* dermal ridge; *d,* upper epidermal layer; *e,* fatty tissue.

KEYNOTE LECTURE
HIGH RESOLUTION 3-D ACOUSTIC DOPPLER VELOCITY AND SEDIMENT FLUX PROFILING IN LABORATORY AND ENVIRONMENTAL STUDIES: POTENTIAL AND LIMITS

Ulrich Lemmin

Environmental Hyd. Lab., ENAC–EPFL 1015 Lausanne, Switzerland, e-mail: ulrich.lemmin@epfl.ch

ABSTRACT

Different aspects of a pulse-to-pulse coherent 3-D acoustic Doppler profiling current profiler with resolution of the turbulence scales are presented. The potential of the instrument system for boundary layer studies in the laboratory, rivers and lakes is revealed.

An ultrasonic constant-beam-width transducer system (1 MHz) is introduced which is capable of generating an extended focal zone by electronically focusing the beam over the desired water depth range. Compared to a plane disc transducer, the higher beam directivity and the reduction in side lobe level leads to an increase of the signal to noise ration by up to 15dB and allows to significantly reduce undesirable spectral broadening effects. Signal treatment methods are discussed which will further reduce spectral broadening effects.

The potential of the same system in directly measuring instantaneous sediment concentration is demonstrated. The resulting acoustic particle flux profiler is a powerful tool for measuring simultaneously profiles of the instantaneous velocity and concentration over the entire water depth of a suspension flow by making use of the backscattering intensity in combination with the simultaneous Doppler phase information. It allows measuring quasi-instantaneous particle flux profiles with a sampling frequency of 25Hz in opaque liquids.

Using the focalised transducer, simultaneous 3-D velocity component profile measurements over the whole water depth are carried out in uniform, open-channel flow and in a small river. They verify existing laws for the distribution of mean velocity, turbulence intensities and Reynolds stresses. They also reveal the presence of coherent structures extending over the whole water depth both in the laboratory channel and in the central part of the river cross section. Coherent structures are aligned in the direction of the mean flow, showing no component in the transversal direction. In the lateral boundary layers of the river, wide adjustment zones are found in which the flow is strongly 3-dimensional.

Experimental results obtained in an open-channel, sediment-laden flow under capacity charge conditions document the event structure of sediment transport by the correlation between sediment concentration peaks and coherent flow structures. Higher order statistical properties of shear stress and of turbulent mass fluxes are compared. It is shown that the coherent structure dynamics are the same in clear water and in sediment-laden flows. Strong changes in the composition of the coherent structure cycle are observed between the near wall layers and the outer layers of the flow. Coherent structures of a burst cycle are found to be important contributors in the mass transport mechanism under highly turbulent flow conditions in open-channel flows. Nearly 50% of the suspended particle transport takes place in coherent structures, which occur during less than 30% of the time.

ACKNOWLEDGEMENTS

This Symposium would not have been possible without the support of many people.

At the institutional side, we would like to thank all the members of the hosting Laboratory of Hydraulic Constructions - LCH, headed by Prof. Anton Schleiss for their commitment, the PSI, Villigen as co-organizing Institute, and the general services of EPFL and the civil engineering section for their logistical support.

Special thanks goes to Renate Bercher from PSI for her availability before and during the Symposium at the reception desk and the organization of the final printing of the proceedings; to Martine Tiercy from LCH for her kind support on the registration and financial matters and to my beloved wife Jolanta De Cesare for her aid on the WEB-site design and the finishing edition of the Symposium proceedings.

Our gratitude also goes to Met-Flow SA in Lausanne, Switzerland and Asahi Thermal and Fluid System Ltd in Nagoya, Japan. Without their support, the Symposium excursion, Student award and the Dinner would not have been possible.

Furthermore we acknowledge the contribution of all the authors, the invited keynote lecturers and the members of the ISUD Award Jury, without them, there would be no such Symposium or Award, not forgetting the joint efforts of the Organizing and Scientific Committees.

SYMPOSIUM PROGRAM

	Monday, 09.09.2002		**Tuesday, 10.09.2002**		**Wednesday, 11.09.2002**
08:30	Registration	08:20	Session 1	08:20	Session 1
09:30	Welcoming Speech	09:50	Coffee break	10:10	Coffee break
09:45	Opening Keynote Lecture	10:10	Keynote Lecture	10:30	Workshop Session
10:30	Coffee break	10:50	Session 2	11:30	Short break
10:50	Session 1		|	11:40	Closure Session
12:00	Lunch break	12:00	Lunch break	12:00	Lunch break
14:00	Session 2	13:30	Excursion Departure	14:00	Joint Committee meeting
15:10	Coffee break		|	15:00	End of Symposium
15:30	Session 3		|		
17:15	Visit of the hydraulic lab.	19:00	Symposium Diner		

Monday sessions

	Opening Keynote Lecture	
09:45 - 10:30	Dolphin Hydrodynamics: Gray's Paradox Revisited	Peter Carpenter

Session 1	Chairman	Giovanni De Cesare
10:50 - 11:10	A Characteristic of the Flow Field on a Heated Rotating Disk	Yasuyuki Miwa
11:10 - 11:30	Signal Processing for Advanced Correlation Ultrasonic Velocity Profiler	Yousuke Sato
11:30 - 11:50	An azimuthal-streamwise structure of an axisymmetric sudden expansion flow	Noriyuki Furuichi
11:50 - 12:00	Discussion	

Session 2	Chairman	Mustafa Altinakar
14:00 - 14:20	Unsteady Free-surface Flow Analysis in Circular Tube using Ultrasonic Doppler Method	Bares Vojtech
14:20 - 14:40	Ultrasonic measurements of instantaneous velocity and suspended concentration in open-channel flow	Massimo Cellino
14:40 - 15:00	Ultrasonic velocity profile measurements in pipes and flumes in a hydraulic laboratory	Helmut Knoblauch
15:00 - 15:10	Discussion	

Session 3	Chairman	Hiroshige Kikura
15:30 - 15:50	Velocity and turbulence measurements in a scour hole using an acoustic Doppler velocity profiler	Adhy Kurniawan
15:50 - 16:10	Elbe River Model: UVP Flow Mapping	Bares Vojtech
16:10 - 16:30	Analysis of coherent flow structures in a bend based on instantaneous-velocity profiling	Blanckaert Koen
16:30 - 16:50	Measurement of 3D flow field in a 90° bend with Ultrasonic Doppler Velocity Profiler	Daniel S. Hersberger
16:50 - 17:00	Discussion	

Tuesday sessions

Session 1	Chairman	Greg King
08:20 - 08:40	An Overview of Experimental Activities at the Thermal Fluid Sciences Laboratory, University of Missouri-Rolla, USA	Akira Tokuhiro
08:40 - 09:00	In-Line Ultrasound Based Rheometry Of Industrial And Model Suspensions Flowing Through Pipes	Jeelani Shaik
09:00 - 09:20	Application of Ultrasound Doppler Velocimetry to flows of hot metallic melts	Sven Eckert
09:20 - 09:40	2D time averaged flow mapping of die entry in flow of highly concentrated shear-thinning and shear-thickening suspensions	Boris Ouriev (Ur'ev)
09:40 - 09:50	Discussion	

	Keynote Lecture	
10:10 - 10:50	High Resolution 3-D Acoustic Doppler Velocity and Sediment Flux Profiling in Laboratory and Environmental Studies: Potential and Limits	Ulrich Lemmin

Session 2	Chairman	Akira Tokuhiro
10:50 - 11:10	Ultrasonic velocity profiler UVP-XW for Ice-slurry flow characterisation	Didier Vuarnoz
11:10 - 11:30	Measurement of Reynolds Stress in Bubbly Flow using Ultrasonic Doppler Method	Hideki Murakawa
11:30 - 11:50	Applicability of Ultrasonic Cavitations Bubbles for Measurement of Ultrasonic Doppler Method	Tsuyoshi Taishi
11:50 - 12:00	Discussion	

Wednesday sessions

Session 1	Chairman	Yasushi Takeda
08:20 - 08:40	Study on the Development of Novel Velocity Profile Measuring Method using Ultrasound Time-Domain Cross-Correlation	Gentaro Yamanaka
08:40 - 09:00	Industrial Application Experiences of New Type Flow-metering System based on Ultrasonic-Doppler Flow Velocity-Profile Measurement	Michitsugu Mori
09:00 - 09:20	Multiline Flow Rate Measurement using Ultrasonic Doppler Method	Sanehiro Wada
09:20 - 09:40	Ultrasound Measurement of Temperature Profiles in Convecting Opaque Fluids	David Andereck
09:40 - 10:00	Ultrasonic propagation properties in a magnetic fluid	Masaaki Motozawa
10:00 - 10:10	Discussion	

	Workshop session	Olivier Mariette
10:30 - 11:30	Workshop presentation with UVP	Various speakers

	Closure session	
11:40 - 11:50	Closure speech	Yasushi Takeda
11:50 - 12:00	"ISUD Asahi Ryunetsu Student Paper Award" ceremony	Organizing Committee & Sponsor

LIST OF PARTICIPANTS

Dr. Mustafa Altinakar
LHE-ICARE-ENAC, EPFL,
CH - 1015 Lausanne, Switzerland
mustafa.altinakar@epfl.ch
Tel.: +41 21 693 3287
Fax: +41 21 693 6767

Prof. David Andereck
Department of Physics, Ohio State University, 174 W. 18th Ave,
Columbus, OH 43210, USA
andereck@mps.ohio-state.edu
Tel.: (614) 292-2360
Fax: (614) 292-7557

Prof. Masanori Aritomi
Tokyo Institute of Technology, 2-12-1 Ohokayama, Meguro-Ku,
Tokyo 152-8550, Japan
maritomi@nr.titech.ac.jp

Mr. Vojtech Bares
Czech Technical University in Prague, Faculty Civil Engineering, Thakurova 7,
Prague 6, 166 29, Czech Republic
bares@lermo.cz
Tel.: +420 2 24354350
Fax: +420 2 24355445

Dr. Koen Blanckaert
LHE-ICARE-ENAC, EPFL,
CH - 1015 Lausanne, Switzerland
koen.blanckaert@epfl.ch
Tel.: +41 21 693 2378
Fax: +41 21 693 6767

Prof. Peter Carpenter
University of Warwick, School of Engineering, Gibbet Hill Road,
Coventry CV4 7A, UK
pwc@eng.warwick.ac.uk
Tel.: +44 024 76 523152
Fax: +44 024 76 418922

Dr. Massimo Cellino
Bonnard & Gardel Consulting, av. de cour 61, CH - 1001 Lausanne, Switzerland
massimo.cellino@bg-21.com
Tel.: +41-21-6181549
Fax: +41-21-6181122

Dr. Giovanni De Cesare
Lab. Hydr. Constr. - LCH, ENAC-EPFL,
CH - 1015 Lausanne, Switzerland
giovanni.decesare@epfl.ch
Tel.: +41-21-693 25 17
Fax: +41-21-693 22 64

Dr. Sven Eckert
Forschungszentrum Rossendorf, P.O.Box 510119, D - 01314 Dresden, Germany
s.eckert@fz-rossendorf.de
Tel.: +49 351 2602132
Fax: +49 351 2602007

Prof. Peter William Egolf
EIVD TIS, route de Cheseaux 1,
CH-1401 Yverdon, Switzerland
peter.egolf@eivd.ch
Tel.: +4124 426 44 79
Fax: +4124 426 44 77

Dr. Walter E. Fischer
Paul Scherrer Institute PSI,
CH-5232 Villigen PSI, Switzerland
walter.fischer@psi.ch
Tel.: +41 56 3103412
Fax: +41 56 3103131

Dr. Noriyuki Furuichi
Gifu University, Yanagido 1-1,
Gifu 501-1193, Japan
furuichi@cc.gifu-u.ac.jp
Tel.: +81-58-293-2538
Fax: +81-58-230-1892

Paul Scherrer Institut
CH-5232 Villigen PSI
Internet

Phone 056 310 21 11
Fax 056 310 21 99
http://www.psi.ch